

AD-A115 295

NAVAL OCEAN RESEARCH AND DEVELOPMENT ACTIVITY NSTL 5--ETC F/G 8/3  
DATA SUMMARY - XCP PROFILES IN THE VICINITY OF THE FAEROE ISLAN--ETC(U)  
APR 82 D A BURNS, N V LOMBARD

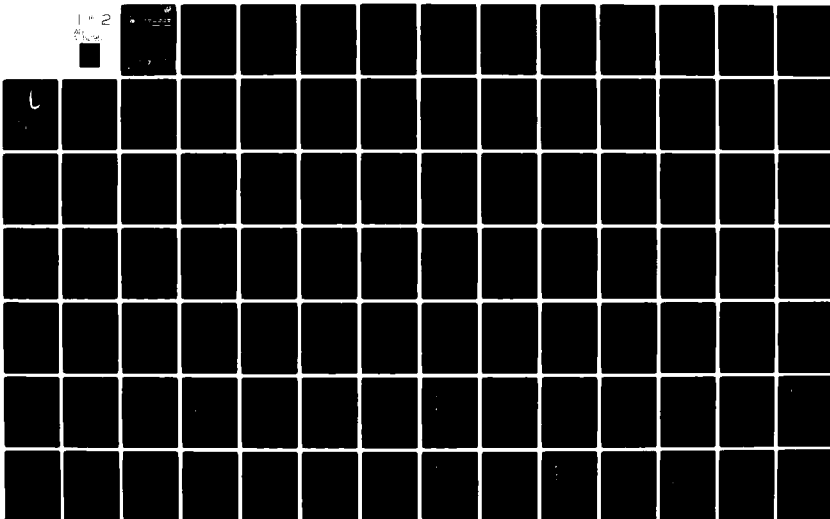
UNCLASSIFIED

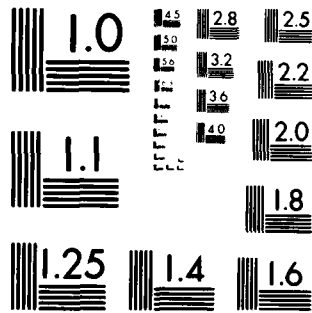
NORDA-TN-142

NL.

1 - 2

6/1/82





MICROCOPY RESOLUTION TEST CHART  
NATIONAL BUREAU OF STANDARDS 1963-A

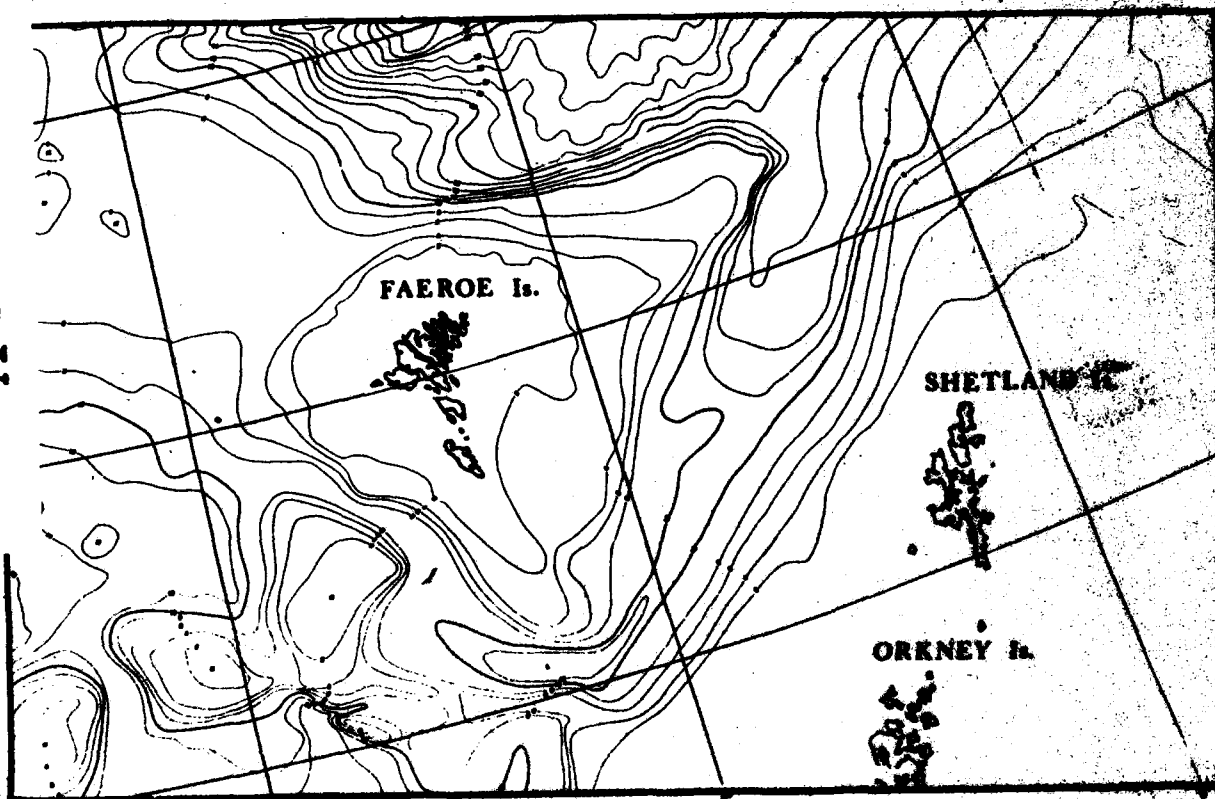
12

Naval Ocean Research and  
Development Activity  
NSTL Station, Mississippi 39529



# Data Summary - XCP Profiles in the Vicinity of the Faeroe Islands During October 1982

AD A 115295



DTIC FILE COPY

DTIC  
ELECTE  
JUN 9 1982  
S D

D.A. Davis

N.V. Lombard

Oceanography Division  
Ocean Science and Technology Laboratory

April 1982

## DISTRIBUTION STATEMENT A

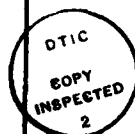
Approved for public release  
Distribution Unlimited

82 06 09 008

# ABSTRACT

In support of the Ocean Measurements Program in the Iceland-Faeroe (Subpolar) oceanic front region, Expendable Current Probes (XCP) were deployed at four time series stations and in four circulation regimes. Forty-six of seventy-three probes deployed transmitted usable data. We discuss data editing and matching of CTD and XCP casts. We present vertical profiles of XCP data and CTD data. We discuss the primary water types present and their relationship to the subpolar front. We discuss the determination and variation of bulk Richardson numbers.

Accession For	
NTIS GRA&I	<input checked="" type="checkbox"/>
DTIC TAB	<input type="checkbox"/>
Unannounced	<input type="checkbox"/>
Justification	
By	
Distribution/	
Availability Codes	
Dist	Avail and/or Special
A	



#### ACKNOWLEDGMENTS

We wish to thank Thomas Sanford, Arthur Bartlett, and Patrick McKeown of Applied Physics Laboratory/University of Washington for extensive equipment preparation and checkout. Patrick McKeown participated in the cruise aboard the USNS KANE. The officers and men of the USNS KANE, E. Weckstrom commanding, performed admirably under adverse weather conditions. Zachariah Hallock served as party chief and provided valuable programming suggestions. Special thanks to A.W. Green for technical editing and constructive criticism of the manuscript. N.V. Lombard works for the Ocean Acoustics Division of NORDA.

## CONTENTS

LIST OF ILLUSTRATIONS AND TABLES	iv
1. Introduction	1
2. Data Collection and Processing	1
3. Hydrography	2
4. XCP and CTD Depth and Temperature Comparisons	3
5. Stratification	4
6. References	5
Appendix A: Expendable Shear Current/Temperature Probe (XCP) Profiles	19
Appendix B: Selected CTD Vertical Profiles and T-S Diagrams	67
Appendix C: Selected XCP and CTD Temperature Profiles	101
Appendix D: Selected Vertical Brunt-Väisälä ( $N^2$ ), Shear ( $S^2$ ), and Bulk Richardson Number (RI-NO) Profiles	117
Appendix E: Log $S^2$ vs Log $N^2$ (Bulk Richardson Numbers)	167

# ILLUSTRATIONS AND TABLES

Figure 1.	Schematic bathymetric relief of the Northeast Atlantic and the Subpolar Front. Cruise Track and primary type III stations.	8
Figure 2.	Vertical section along Line AB	9
Figure 3.	Temperature section along Line AB	10
Figure 4.	Temperature field at 100 m along Line AB	11
Figure 5.	Crossing the front (U component of current)	12
Figure 6.	Crossing the front (V component of current)	13
Figure 7.	Derivative of CTD (Cast 109076) temperature with depth	
Figure 8.	Derivative of CP temperature with depth - XCP 504	15
Figure 9.	Geomagnetic activity during October 1980, for Leirvogur, ICELAND, and Anchorage, Alaska	16
Table 1.	XCP Summary (Cruise 270980 - Phase II)	17
Table 2.	Data Summary	18

## DATA SUMMARY:

### XCP PROFILES IN THE VICINITY OF THE FAEROE ISLANDS DURING OCTOBER 1980

#### 1. INTRODUCTION

During 14 October - 3 November 1980, oceanographic operations were conducted aboard the USNS KANE (Cruise 270980, Phase II) in support of the Ocean Measurements Program (OMP) in the Iceland-Faeroe (Subpolar) oceanic front region.

Phase II objectives were:

- (a) To assess a complex oceanographic environment in the vicinity of an oceanic front, and
- (b) To describe the temporal and spatial distribution of fine-scale structure, vertical stability, and mixed layer depth in a dynamic oceanic region.

Hallock (1981) has reported in summary detail on operations during all three phases, and Teague (1981a, 1981b) has compiled two volumes of CTD profile data taken during the cruise.

In support of the above objectives, Expendable Current Probes (XCP) were deployed at four time series stations that were occupied for an inertial (13 hours) period and in four circulation regimes:

- (a) South of the Iceland-Faeroe Ridge
- (b) Within the Subpolar front
- (c) North of the front
- (d) On the Norway side of the eastern extension of the front

It was hoped that XCP data would provide insight into:

- (a) Variability of shear due to inertial modulation
- (b) Bulk Richardson numbers might be derived from XCP and CTD data
- (c) Estimates of shear and Richardson number variability might be determined.
- (d) Effects of intense geomagnetic activity on probe performance

#### 2. DATA COLLECTION AND PROCESSING

Vertical profiles of current velocity between about 25 m and 800 m were obtained with an XCP system (Sanford, 1980). The instrument is essentially an elongated XBT fitted with special electronics and sensors to detect the weak electric potential induced by the movement of sea water through the earth's magnetic field. The output is a velocity profile related to an unknown depth independent reference velocity. The probes also transmit a temperature profile that can be used to make depth comparisons with CTD casts (Table 1) when available. Performance trials indicated that the system has an rms uncertainty of about 1 cm/s (Sanford, 1980).

Conductivity, temperature and depth (CTD) measurements were taken with a Neil Brown Mark III CTD. Instrumentation details are described by Teague (1981a). RMS uncertainty in temperature and salinity are about 0.005°C and 0.005 g/kg, respectively.

Forty-six of seventy-three probes deployed transmitted usable data (Table 1). Four of these forty-six probes had defective temperature outputs, but the u and v current profiles appeared reasonable (Appendix A) in comparisons with others obtained in nearby profiles.

The Applied Physics Laboratory/University of Washington (APL/UAW) furnished a set of edited profiles with a vertical sample interval of about 2 to 3 meters. We interpolated these profiles, using a cubic spline, to 1 meter intervals, so they would be compatible with the 1 meter NAVOCEANO CTD data file.

### 3. HYDROGRAPHY

The hydrography in the vicinity of the Faeroe Islands is dominated by the Iceland/Faeroe Ridge and the Subpolar front (Fig. 1). Both features tend to separate the cold, less saline arctic and subarctic waters from the warm, saline Atlantic waters. The surface expression of the front is generally taken as the 35.0 g/kg isohaline, which represents the zone of maximum horizontal salinity gradients, while the vertical expression of the front is most easily visualized when displayed as the zone separating the several water types present. This technique has been discussed by Hermann (1967) and Hansen (1979).

The simplified representation shown in Figure 2 gives some idea of the areal extent of this front for a selected region. Its vertical scope is over several hundreds of meters, and its horizontal scale is over hundreds of kilometers. The shaded area around the solid line indicates that the front is rich in fine structure and many degrees of mixing intensities are possible. The solid line labeled 100 represents the approximate boundary below which the water masses contain no Atlantic type waters. The several water types used to determine this line were: Modified North Atlantic Water (MNA,  $T=8.5^{\circ}\text{C}$ ,  $S=35.24$  g/kg), Norwegian Sea Deep Water (NS,  $T=-0.5^{\circ}\text{C}$ ,  $S=34.92$  g/kg) and North Icelandic Winter Water/Arctic Intermediate Water (NI/AI,  $T=3.0^{\circ}\text{C}$ ,  $S=34.78$  g/kg). Traditionally, NI/AI water has a salinity of 34.88 g/kg, but on the basis of observations we have used 34.78 g/kg. Meincke (1978) used this same salinity value attributing its decrease to a 20 year trend in this area.

This front region is a complex oceanographic area resulting from the mixing and interacting of several water types with significantly different characteristics. Modified North Atlantic Water dominates the surface flow. North Icelandic Winter Water and Arctic Intermediate Water are found at intermediate depths. Norwegian Sea Deep Water, which is formed by the surface cooling of North Atlantic Water, sinks along the polar front northwest of the Faeroe Islands and spreads throughout the area as a southward intermediate and deep flow, with the Iceland-Faeroe Ridge and polar front acting as an effective barrier in preventing the colder waters from "overflowing" into the northeastern Atlantic (Hansen, 1979). Vertical oscillations of several hundreds of meters with horizontal length scales of 60 km or less appear to occur.

Mysak (1977) used hydrographic data to show the presence of isopycnal oscillations with horizontal length scales of 30-60 km. Analysis of current meter data indicated energy peaks at almost all depths of 2-3 days. He attributed these

oscillations to baroclinic instability in the Norwegian Current. Figure 3 indicates that vertical and horizontal oscillations occur throughout the water column in the frontal zone.

Oscillations with periods between 8 to 11 days and from 2 to 5 days have been reported by Meincke and Kvinge (1978) from one year observations of current meter records between Iceland and Scotland at two locations.

Hansen (1979) presented evidence for the existence of eddies and meanders with horizontal scales on the order of 30 to 50 km and vertical scales on the order of 100 to 200 m, extending down to about 500 m. Figure 4 indicates the presence of a cyclonic eddy or meander at the 100 m level across the front. The barbed arrows in Figure 4 show the relative current along the 100 m depth. Shear probes 546, 547, and 548 show significantly different patterns in both speed and direction. Shear probe 548 shows a northeast current at about 45 cm/sec, probe 547 a northwest current at 20 cm/sec, and probe 546 a southeast shear at about 10 cm/sec. Figures 5 and 6 show the vertical u and v current variation for the three probes. Most of the variation appears in the u component, not only in amplitude but in phase as well, particularly when comparing probes 546 and 547 between 100 m and 300 m where a 180° phase shift is indicated. Both u and v components of probe 546 appear to indicate a significant change in speed at about 200 m and 400 m. That change could indicate where probe 546 entered and left the strongest part of the front (Fig. 2).

From visual inspection of Figures 2, 5, and 6 the following observations are made:

<u>Shear Probe</u>	<u>Component</u>	<u>Comments</u>
546	u,v	150-250 m probe crosses through front
547	u	150-250 m probe crosses through front
548	u,v	400-450 m probe crosses through front

The resulting complex water mass distribution appears to be a shallow phenomenon, with the deeper water below about 600 m being more uniform, occurring throughout the year. Countryman (1969) reported on similar conditions during July and August 1963, as did Meincke (1978) during June 1977 and Hansen (1979) during September 1973.

#### 4. XCP AND CTD DEPTH AND TEMPERATURE COMPARISONS

Due to adverse weather throughout much of the cruise, synoptic drops of XCP and CTD were prohibited. Time differences of one-half hour and greater between XCP and CTD deployment were common (Table 1).

XCP depths are determined from a quadratic empirical equation that incorporates a nominal fall rate of about 4.5 m/sec. Varying deployment conditions may cause significant deviations between true depth and the values calculated by the formula, so some corrections of probe depth errors should be attempted.

An accepted method of checking shear probe depth data is to make a comparison between temperature-depth profiles derived from CTD (Appendix B) records and the temperature profiles from the XCP cast. Green and Saunders (1981) showed a

statistical method for making probe depth corrections. Their method is most applicable to cases in which CTD and XCP profiles are nearly simultaneous. Since this condition was rare during these operations a more direct simplified check was used. The few cases where direct CTD/XCP intercomparisons were made showed that depth and temperature corrections were small.

In most cases there was a thoroughly mixed surface layer overlying a sharp thermocline. The surface layer temperature was used as the reference for XCP temperature offset correction, and the depth of the mixed layer furnished a distinct reference depth for probe profiles. The near surface thermocline or depth of mixed layer was determined by the depth at which the thermal gradient exceeded  $5.6 \times 10^{-3} \text{ }^{\circ}\text{C/m}$  (James, 1966).

Figures 7 and 8 are an example of the vertical temperature derivative ( $^{\circ}\text{C/m}$ ) for shear probe 504. The dashed vertical lines are at plus and minus  $5.6 \times 10^{-3} \text{ }^{\circ}\text{C/m}$ , the temperature gradient boundaries used in defining the bottom of the mixed layer. Depth of the bottom of the mixed layer is indicated in both figures, but more clearly in Figure 7. Note that the two depths do not agree because the depth determined from the shear probed data was somewhat shallower due to the assumed fall rate of the probe. Note, also, however, that using this method can result in defining several deeper layer depths. These secondary layer depths can usually be distinguished from the near-surface layer depth. Since this method of determining layer depths is subjective, visual inspection of the smoothed profiles is mandatory and some "eyeballing" is unavoidable.

Smoothed temperature profiles of XCP and CTD casts are located in Appendix C. Aside from several instances of obvious horizontal temperature offsets the smoothed profiles track each other fairly consistently. Some of the profile differences are due to finestructure detail caused by temporal and spatial variations in the water column, while other variations occur as a result of the nonlinearity characteristics of the XCP temperature probe.

There appears to be generally good agreement between CTDs and XCPs on the depth of the mixed layer. Four of the drops indicated no depth difference, four indicated a deeper depth as determined by the shear probe, and six indicated a deeper depth as determined by the CTD. Maximum difference in depth was -34 meters (drop 525) where the shear probe recorded a deeper depth to the bottom of the mixed layer. These errors can be attributed to uncertainties in launch time start and probe dynamic at profile initiation (Green and Saunders, 1981), as well as rich finestructure variability in the data.

## 5. STRATIFICATION

The Richardson number ( $Ri$ ) is an indicator of dynamical stability of a stratified shear flow:

$$Ri = \frac{N^2}{S^2}$$

where  $N$  = Brunt-Väisälä frequency and

$S$  = current shear

In general, for  $Ri > 0.25$ , disturbances of the flow (such as internal gravity waves) do not grow due to the stabilizing effect of the static stability. When  $Ri < 0.25$ , flow disturbances grow rapidly and lead to turbulence or overturning of the stratification.

Calculating Richardson numbers over a fixed vertical interval (bulk Richardson number) may not be representative of the flow at some particular depth, since the largest values of vertical density and velocity gradients occur in thin layers of various thickness that will most likely be randomly located with respect to any feature (Federov, 1978). Averaging vertical gradients over large depth intervals may lead to an overestimate of the Richardson number since the density gradient may increase more rapidly than the vertical velocity gradient.

Smoothed one meter vertical profiles of Brunt-Väisälä frequency ( $N^2$ ), shear ( $S^2$ ), and bulk Richardson number ( $Ri$ ) are presented in Appendix D, while scatter plots of bulk Richardson numbers are presented in Appendix E. The  $Ri$  profiles in Appendix D were made from values of  $N^2$  and  $S^2$  that had an estimated signal-to-noise ratio of at least one. These values fall in quadrant 1 of the log-log plots in Appendix E.

The depth of bulk maximum Richardson number (smoothed 1 m interval) varied from about 85 m to about 505 m (Table 2). Bulk Richardson number profiles indicated a wide range of variability. In homogeneous, well-mixed zones  $Ri$  approached or was equal to zero, particularly in the deeper Norwegian Sea water below about 500 m. Separating zones of low  $Ri$  values are interface layers with larger  $Ri$  values (up to about 47, XCP 534 at 72 m) just below the bottom of the mixed layer. Evans (1981) found similar inter-fingering of high (up to 100) and low (0)  $Ri$  numbers in tropical Atlantic waters that showed evidence of salt fingering or thermohaline staircase structure. Evans claims that these high values (higher than typical thermocline values of 1 to 3) indicate stable flow across the interfaces and that the salt-finger fields will be undisturbed. In these cases the microscale variability in temperature and salinity will be intense.

Estimated values of  $Ri$  when passing through the strongest part of the subpolar front were:  $Ri = 5$  at 425 m for XCP 548;  $Ri = 16$  at 374 m for XCP 547;  $Ri = 19$  at 176 m for XCP 546. In the vicinity of the front, shear varied in both magnitude and direction (Figures 4, 5, 6).

There did not appear to be any obvious overall relationship between the depths of maximum  $N^2$  and  $S^2$  except that at several stations (504, 534, 547) a maximum in both  $N^2$  and  $S^2$  occurred just below the bottom of a well-defined mixed layer. The maximum was usually indicated by a distinct sharp signature in  $N^2$  rather than in  $S^2$ . This is consistent with the observation that the diffusion of momentum by the shear is greater than the diffusion of the density due to the vertical constraint of gravity.

Successful probe operation is dependent upon the magnitude and stability of the earth's geomagnetic field. During periods of intense magnetic activity or magnetotelluric disturbances, data contamination may occur. This is particularly true at higher geomagnetic latitudes where the earth's magnetic field is more active. Figure 9 is a plot of the daily indices of geomagnetic activity ( $A_k$ ) for Anchorage, Alaska, and Leirvogur, Iceland. Although several major geomagnetic storms did occur at operational latitudes during the period 11 and 23 October, with diminished amplitude at Leirvogur compared to Anchorage, no discernible effect was noted on probe performance.

## 6. REFERENCES

Countryman, Kenneth A. (1969). Some Summer Oceanographic Features of the Norwegian Sea, Summer 1963. TR-216, Naval Oceanographic Office, NSTL Station, Miss.

- Evans, David L. (1981). Velocity Shear in a Thermohaline Staircase. *Deep Sea Res.* (28A), 1409-1415.
- Evans, K.N. (1979). YVETTE - A Free Fall Shear Profiler. *Deep Sea Res.* 26(6A), 703-718.
- Federov, K.N. (1978). The Thermohaline Finestructure of the Ocean. Institute of Oceanology of the Academy of Sciences, Moscow, USSR, 170 p.
- Green, A.W. and K.D. Saunders. (1981). Theoretical and Empirical Fall Rates of XCP's and XBT's. *Oceans*, September 1981, p. 382-386.
- Hallock, Zachariah R. (1980). The Fast and Easy Binary (FEB) File. TN7210-12-80, Naval Oceanographic Office, NSTL Station, Miss.
- Hallock, Zachariah R., et al. (1981). Report of Operations USNS KANE Northeast Atlantic and Norwegian Sea Survey Operation 270980, Phases I, II, III, 16 September-28 November 1980 Ocean Measurements Program. OCS 270980, Naval Oceanographic Office, NSTL Station, Miss.
- Hansen, B. and J. Meincke. (1979). Eddies and Meanders in the Iceland-Faeroe Ridge Area. *Deep Sea Res.*(26A), 1067-1082.
- Hermann, F. (1967). The TS-Diagram Analysis of the Water Masses Over the Iceland-Faeroe Ridge and in the Faeroe-Bank Channel. *Rapp. P. - v. Recm. Cons. perm. int. Explor. Mer* 157, 139-149.
- James, Richard W. (1966). ASWEPS Manual Volume 5, Ocean Thermal Structure Forecasting. SP-105, Naval Oceanographic Office, NSTL Station, Miss.
- Meincke, J. (1978). On the Distribution of Low Salinity Intermediate Waters Around the Faeroes. *Deutsche Hydrog. Zeit.* 31, 50-64.
- Meincke, J. and T. Kvinge. (1978). On the Atmospheric Forcing of Overflow Events. International Council for the Exploration of the Sea, C.M. 1978/C;9.
- Muller, T.J., et al. (1979). Overflow '73: The Distribution of Water Masses on the Greenland-Scotland Ridge in August/September 1973 - A Data Report. *Berichte aus dem Institut fur Meereskunde an der Christian-Albrechts-Universitat Kiel*, Nr 62.
- Mysak, Lawrence A. and Friedrich Schott. (1977). Evidence for Baroclinic Instability of the Norwegian Current. *J. Geophys. Res.* 82(15), 2087-2095.
- Newman, Fred C., et al. (1981). Some Methods of Calculating Richardson Number from Observed Data. SAI 82-414-WA, Science Applications, Inc., McLean, Va.
- Sanford, Thomas B. (1980). Shear Probe Data. In: *Oceanic Environmental Background Observations in the Sargasso Sea During September 1979*, Compiled and edited by Henry Perkins. Section 7.0, pp. 189-230. NORDA Technical Note 58. Naval Ocean Research and Development Activity, NSTL Station, Miss.
- Teague, William J. (1981a). Data Summary CTD Profiles in the Northeast Atlantic and Norwegian Sea September-November 1980, Volume 1 of 2. Naval Oceanographic Office, NSTL Station, Miss.

Teague, William J. (1981b). Data Summary CTD Profiles in the Northeast Atlantic and Norwegian Sea September-November 1980, Volume 2 of 2. Naval Oceanographic Office, NSTL Station, Miss.

Willebrand, Jurgen and Jens Meincke. (1980). Statistical Analysis of Fluctuations in the Iceland-Scotland Frontal Zone. Deep Sea Res. 27A, 1047-1066.

Worthington, L.V. (1970). The Norwegian Sea as a Mediterranean Basin. Deep Sea Res. 17, 77-84.

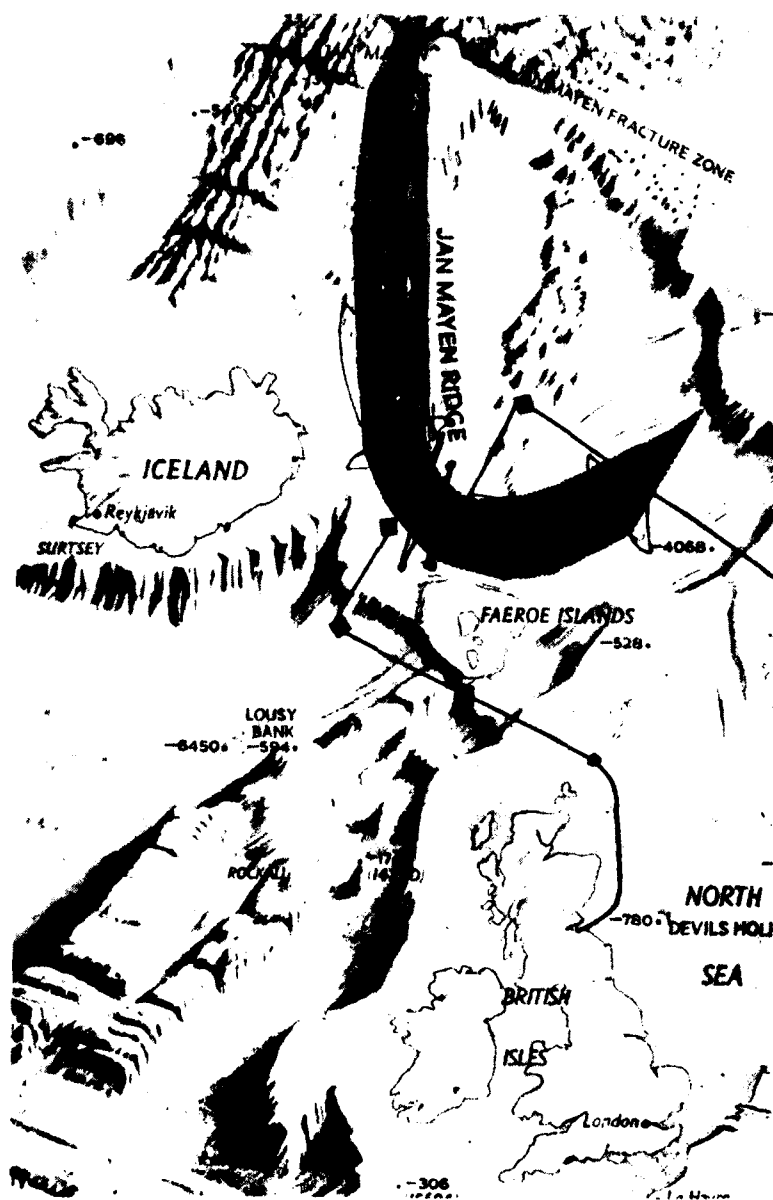


Figure 1. Schematic bathymetric relief of the Northeast Atlantic and the Subpolar Front. Cruise Track and primary (◆) type III stations.

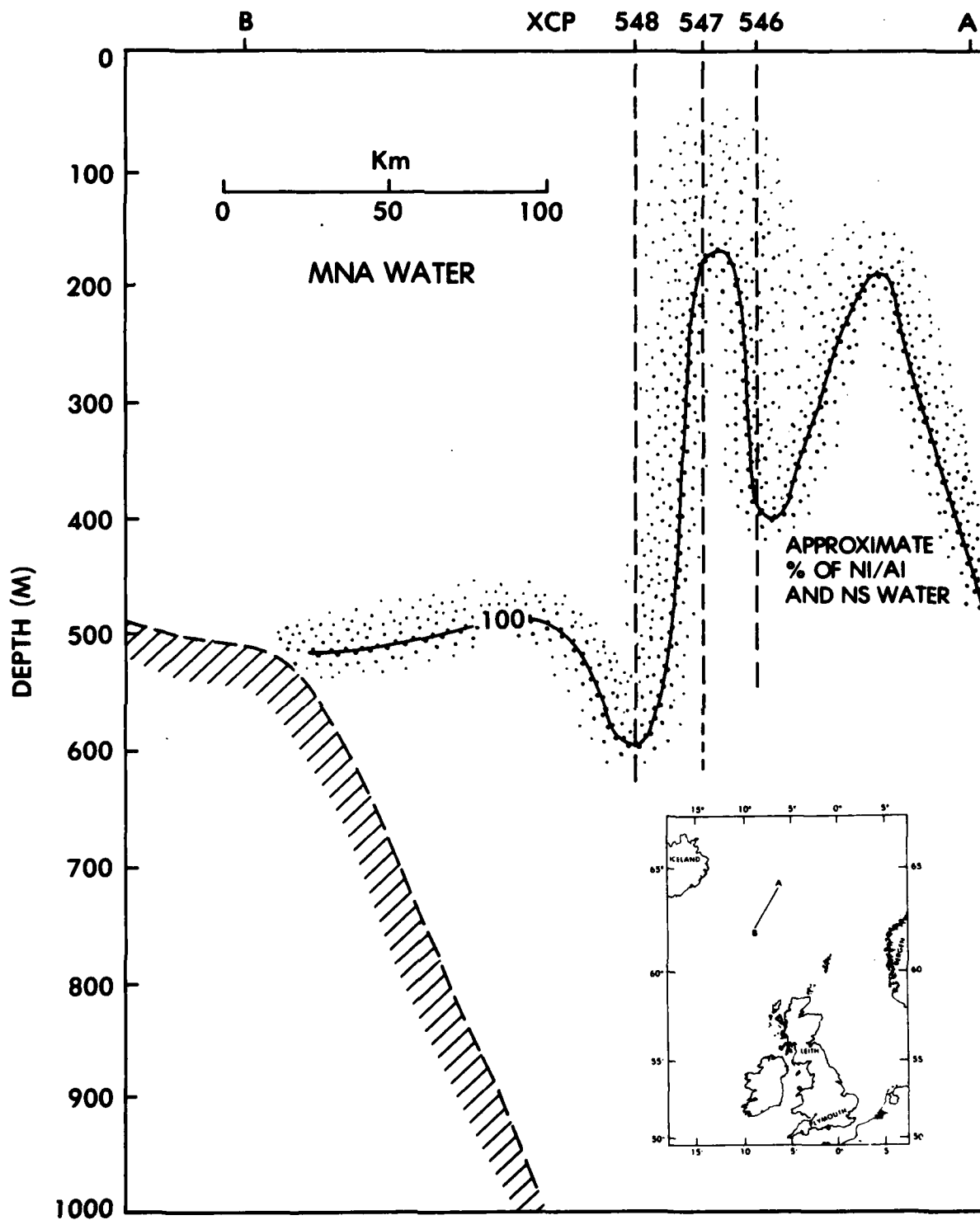


Figure 2. Vertical section along Line AB

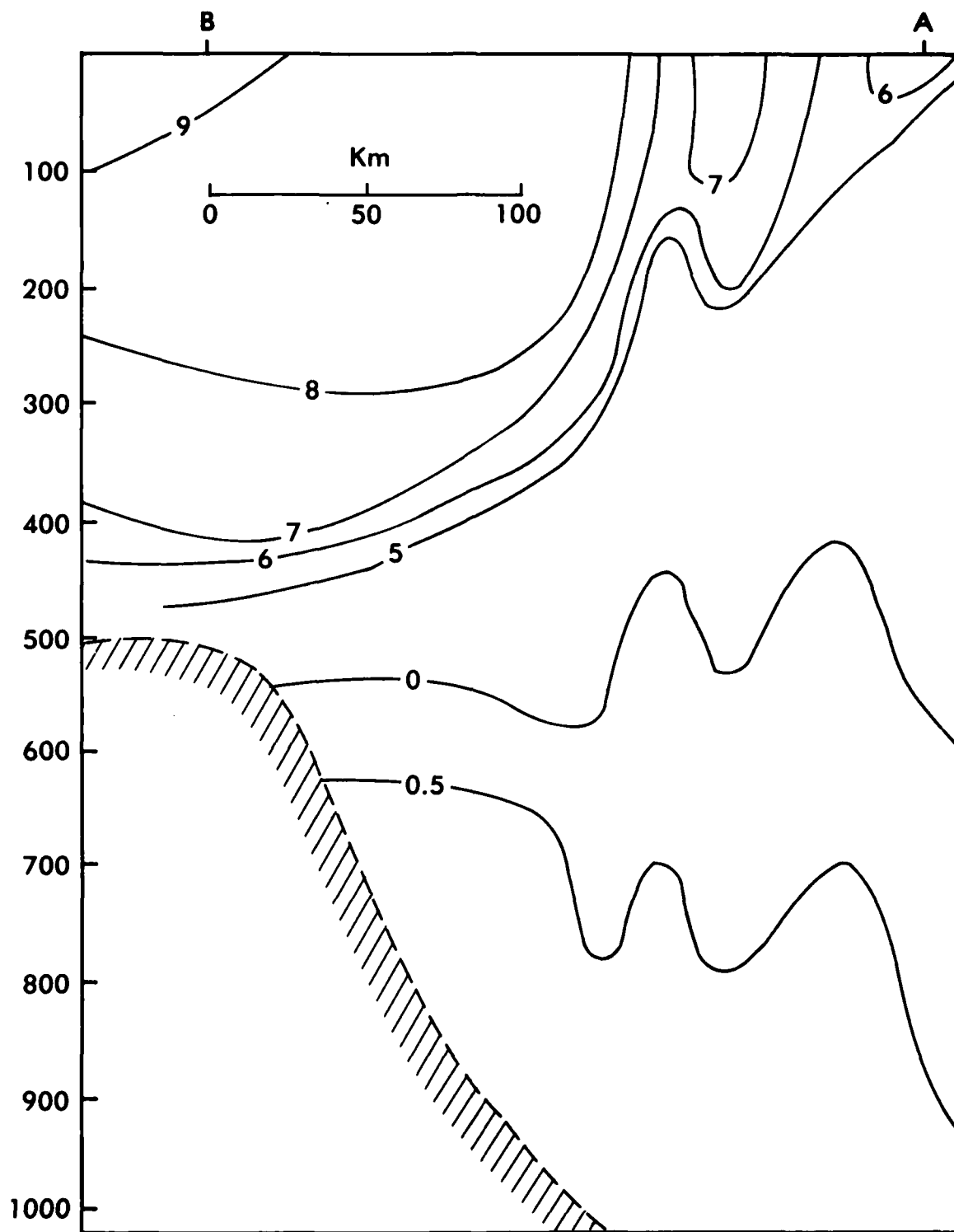


Figure 3. Temperature section along Line AB

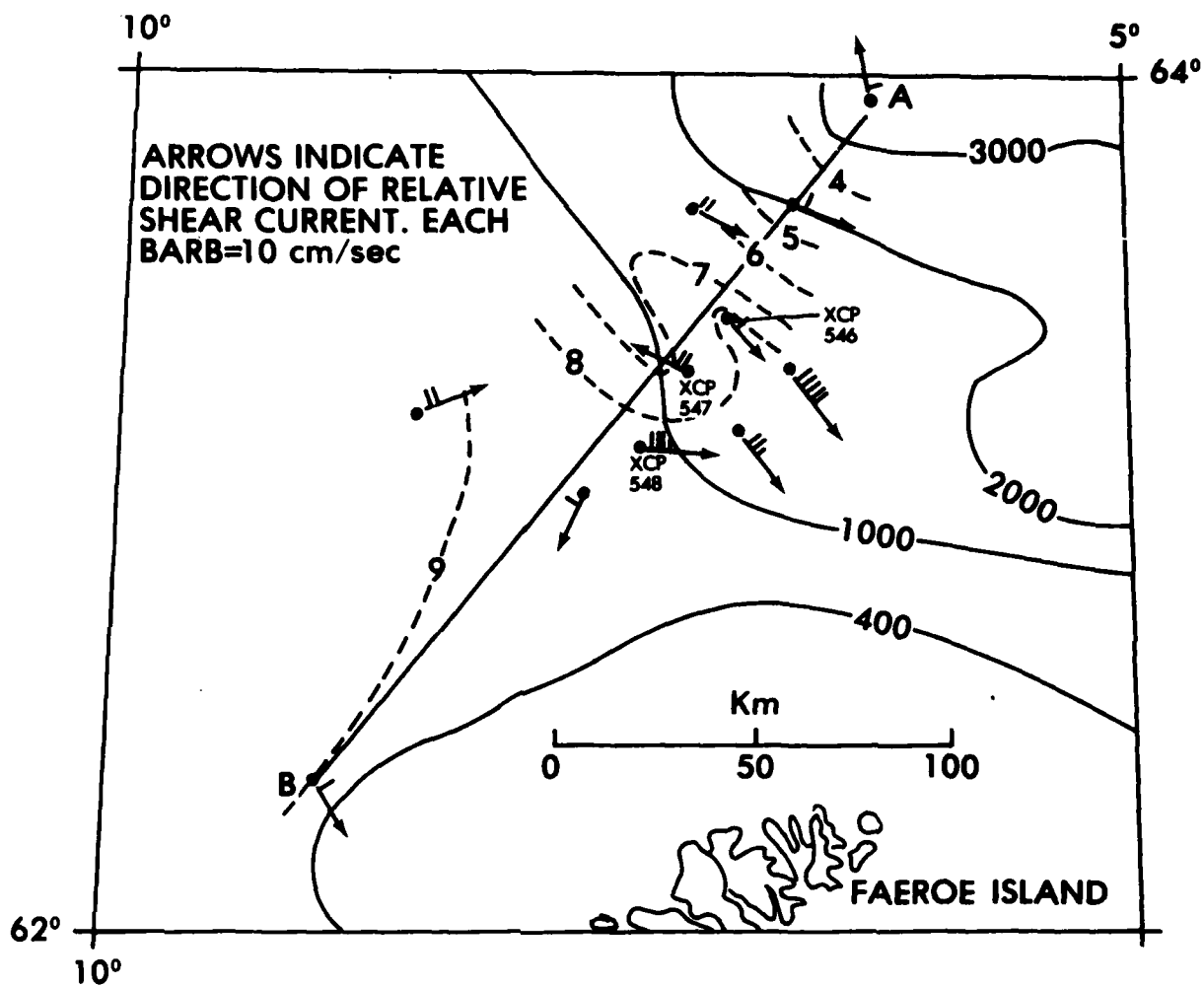


Figure 4. Temperature field at 100 m along Line AB

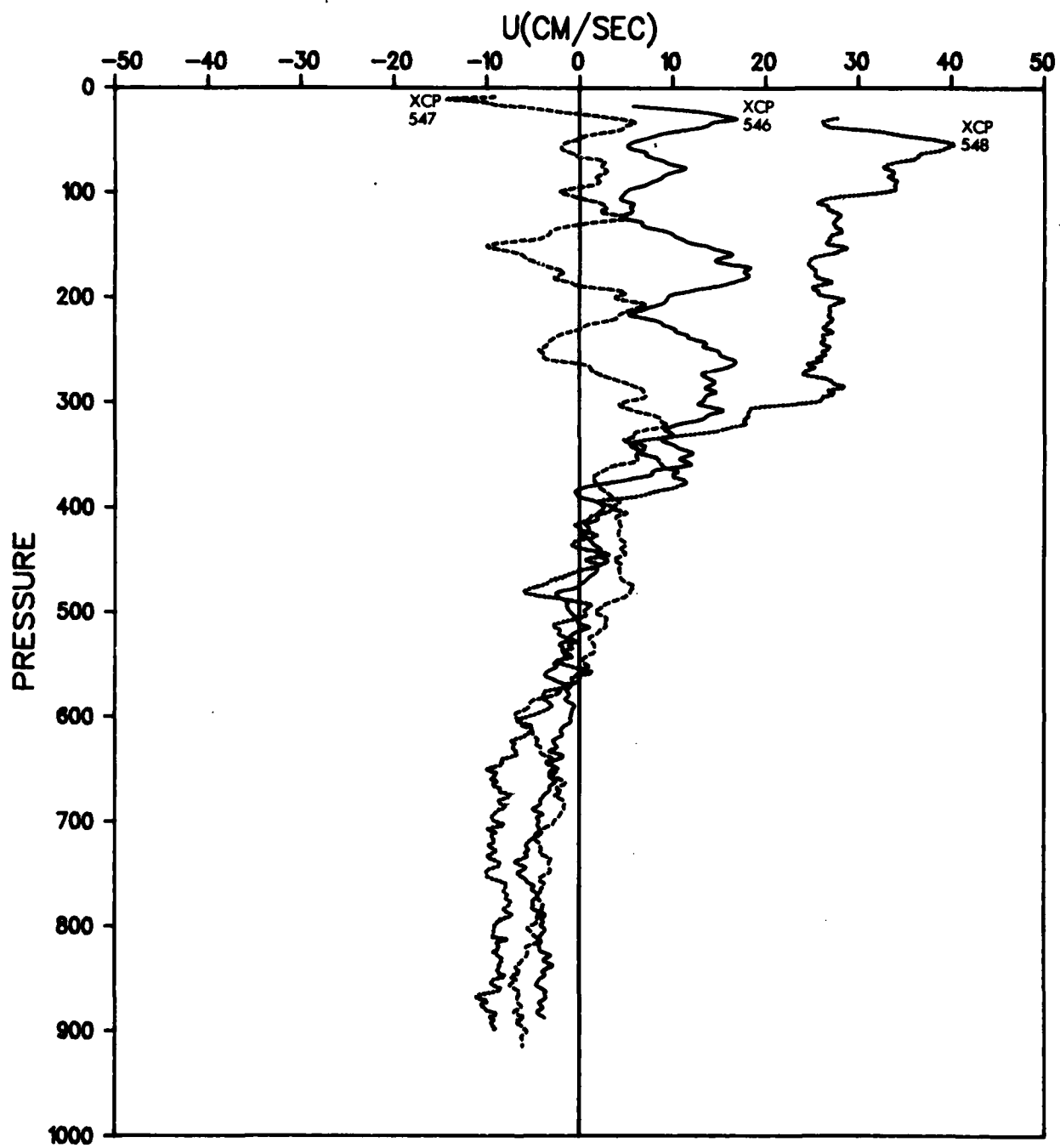


Figure 5. Crossing the front (U component of current)

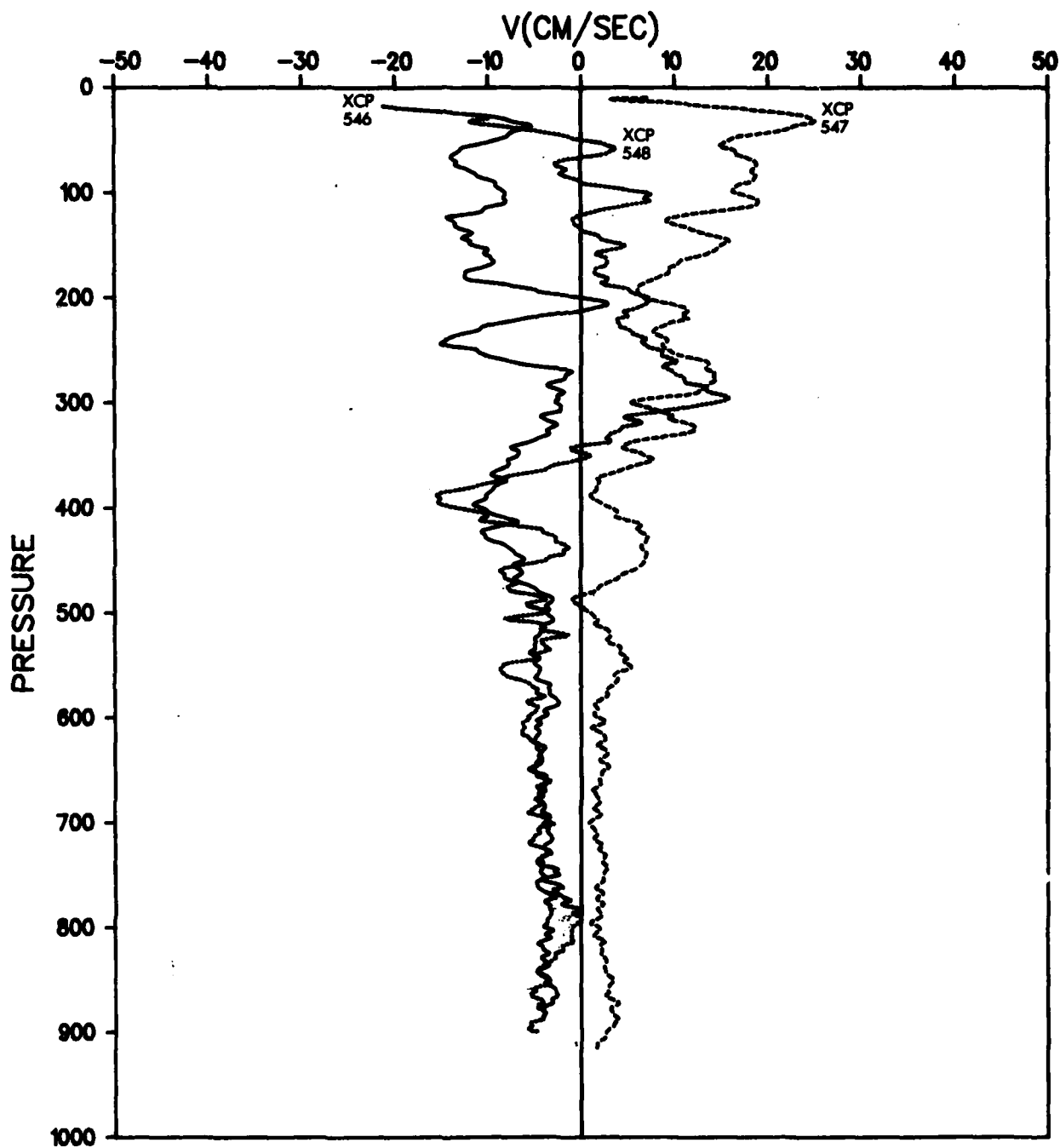


Figure 6. Crossing the front (V component of current)

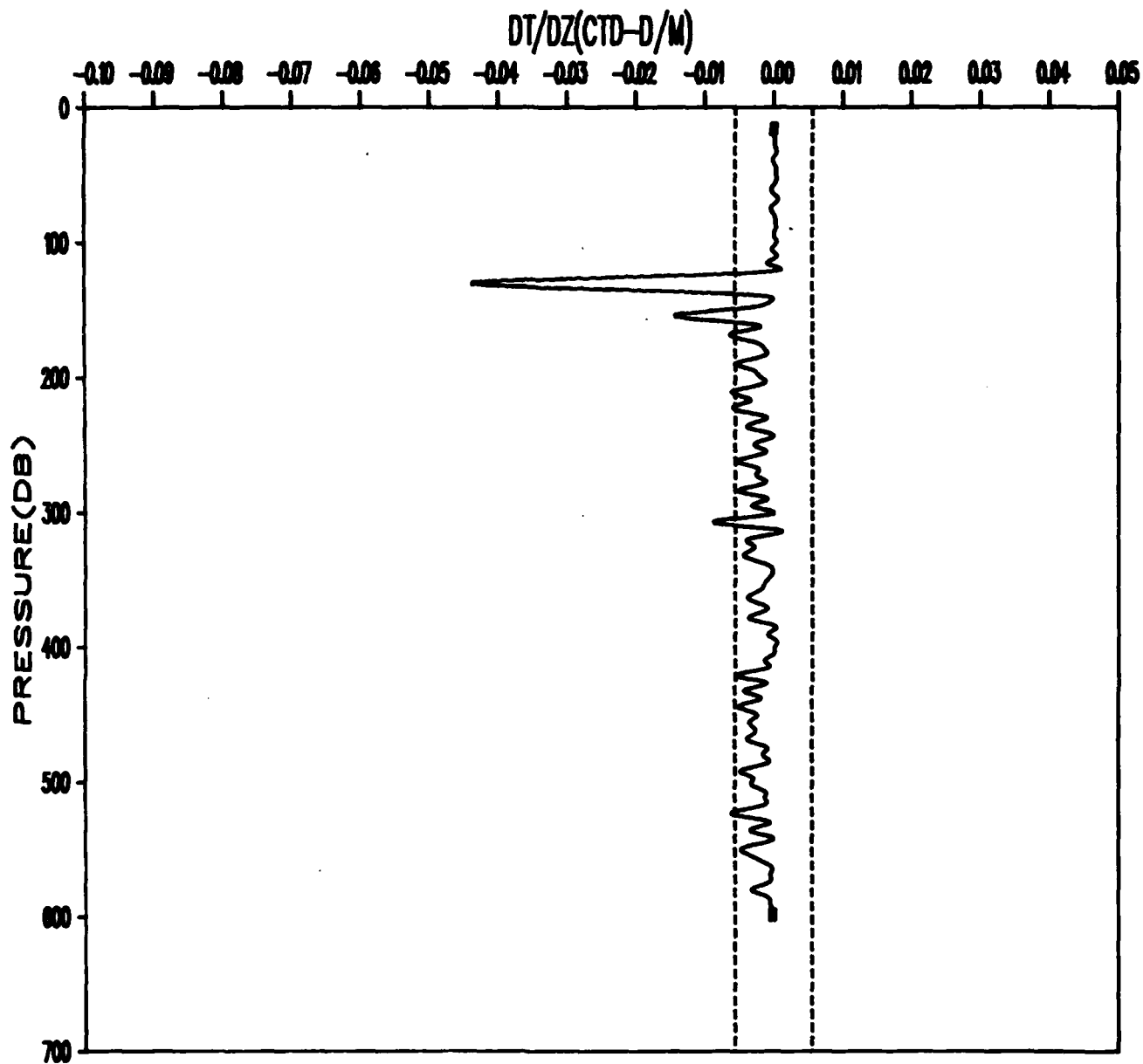


Figure 7. Derivative of CTD (Cast 109076) temperature with depth

FILE KANE  
SEGMENT C 504

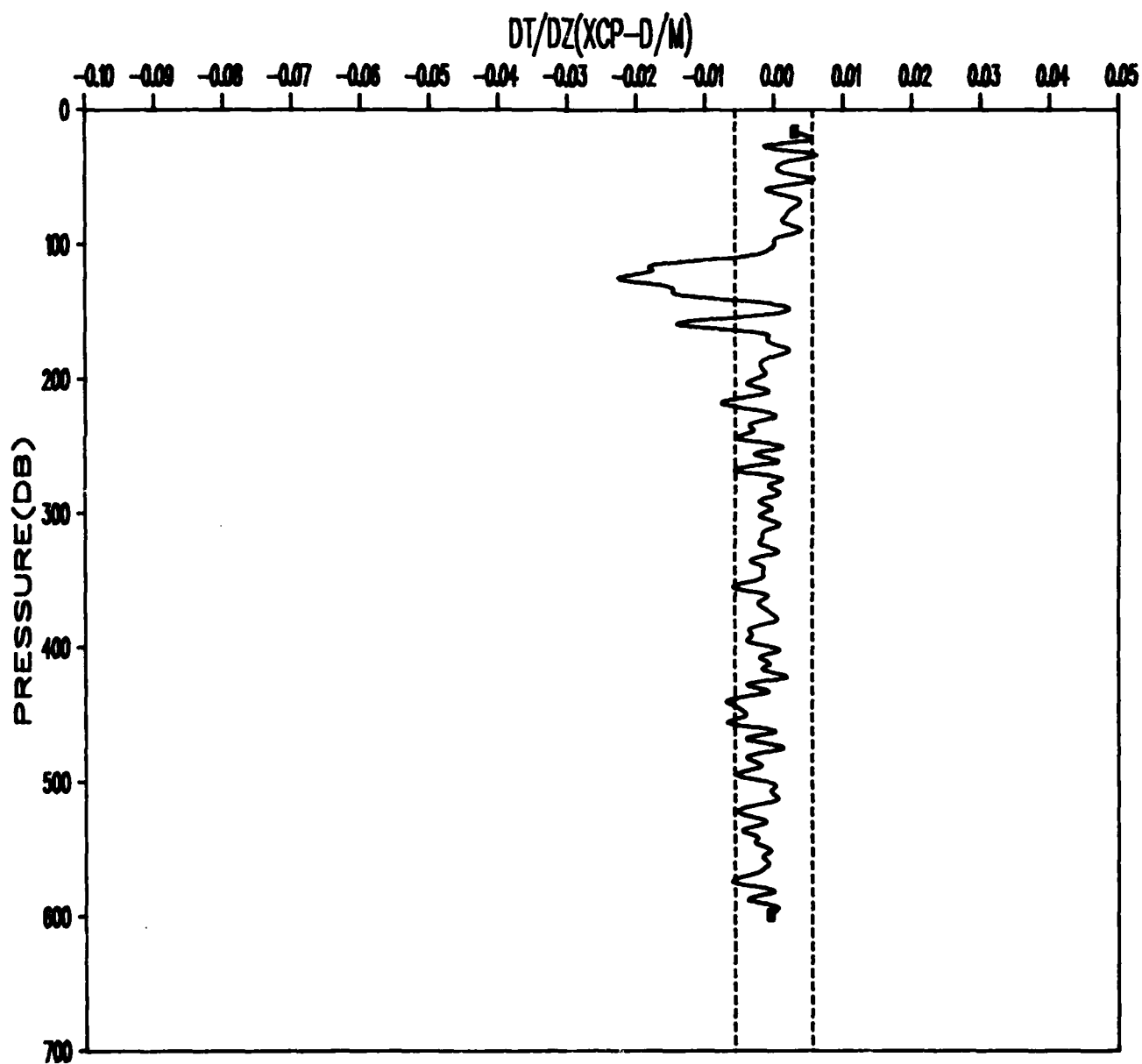
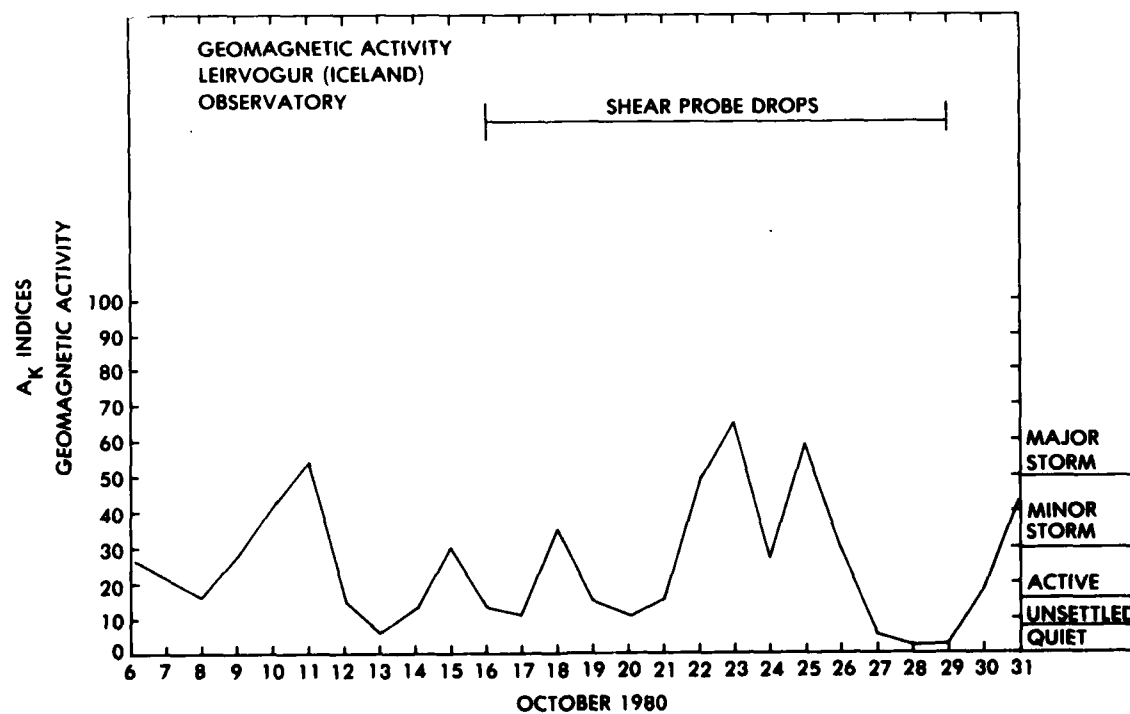
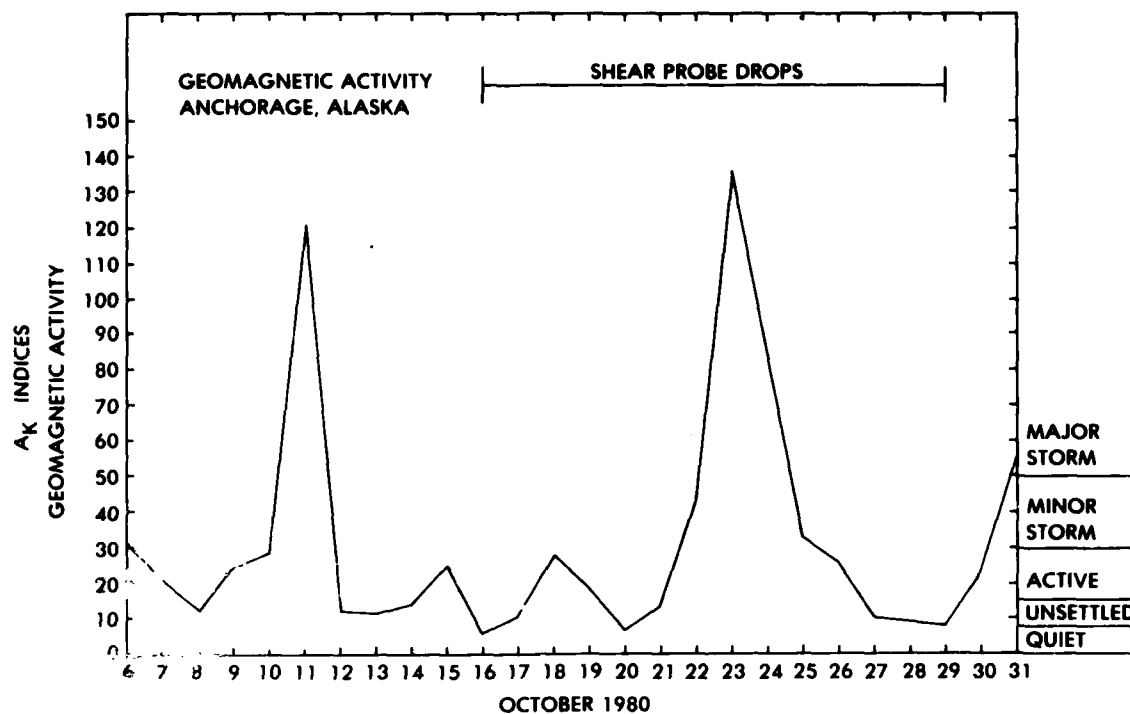


Figure 8. Derivative of XCP temperature with depth - XCP 504



**Figure 9. Geomagnetic activity during October 1980, for Leirvogur, ICELAND, and Anchorage, Alaska**

Table 1. XCP Summary (Cruise 270980 - Phase II)

XCP DROP	LATITUDE	LONGITUDE	JULIAN DAY/TIME (Z)	NEAREST CTD CAST	LATITUDE	LONGITUDE	JULIAN DAY/ START TIME (Z)	JULIAN DAY/ END TIME (Z)	COMMENTS
502	60°22.8'N	07°02.8'W	290/0837	105073	60°38.8'N	07°21.4'W	290/1659	290/1714	Time Series No. 1
503	60°40.0'N	07°18.3'W	/1813	109076	61°39.1'N	10°13.9'W	291/1156	291/1211	
504	61°37.7'N	10°12.9'W	291/1256	109078	61°37.7'N	10°12.6'W	/1640	/1925	
506	61°38.4'N	10°14.3'W	/1548	109079	61°37.1'N	10°13.0'W	/2004	/2325	
507	61°37.1'N	10°12.9'W	/2004	109080	61°37.1'N	10°13.0'W	/2035	/2325	Time Series No. 2
508	61°37.1'N	10°12.9'W	/2015	109081	61°37.5'N	10°13.5'W	292/0040	292/0336	
510	61°38.1'N	10°13.4'W	292/0010	109082	61°36.8'N	10°13.2'W	/0505	/0818	
512	61°37.1'N	10°12.8'W	/0436	109083	61°37.9'N	10°12.9'W	/0920	/1203	
513	61°37.9'N	10°13.5'W	/0856	109085	61°38.6'N	10°12.4'W	/1349	/1636	Time Series No. 3
514	61°38.0'N	10°12.6'W	/1308	110084	61°36.6'N	10°12.4'W	/1349	/1636	
515	61°37.6'N	10°13.2'W	/1730	110085	61°36.6'N	10°12.4'W	/1349	/1636	
517	61°58.7'N	09°37.5'W	/2056	110086	62°23.2'N	09°05.0'W	293/0142	293/0154	
519	62°22.8'N	09°04.8'W	293/0121	110087	62°48.1'N	08°51.7'W	/0530	/0540	Time Series No. 4
520	62°45.2'N	08°32.6'W	/0454	110088	63°41.7'N	07°12.8'W	/2212	/2237	
525	63°42.2'N	07°12.7'W	/2342	117091	63°42.7'N	07°09.0'W	294/0415	294/0702	
527	63°42.3'N	07°09.6'W	294/0739	117093	63°42.7'N	07°09.6'W	/0825	/1120	
528	63°43.2'N	07°06.5'W	/0750	117094	63°43.7'N	07°09.0'W	/1254	/1525	Time Series No. 5
530	63°43.5'N	07°09.0'W	/1236	117095	63°42.9'N	07°09.1'W	/2029	/2321	
533	63°42.9'N	07°09.9'W	/2002	117097	63°43.5'N	06°40.5'W	295/1320	295/1354	
534	64°08.0'N	06°04.9'W	295/1302	122103	64°08.0'N	06°04.0'W	/1545	/1545	
535	63°59.9'N	06°15.5'W	/1509	123104	63°59.5'N	06°15.4'W	/2006	/2025	Time Series No. 6
538	63°44.7'N	06°42.7'W	/2106	126106	63°43.5'N	06°40.5'W	/2240	/2309	
539	63°35.8'N	06°53.1'W	296/0032	128107	63°36.2'N	06°51.6'W	/0331	/0351	
542	63°34.4'N	06°55.1'W	/0129	130108	63°27.7'N	07°04.0'W	296/0331	296/0351	
543	63°32.6'N	06°58.4'W	/0156	130108	63°27.7'N	07°04.0'W	/0331	/0351	Time Series No. 7
544	63°50.8'N	06°59.7'W	/0223	130108	63°27.7'N	07°04.0'W	/0331	/0351	
546	63°28.0'N	07°02.5'W	/0312	130108	63°27.7'N	07°04.0'W	/0331	/0351	
547	63°20.5'N	07°15.8'W	/0548	131109	63°20.4'N	07°16.0'W	/0609	/0631	
548	63°12.0'N	07°26.6'W	/0842	132110	63°12.3'N	07°25.9'W	/0901	/0924	Time Series No. 8
549	63°03.7'N	07°40.1'W	/1602	133111	63°04.3'N	07°39.5'W	/1643	/1703	
550	63°13.4'N	06°55.6'W	297/0350	136116	63°13.7'N	06°54.9'W	297/0412	297/0431	
551	63°21.2'N	06°44.8'W	/0620	137117	63°20.7'N	06°41.9'W	/0719	/0742	
556	66°00.1'N	02°00.3'W	301/0025	171148	66°59.8'N	02°00.2'W	301/0046	301/0333	Time Series No. 9
558	65°57.6'N	02°01.0'W	/0419	171148	66°59.8'N	02°00.2'W	/0046	/0333	
559	65°59.9'N	02°01.1'W	/0455	171149	66°03.1'N	02°01.4'W	/0516	/0803	
560	66°00.1'N	02°00.3'W	/0854	171150	66°00.0'N	01°59.5'W	/0856	/1148	
561	66°00.1'N	02°00.0'W	301/1235	171150	66°00.0'N	01°59.5'W	/0856	/1148	Time Series No. 10
562	66°00.5'N	02°00.7'W	/1633	171151	66°00.0'N	02°00.8'W	/1307	/1601	
563	65°00.2'N	00°59.2'E	302/2325	175155	65°00.4'N	01°01.4'E	302/2116	302/2208	
564	65°00.1'N	00°58.9'E	303/0339	171157	65°00.3'N	00°57.7'E	303/0414	303/0708	
566	64°59.7'N	01°00.3'E	/0734	171158	64°59.7'N	00°59.6'E	/0811	/1056	Time Series No. 11
567	65°00.0'N	00°59.4'E	/1131	171159	64°59.7'N	00°59.6'E	/1153	/1445	
568	64°59.8'N	01°00.0'E	/1532	175160	64°59.7'N	01°00.2'E	/1549	/1837	
569	65°00.3'N	00°59.2'E	/1912	175161	65°00.4'N	00°59.4'E	/1939	/2227	
571	65°00.5'N	00°56.5'E	/2320	175161	65°00.4'N	00°59.4'E	/1939	/2227	Time Series No. 12
573	65°00.0'N	00°59.6'E	/2552	175161	65°00.4'N	00°59.4'E	/1939	/2227	

### Table 2. Data Summary

Probe Drop	Data Range (m)	Bottom of Mixed Layer (m)	Depth (m) Max S <sub>2</sub>	Depth (m) Max N <sub>2</sub>	MEDIAN VALUE OF		MEAN VALUE OF	
					$\frac{S^2}{\times 10^{-4} \times \text{Sec}^{-2}}$	$\frac{N^2}{\times 10^{-4} \times \text{Sec}^{-2}}$	$\frac{S^2}{\times 10^{-4} \times \text{Sec}^{-2}}$	$\frac{N^2}{\times 10^{-4} \times \text{Sec}^{-2}}$
503	25-504	120	224	452	.267	.106	.394	.148
504	16-599	105	115	130	.102	.021	.157	.040
517	25-660	160	576	612	.143	.057	.385	.115
519	20-509	80	461	464	.114	.052	.414	.114
520	20-460	120	123	340	.245	.110	.615	.132
525	15-892	90	573	121	.173	.026	.330	.074
534	23-891	60	66	73	.151	.029	.222	.087
535	27-902	50	105	56	.086	.031	.240	.082
538	20-883	100	650	109	.313	.017	.626	.073
546	18-888	100	198	234	.091	.027	.194	.086
547	19-915	100	118	104	.069	.021	.177	.087
548	30-900	90	304	424	.163	.042	.272	.096
549	20-792	180	351	407	.122	.044	.277	.106
550	26-892	90	218	309	.087	.040	.222	.094
551	25-918	110	275	321	.095	.029	.241	.097
563	20-908	80	79	76	.084	.059	.144	.090

**Appendix A:**  
**Expendable Shear Current/Temperature**  
**Probe (XCP) Profiles**

**COMMENTS:**

**1 m Smoothed and Interpolated Profiles**  
**No Temperature Profile for:**

XCP 507	Fig. A-5
XCP 535	Fig. A-21
XCP 549	Fig. A-30
XCP 571	Fig. A-45

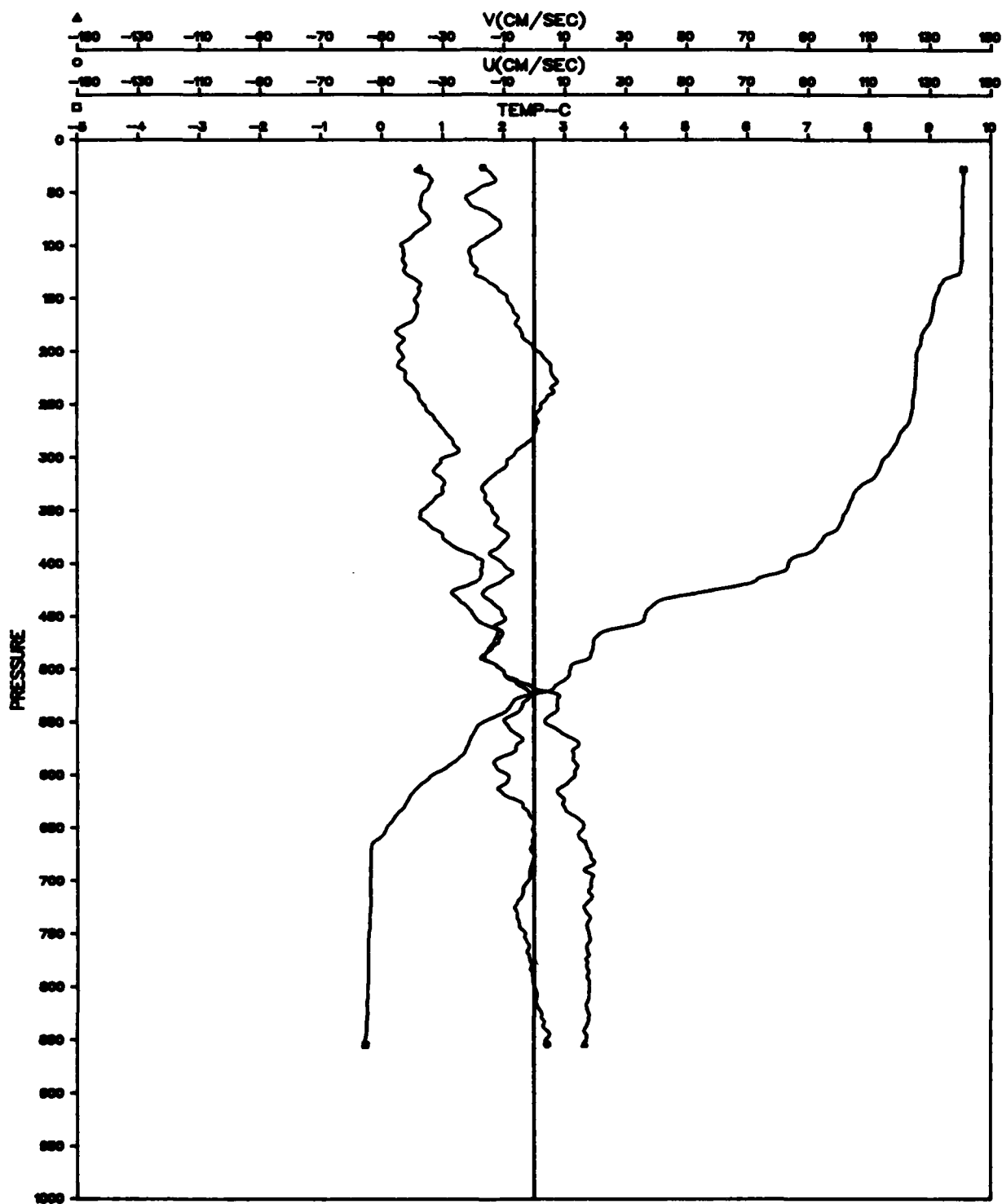


Figure A-1. File: KANE, Segment: C 502

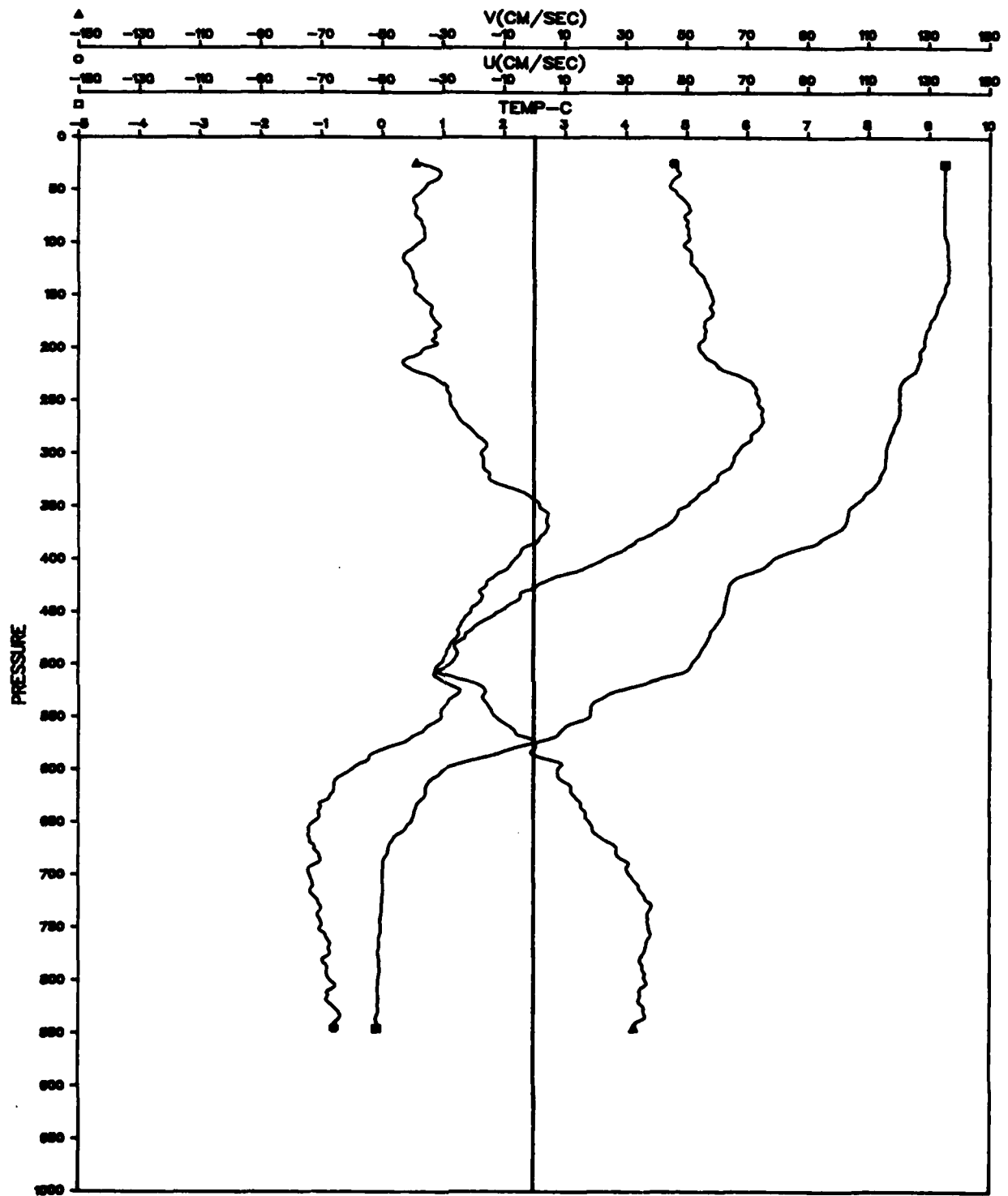


Figure A-2. File: KANE, Segment: C 503

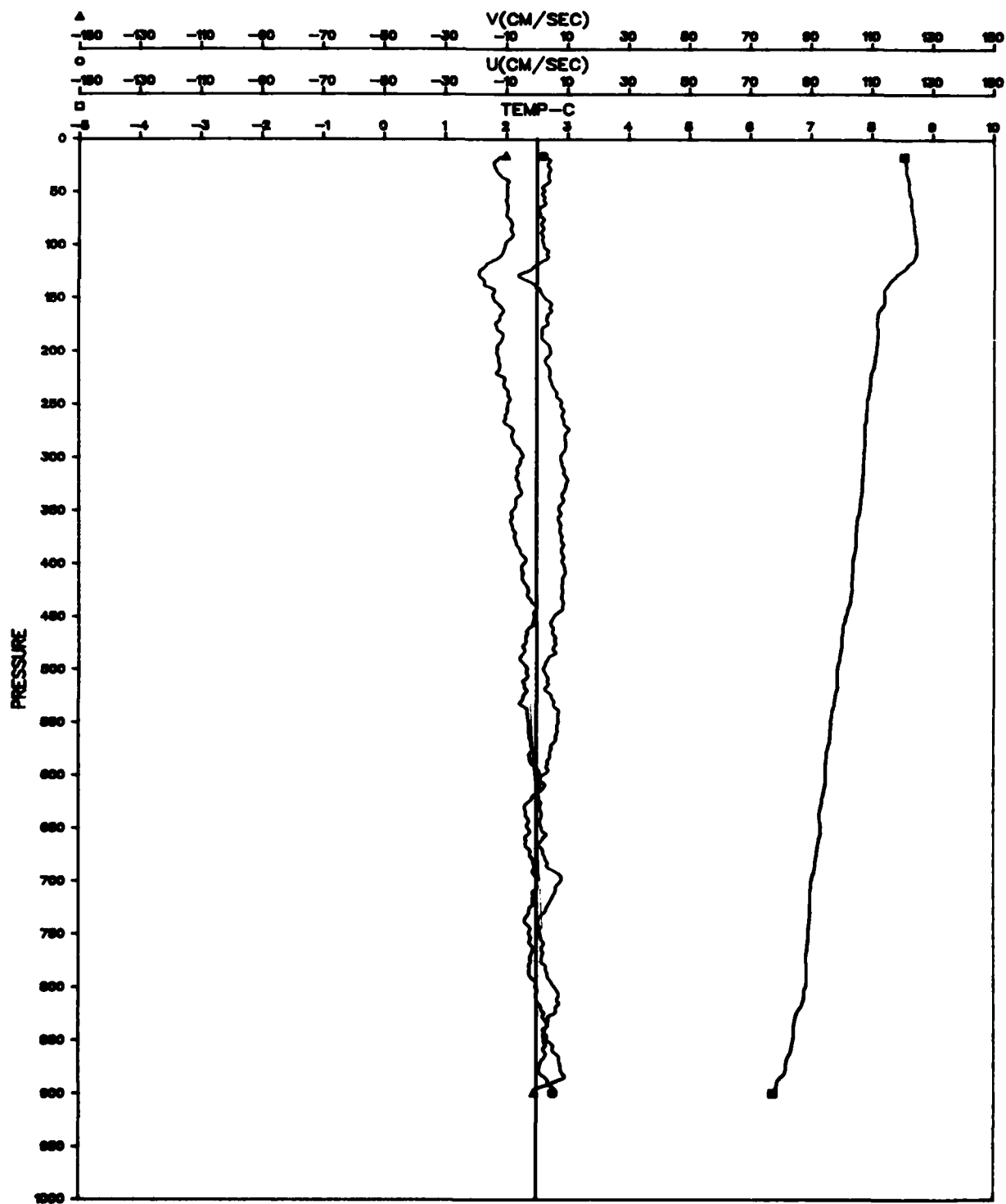


Figure A-3. File: KANE, Segment: C 504

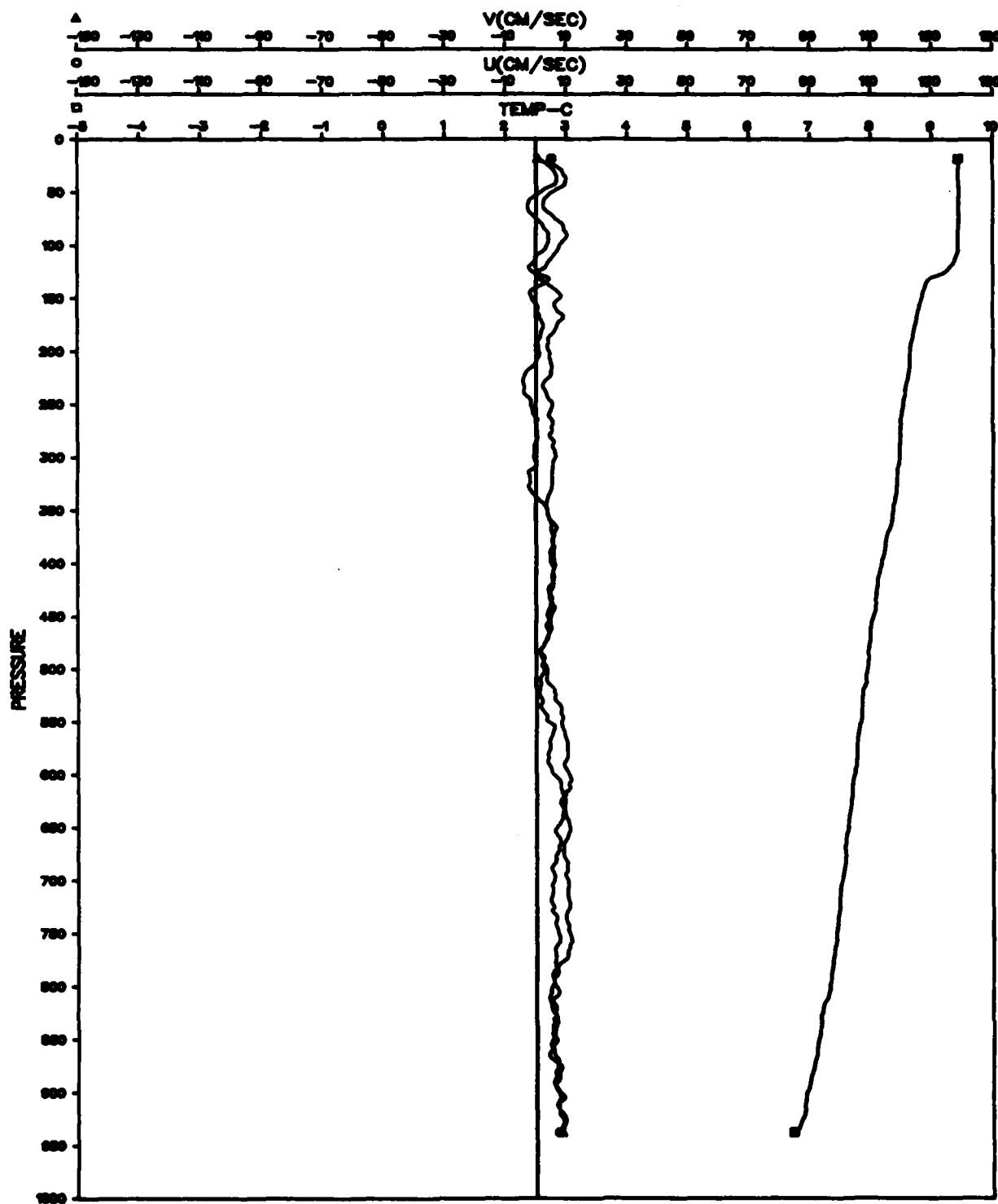


Figure A-4. File: KANE, Segment: C 506

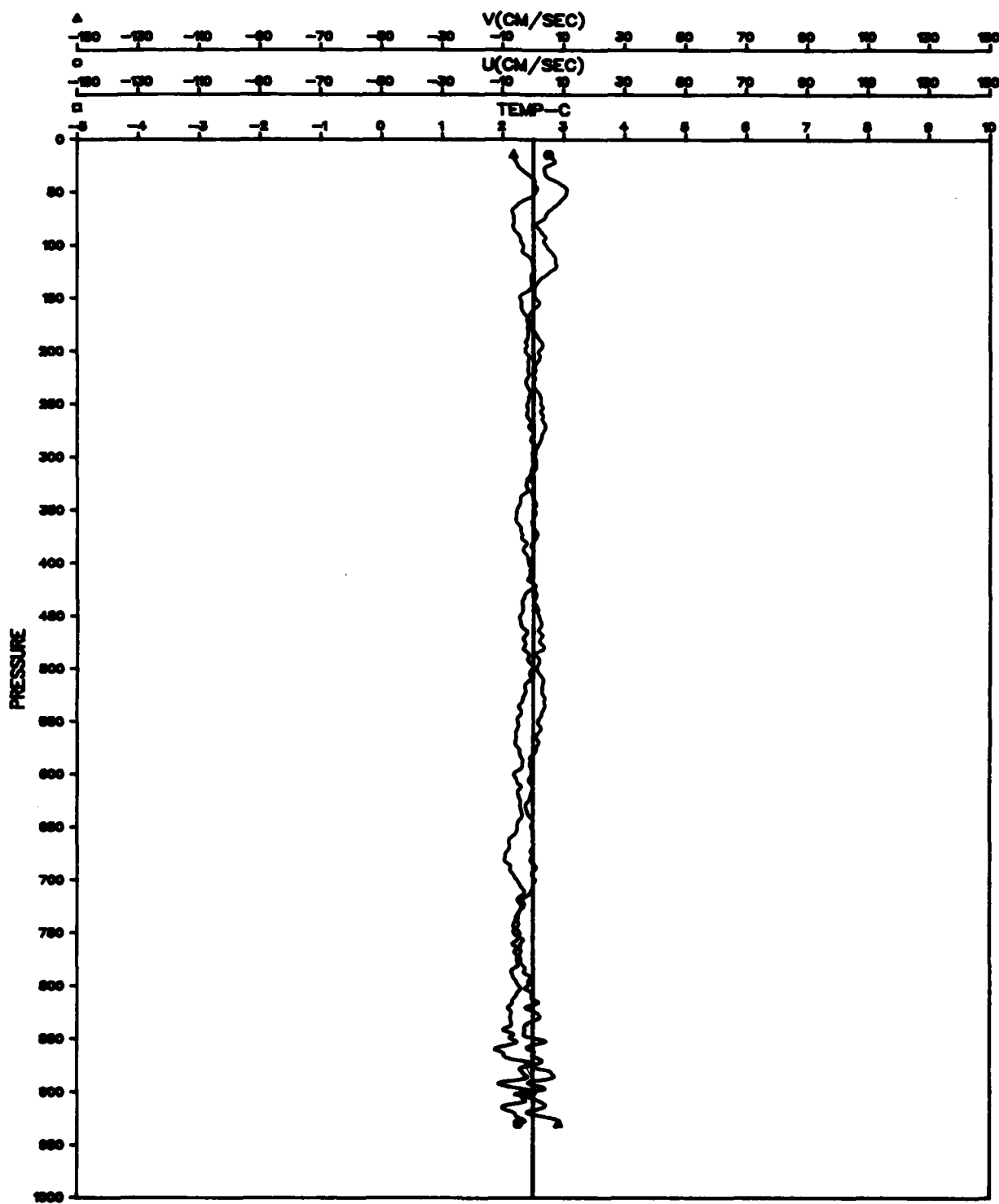


Figure A-5. File: KANE, Segment: C 507

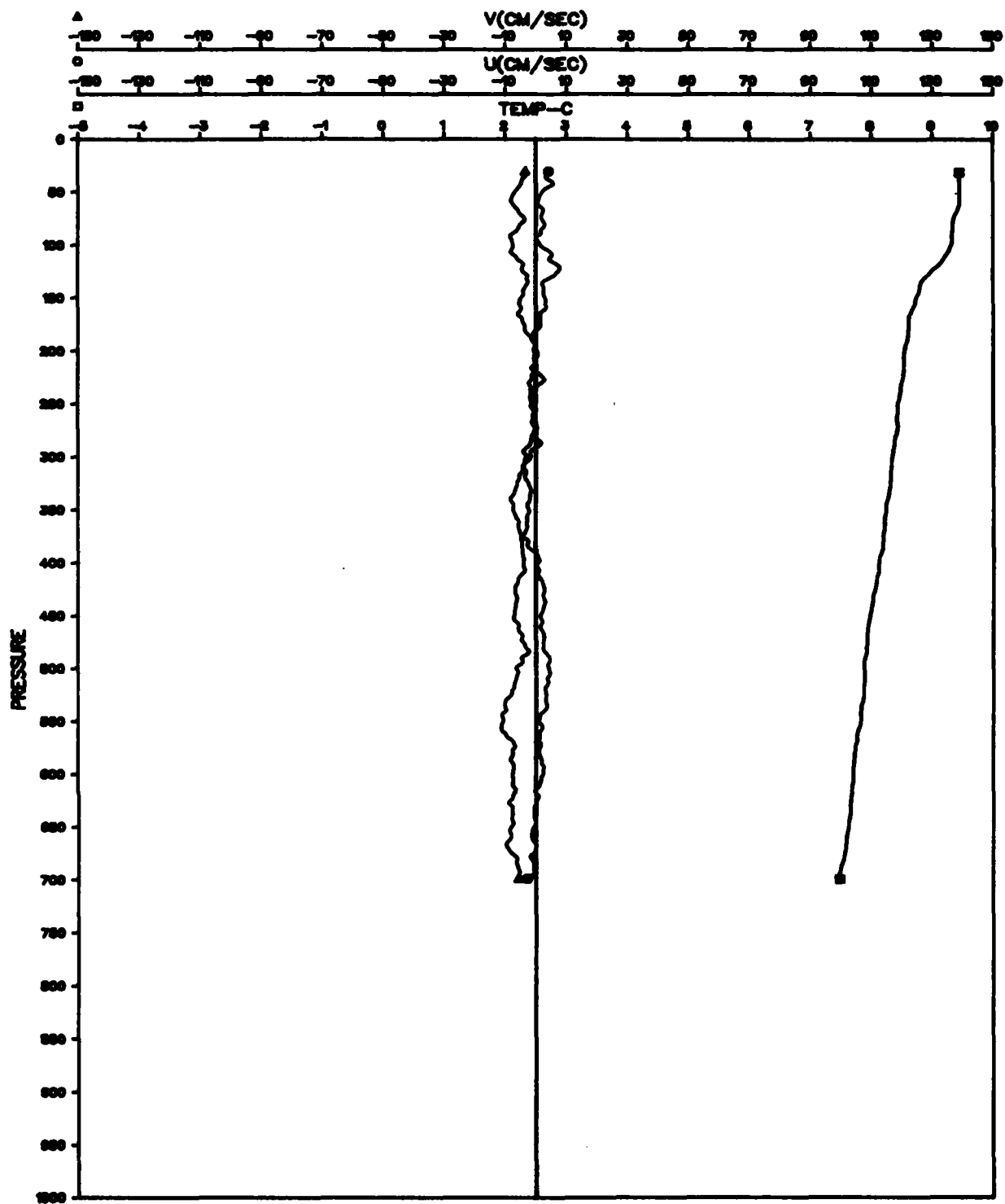


Figure A-6. File: KANE, Segment: C 508

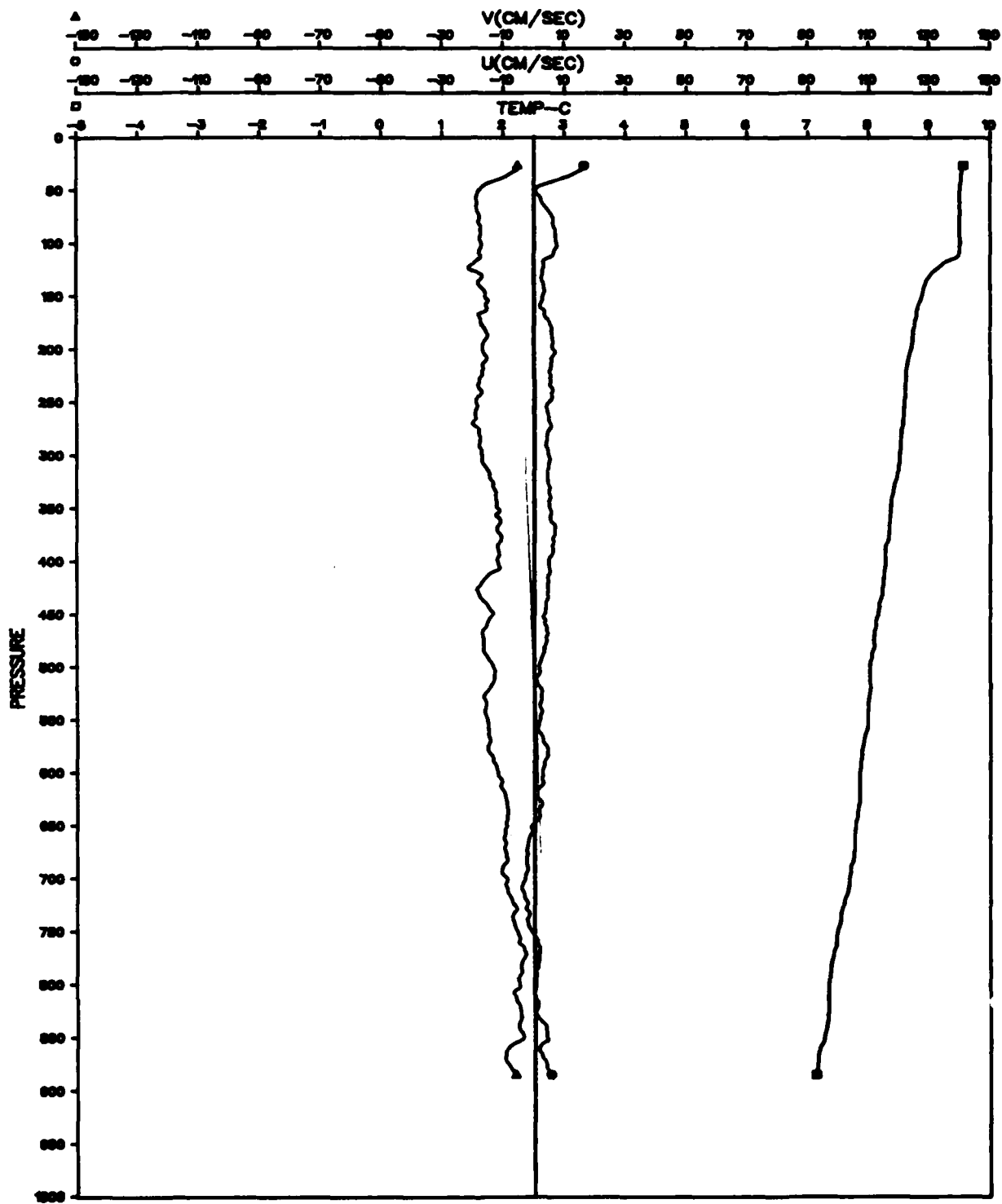


Figure A-7. File: KANE, Segment: C 510

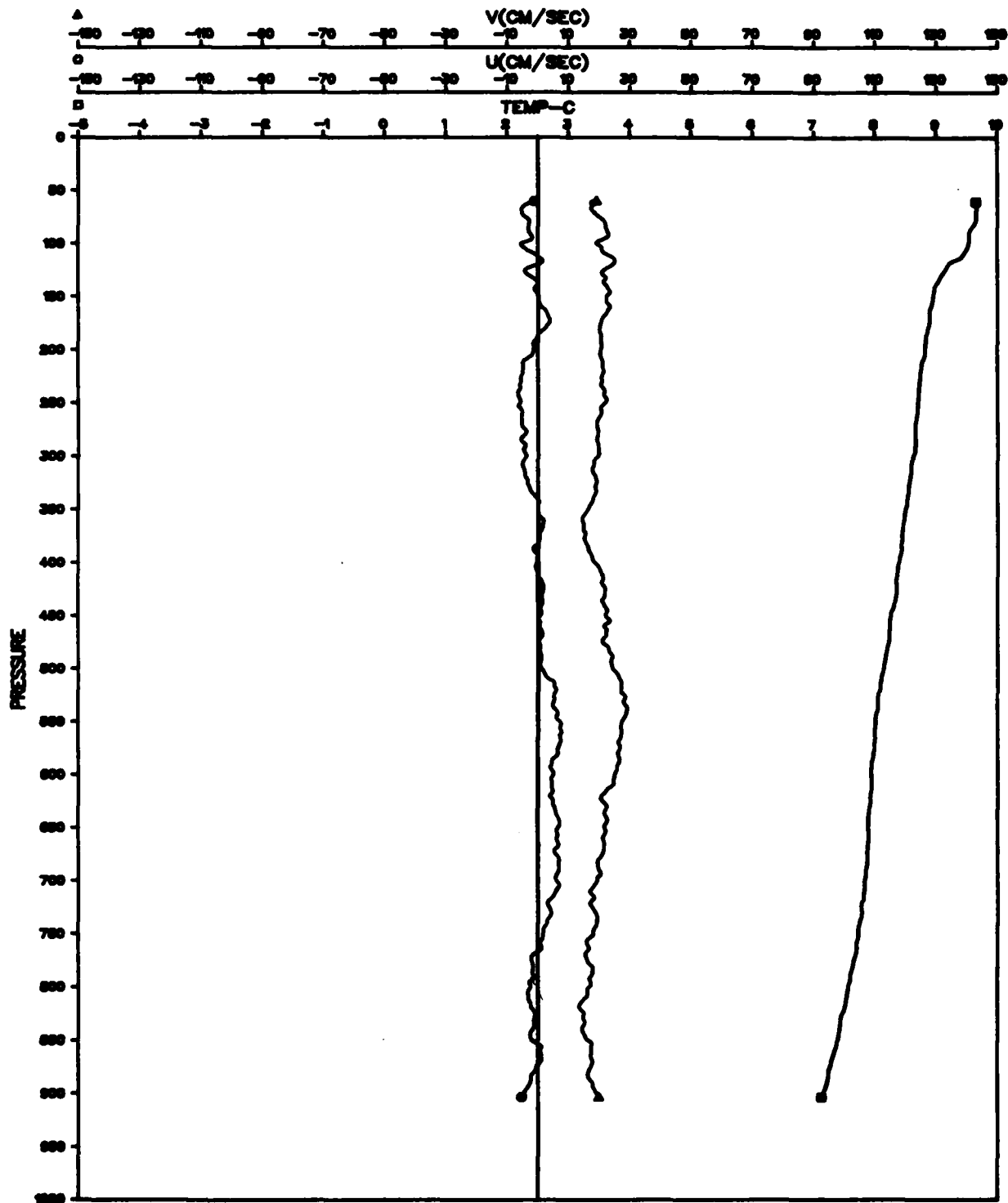


Figure A-8. File: KANE, Segment: C 512

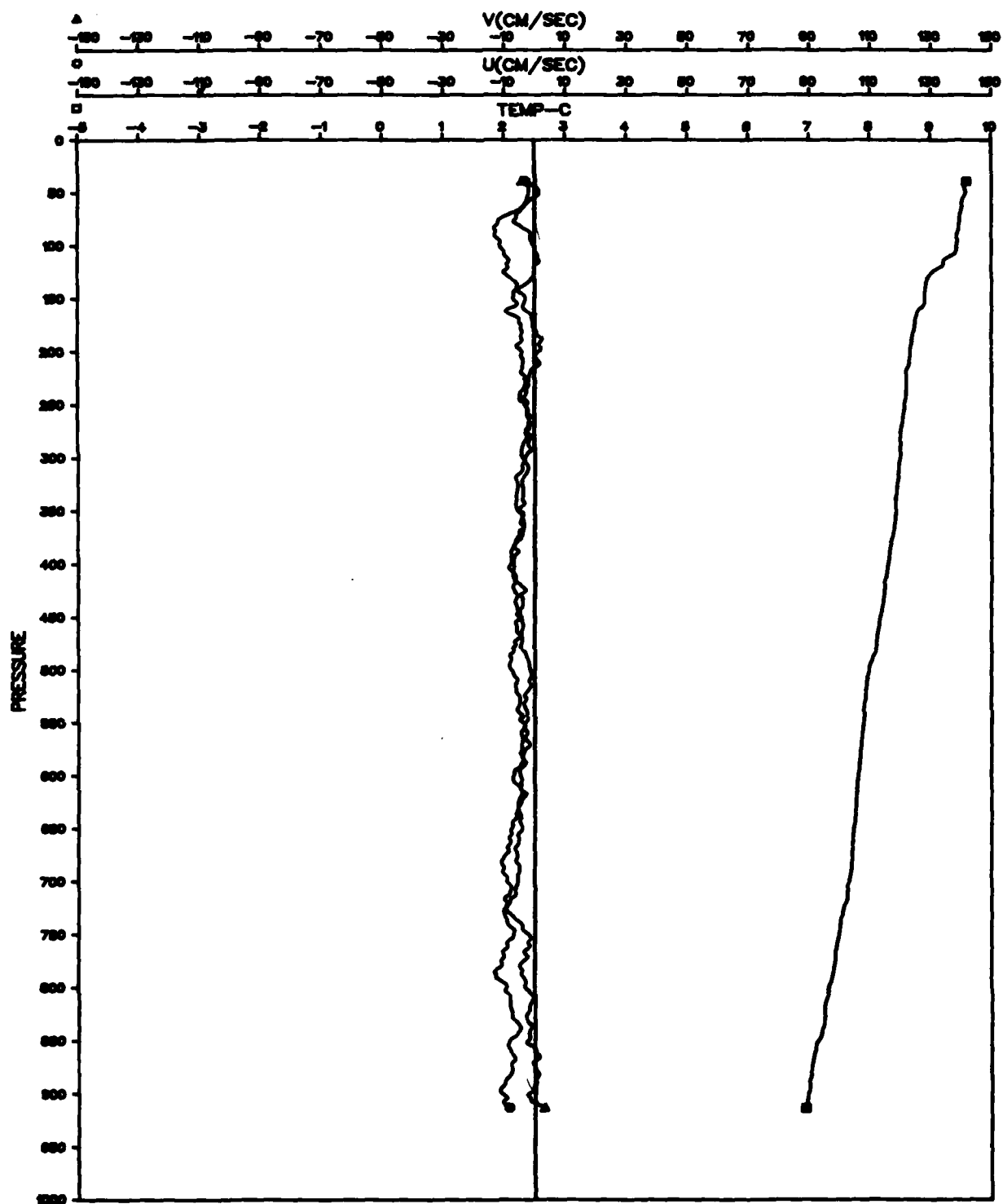


Figure A-9. File: KANE, Segment: C 513

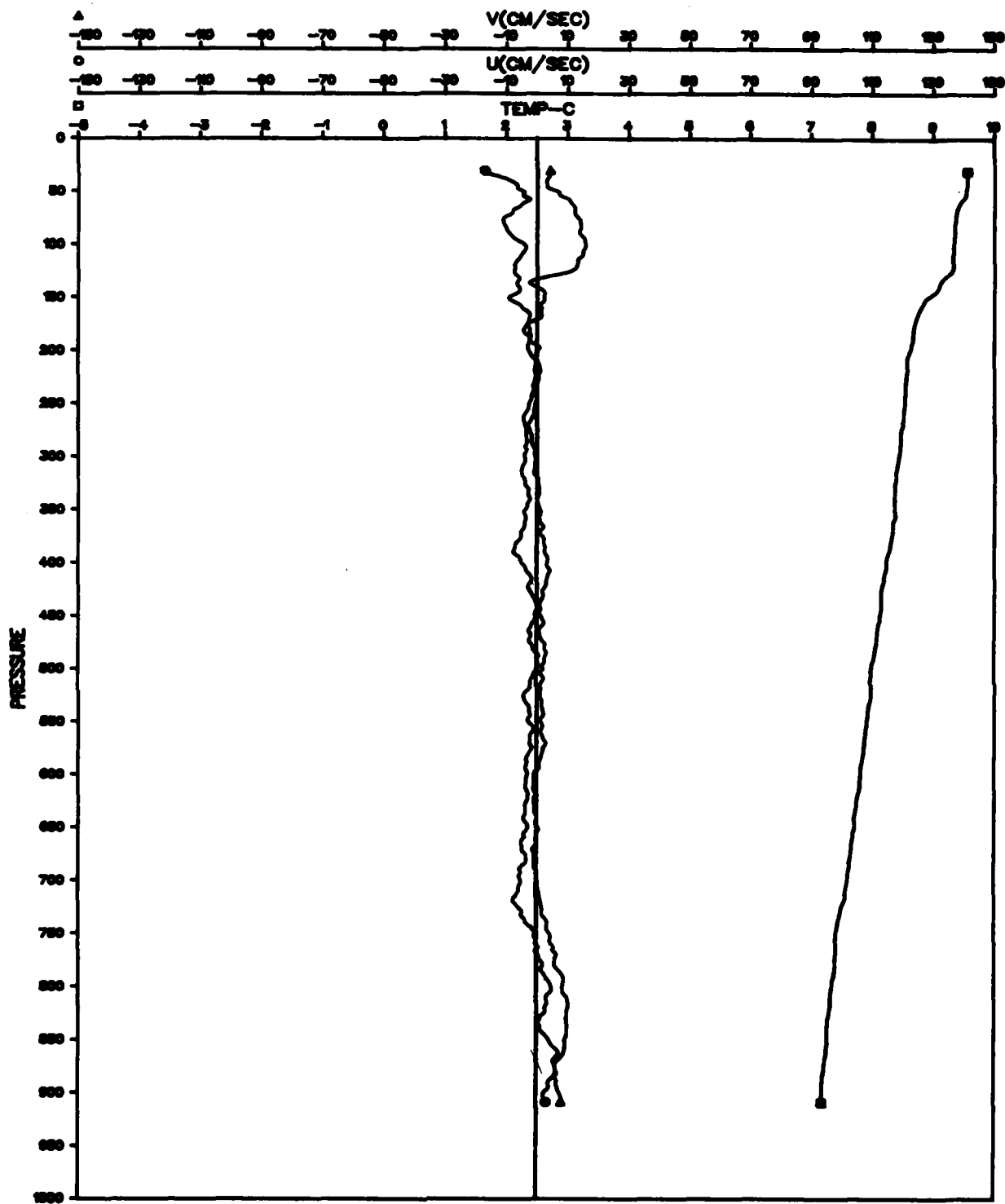


Figure A-10. File: KANE, Segment: C 514

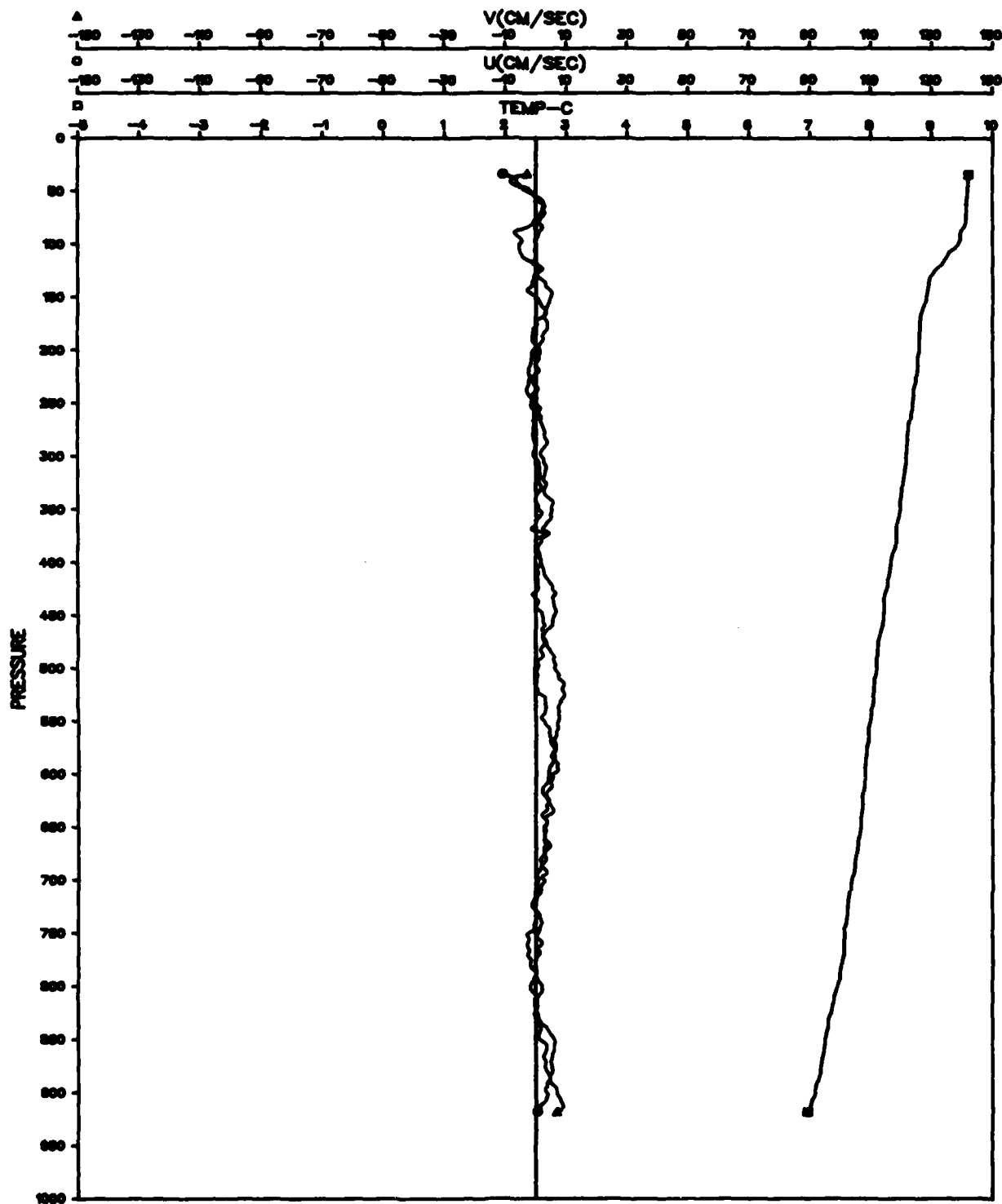


Figure A-11. File: KANE, Segment: C 515

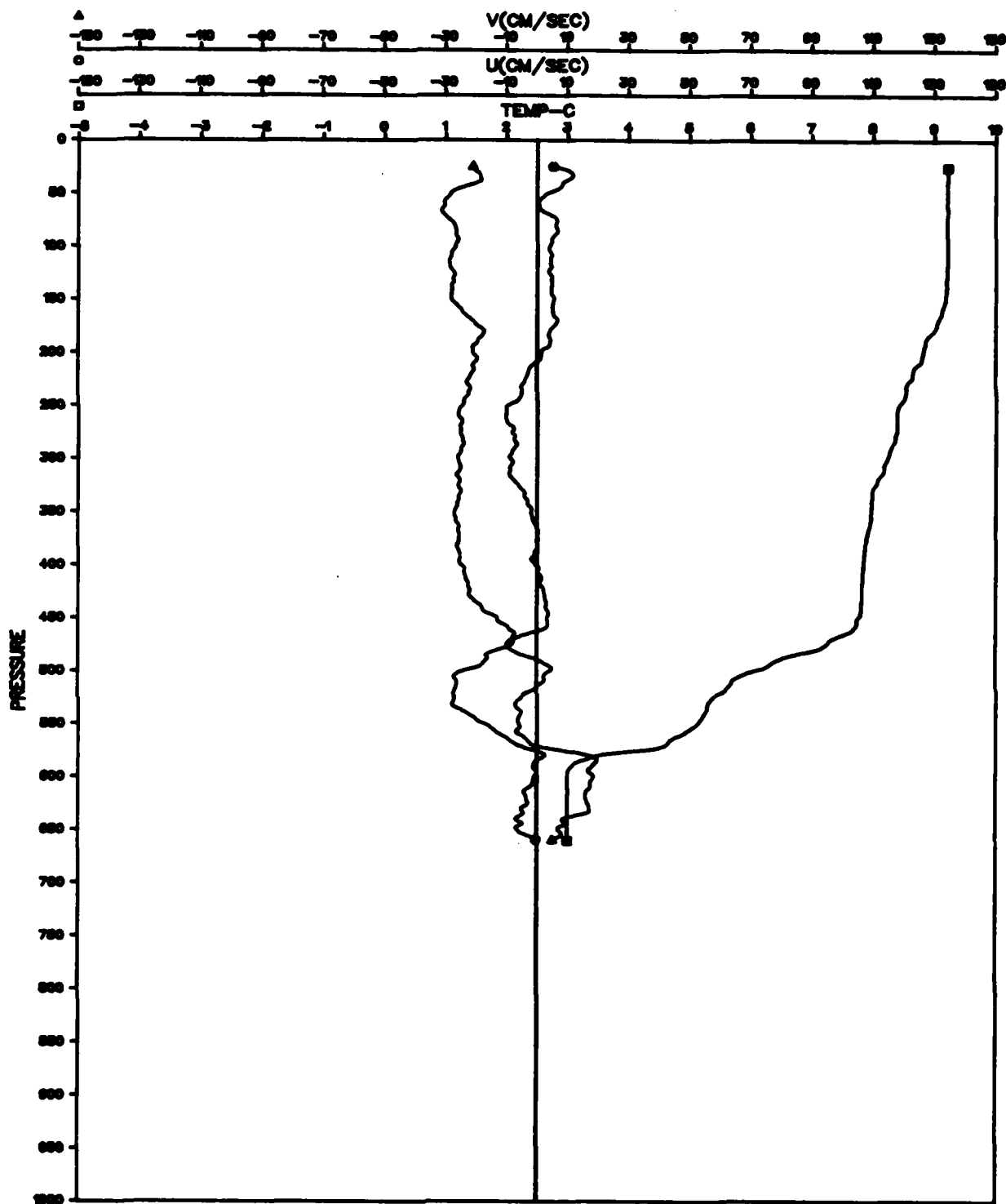


Figure A-12. File: KANE, Segment: C 517

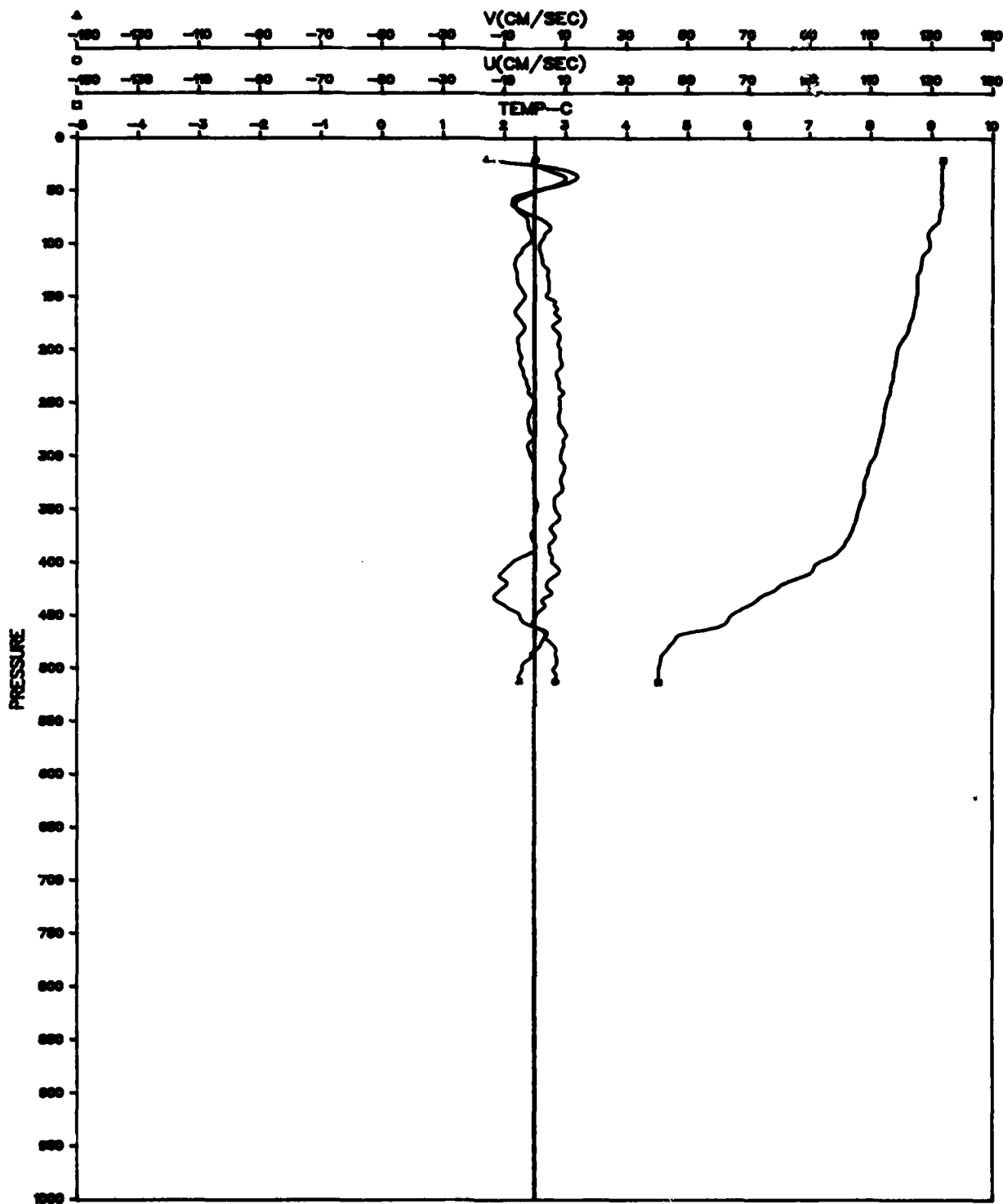


Figure A-13. File: KANE, Segment: C 519

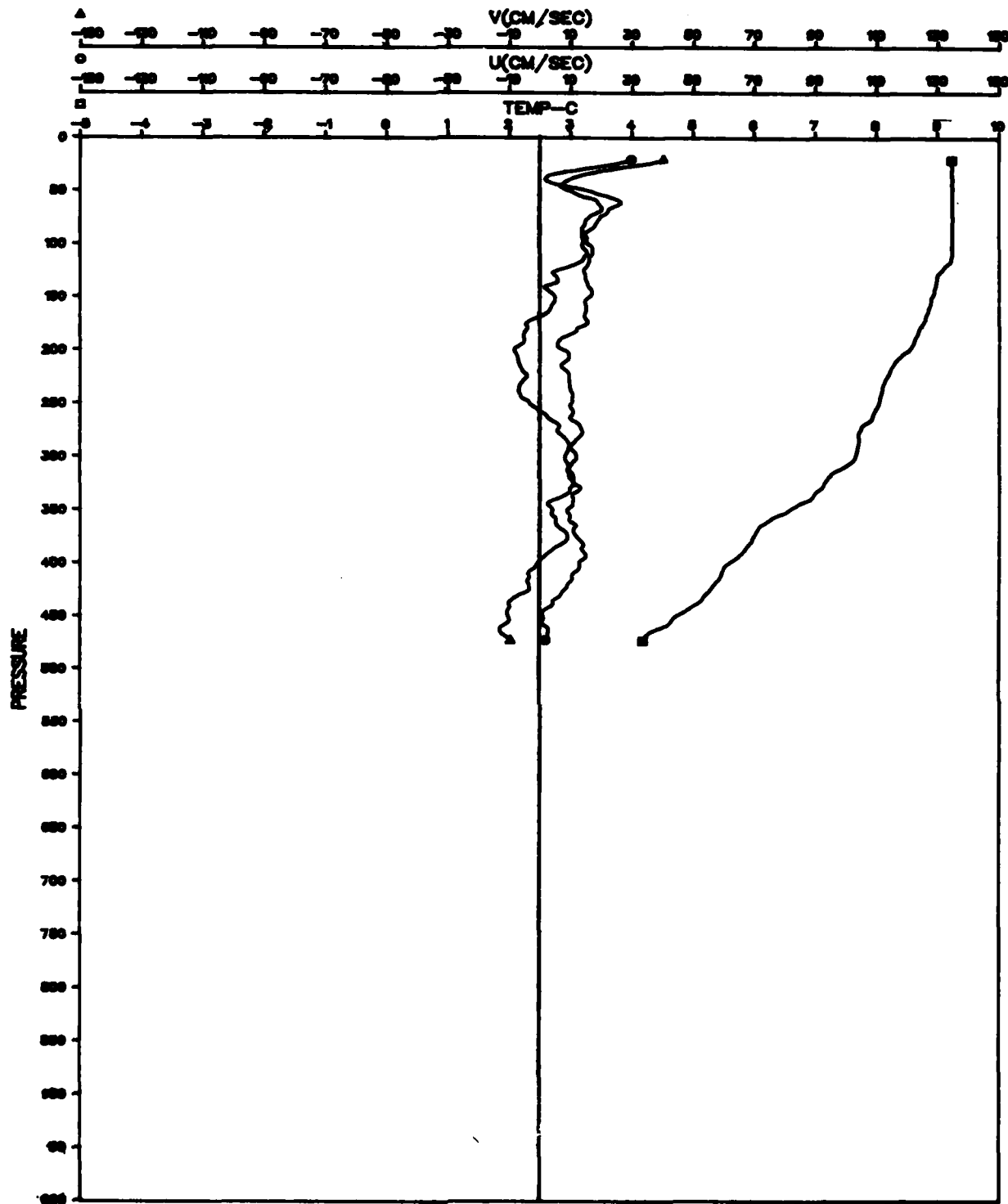


Figure A-14. File: KANE, Segment: C 520

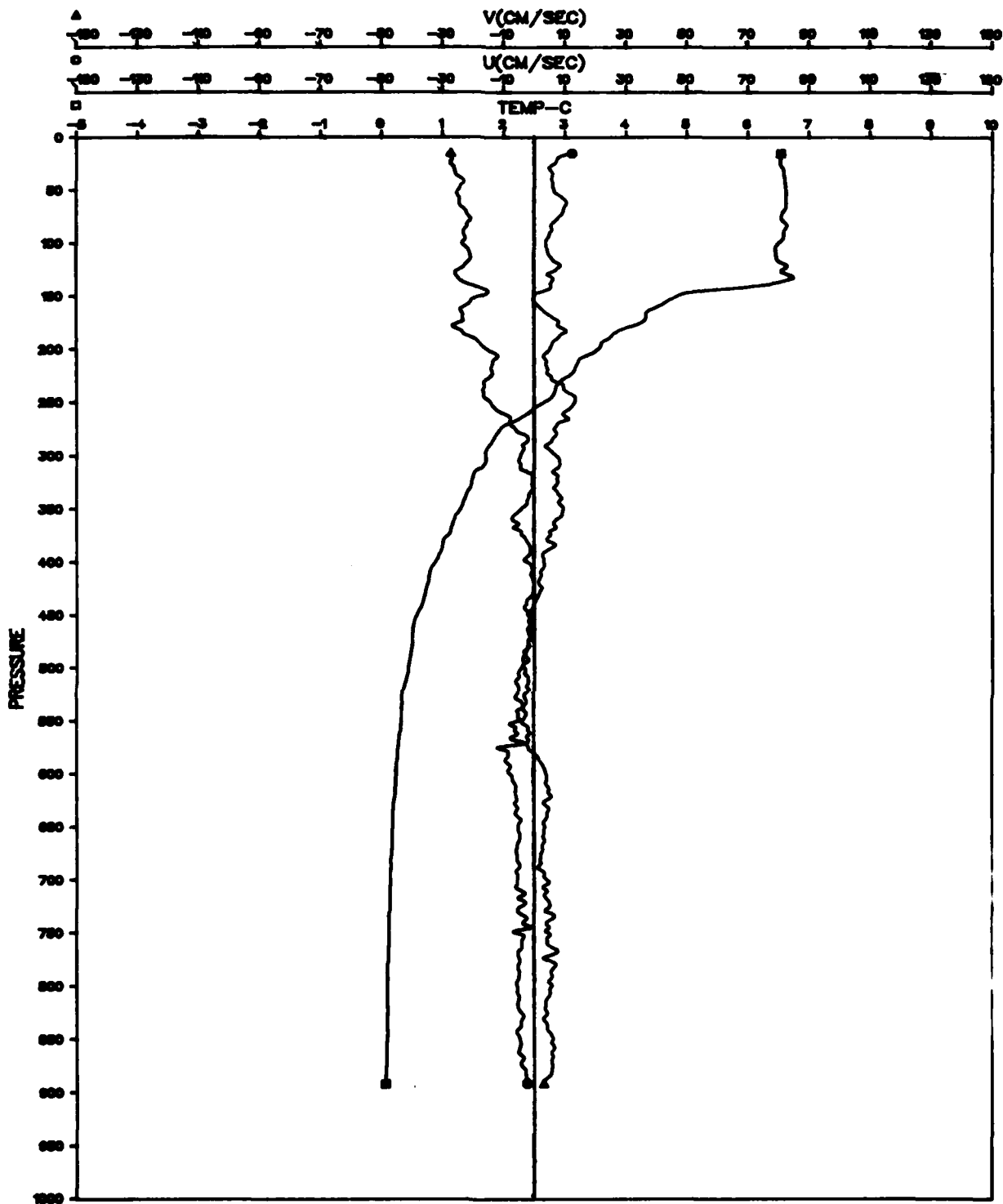


Figure A-15. File: KANE, Segment: C 525

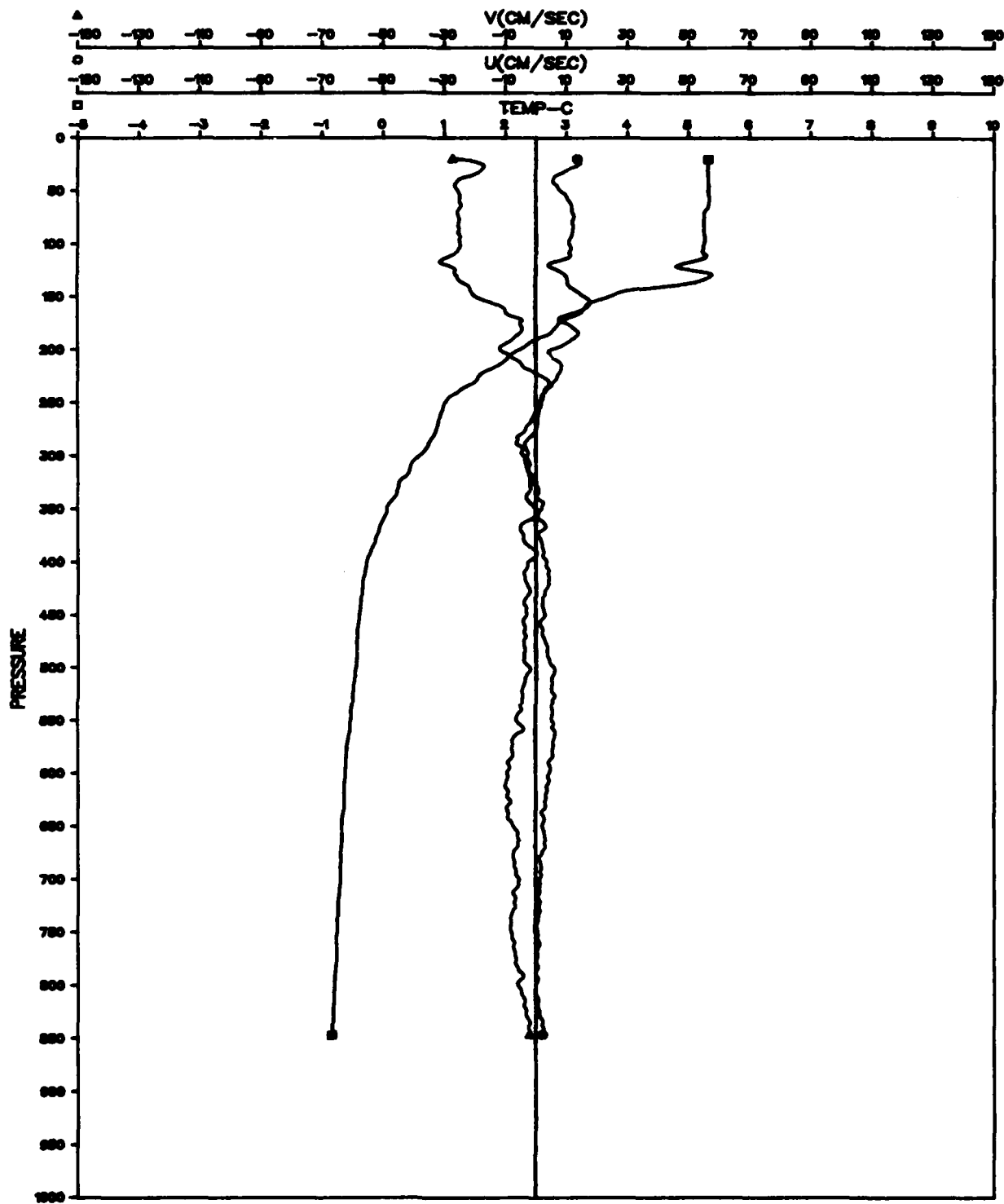


Figure A-16. File: KANE, Segment: C 527

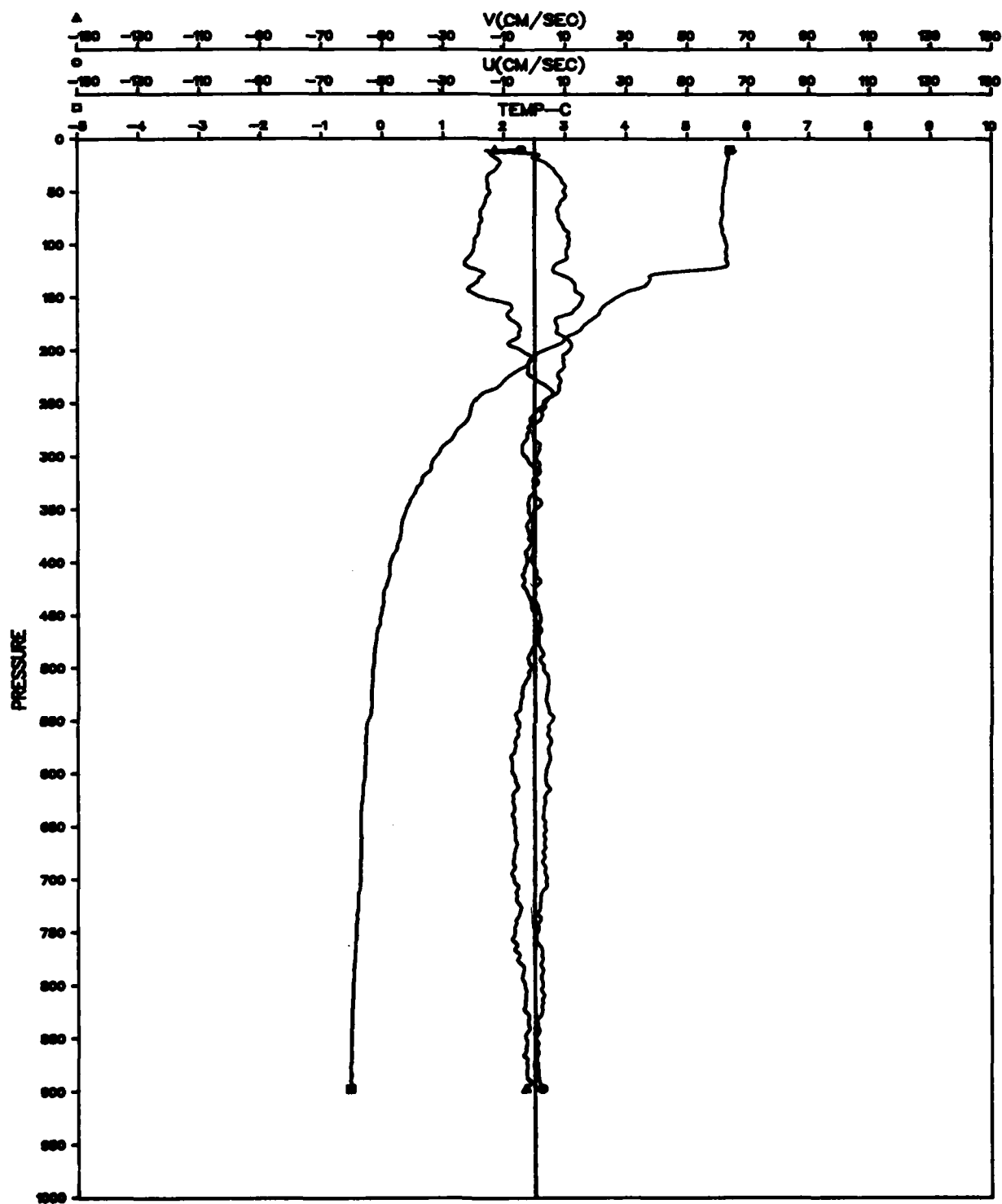


Figure A-17. File: KANE, Segment: C 528

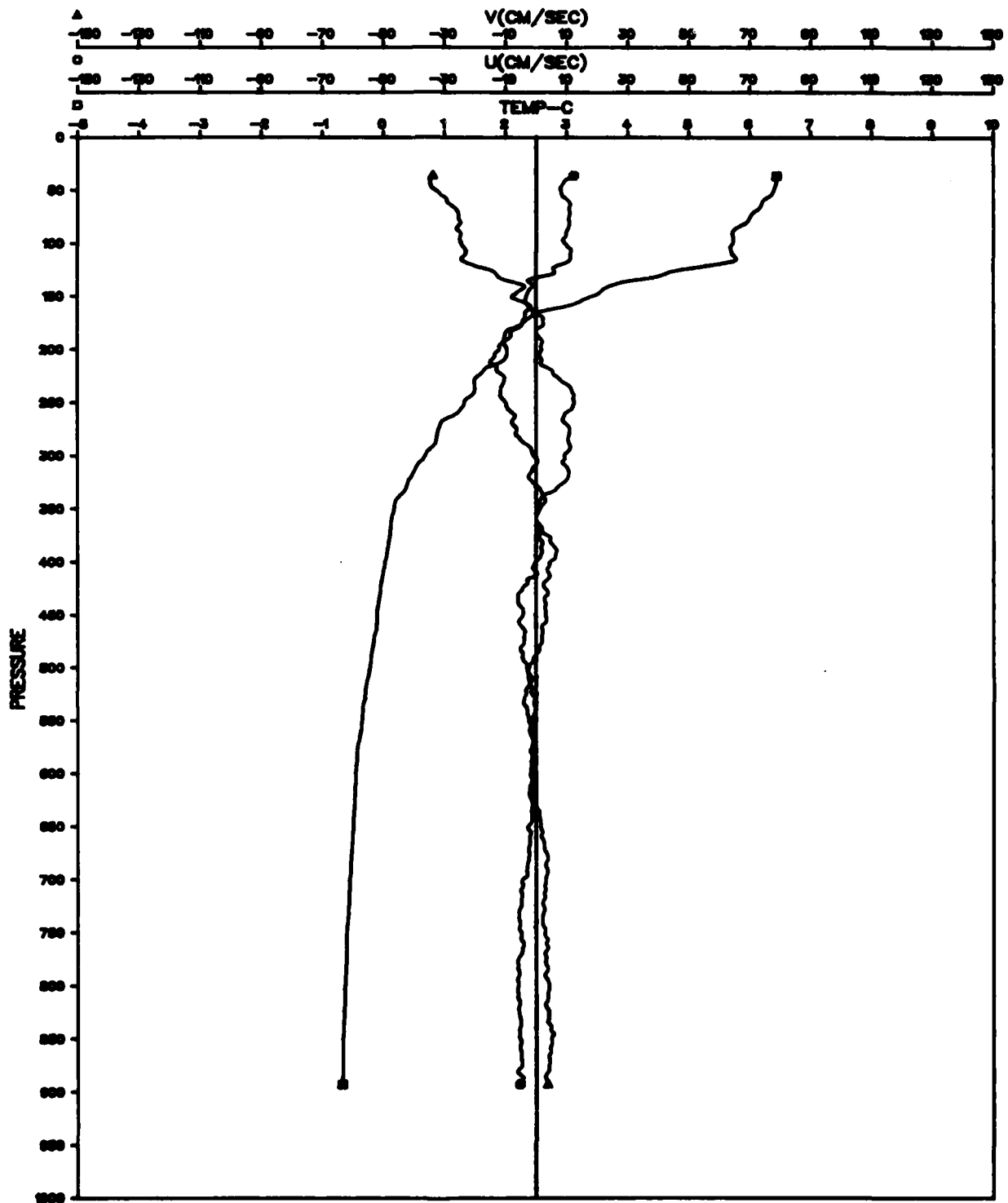


Figure A-18. File: KANE, Segment: C 530

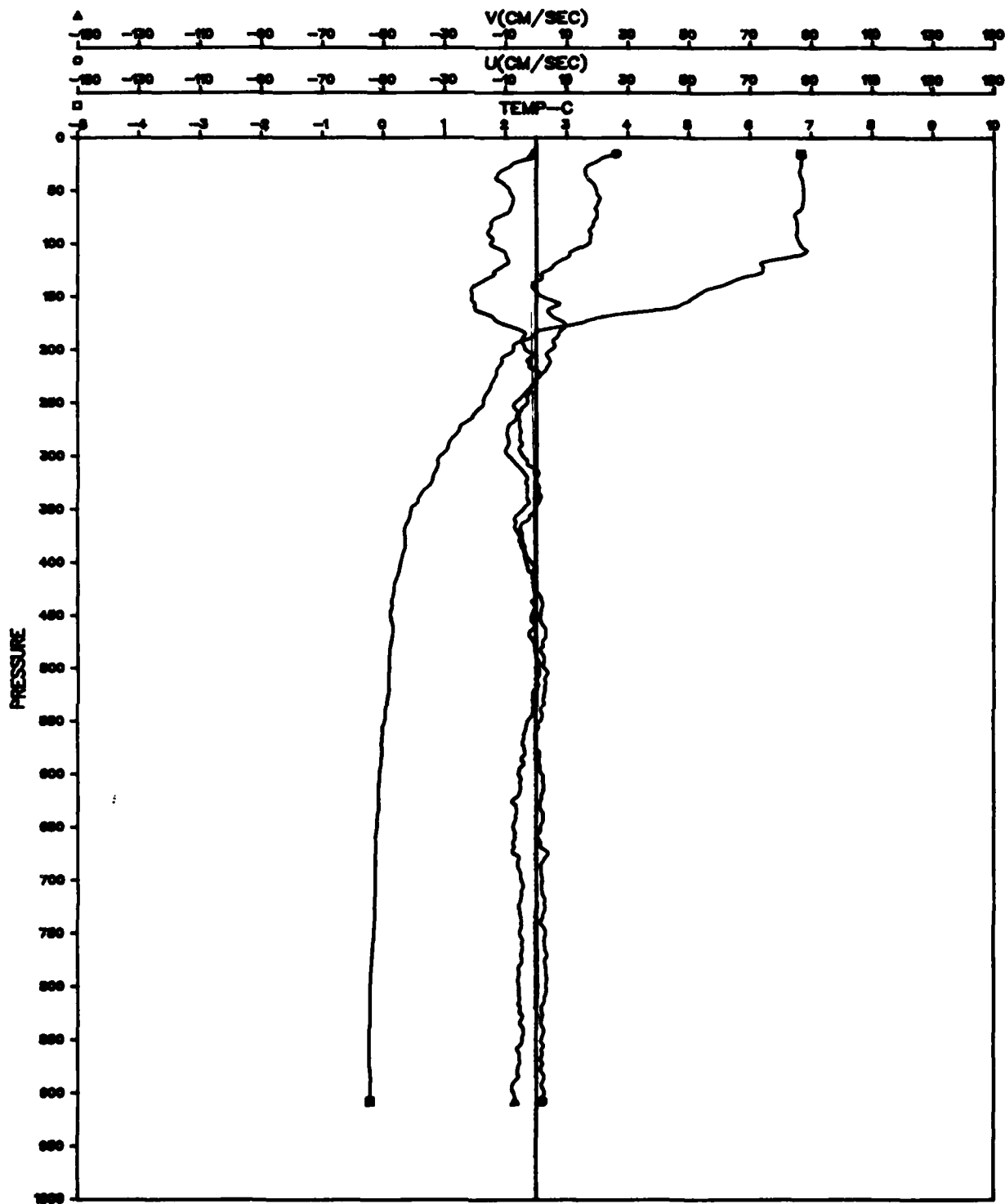


Figure A-19. File: KANE, Segment: C 533

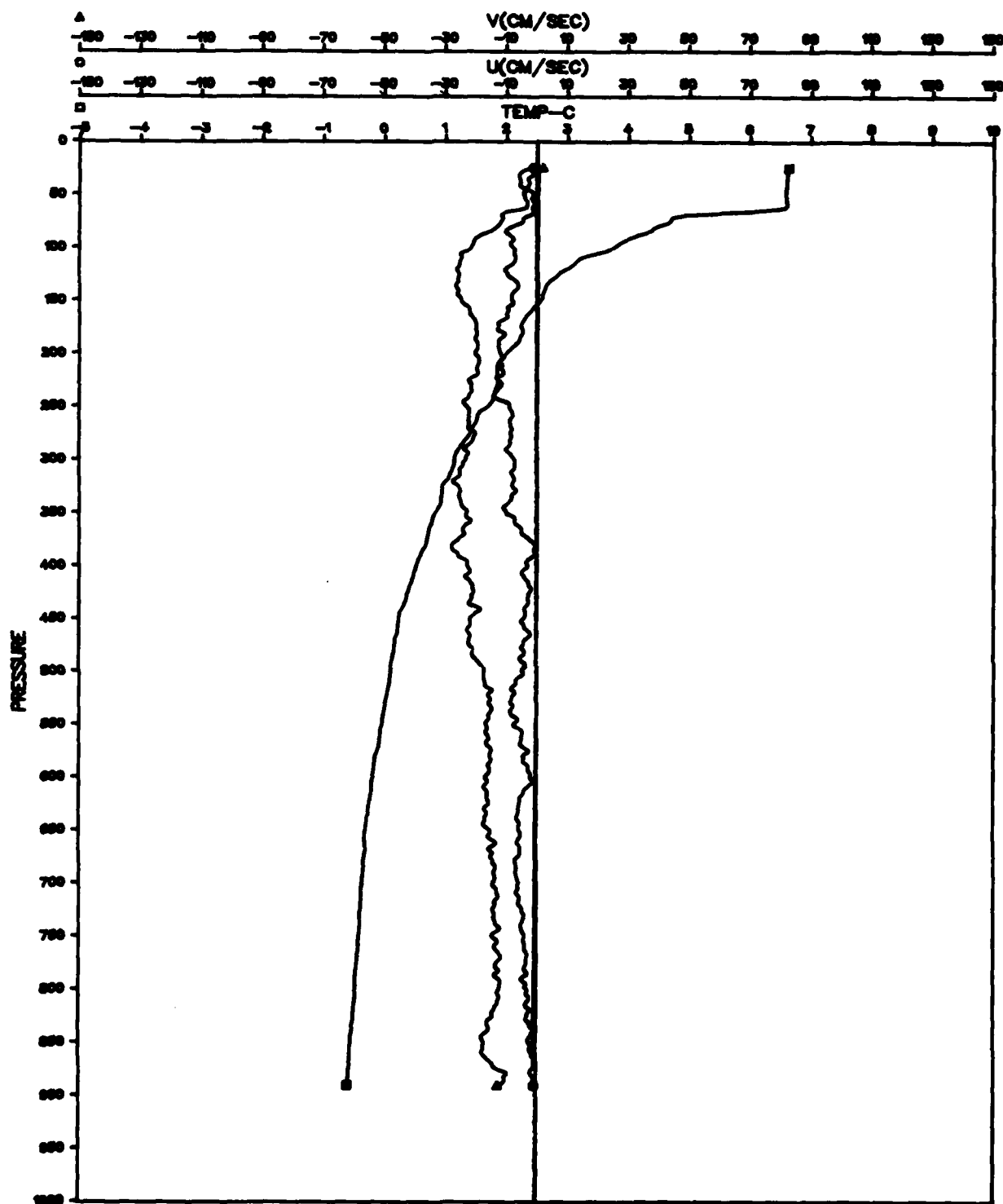


Figure A-20. File: KANE, Segment: C 534

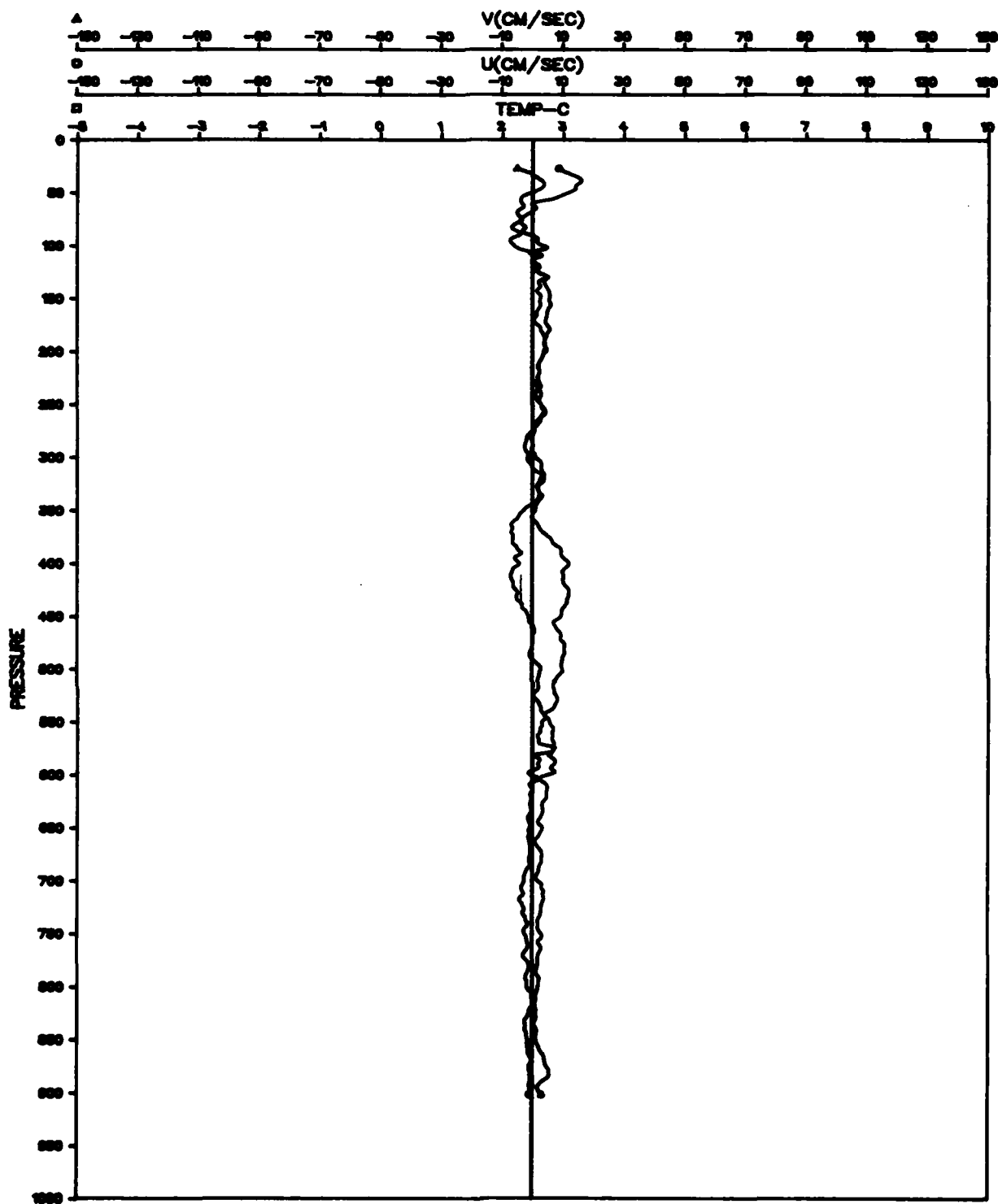


Figure A-21. File: KANE, Segment: C 535

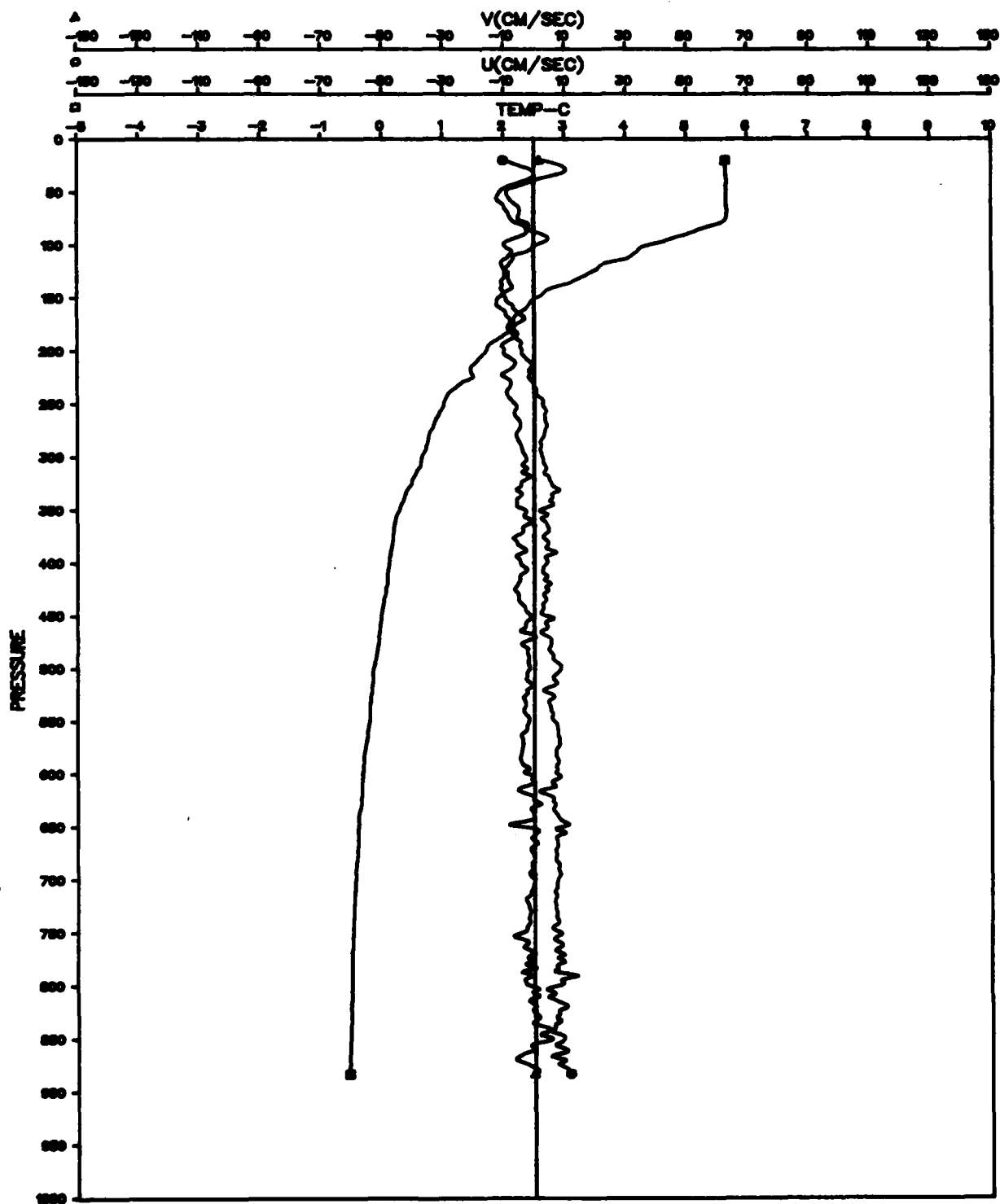


Figure A-22. File: KANE, Segment: C 538

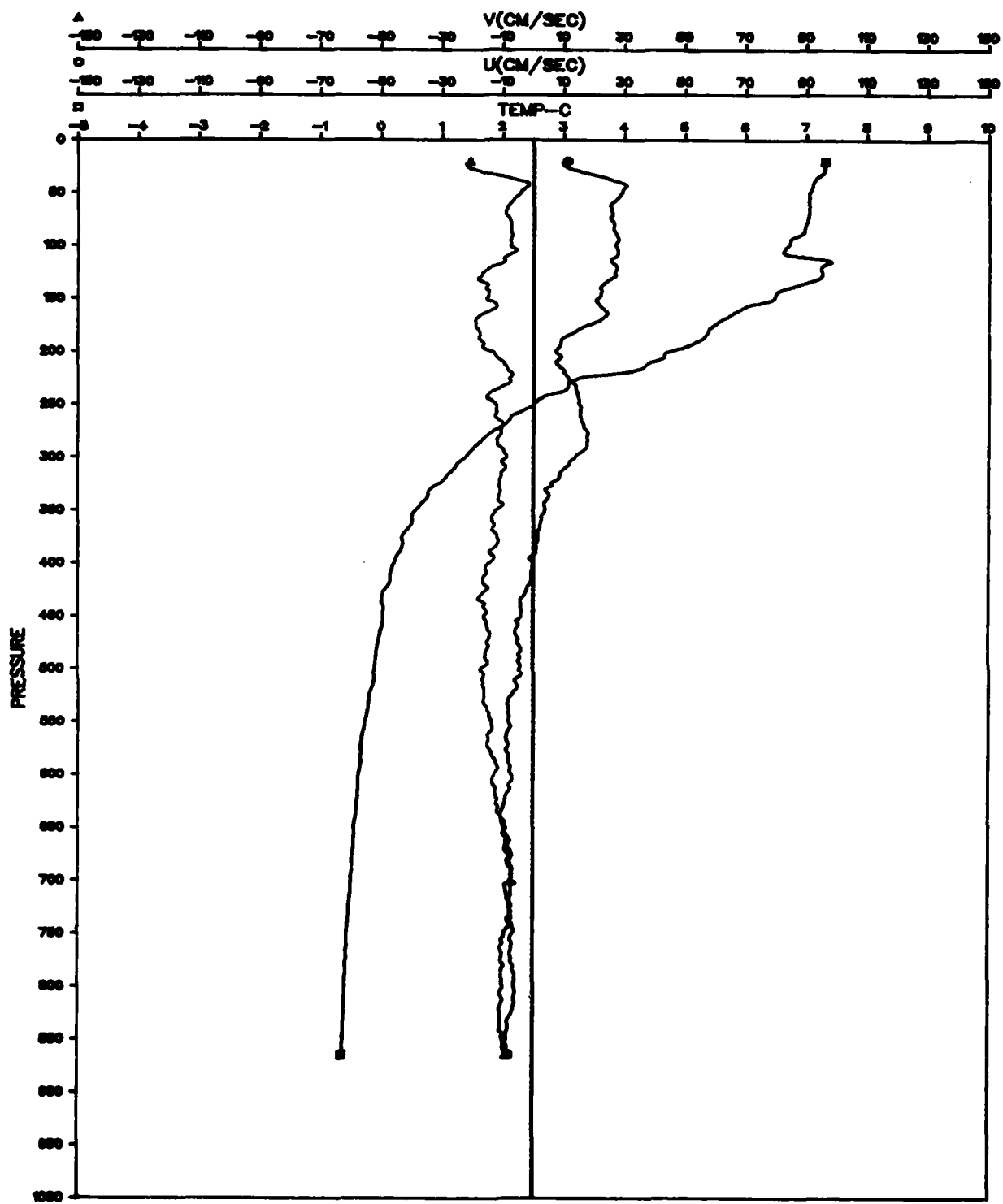


Figure A-23. File: KANE, Segment: C 539

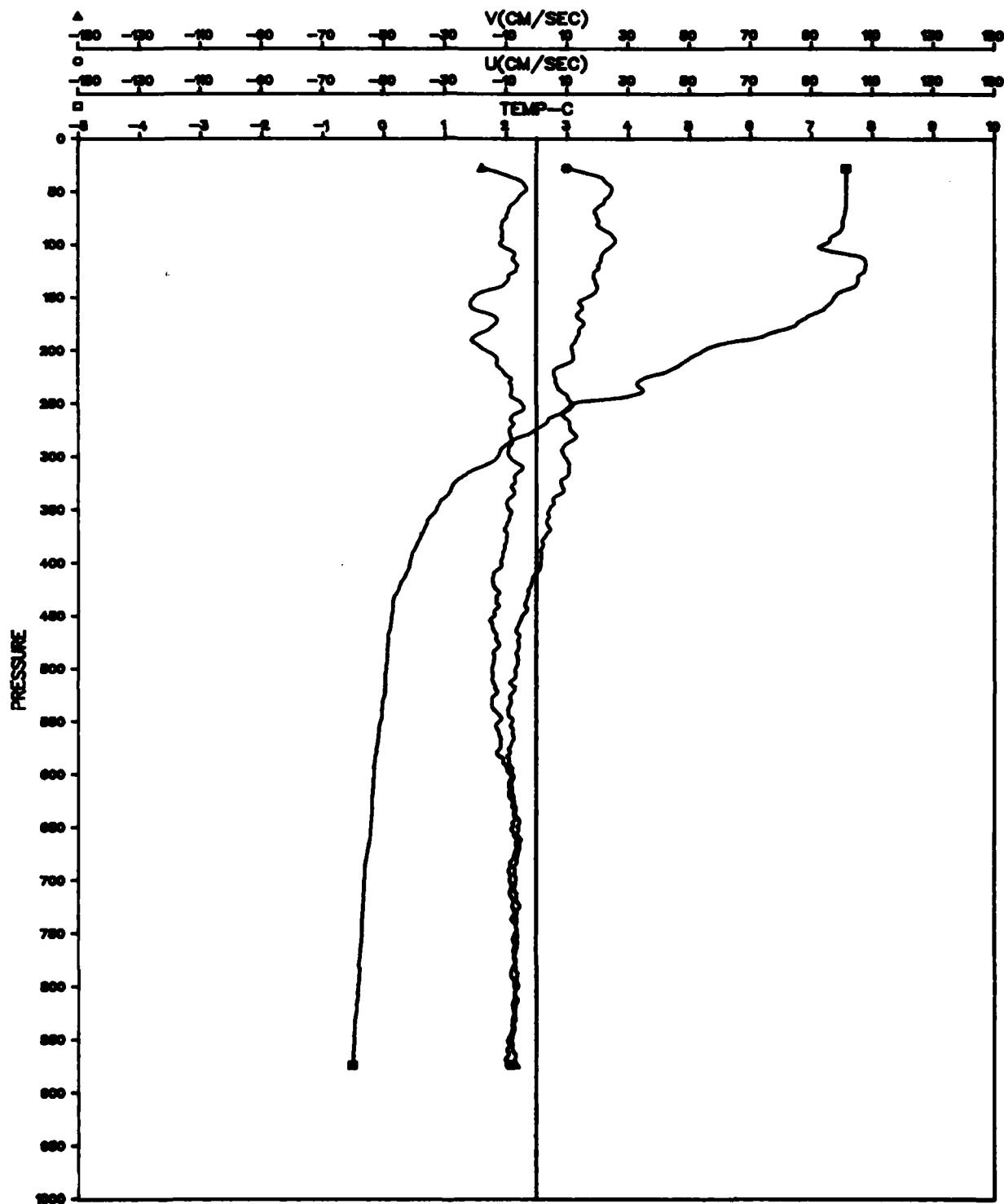


Figure A-24. File: KANE, Segment: C 542

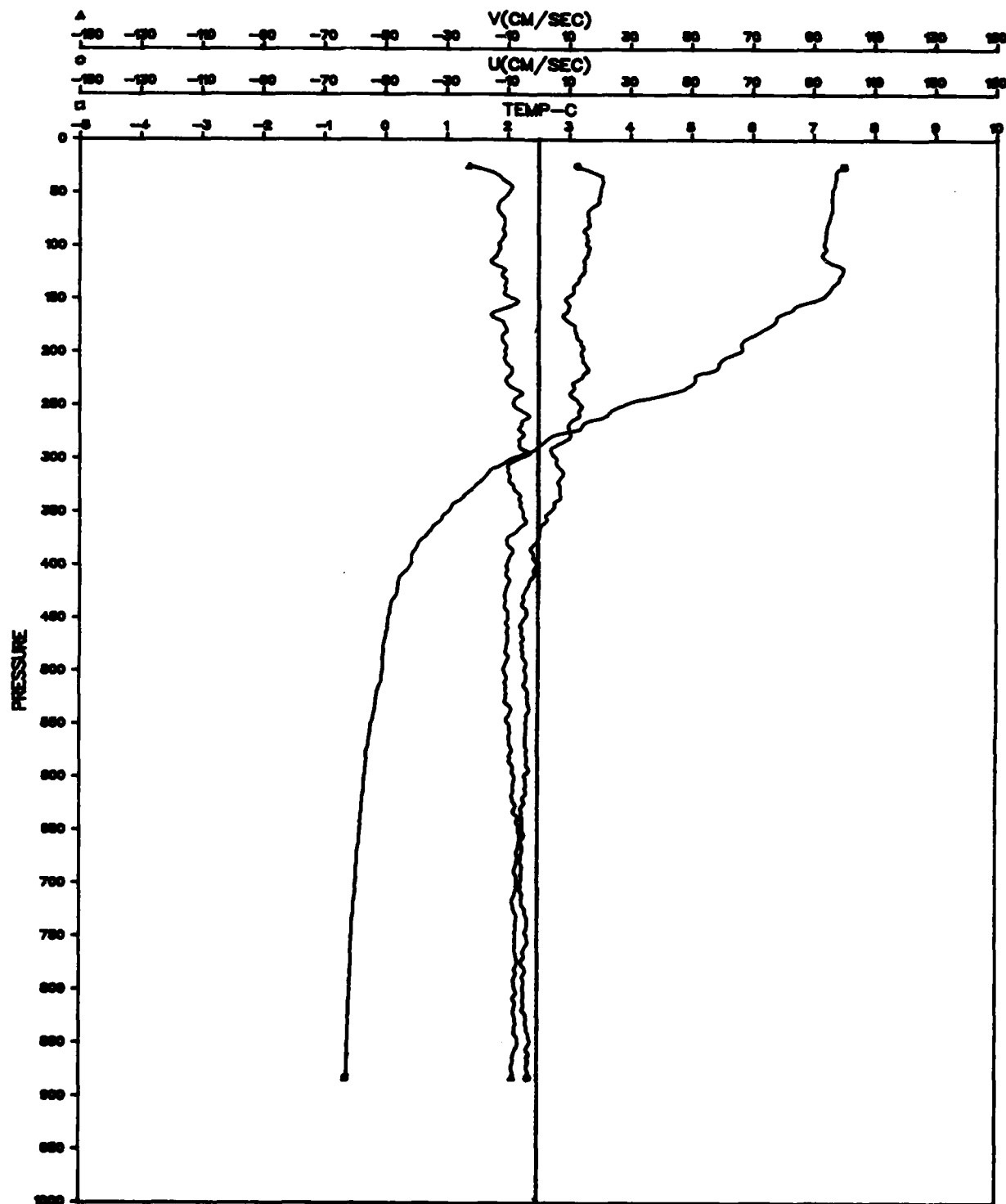


Figure A-25. File: KANE, Segment: C 543

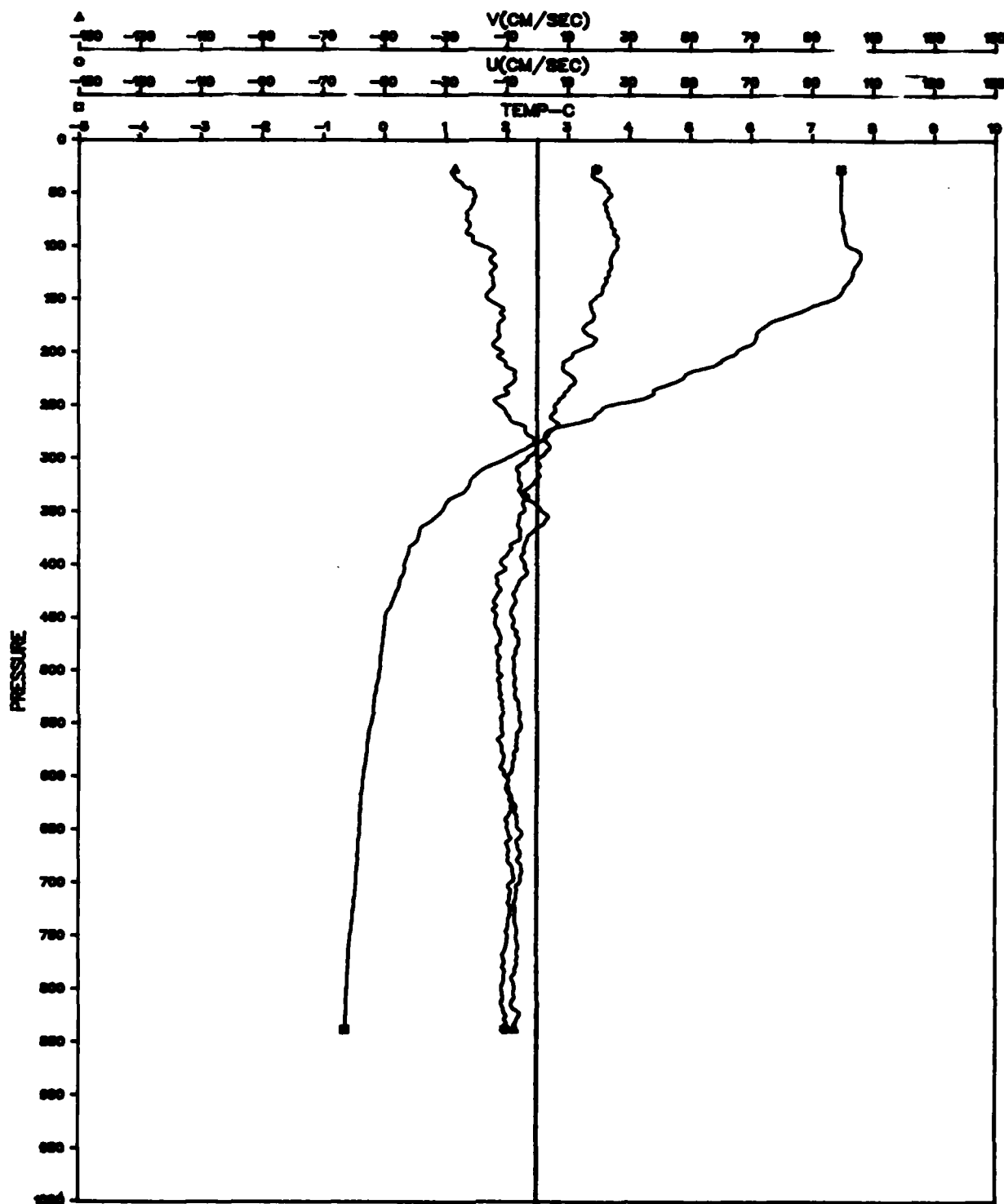


Figure A-26. File: KANE, Segment: C 544

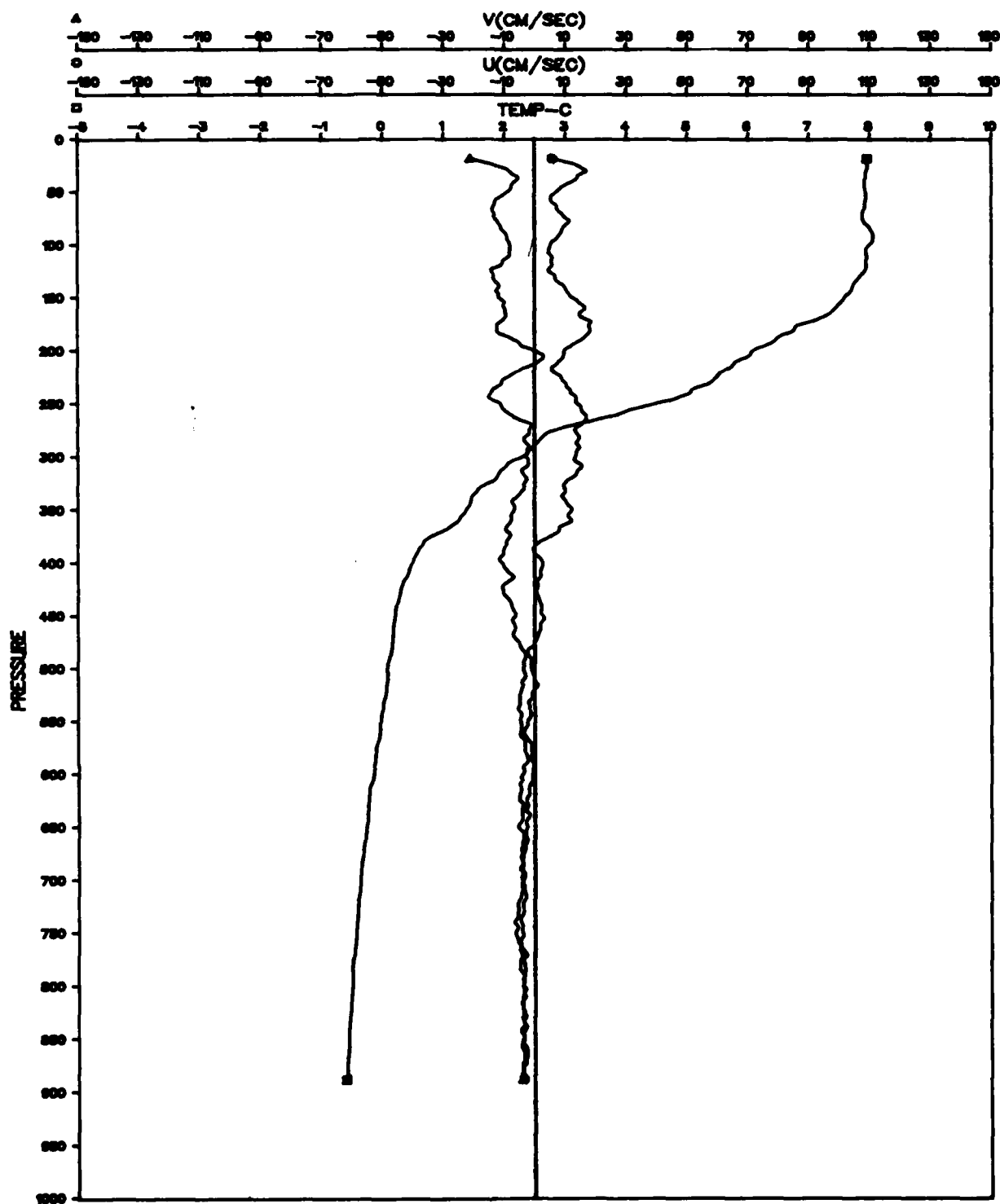


Figure A-27. File: KANE, Segment: C 546

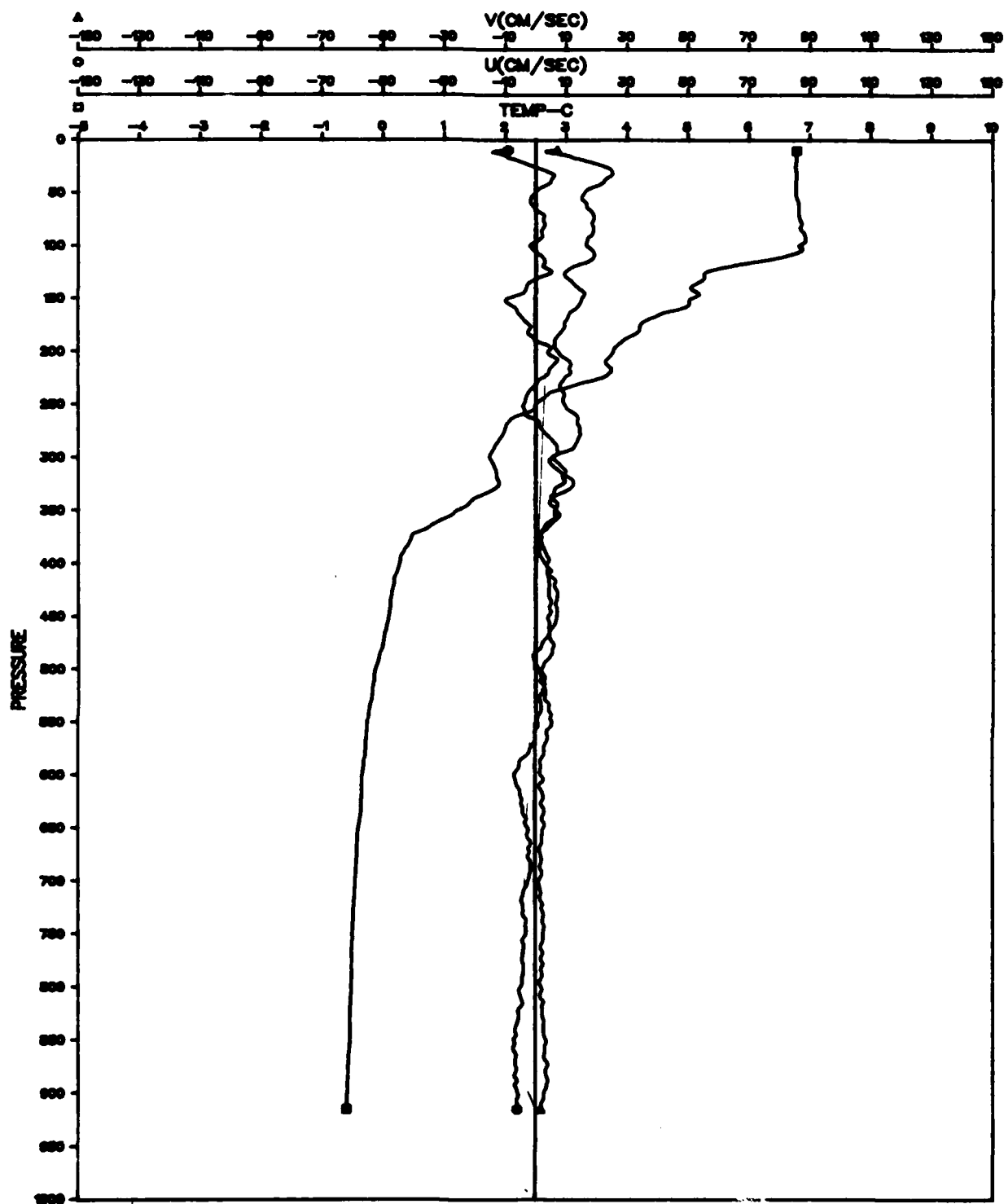


Figure A-28. File: KANE, Segment: C 547

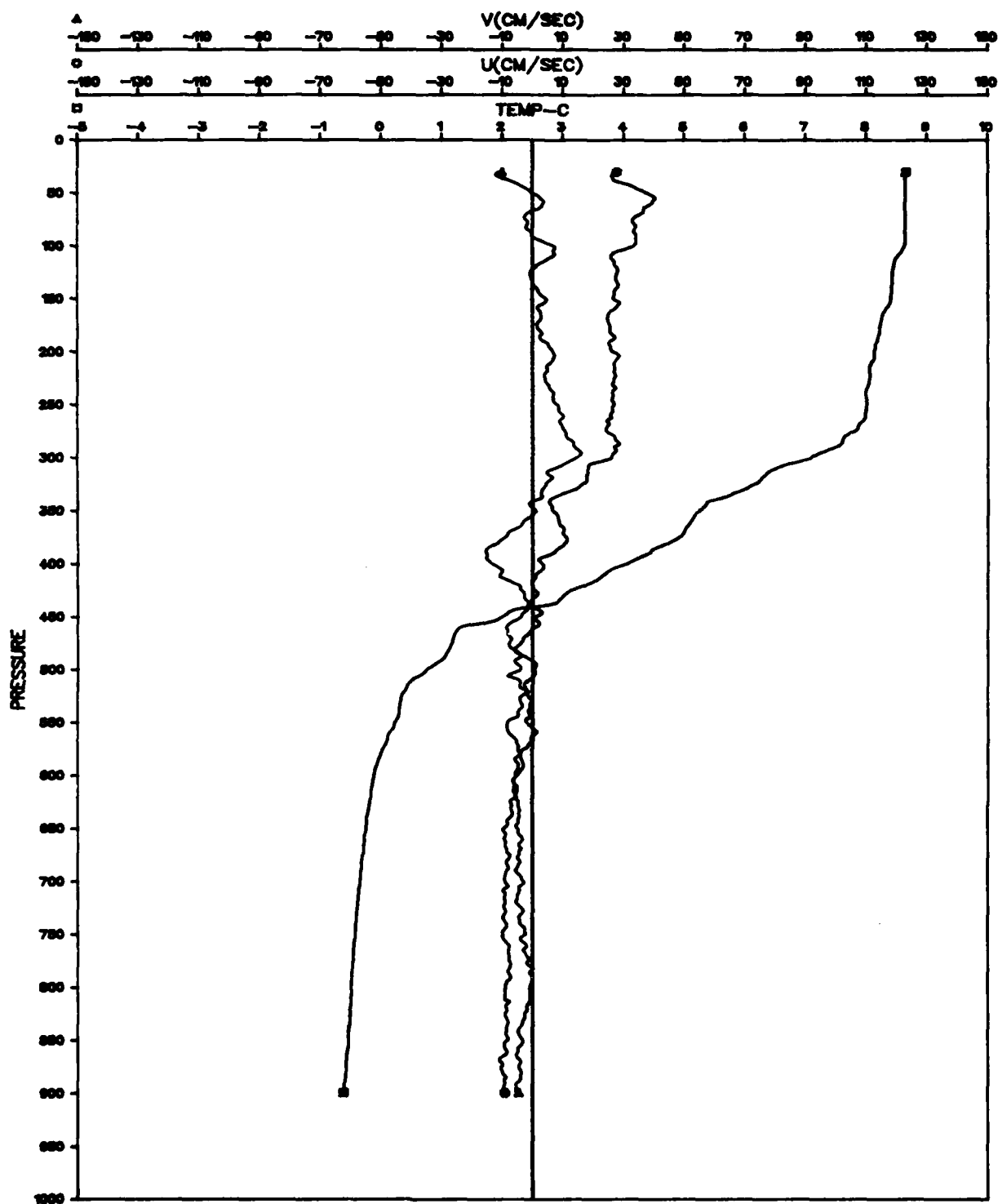


Figure A-29. File: KANE, Segment: C 548

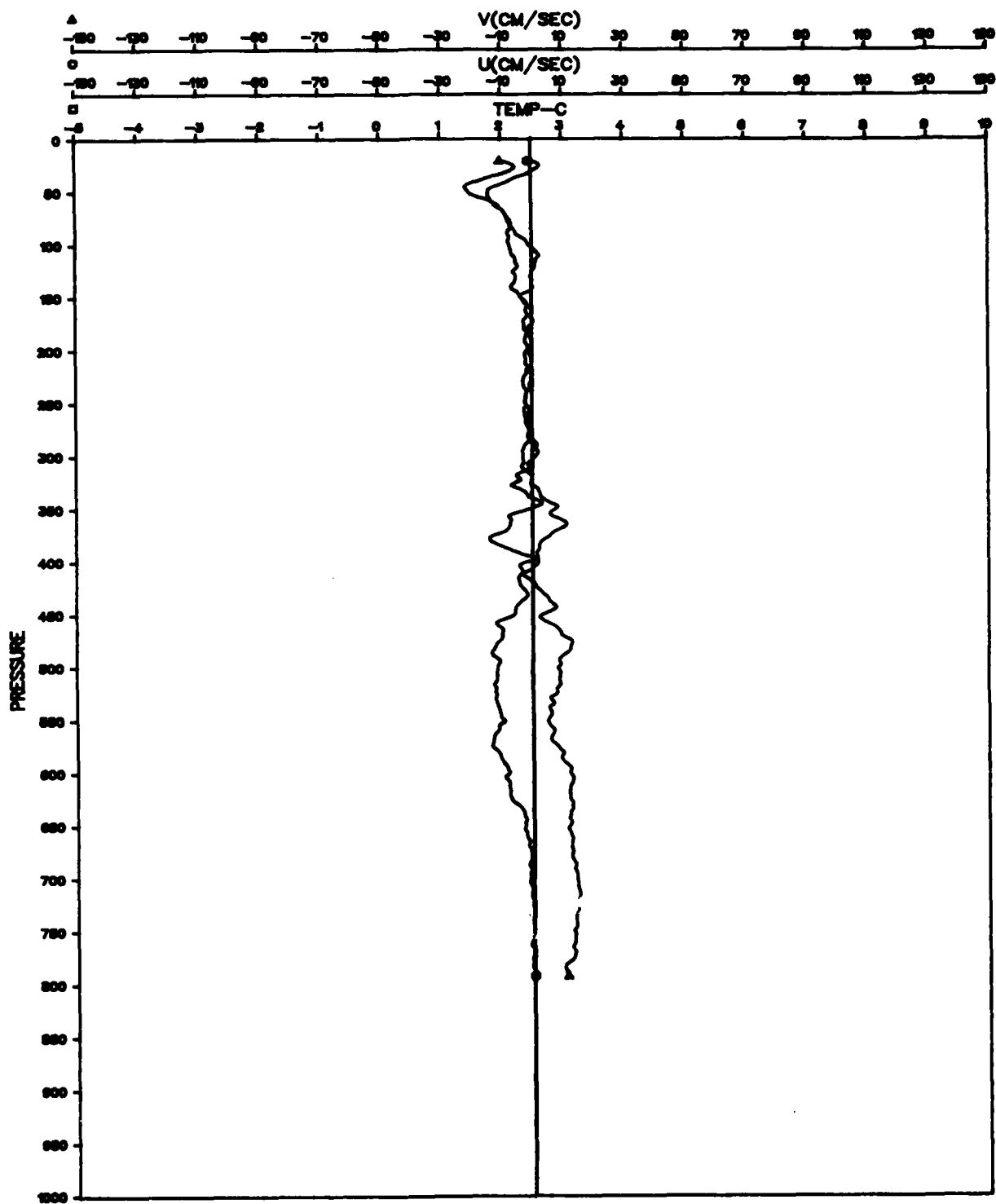


Figure A-30. File: KANE, Segment: C 549

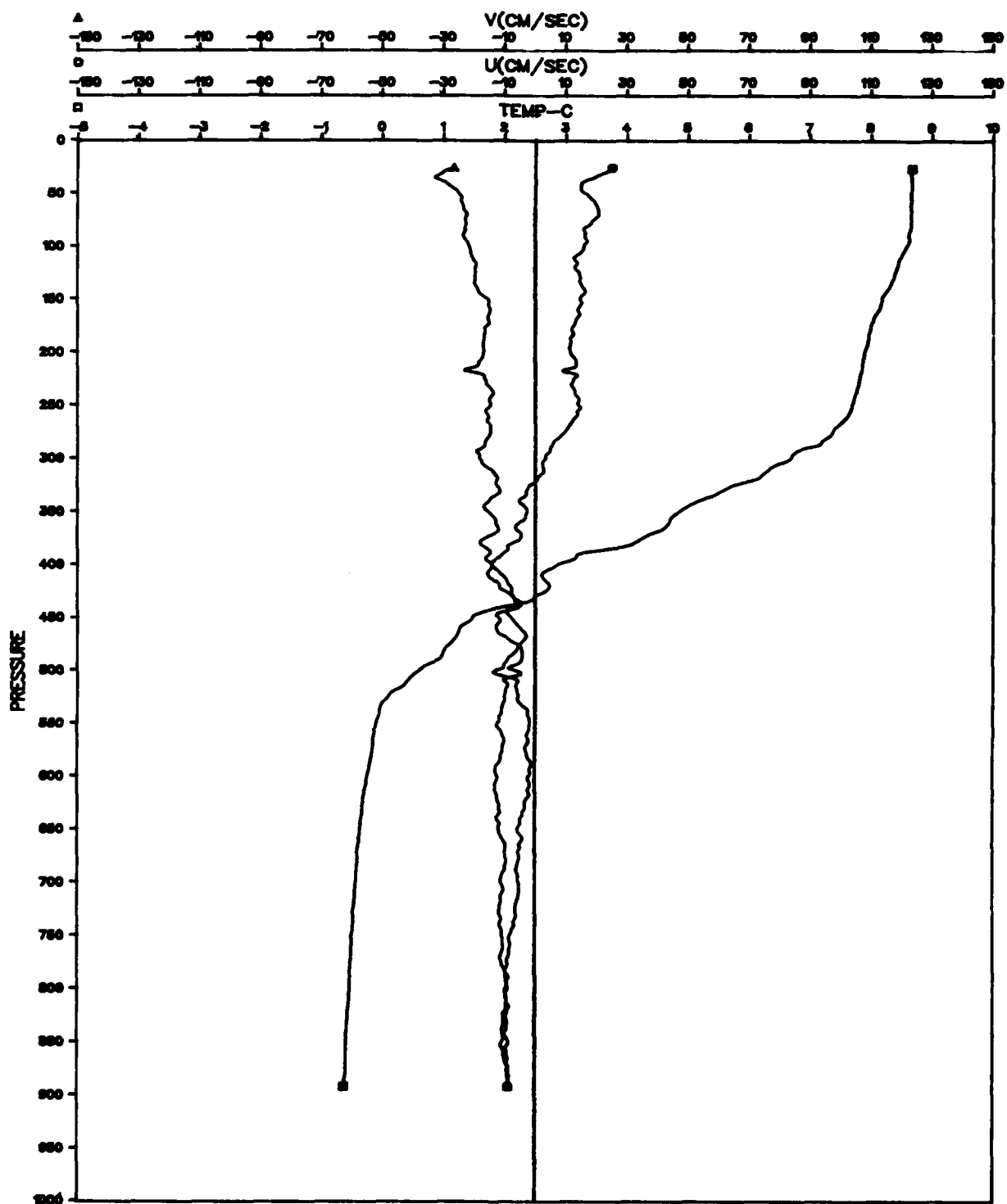


Figure A-31. File: KANE, Segment: C 550

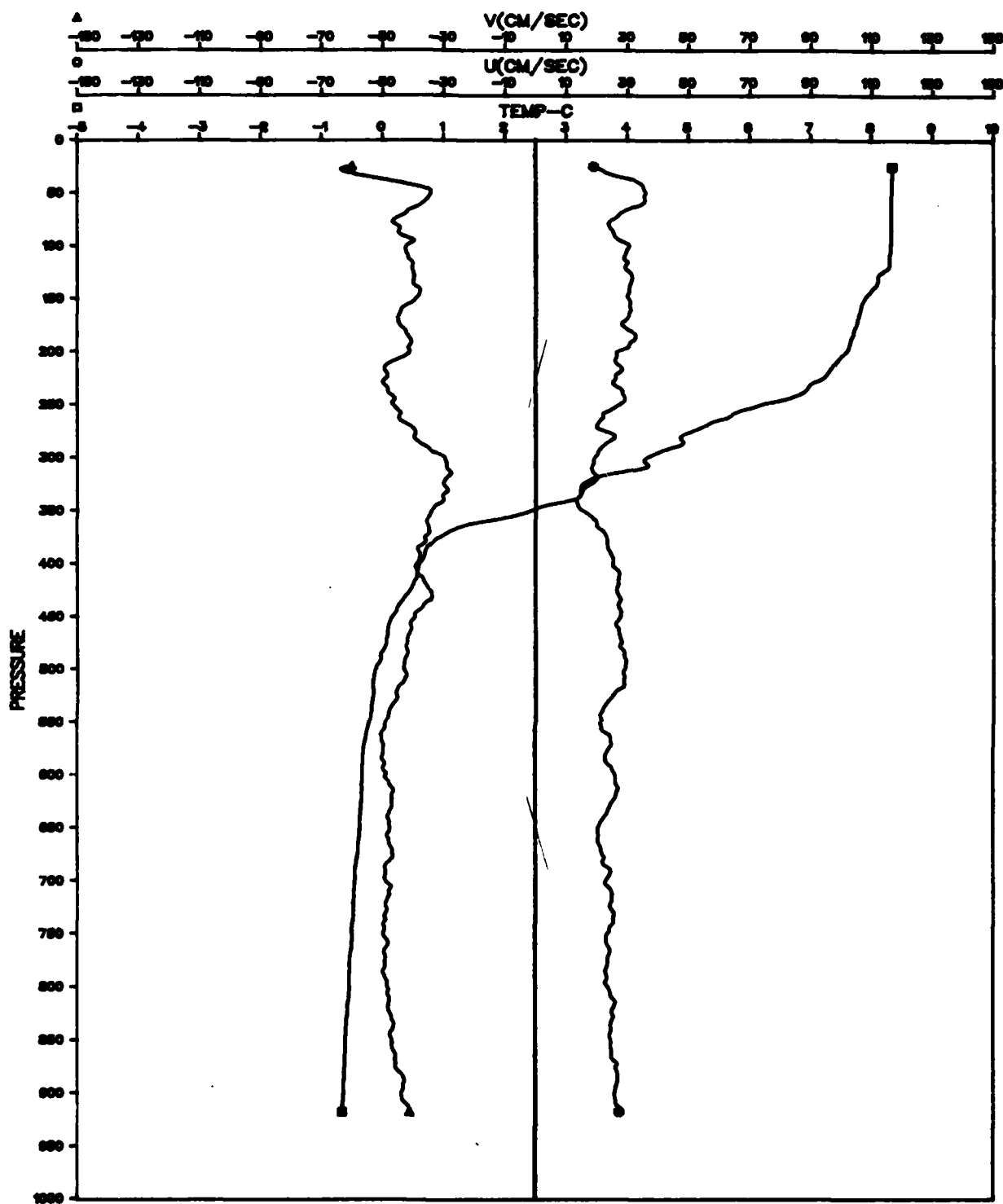


Figure A-32. File: KANE, Segment: C 551

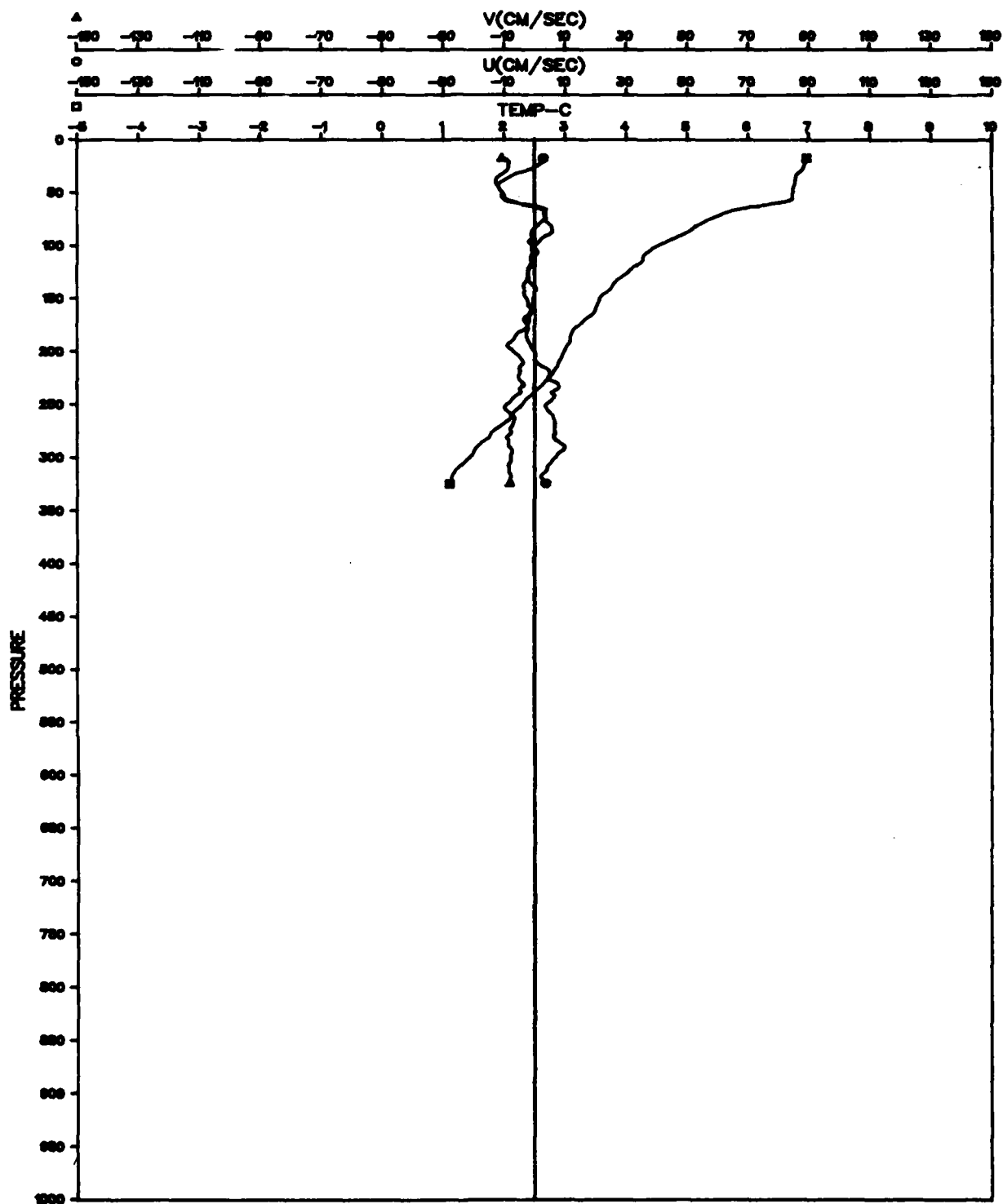


Figure A-33. File: KANE, Segment: C 556

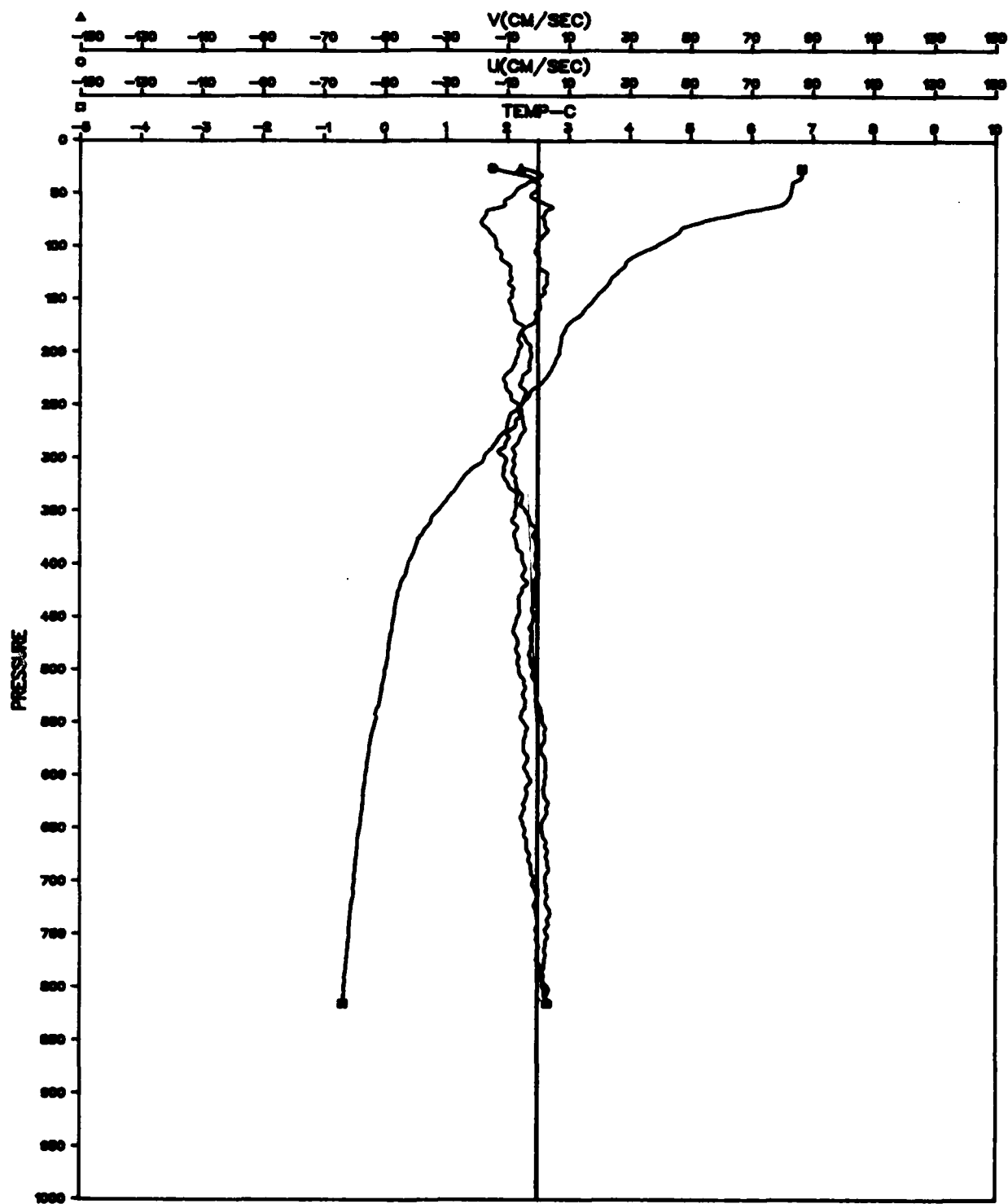


Figure A-34. File: KANE, Segment: C 558

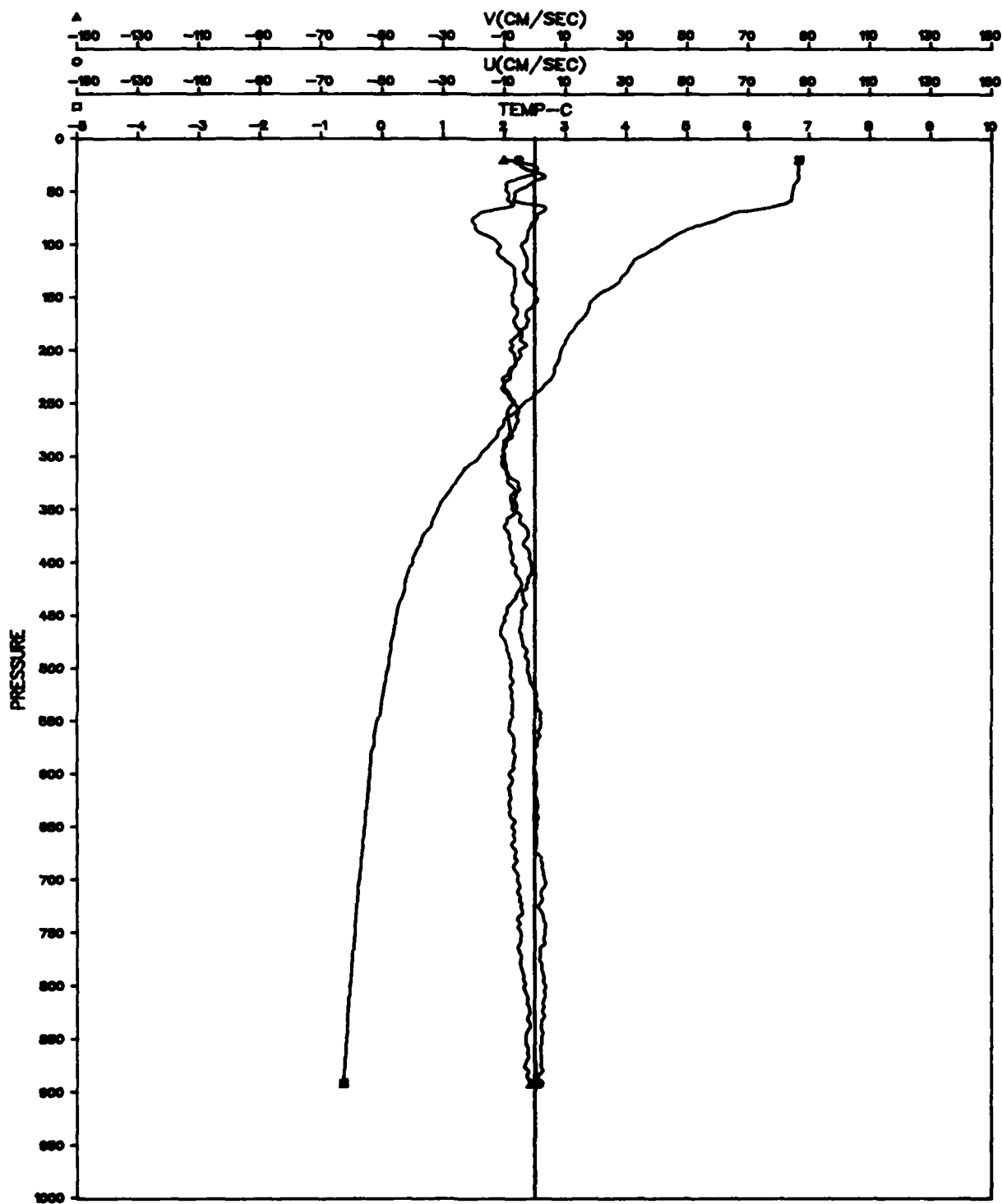


Figure A-35. File: KANE, Segment: C 559

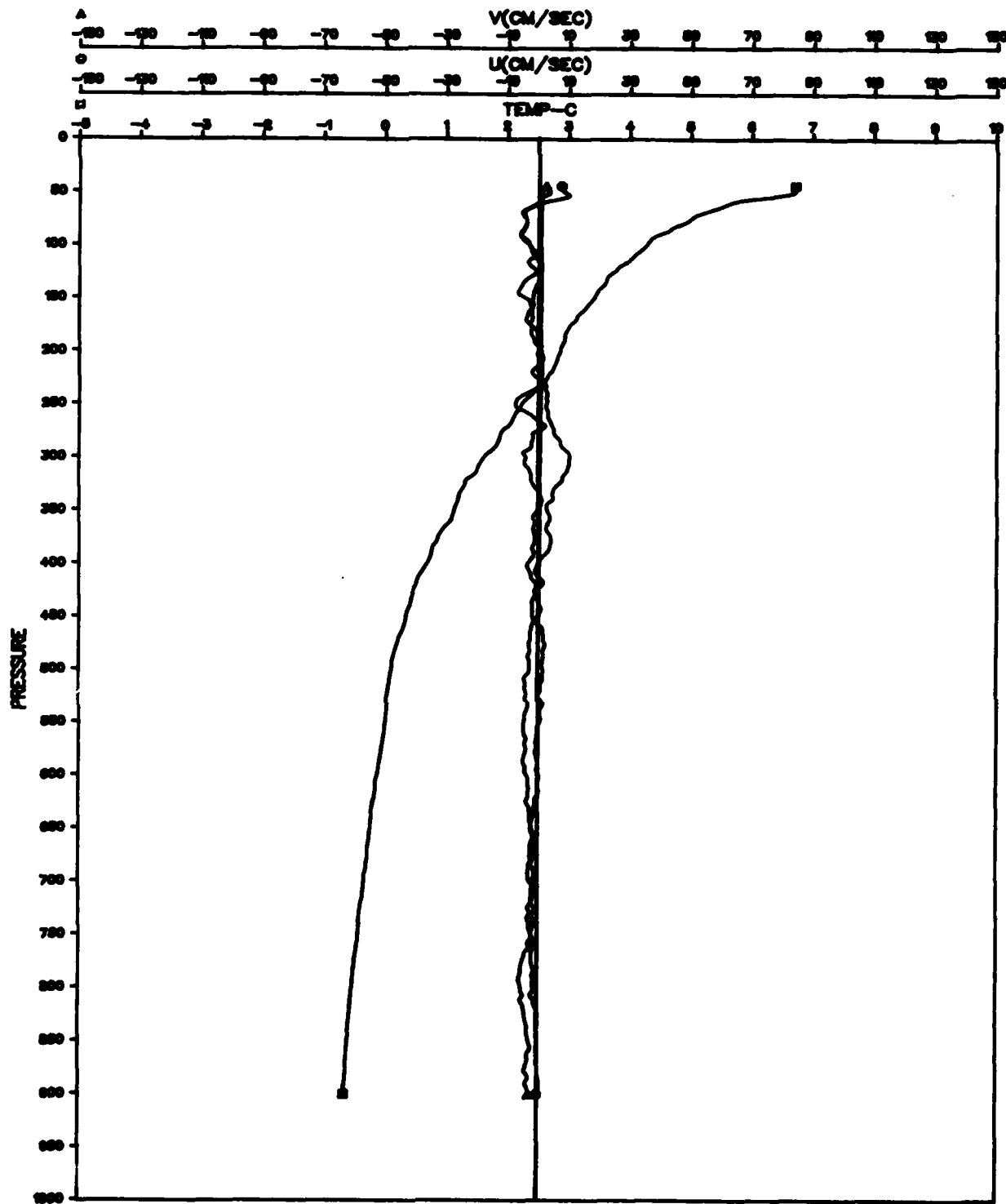


Figure A-36. File: KANE, Segment: C 560

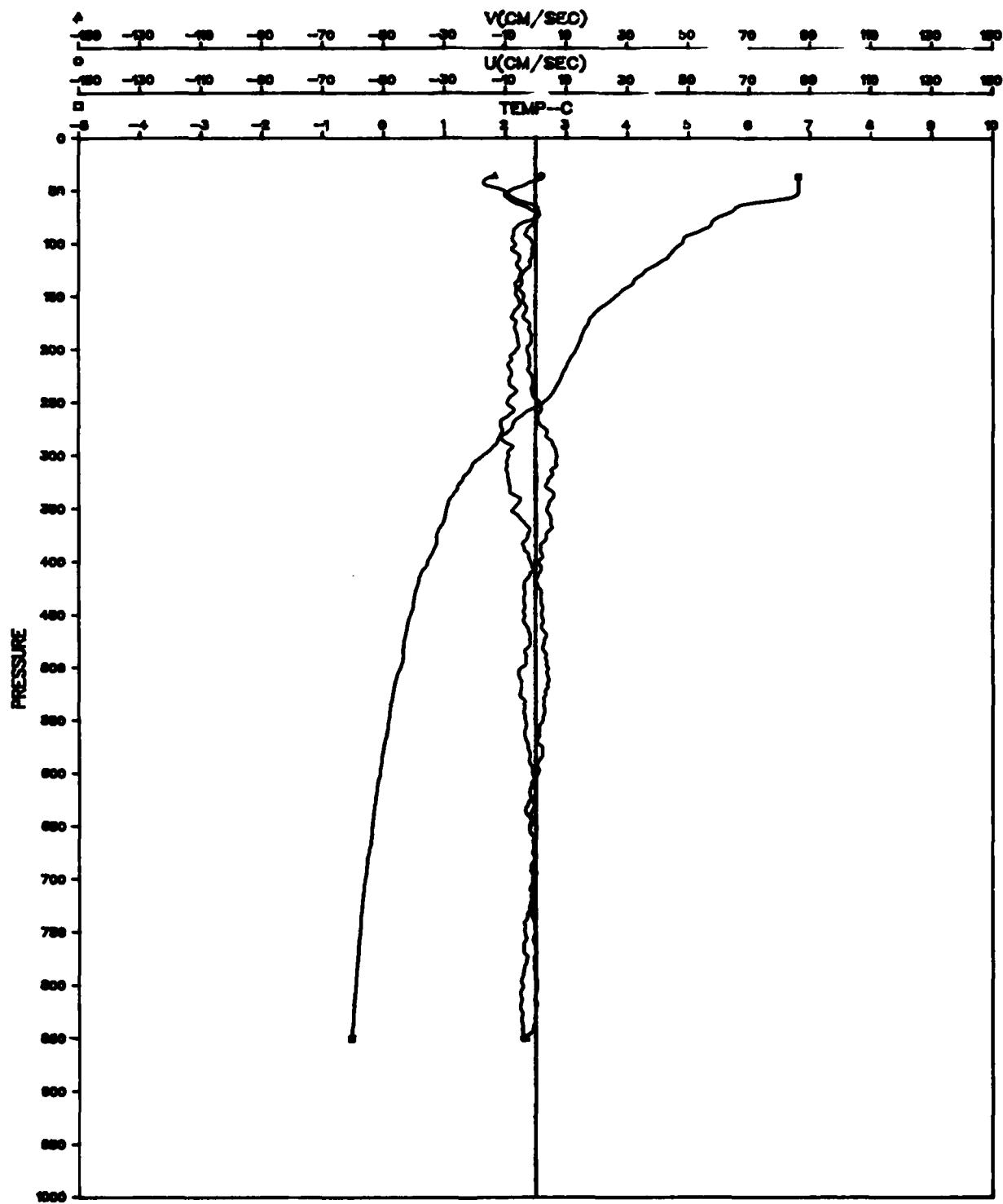


Figure A-37. File: KANE, Segment: C 561

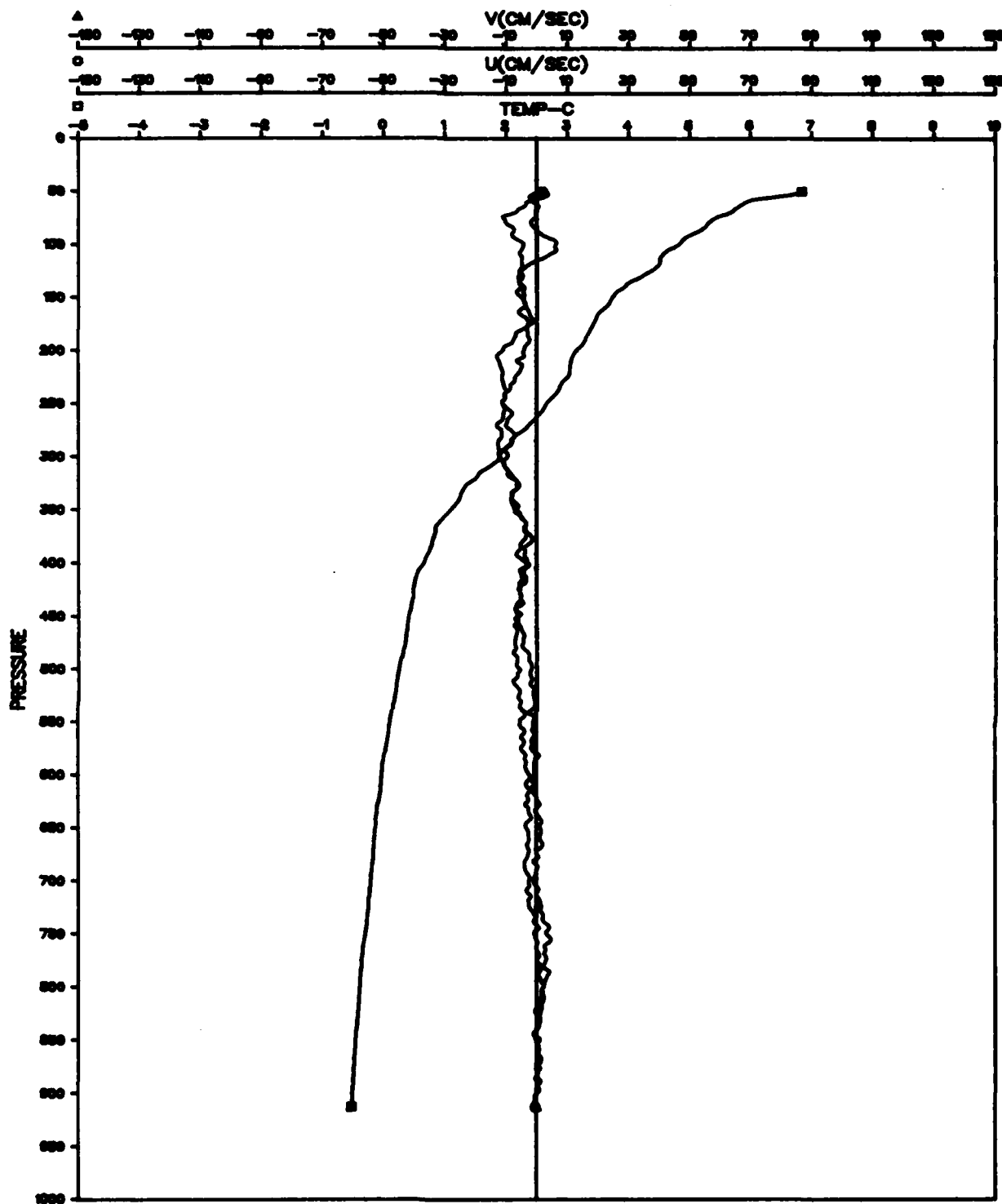


Figure A-38. File: KANE, Segment: C 562

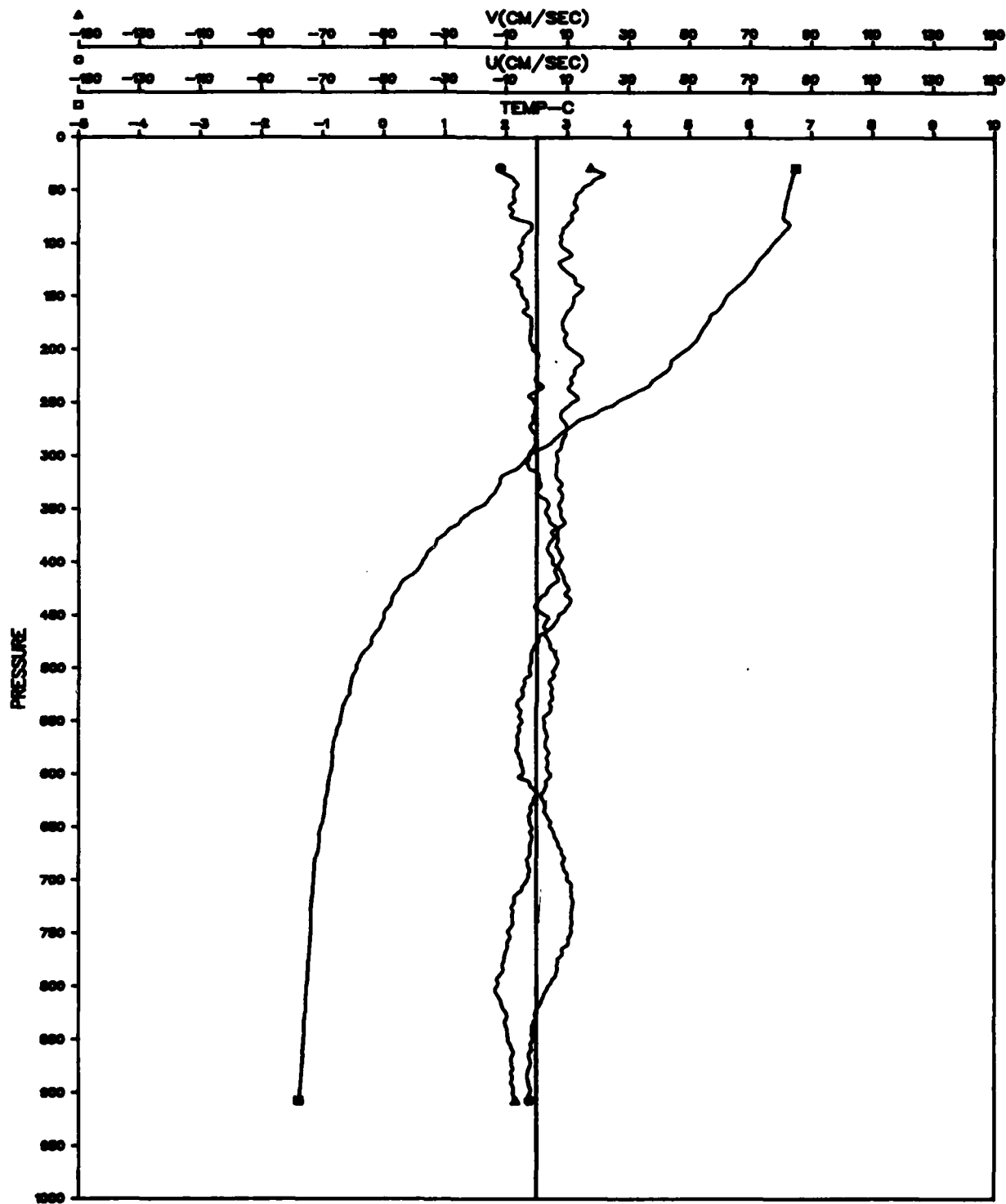


Figure A-39. File: KANE, Segment: C 563

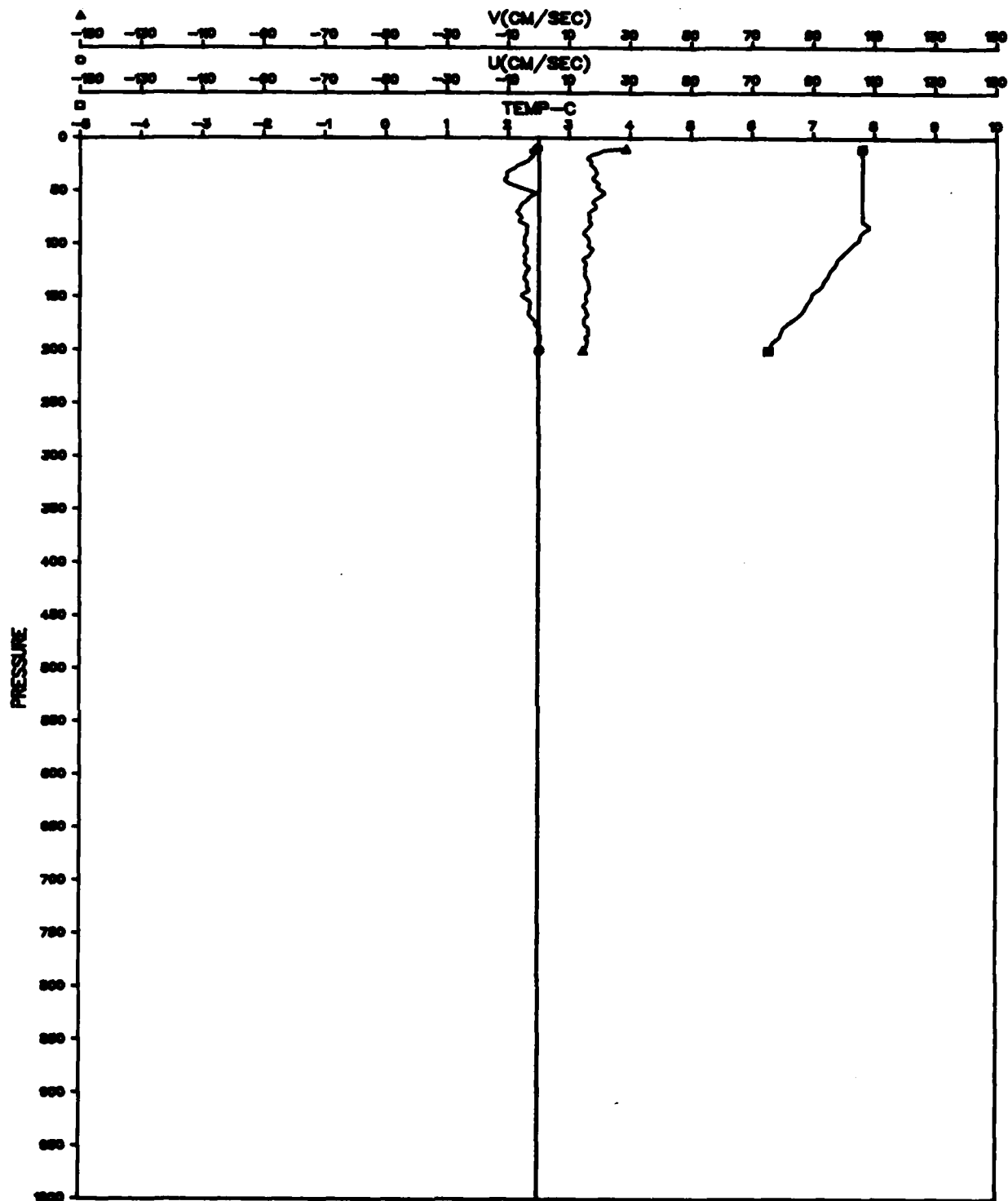


Figure A-40. File: KANE, Segment: C 564

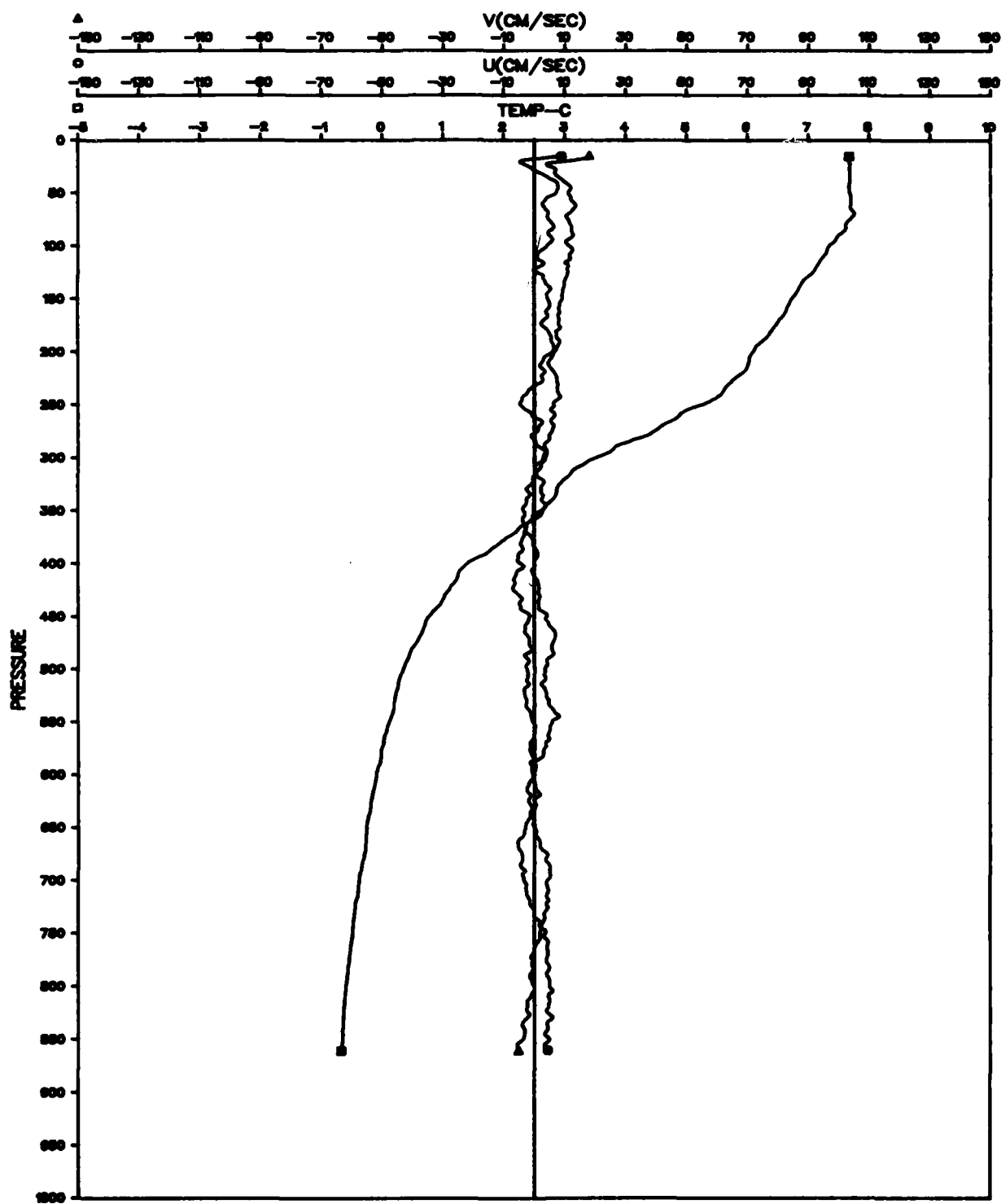


Figure A-41. File: KANE, Segment: C 566

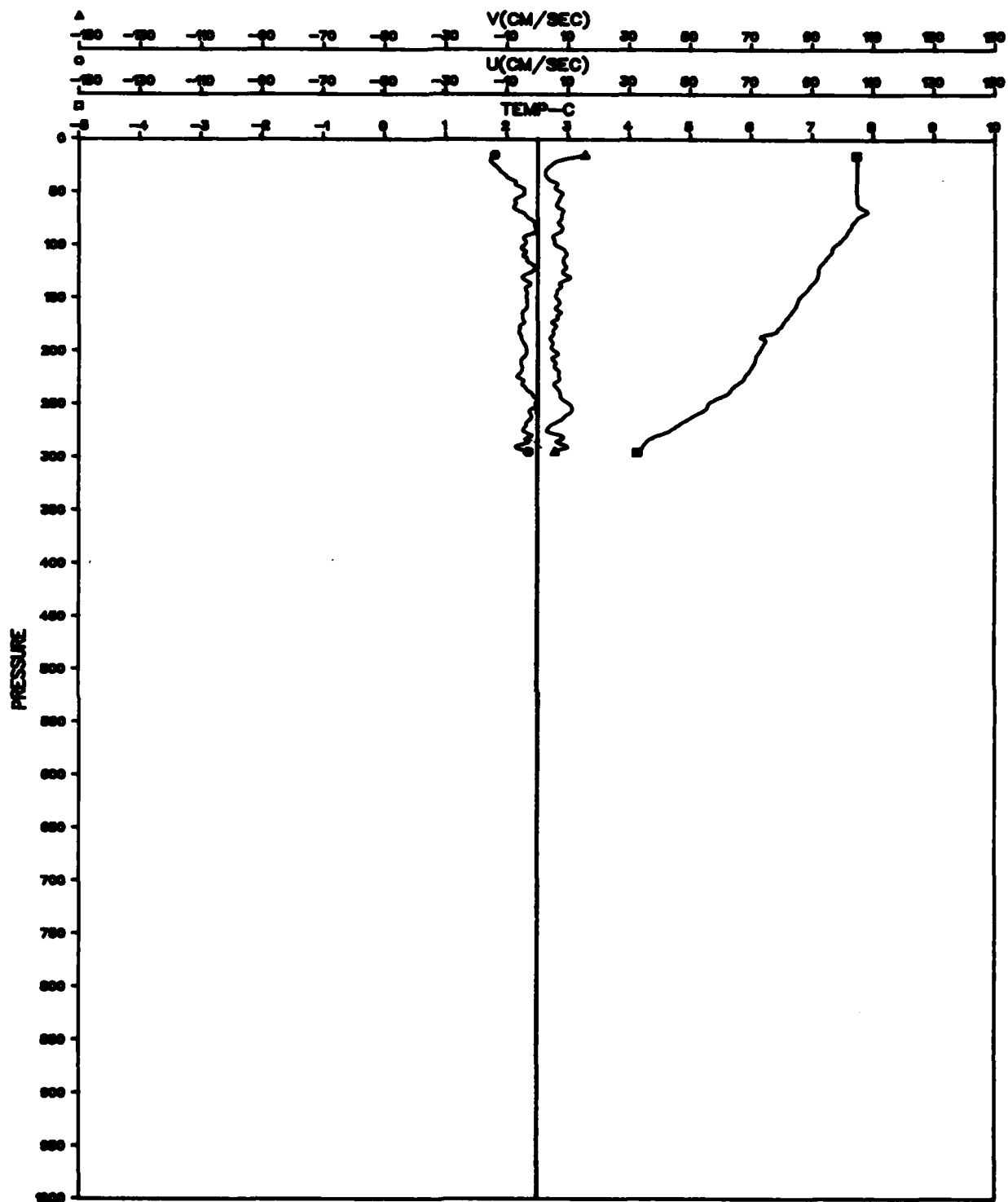


Figure A-42. File: KANE, Segment: C 567

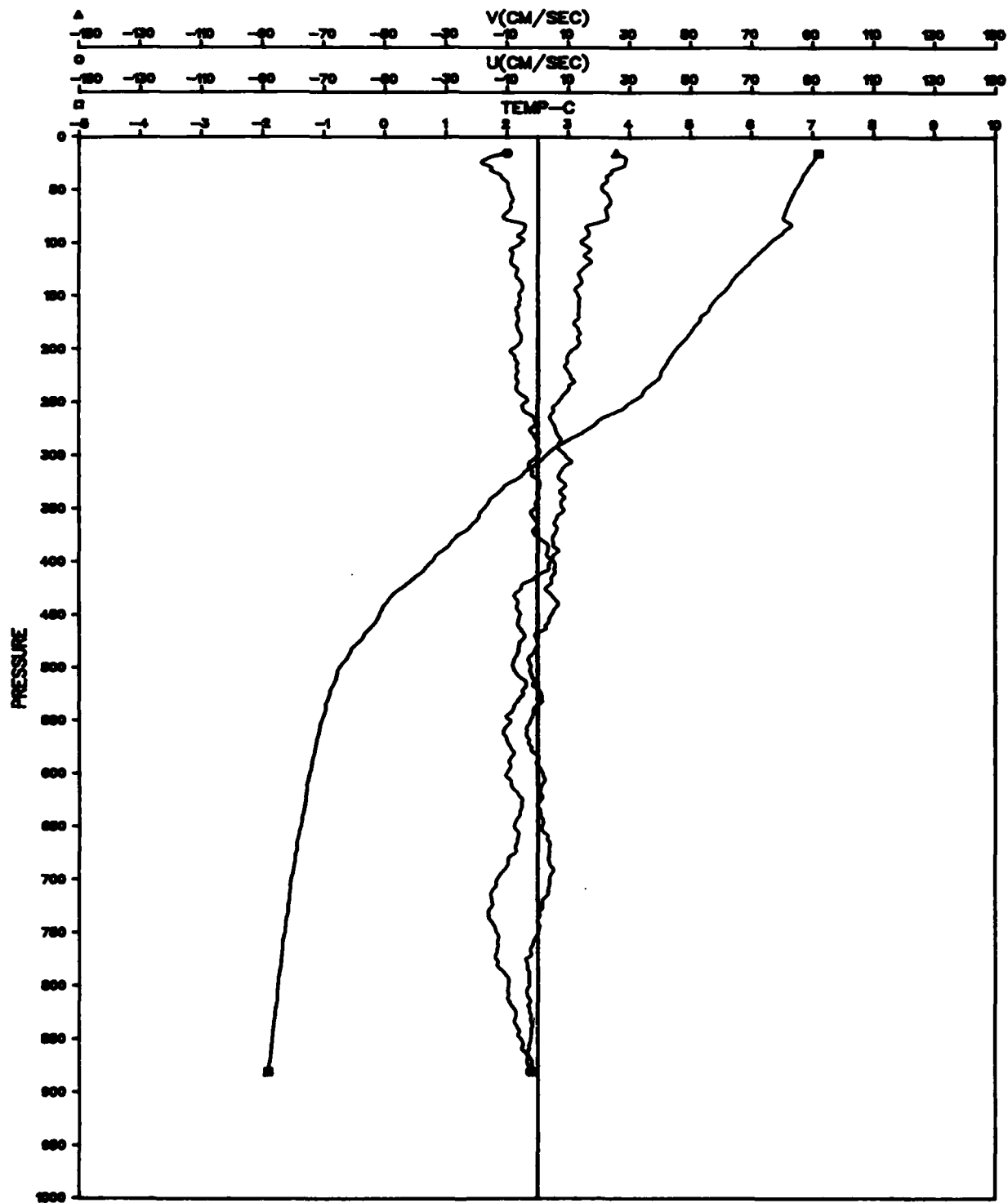


Figure A-43. File: KANE, Segment: C 568

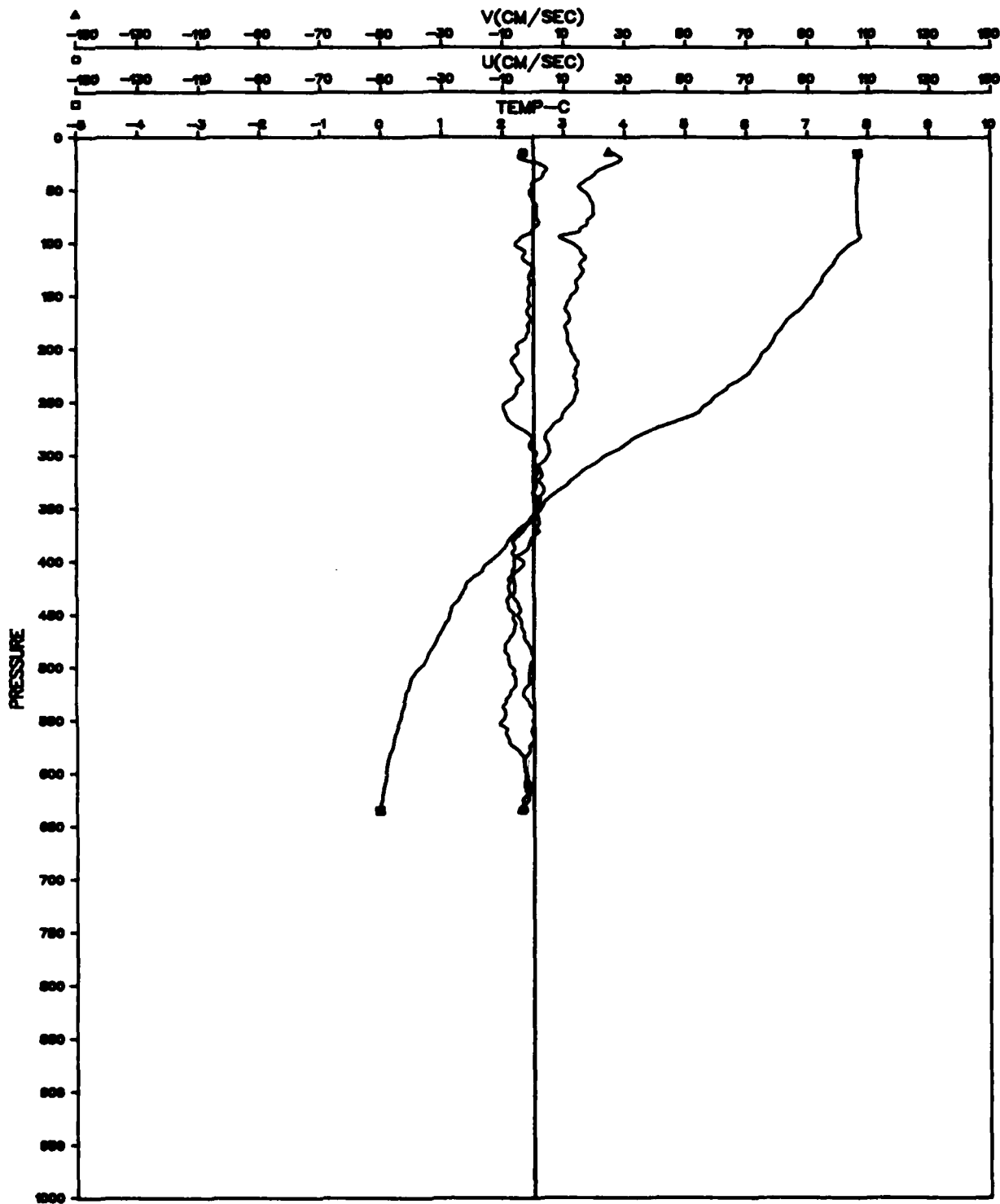


Figure A-44. File: KANE, Segment: C 569

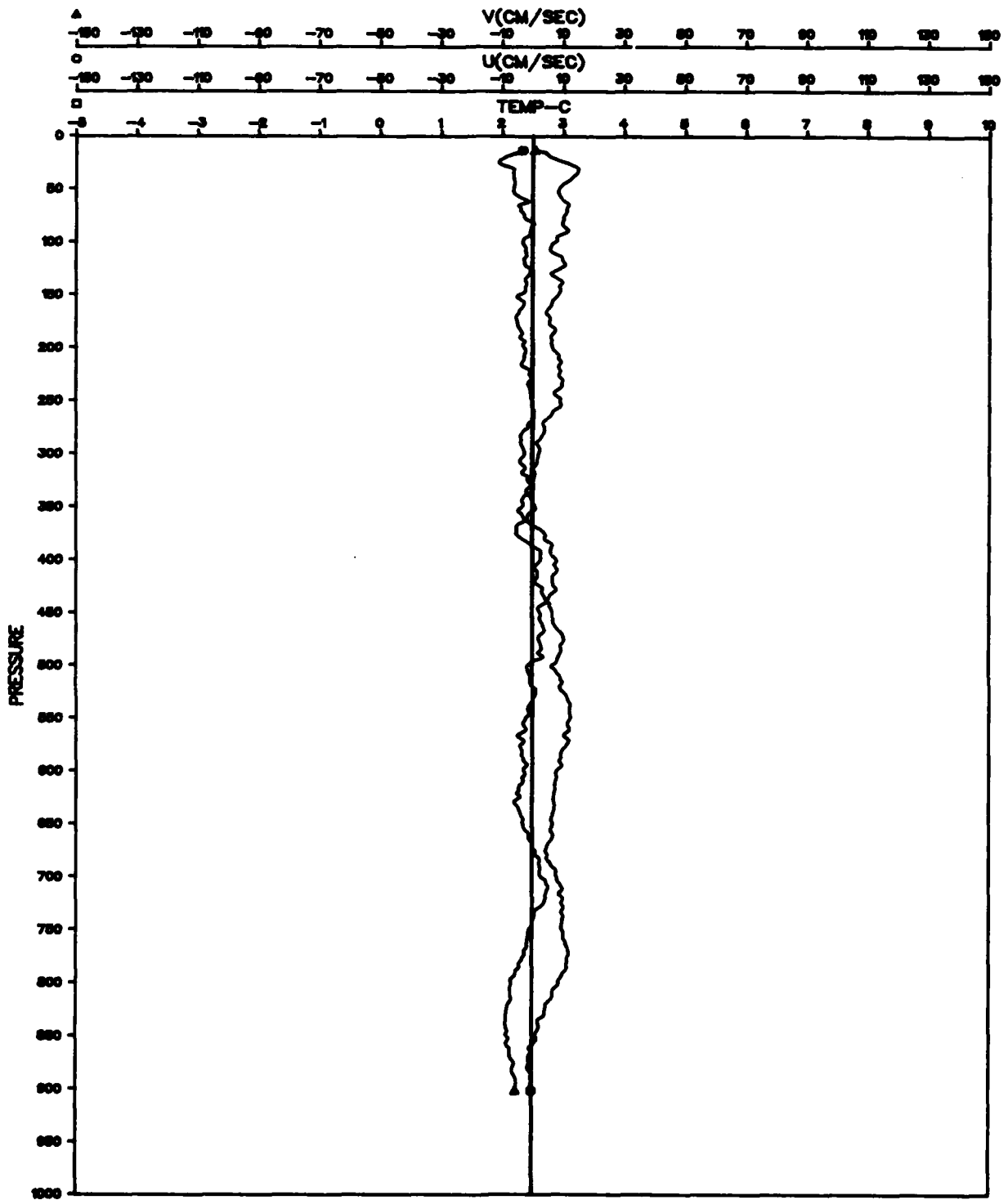


Figure A-45. File: KANE, Segment: C 571

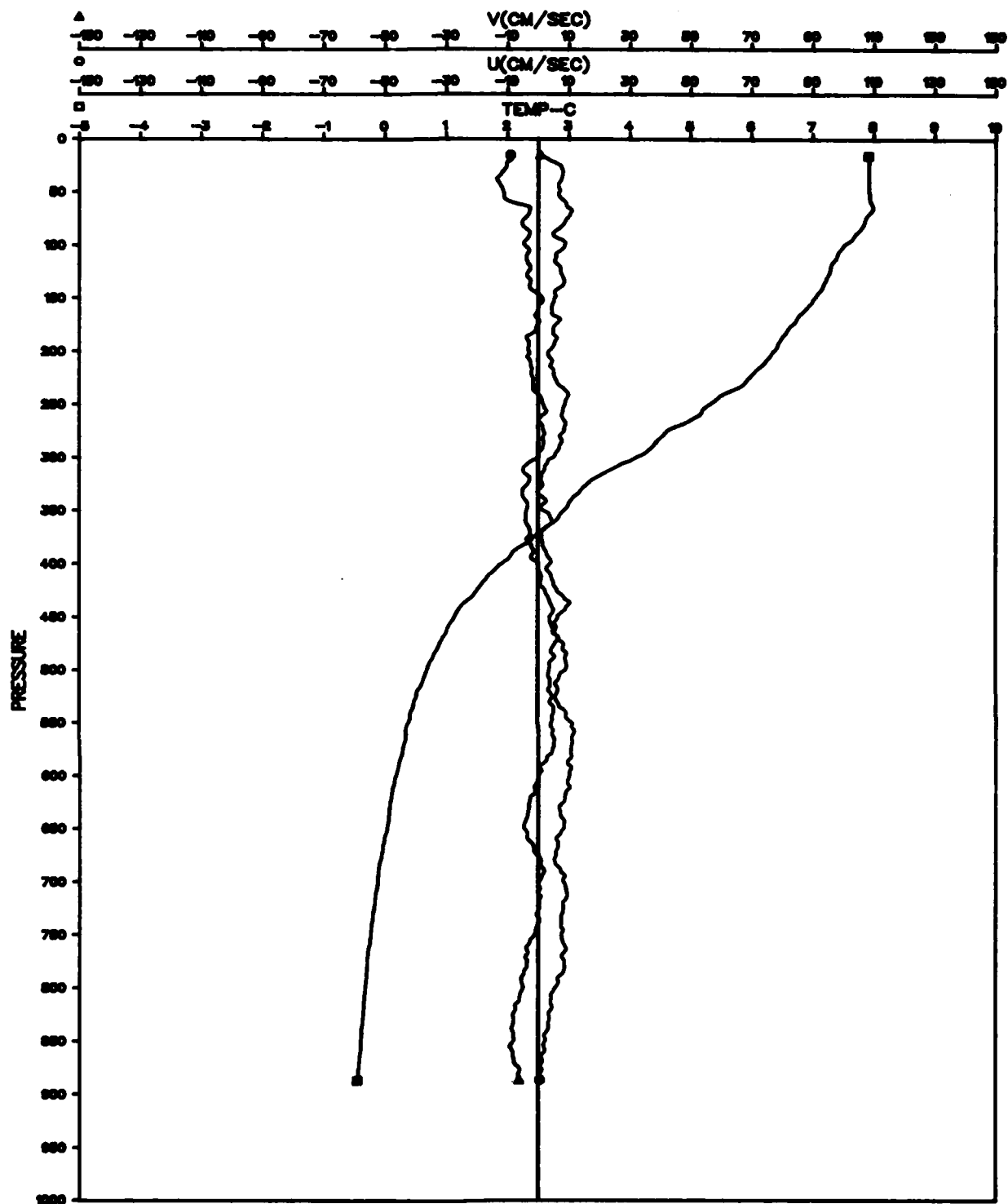


Figure A-46. File: KANE, Segment: C 573

**Appendix B:**  
**Selected CTD Vertical Profiles**  
**and T-S Diagrams**

**COMMENTS:**

**Low Pass Filtered 1 m Resolution Subsampling Interval 1 m**

**Data Truncated Below 1000 m:**

**Stations 117091**  
**122103**  
**123104**  
**126106**  
**130108**  
**130109**  
**132110**  
**136116**  
**137117**  
**175155**

**For Complete Profile See Teague, 1981**

**PRECEDING PAGE BLANK-NOT FILMED**

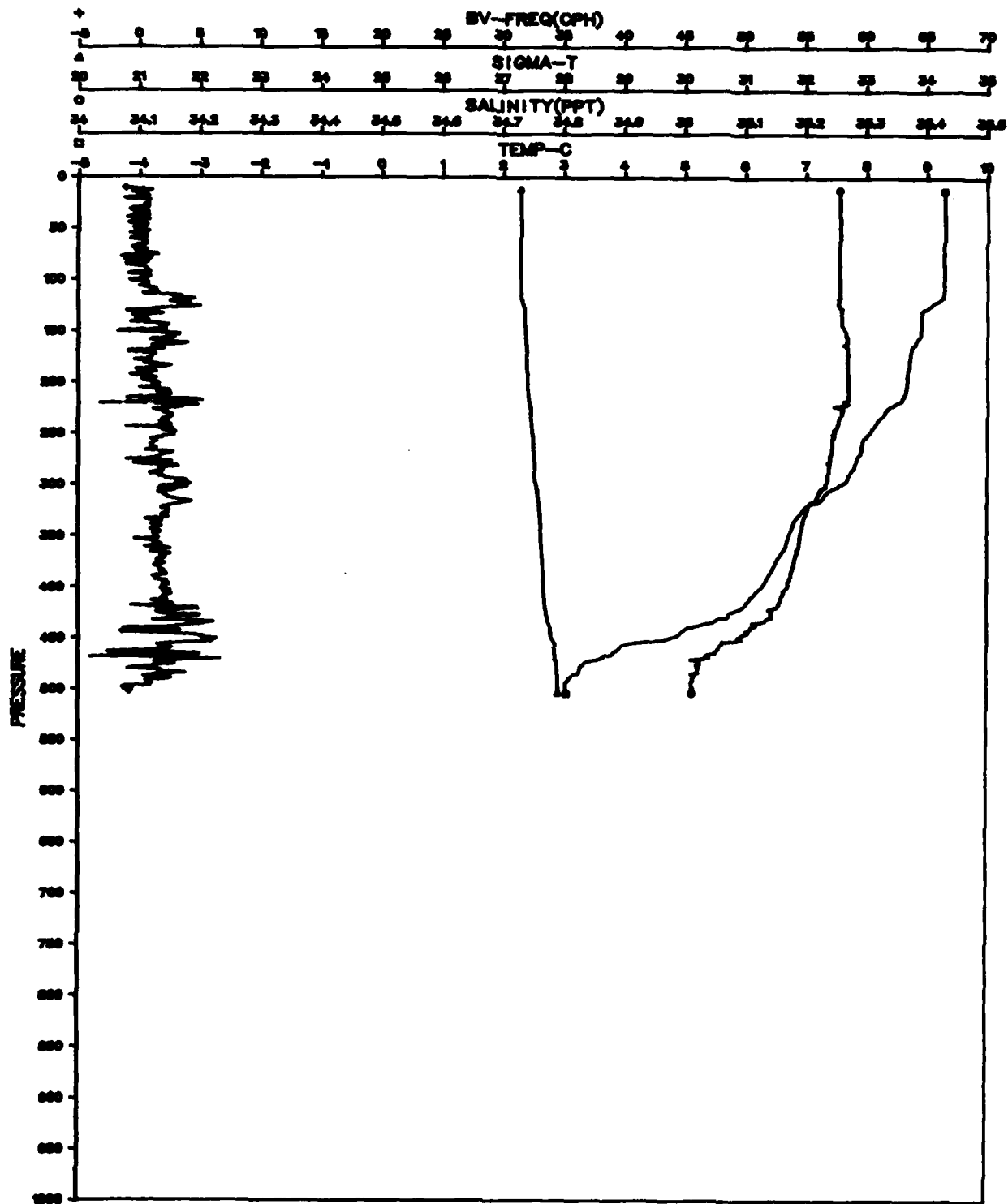


Figure B-1. File: 270980, Segment: 105073

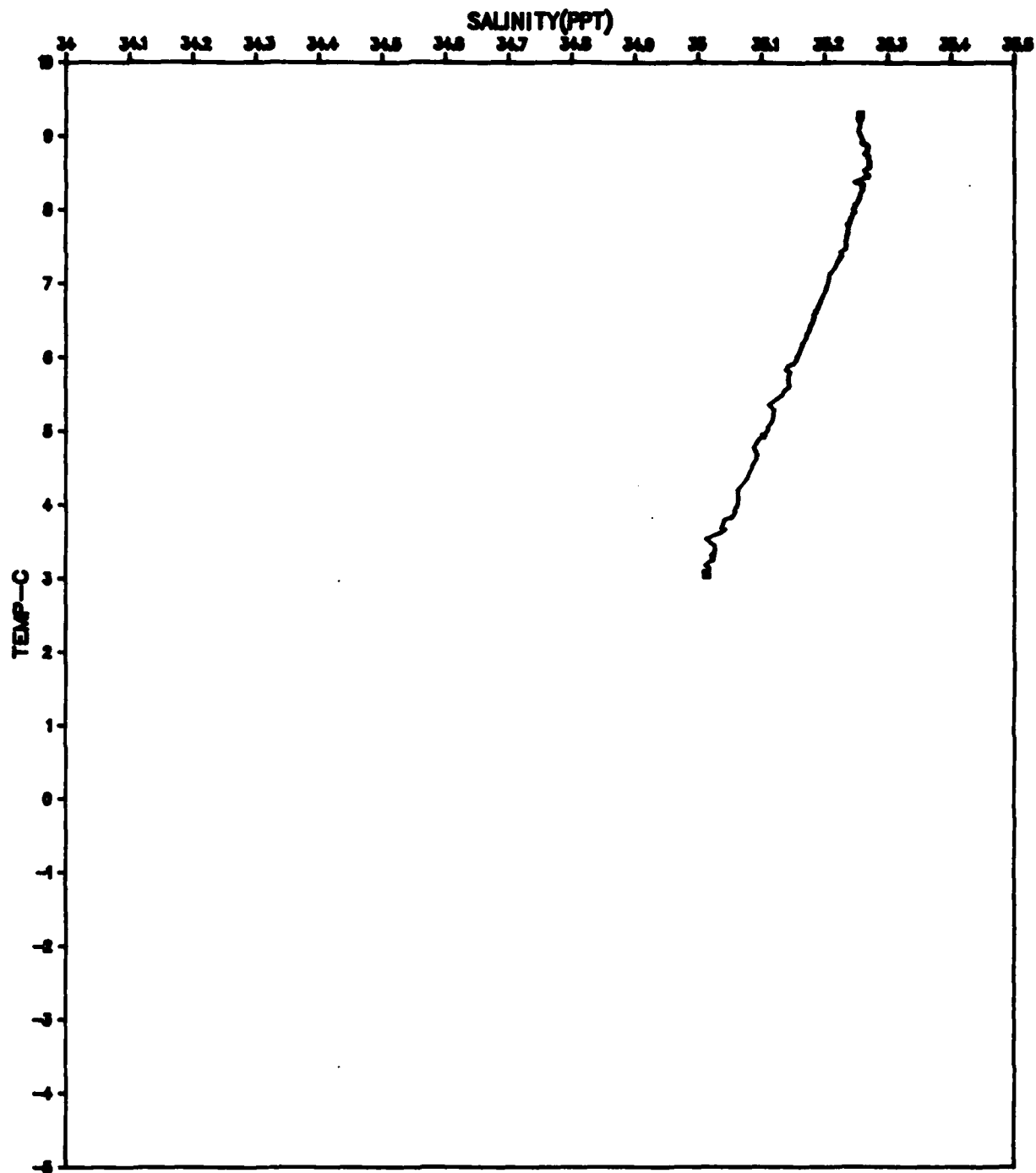


Figure B-2. File: 270980, Segment: 105073

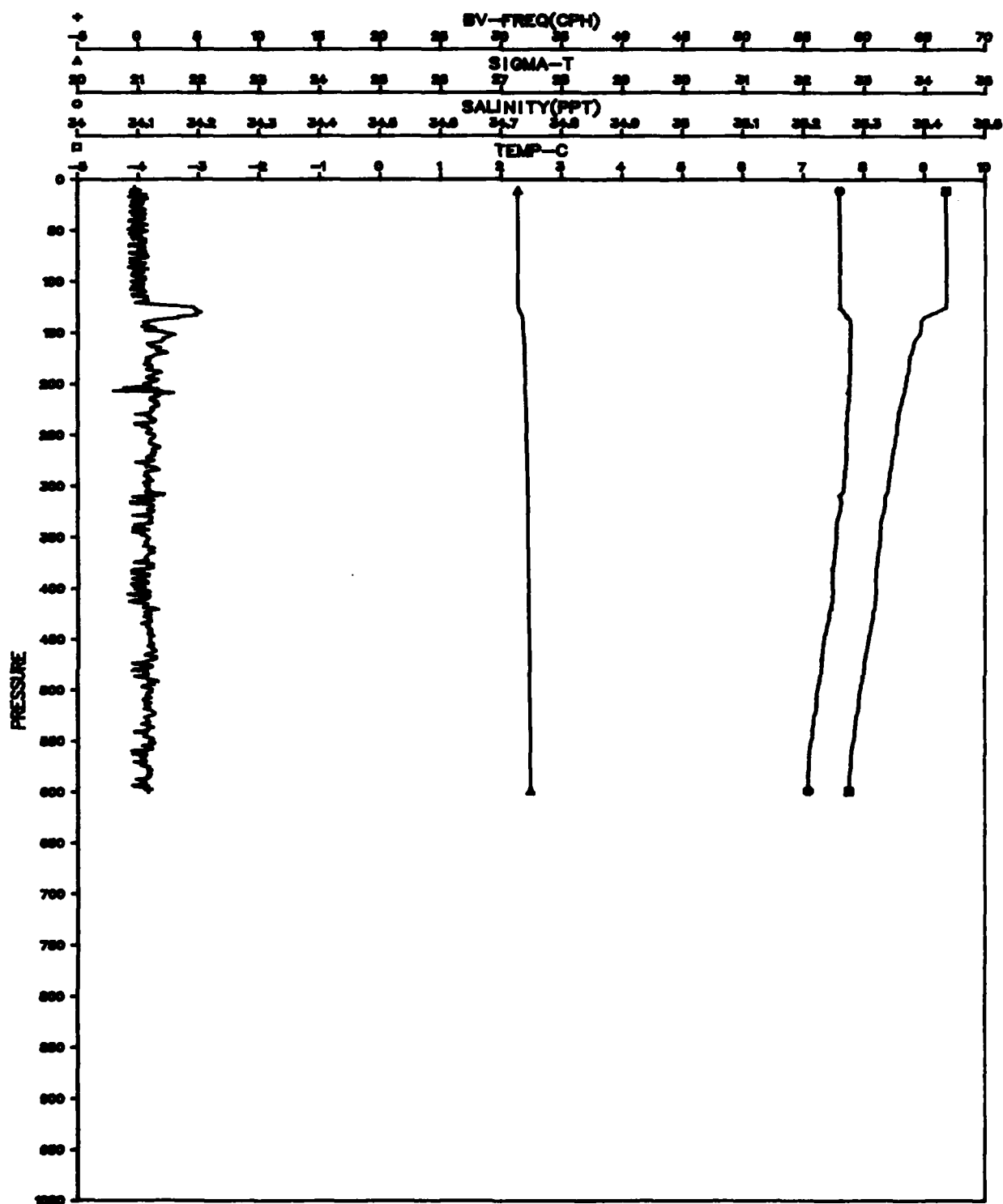


Figure B-3. File: 270980, Segment: 109076

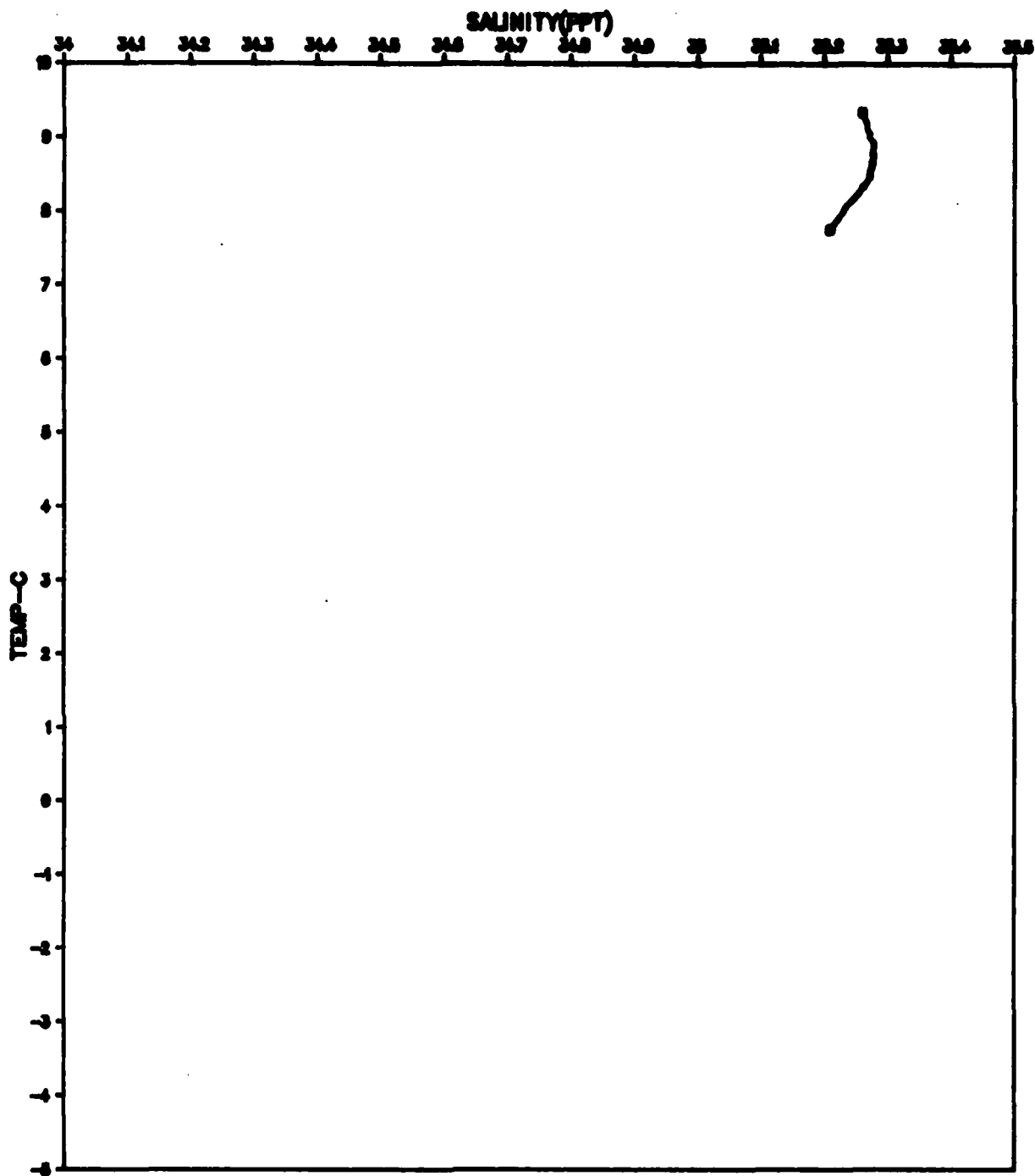


Figure B-4. File: 270980, Segment: 109076

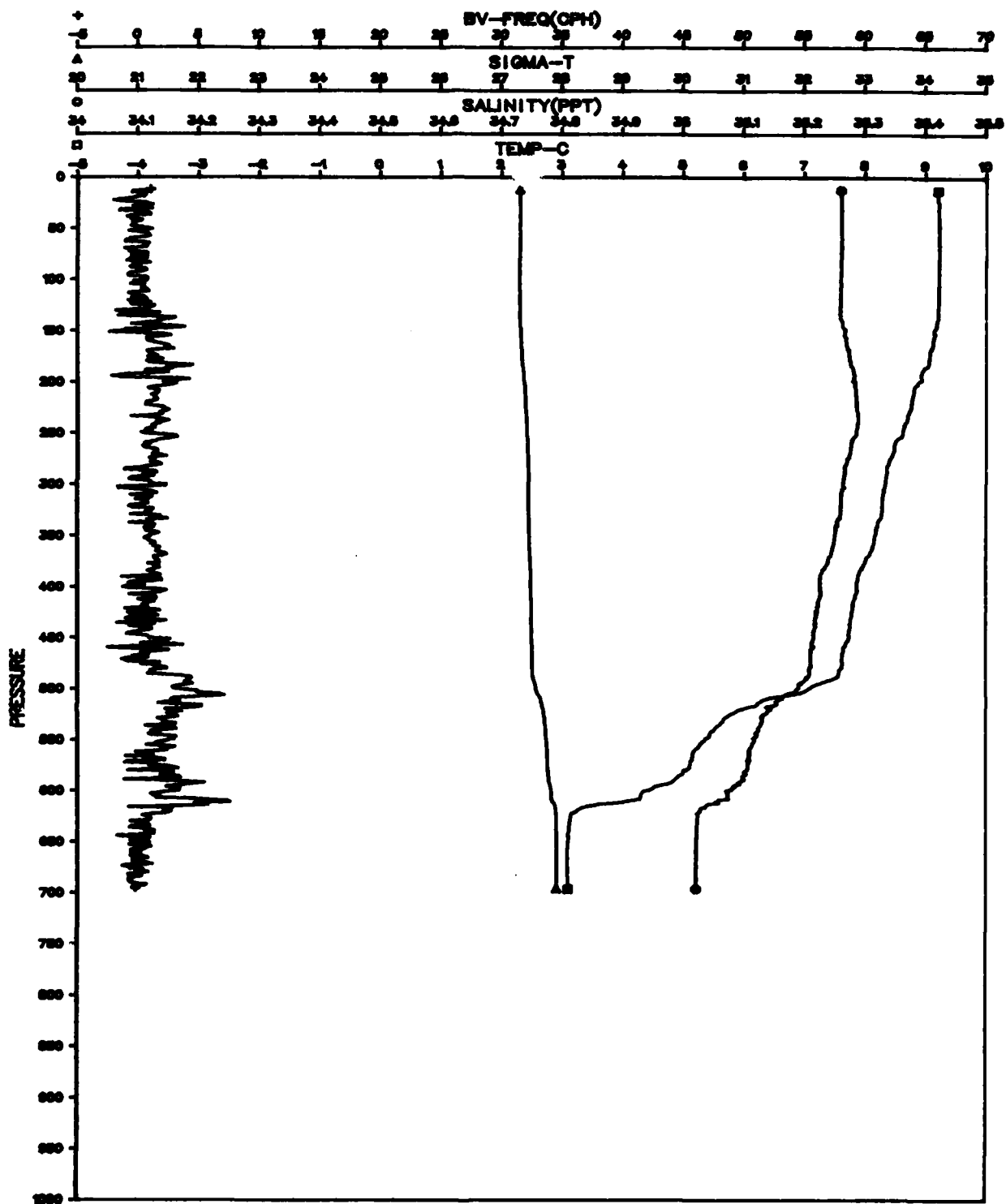


Figure B-5. File: 270980, Segment: 110084

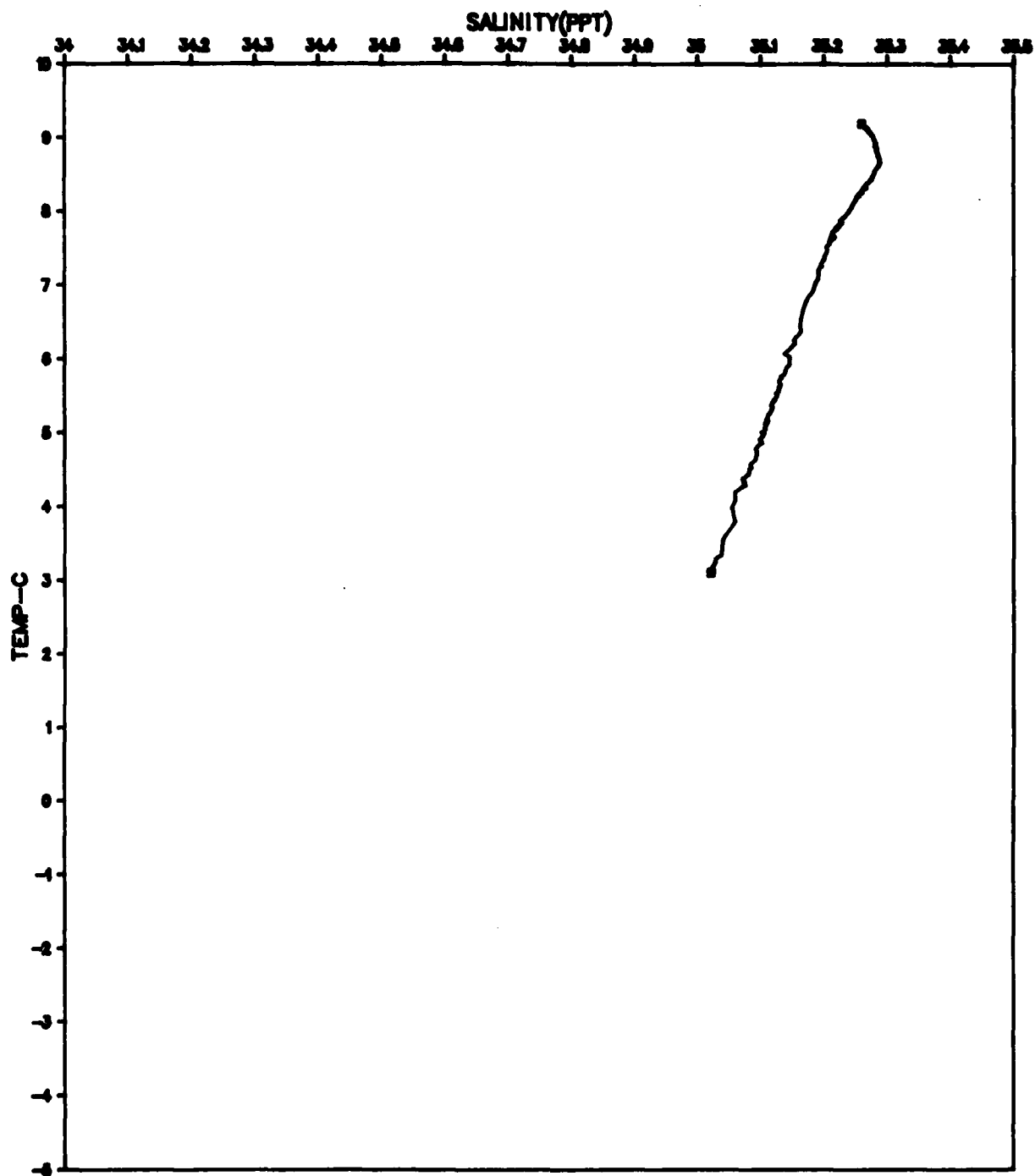


Figure B-6. File: 270980, Segment: 110084

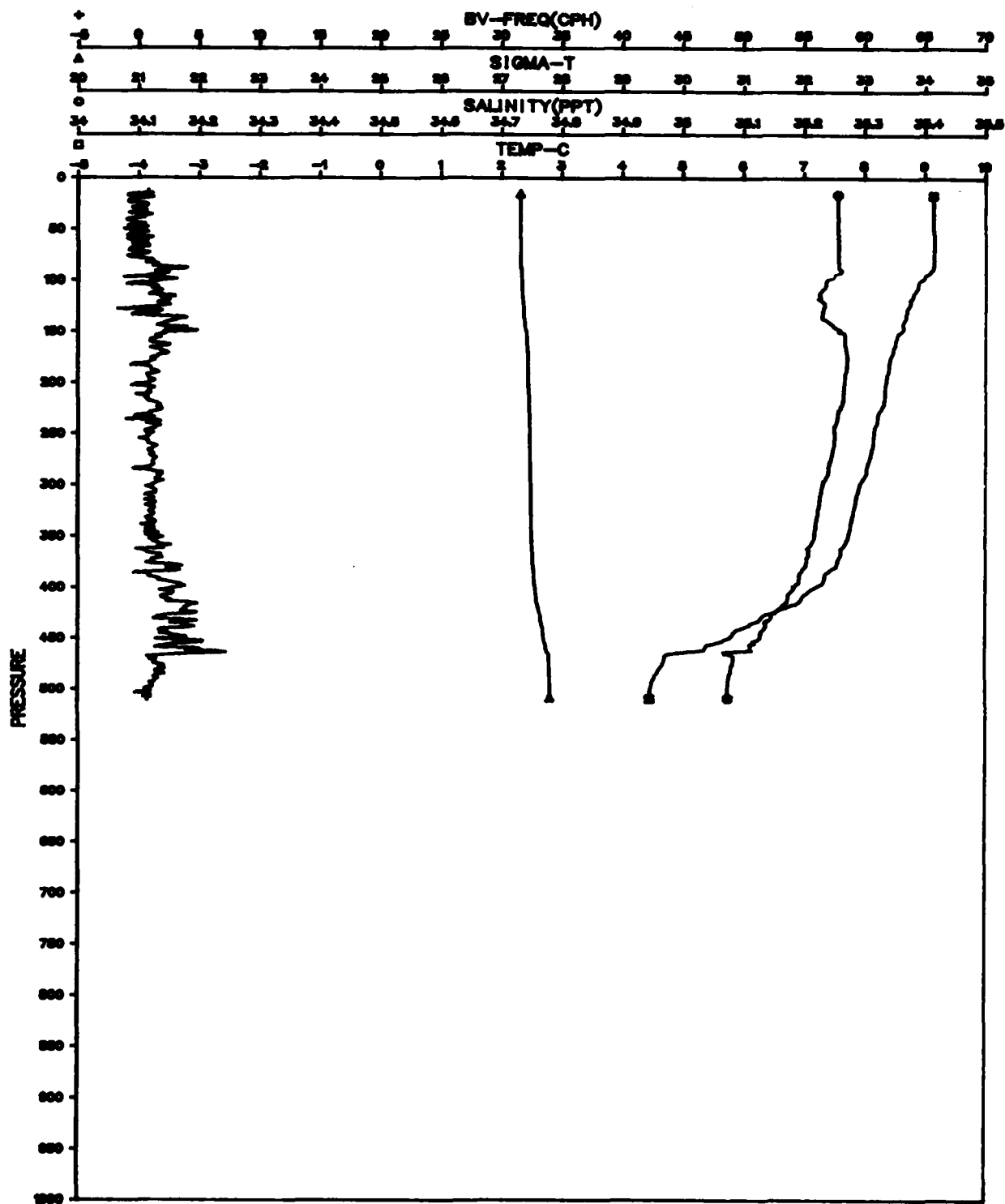


Figure B-7. File: 270980, Segment: 111085

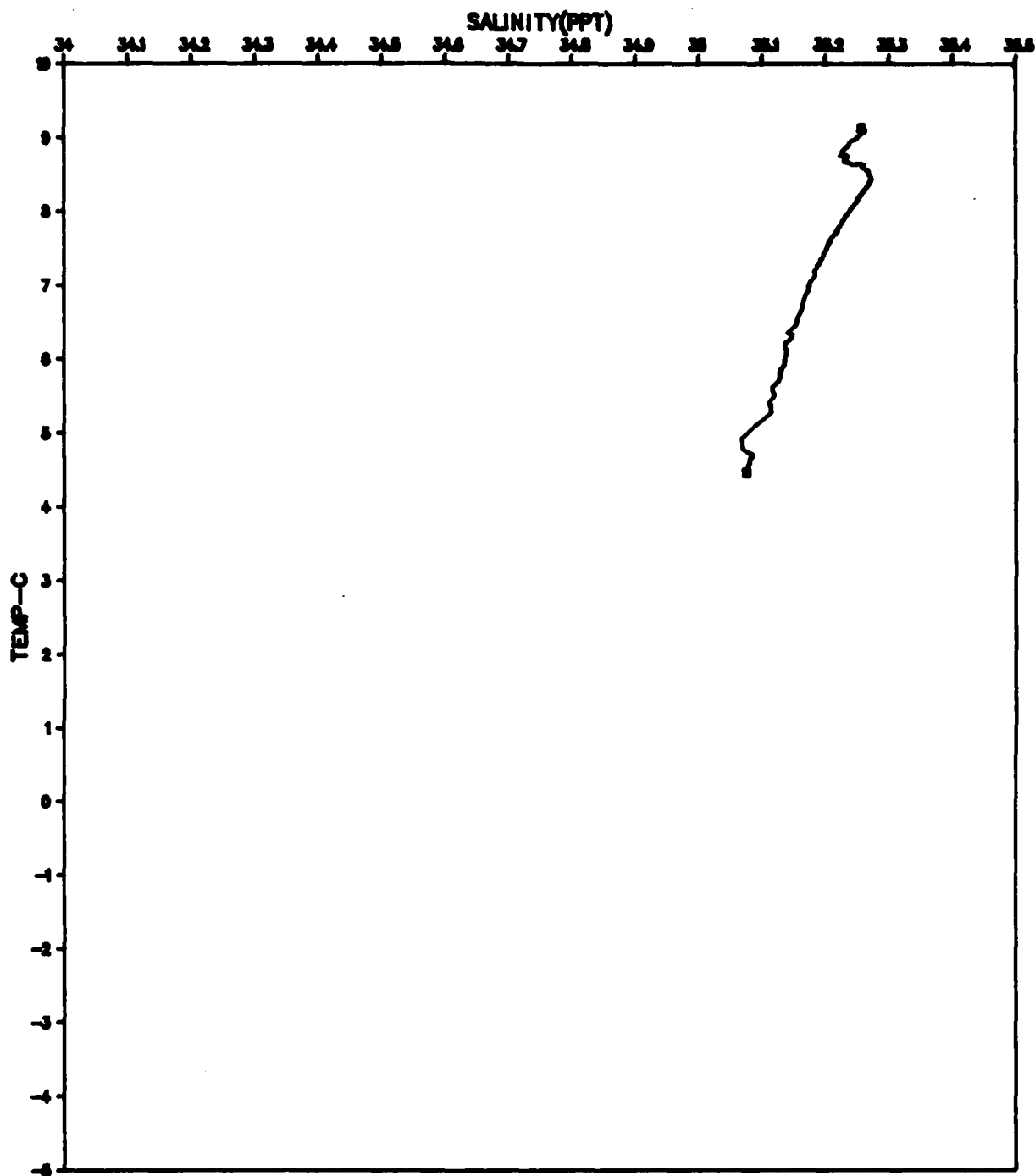


Figure B-8. File: 270980, Segment: 111085

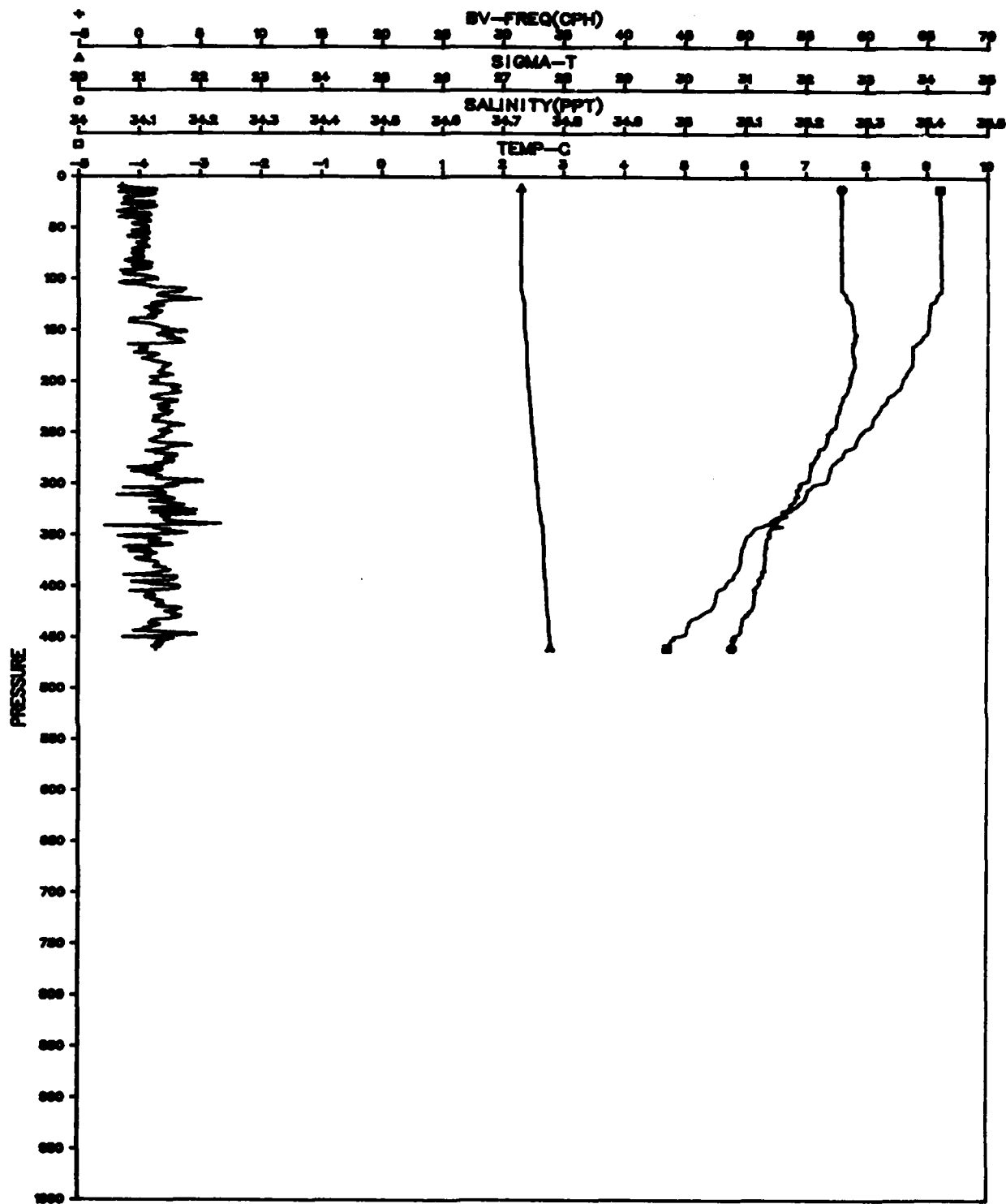


Figure B-9. File: 270980, Segment: 112086

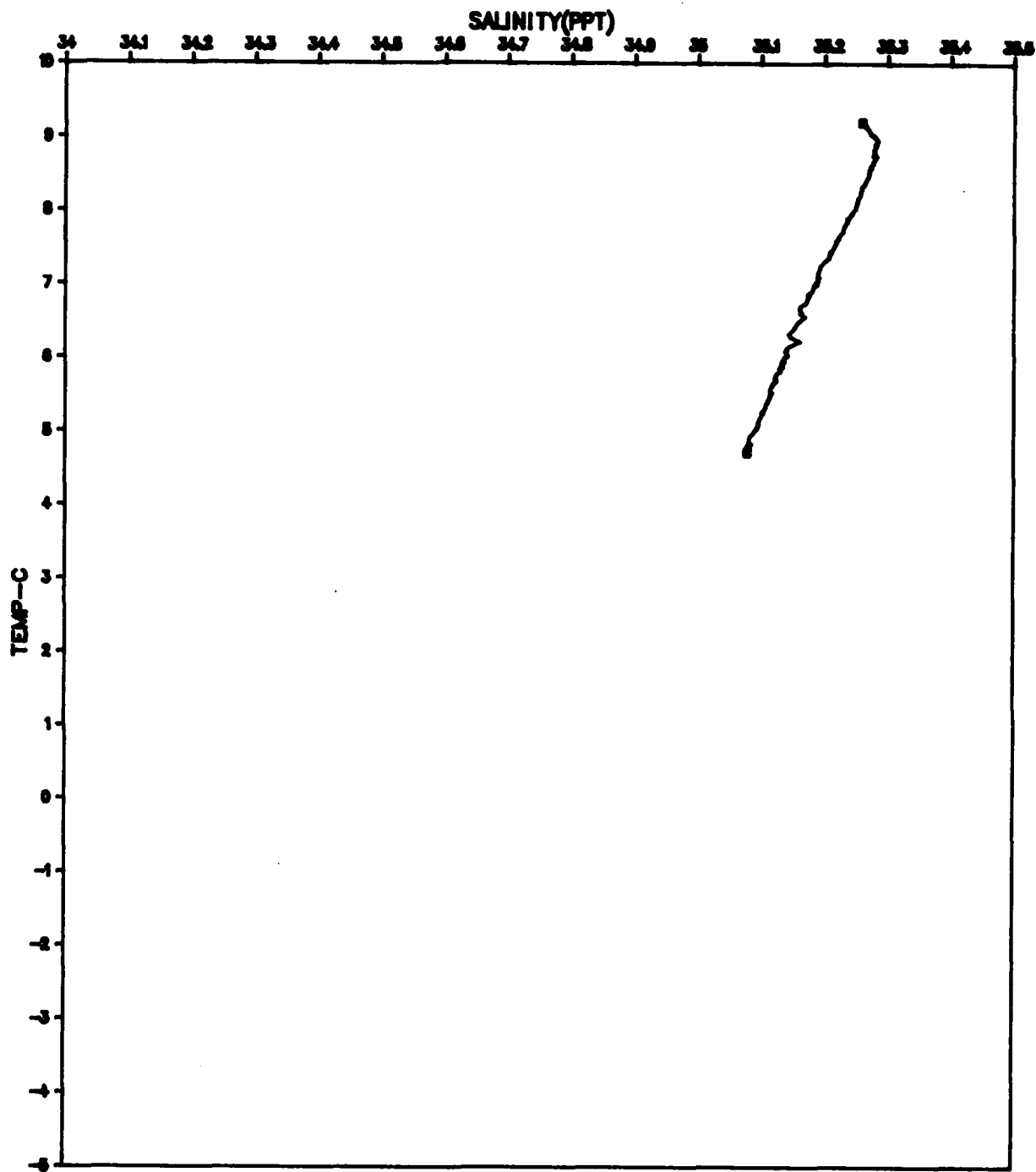


Figure B-10. File: 270980, Segment: 112086

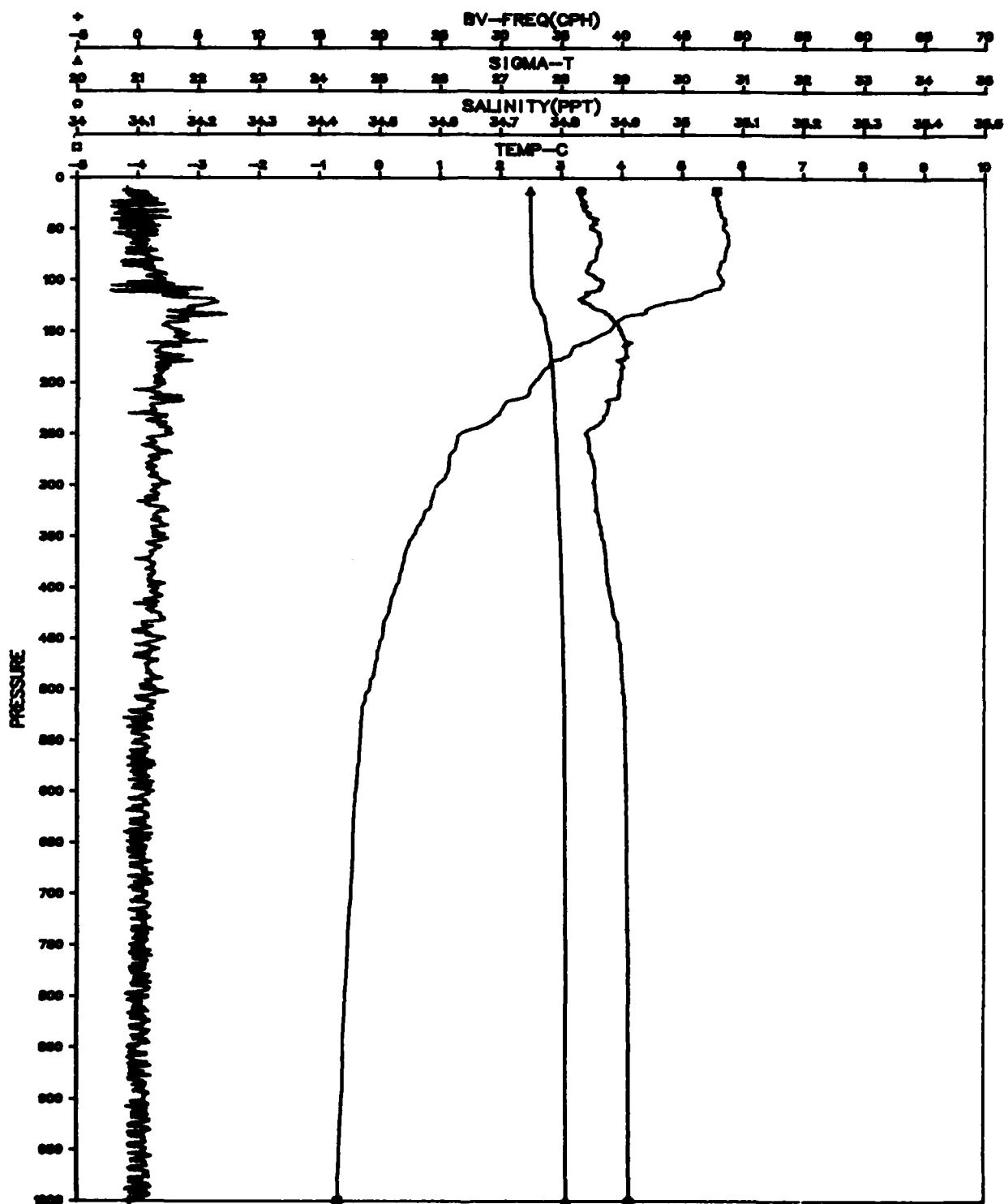


Figure B-11. File: 270980, Segment: 117091

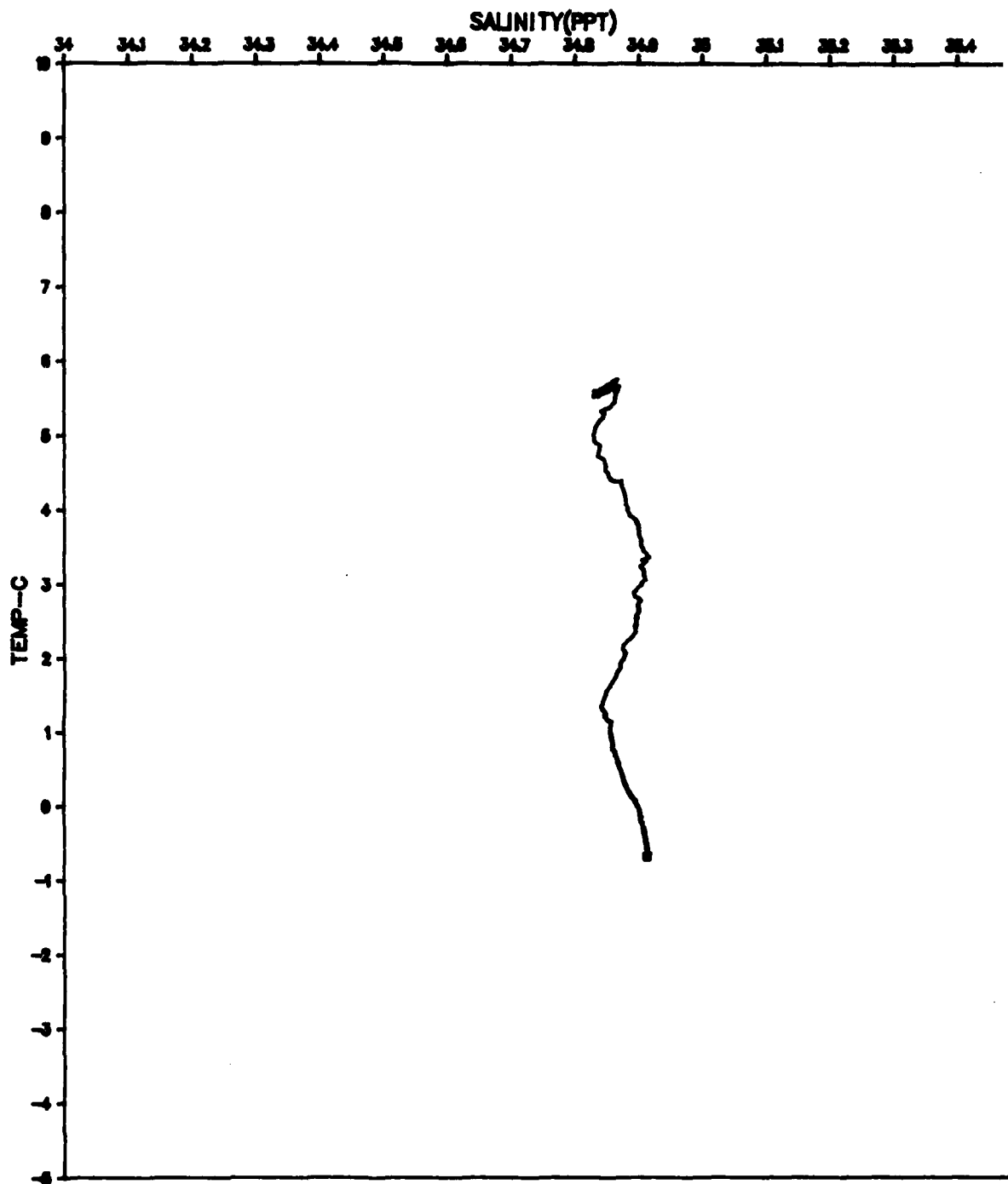


Figure B-12. File: 270980, Segment: 117091

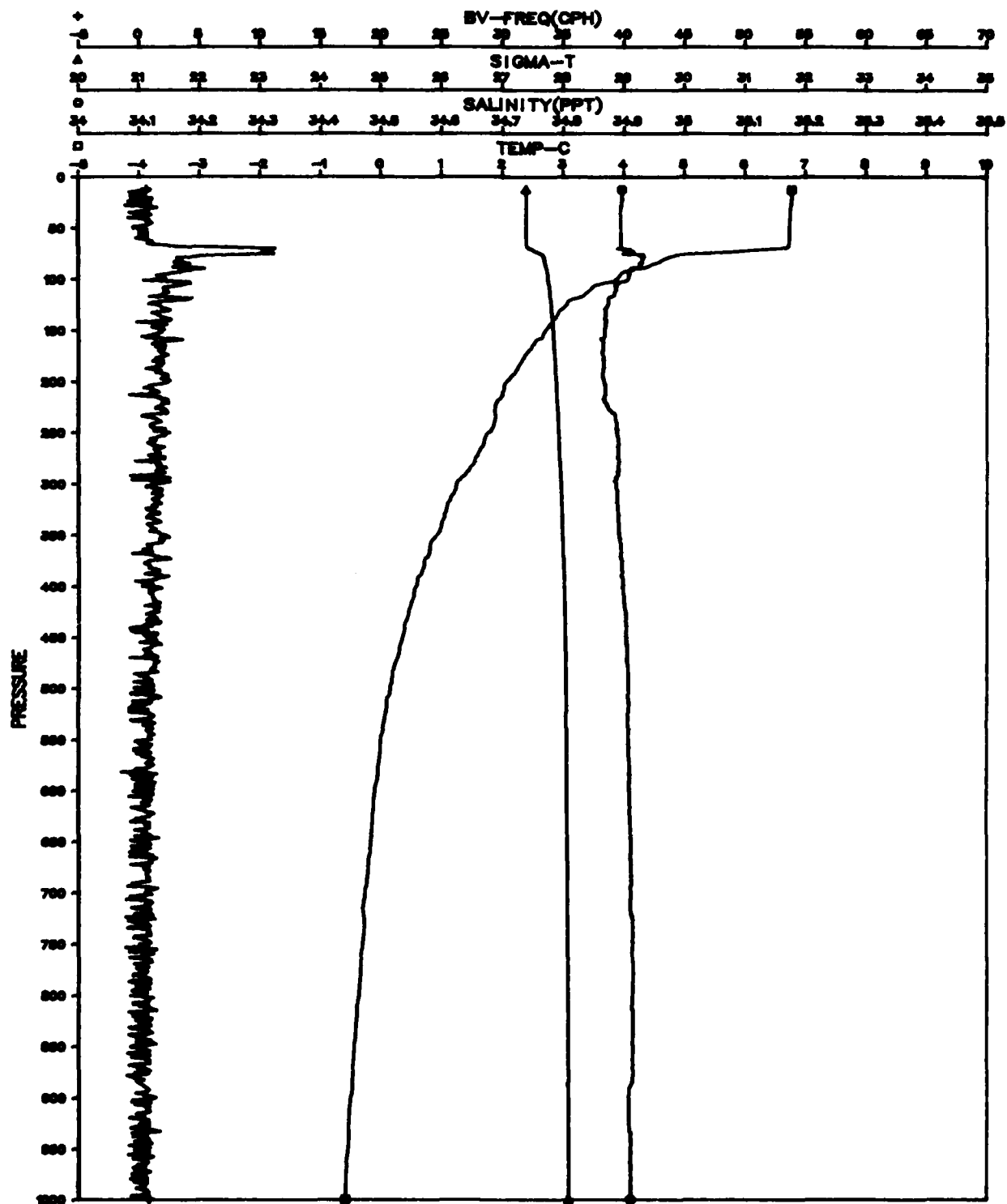


Figure B-13. File: 270980, Segment: 122103

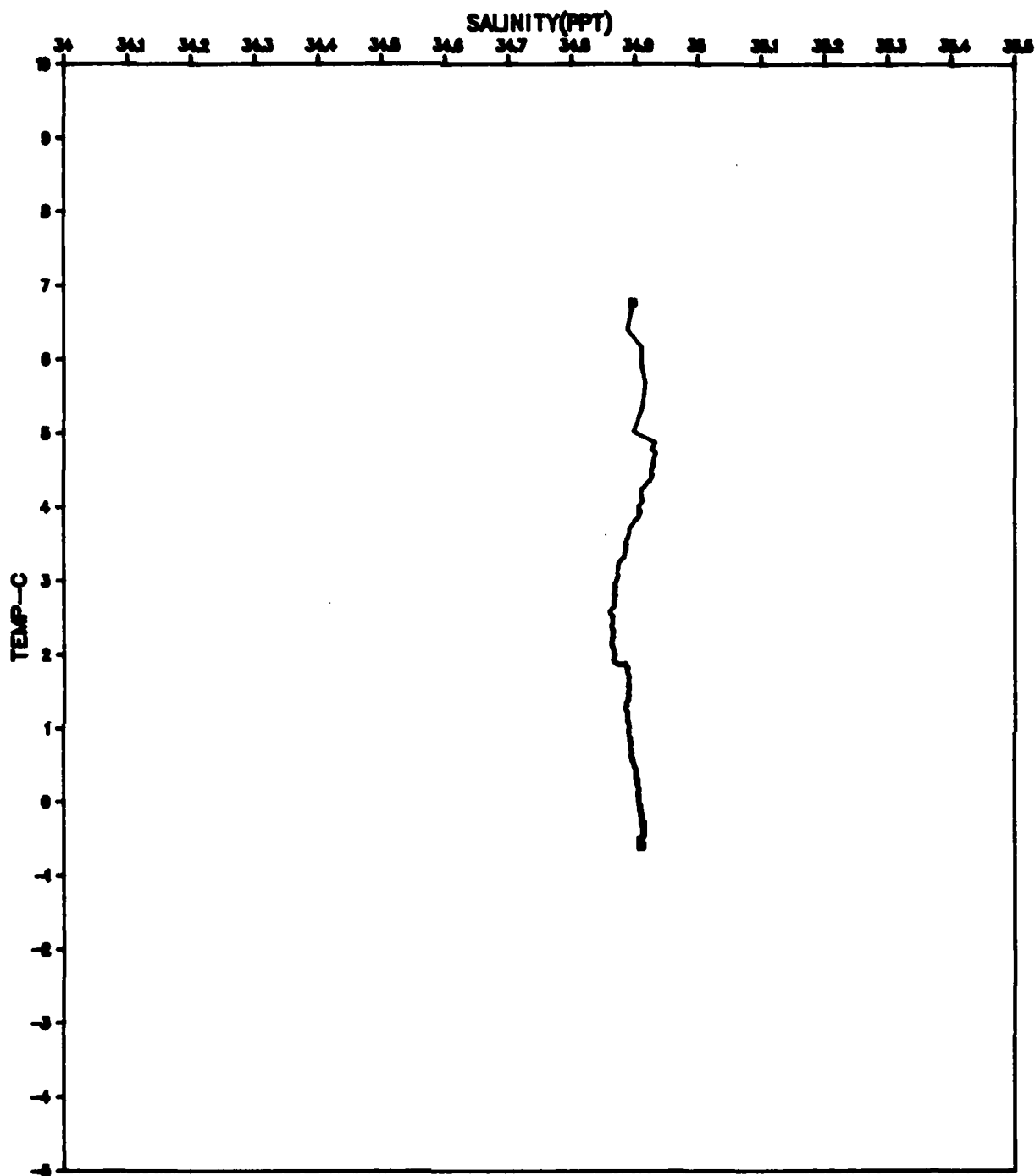


Figure B-14. File: 270980, Segment: 122103

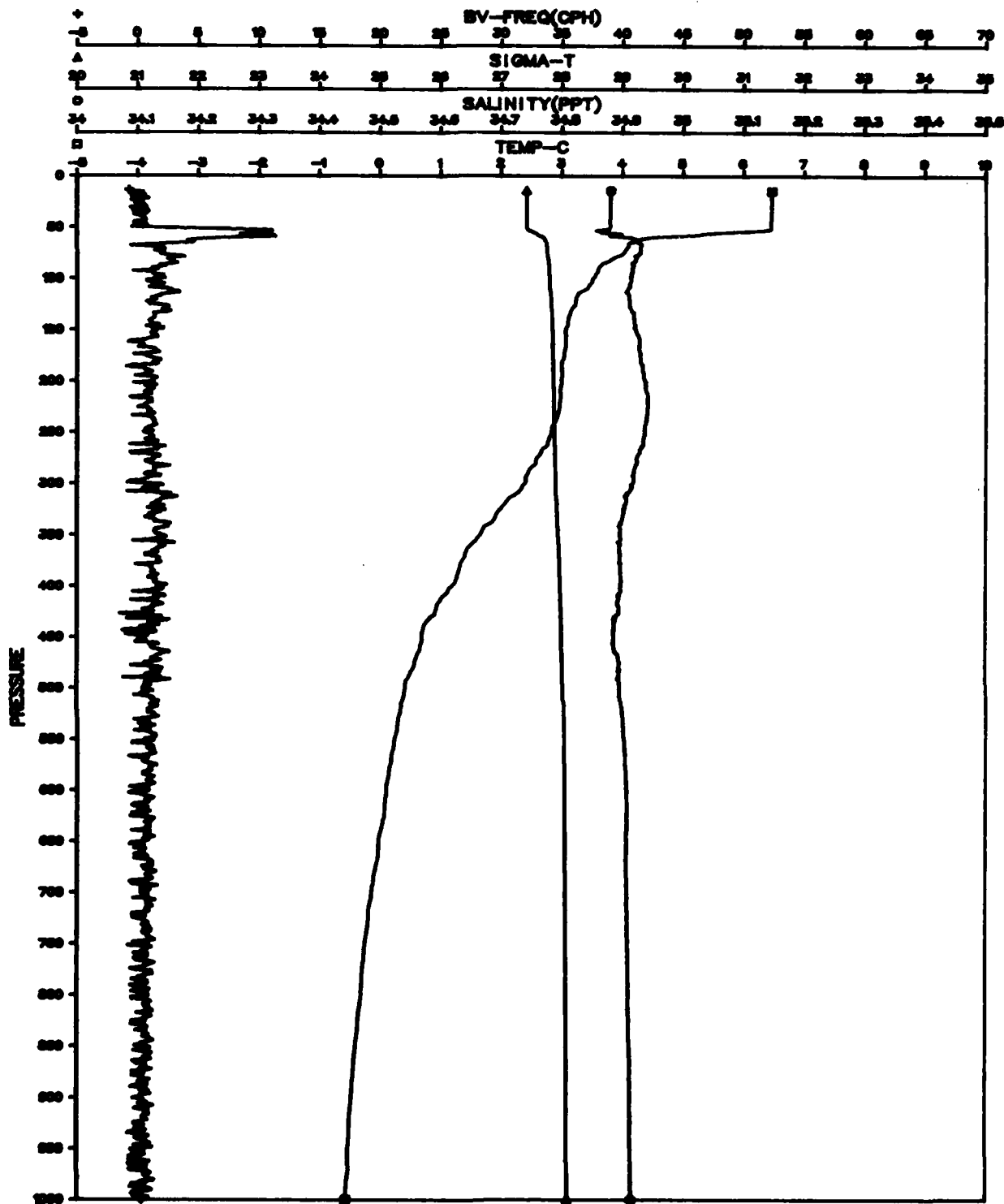


Figure B-15. File: 270980, Segment: 123104

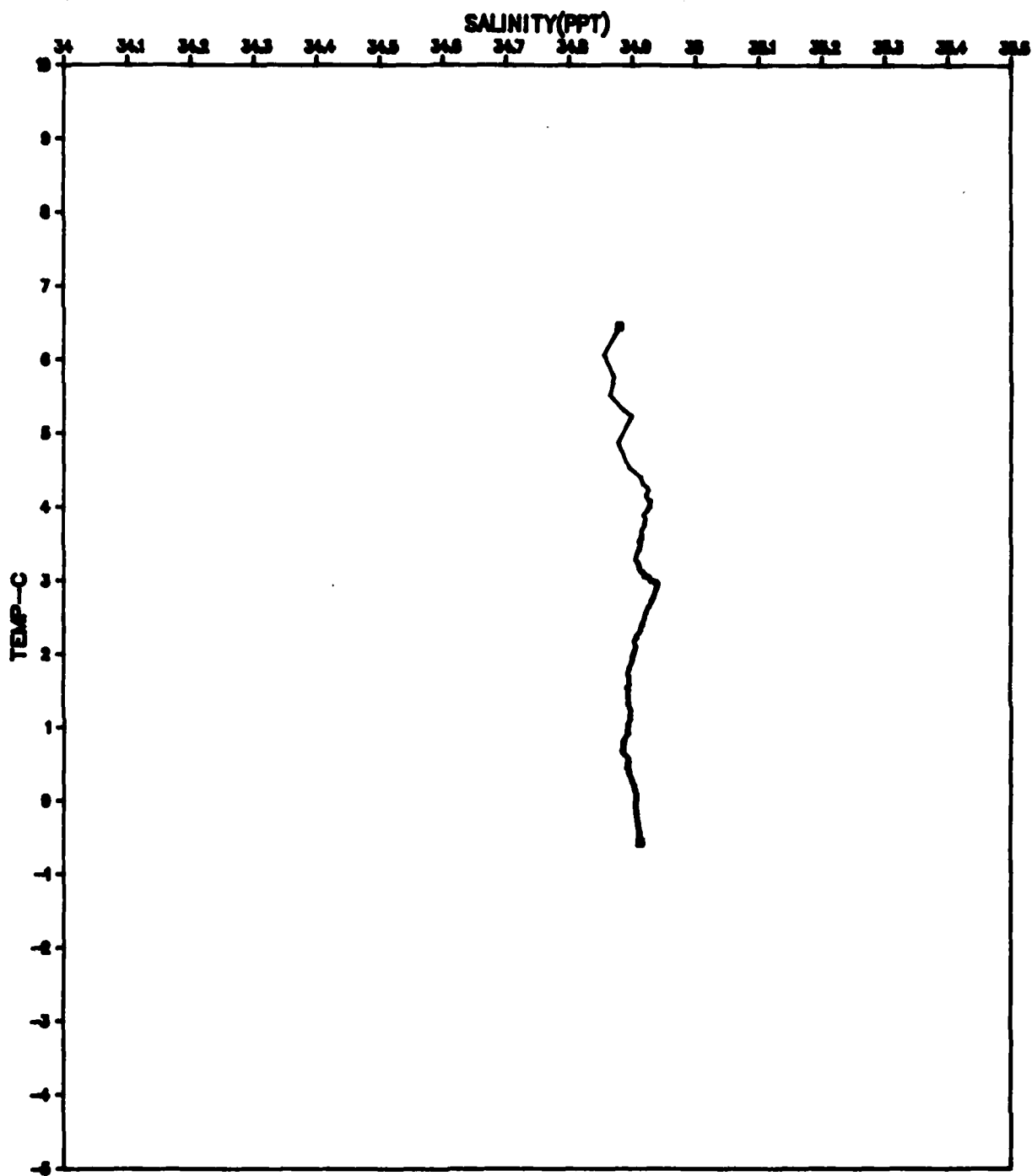


Figure B-16. File: 270980, Segment: 123104

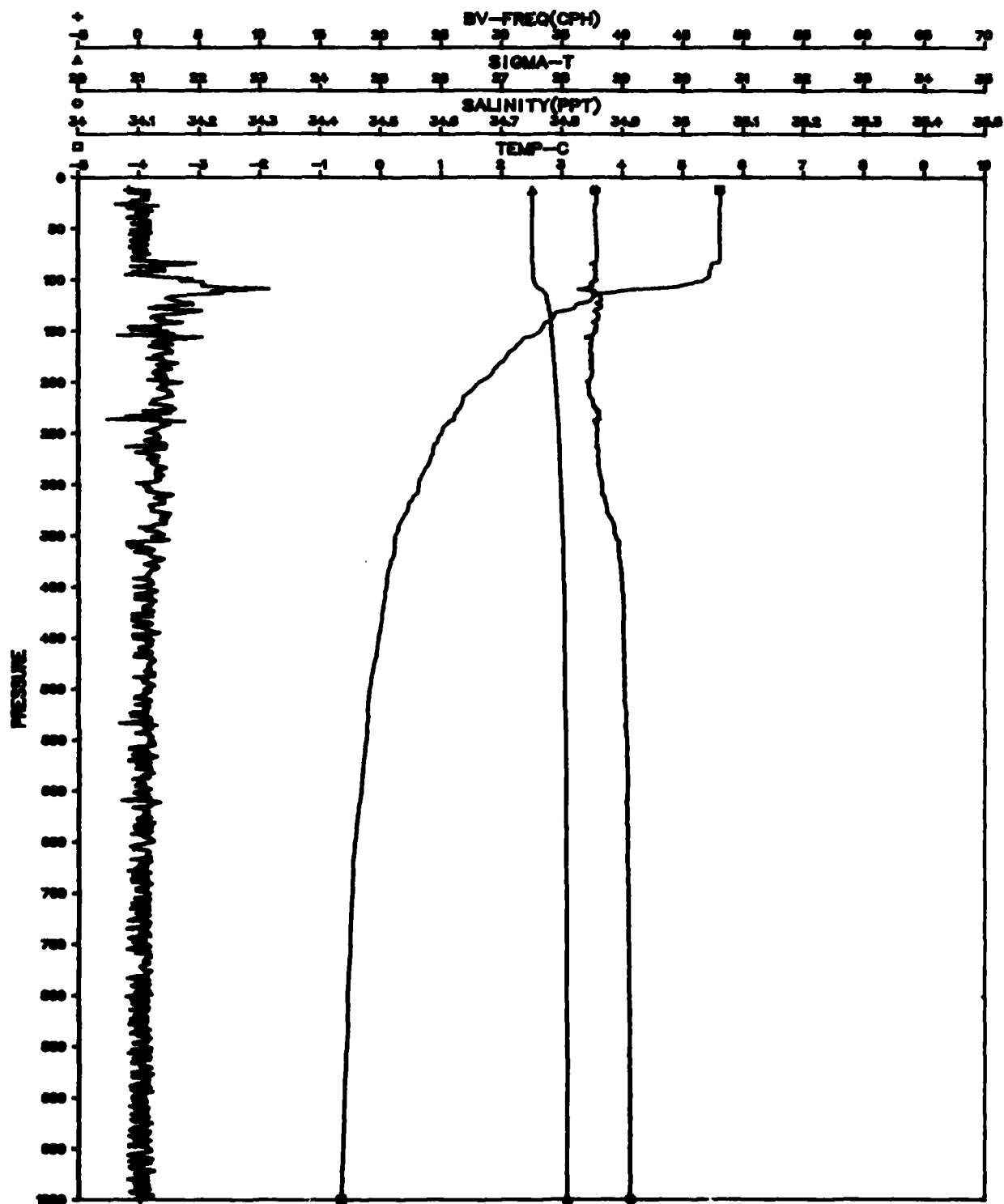


Figure B-17. File: 270980, Segment: 126106

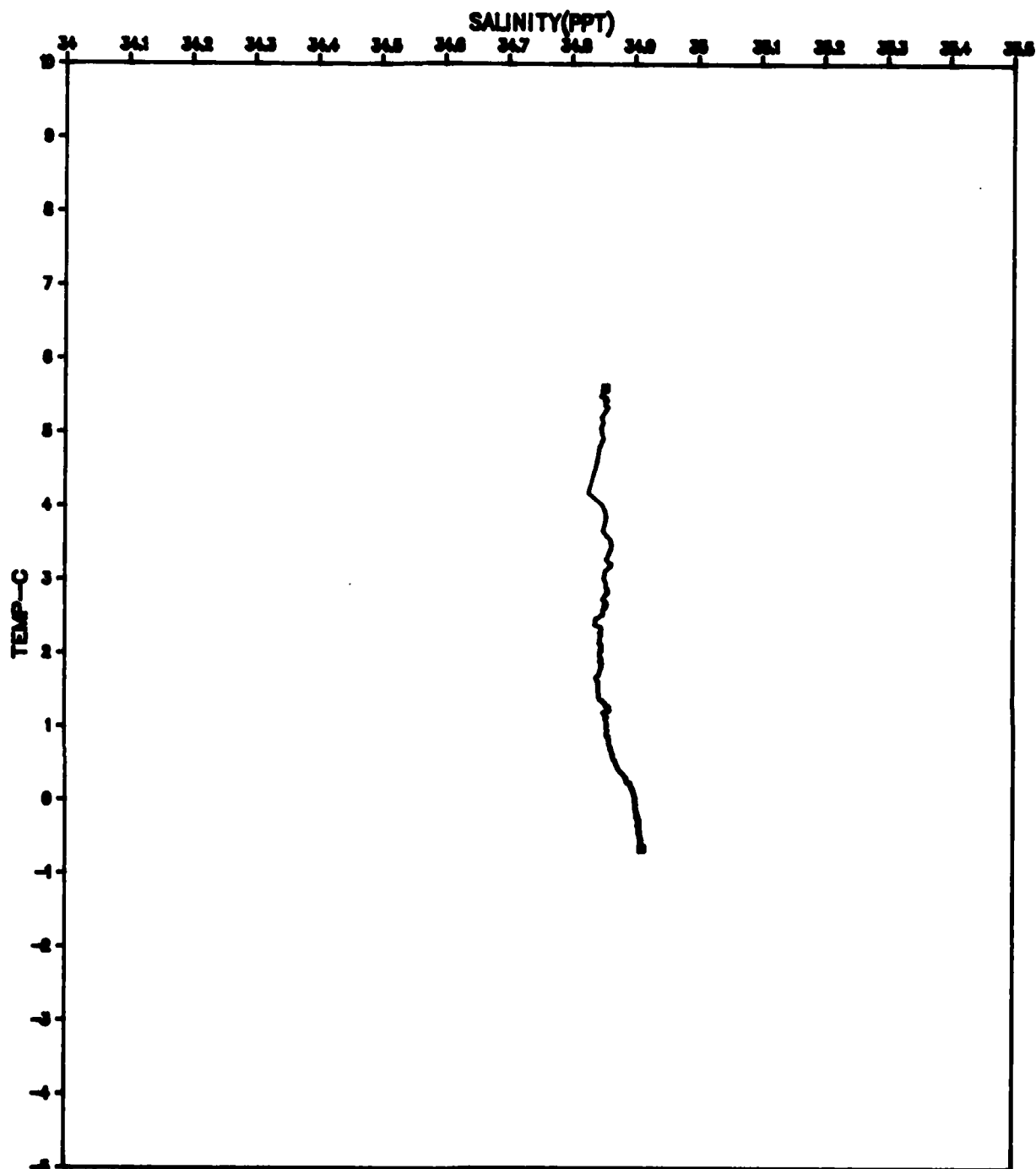


Figure B-18. File: 270980, Segment: 126106

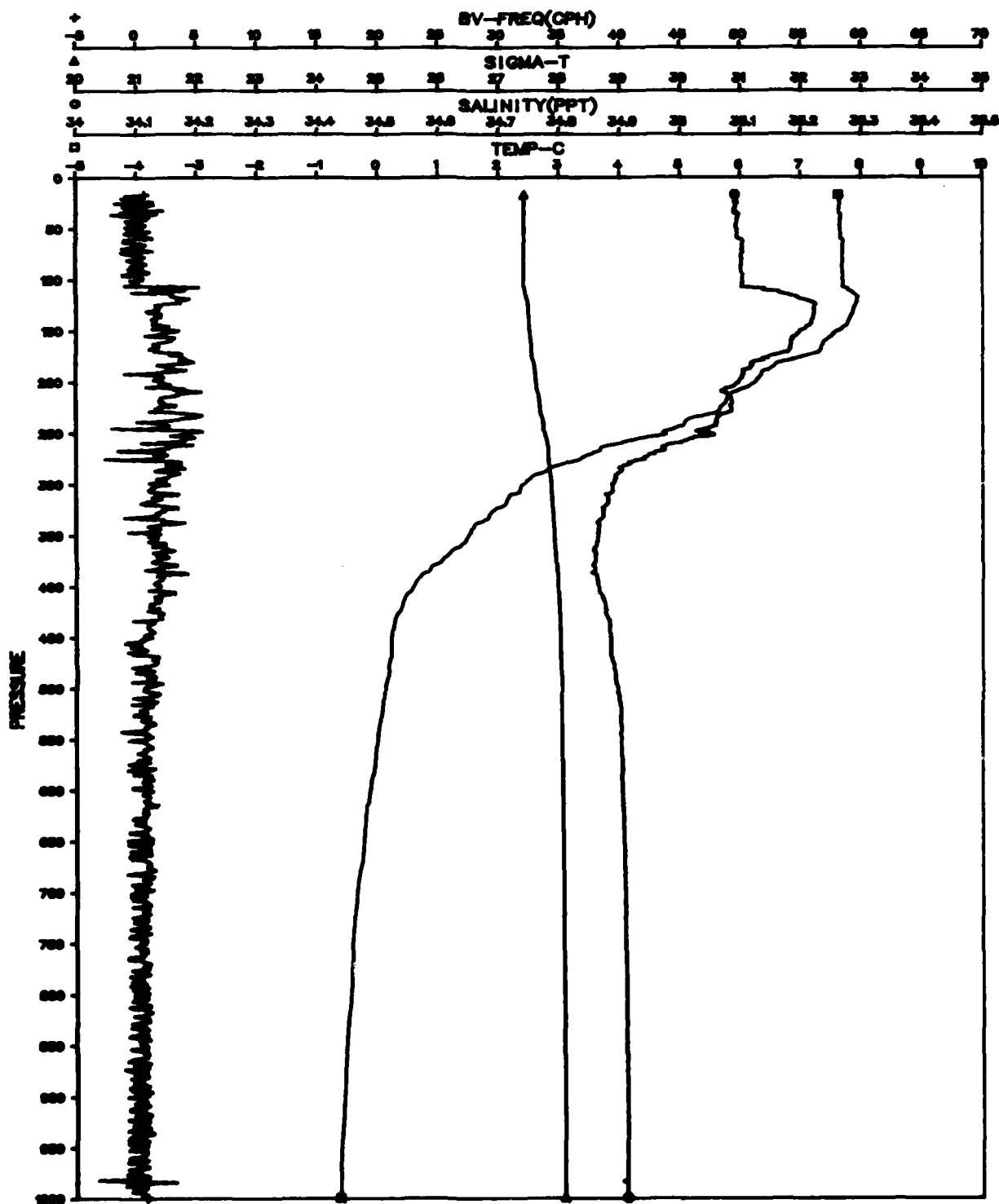


Figure B-19. File: 270980, Segment: 130108

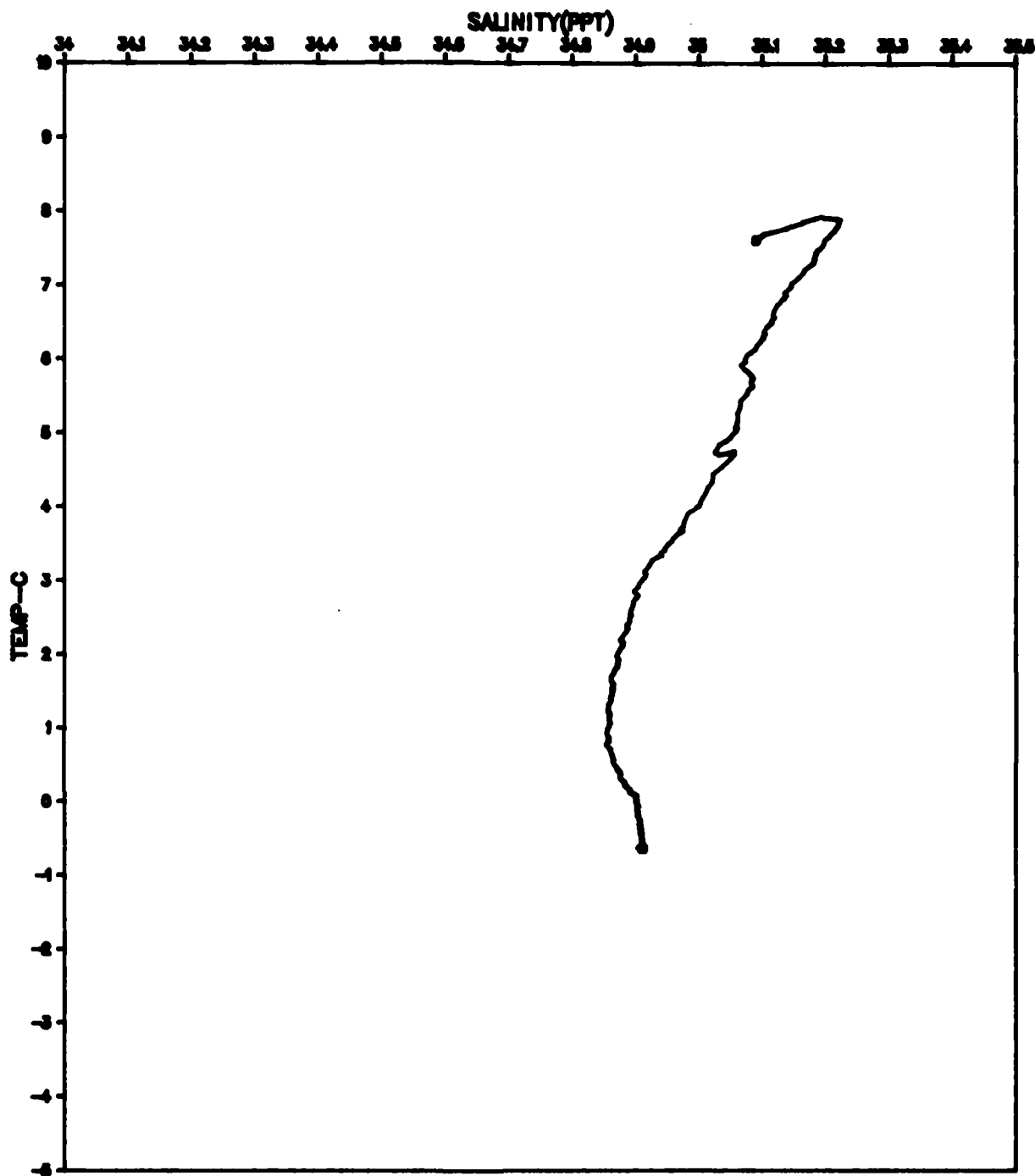


Figure B-20. File: 270980, Segment: 130108

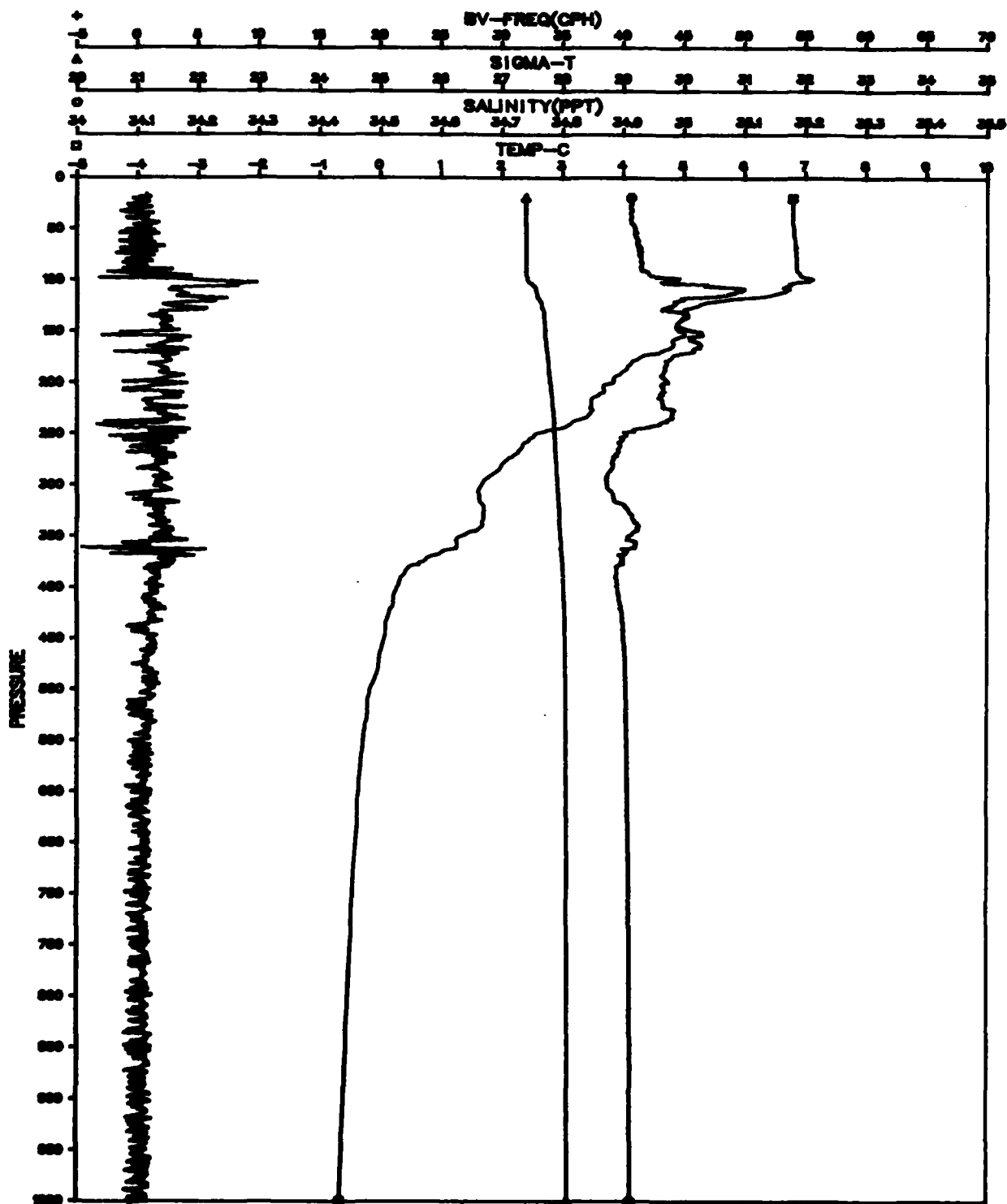


Figure B-21. File: 270980, Segment: 131109



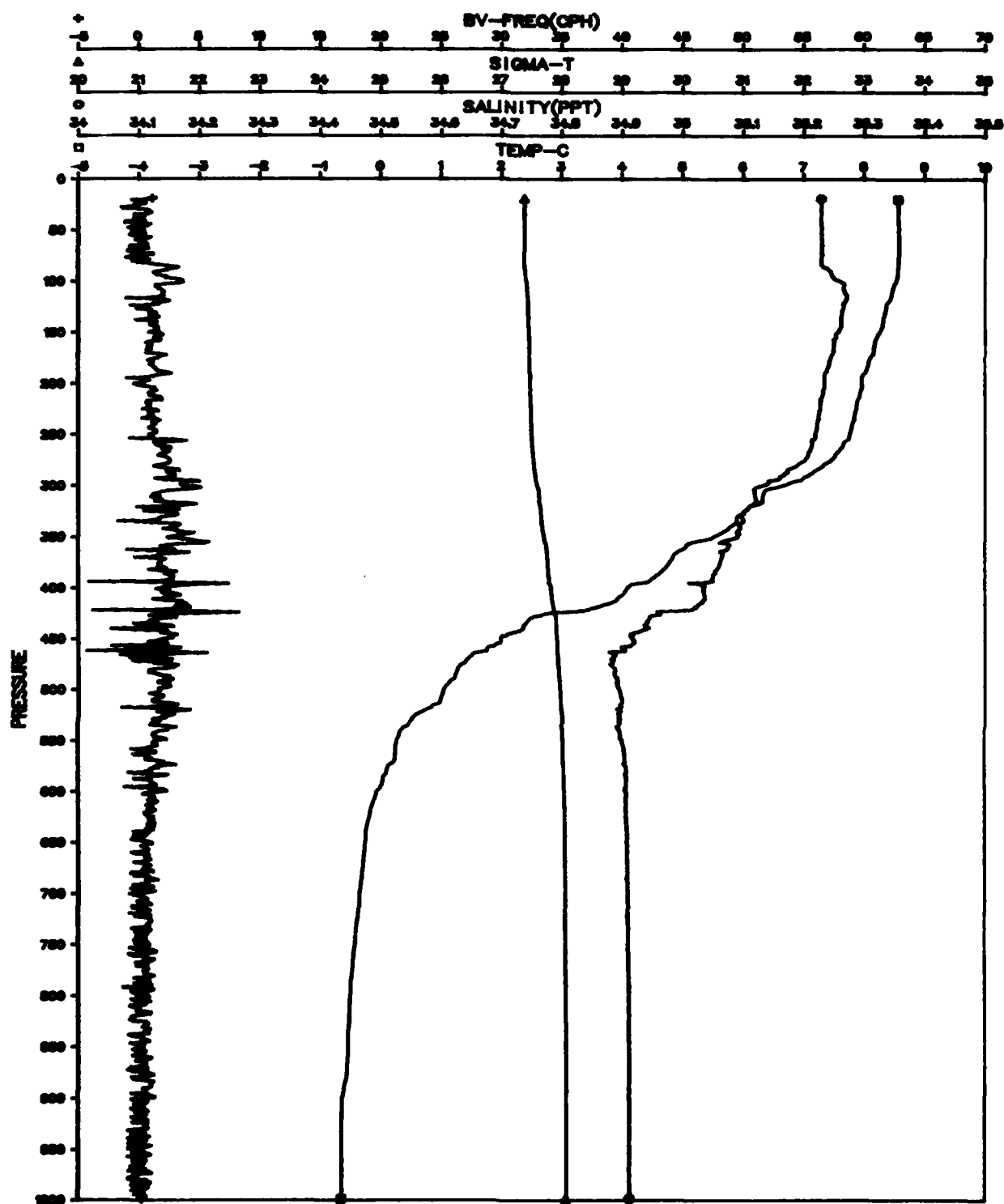


Figure B-23. File: 270980, Segment: 132110

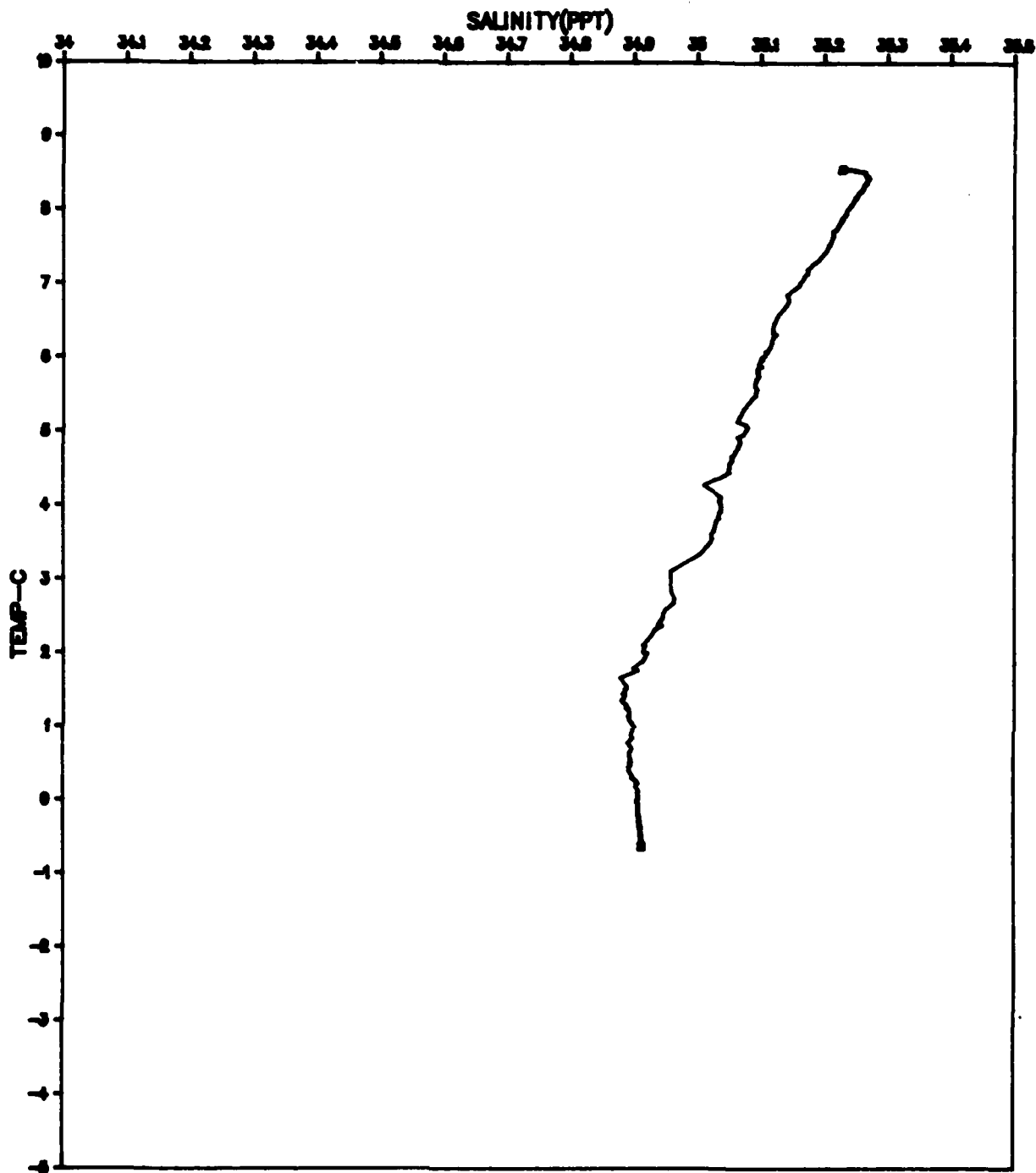


Figure B-24. File: 270980, Segment: 132110

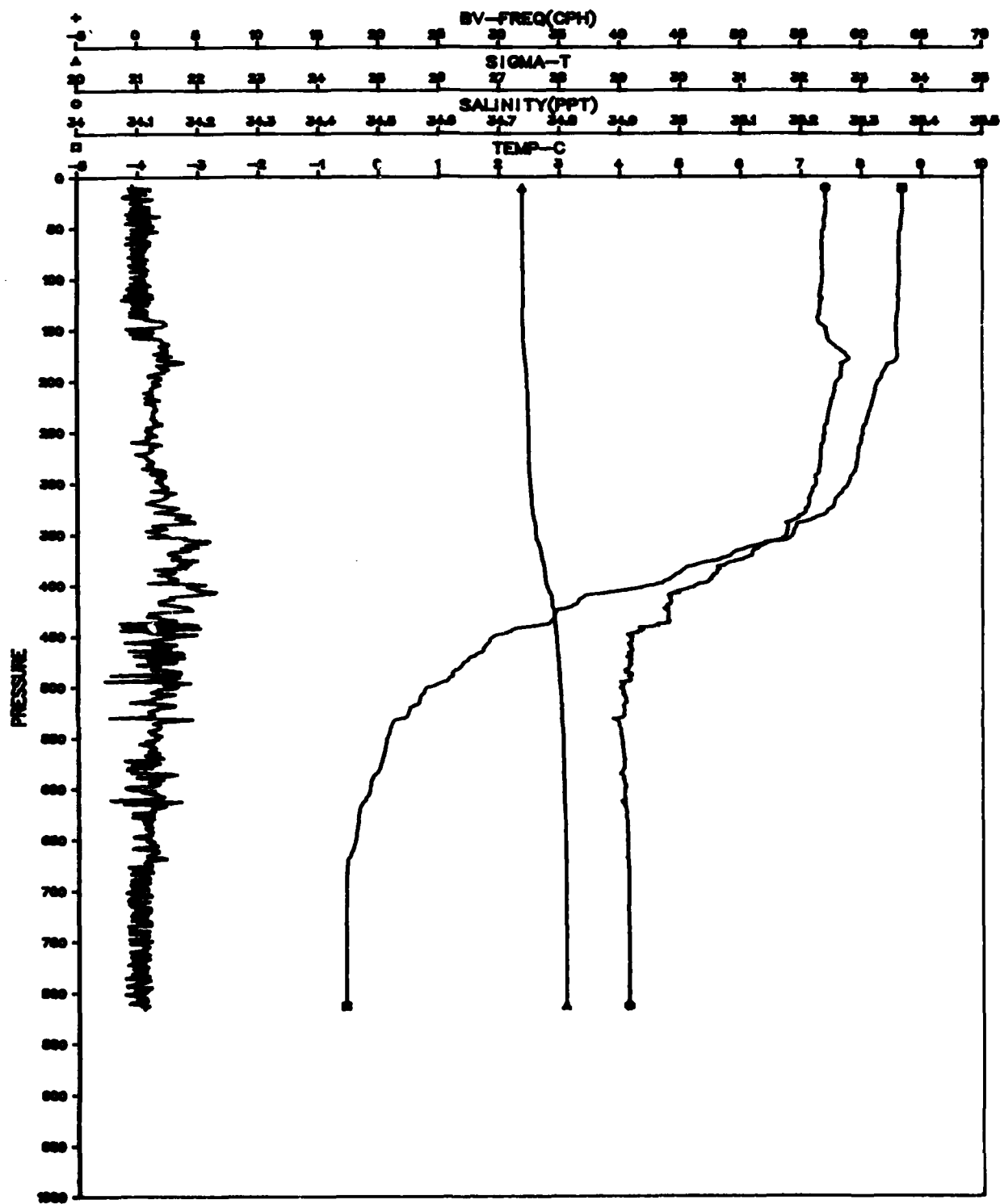


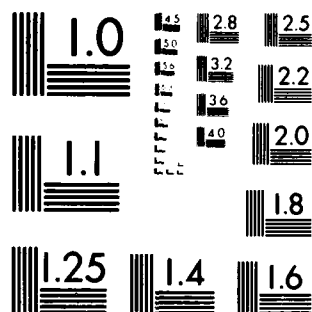
Figure B-25. File: 270980, Segment: 133111

NAVAL OCEAN RESEARCH AND DEVELOPMENT ACTIVITY NSTL S--ETC F/G 8/3  
DATA SUMMARY - XCP PROFILES IN THE VICINITY OF THE FAEROE ISLAND--ETC(U)  
APR 82 D A BURNS, N V LOMBARD  
NORDA-TN-142 NL

NL

$$A_1 = \{1, 2, 4, 6\}$$

END  
DATE  
FILMED  
7 82  
DTIC



MICROCOPY RESOLUTION TEST CHART  
NATIONAL BUREAU OF STANDARDS 1963-A

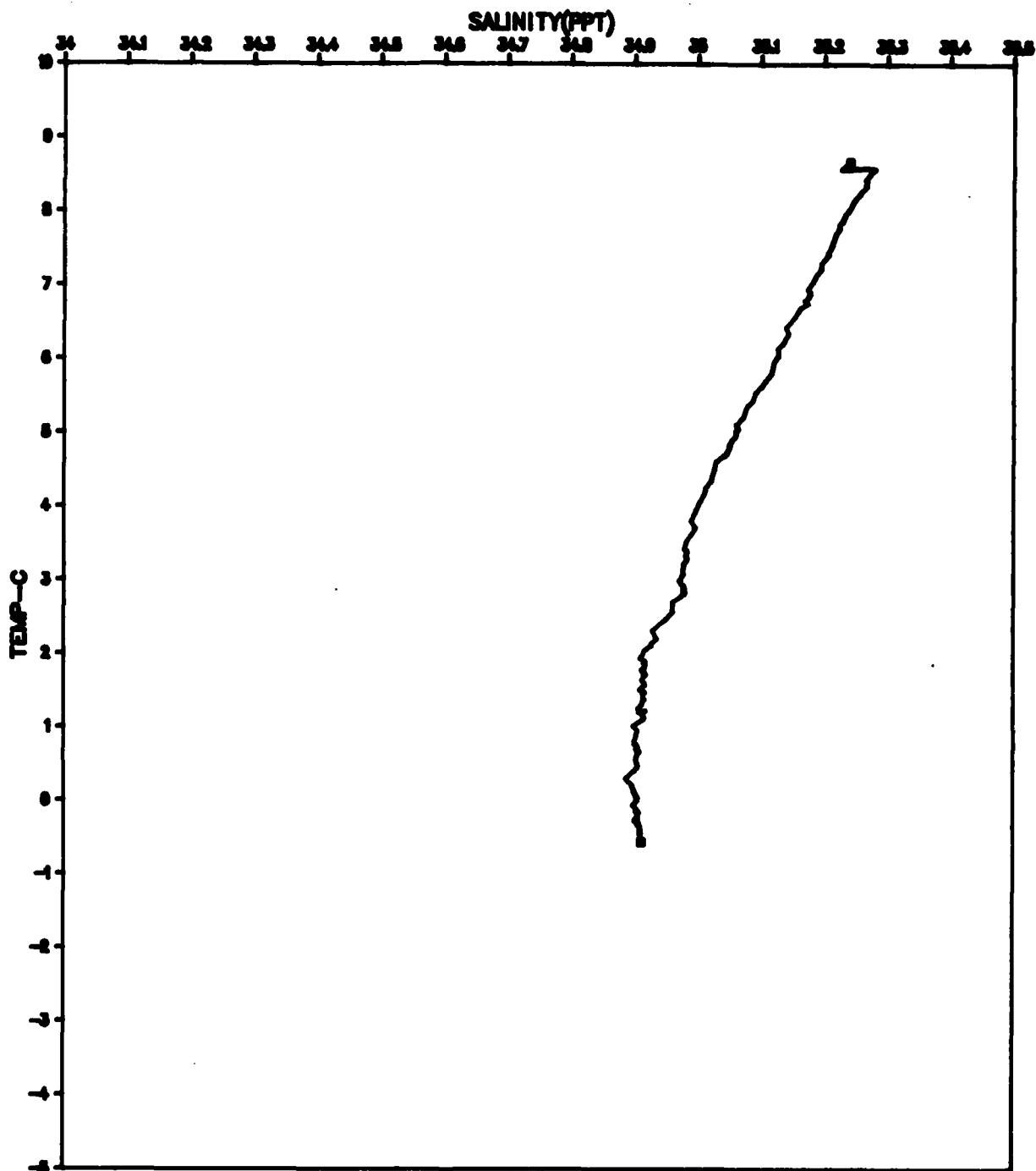


Figure B-26. File: 270980, Segment: 133111

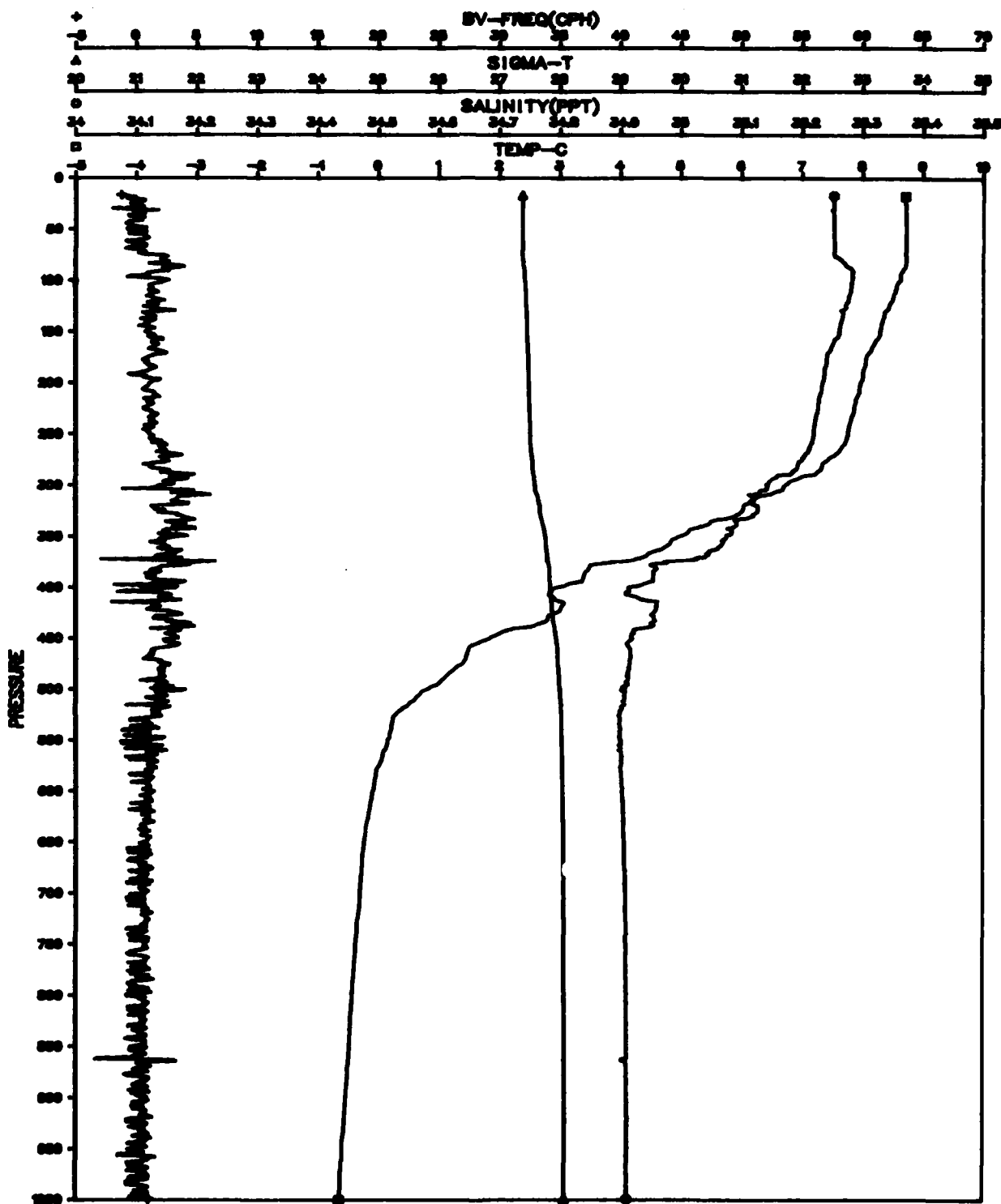


Figure B-27. File: 270980, Segment: 136116

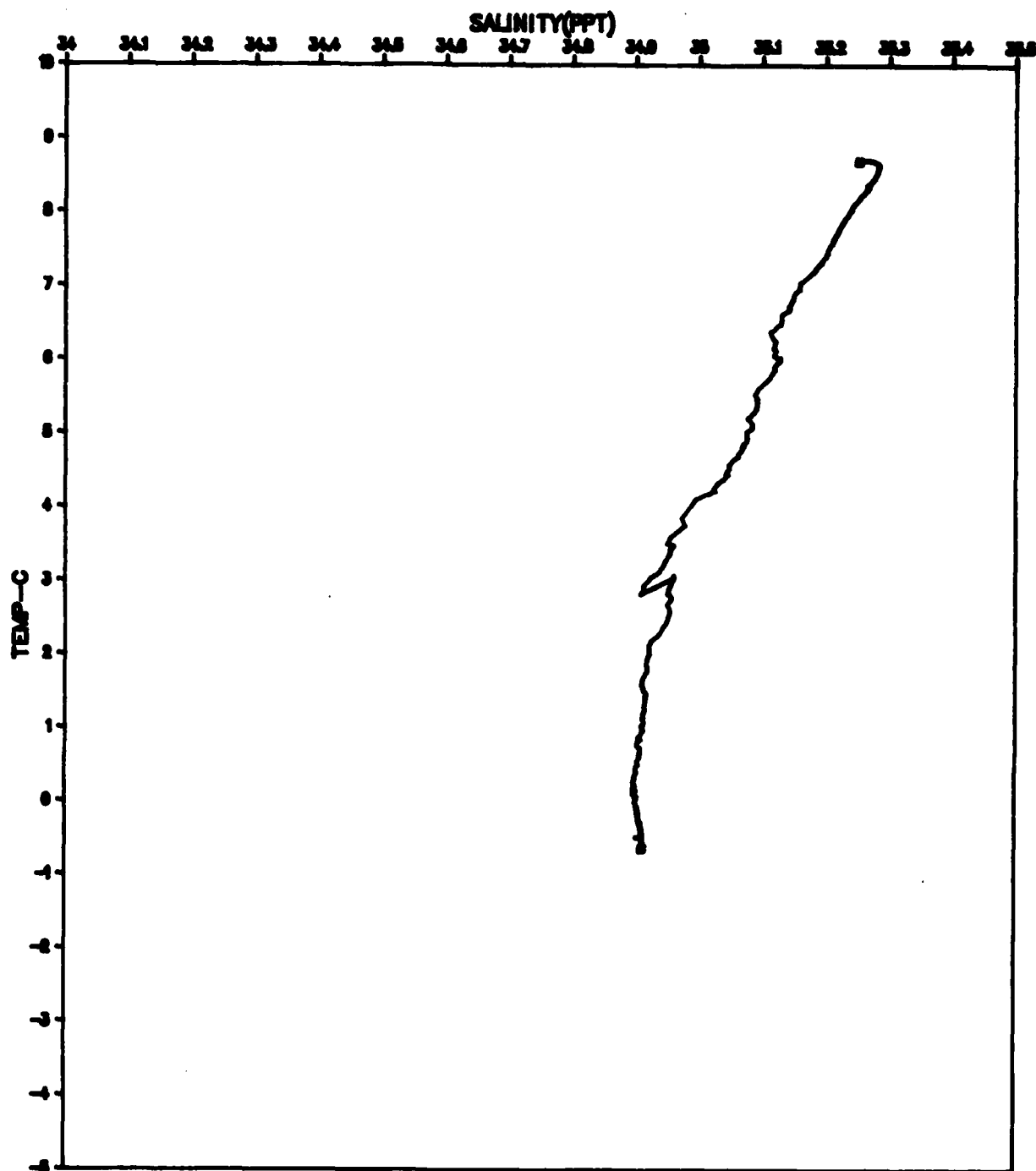


Figure B-28. File: 270980, Segment: 136116

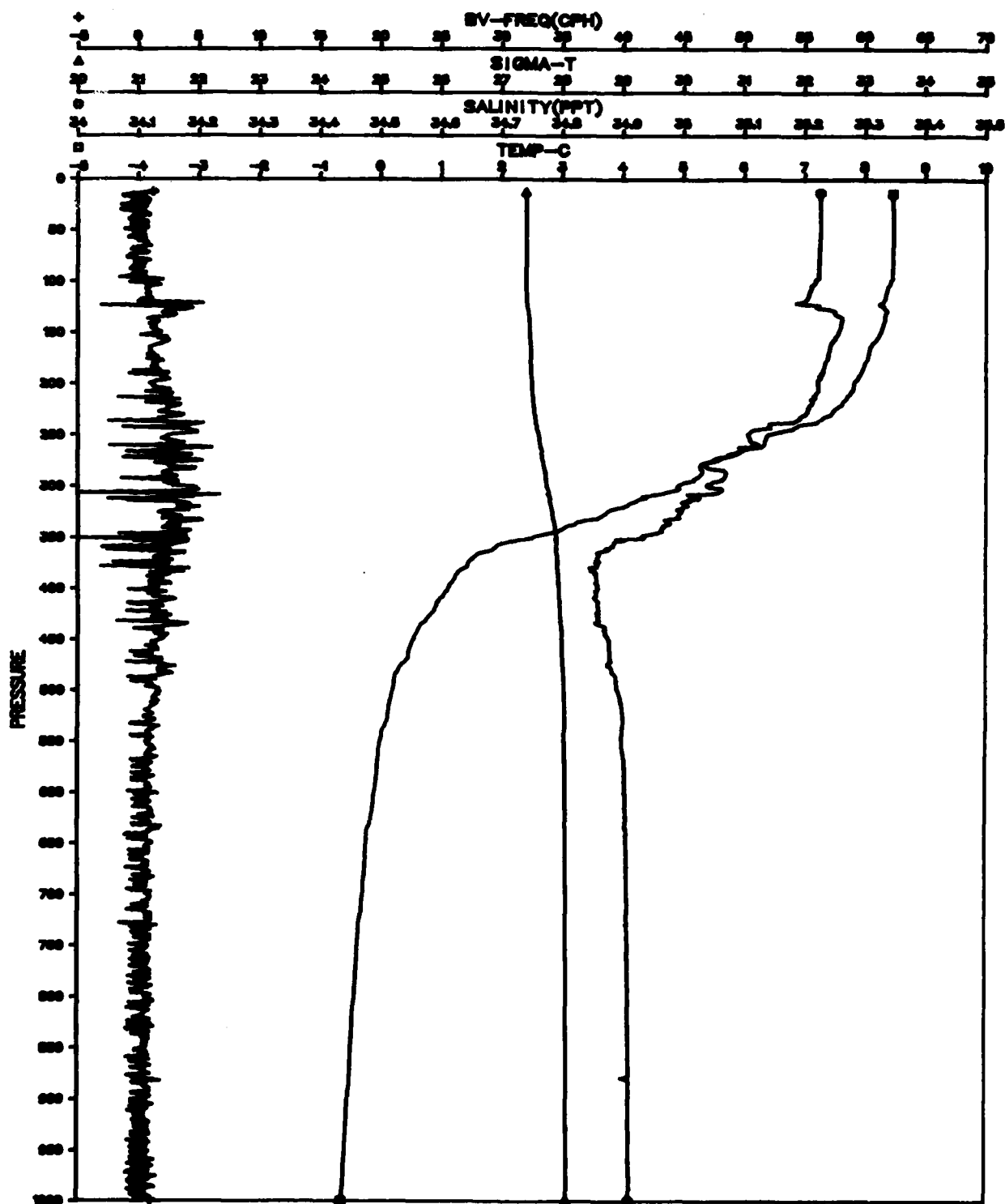


Figure B-29. File: 270980, Segment: 137117

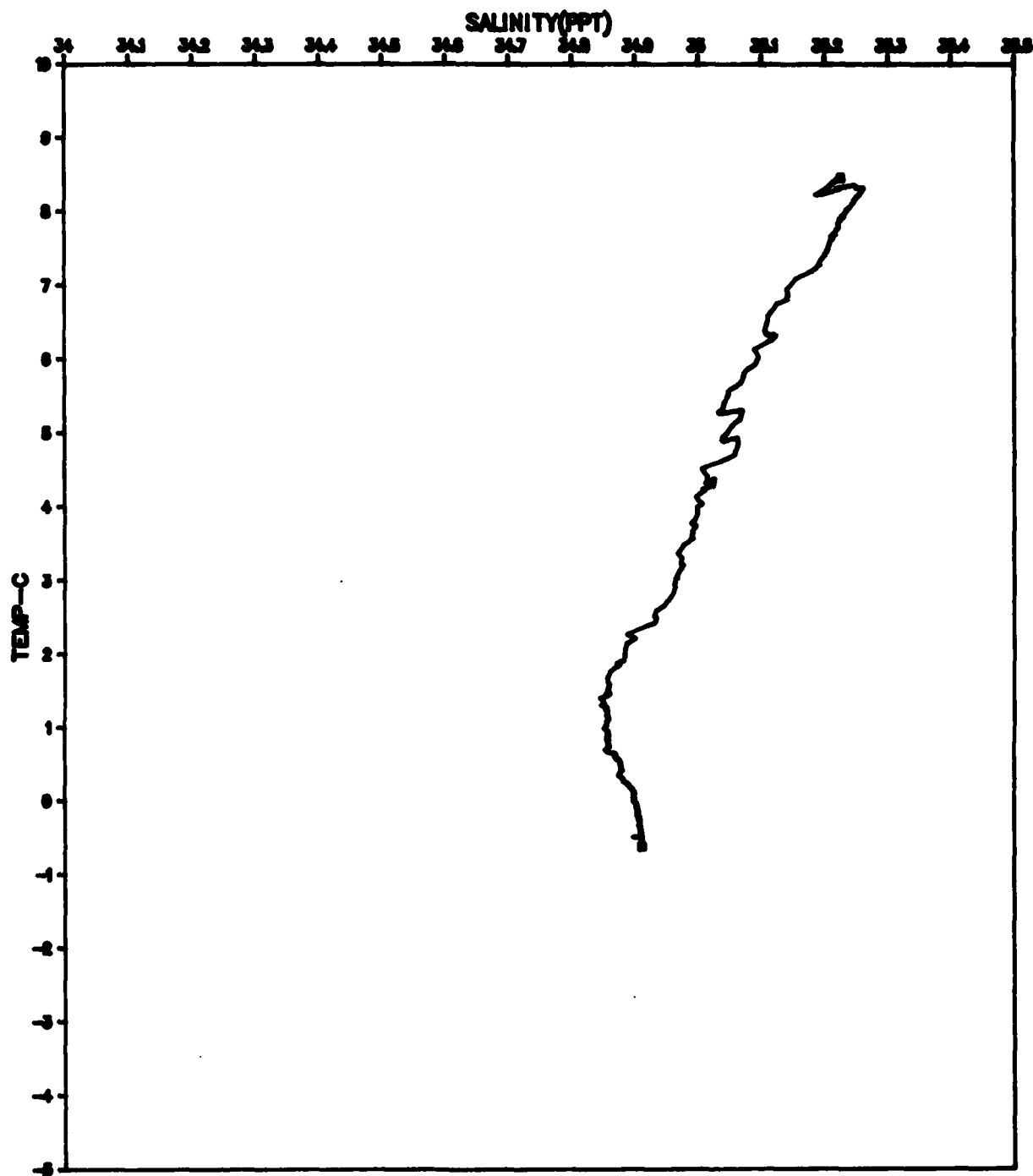


Figure B-30. File: 270980, Segment: 137117

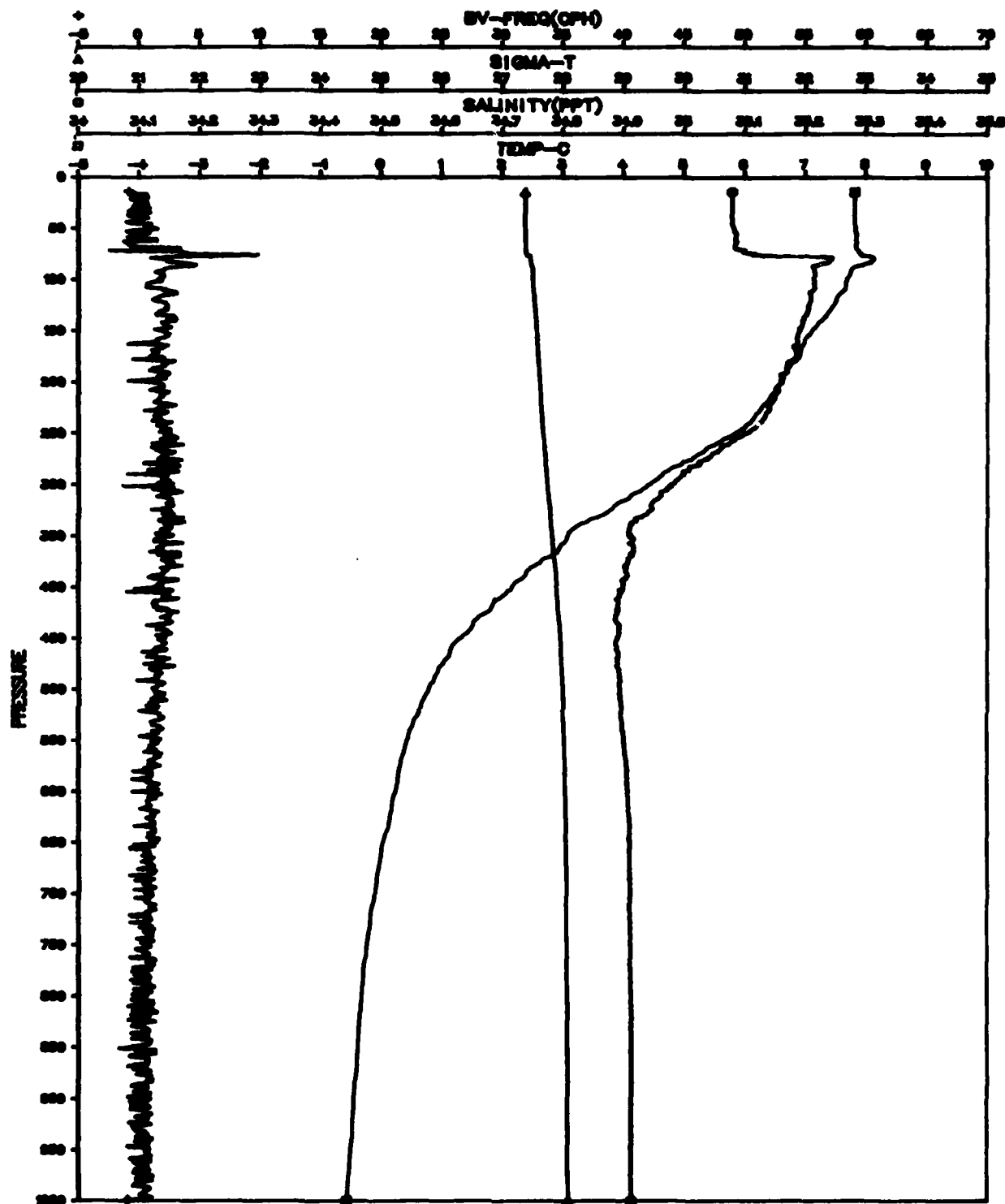


Figure B-31. File: 270980, Segment: 175155

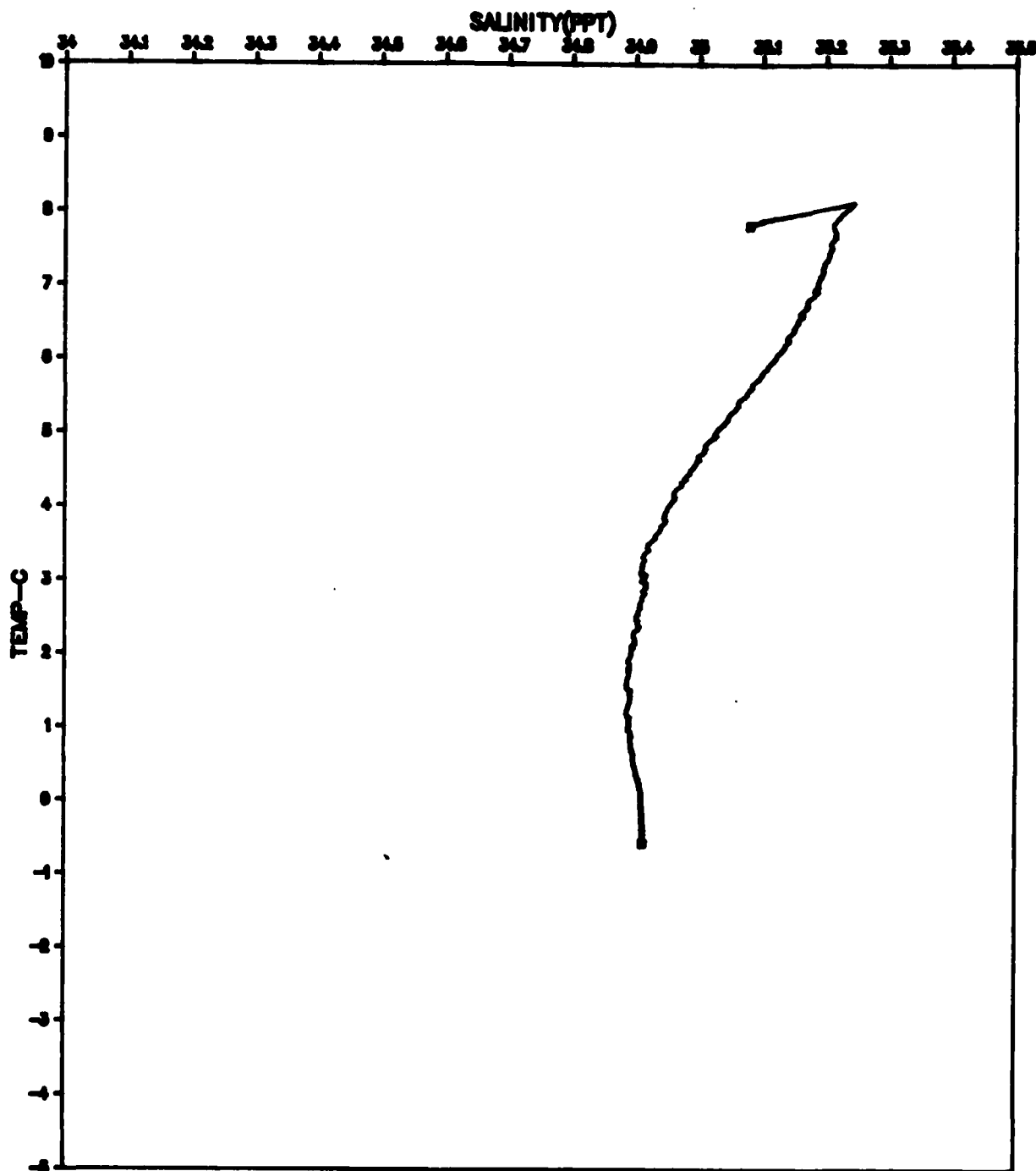


Figure B-32. File: 270980, Segment:175155

**Appendix C:**  
**Selected XCP and CTD**  
**Temperature Profiles**

**COMMENTS:**  
**Low Pass Filtered 10 m Resolution Subsampling Interval 1 m**

**FIGURE PAGE BLANK-NOT FILMED**

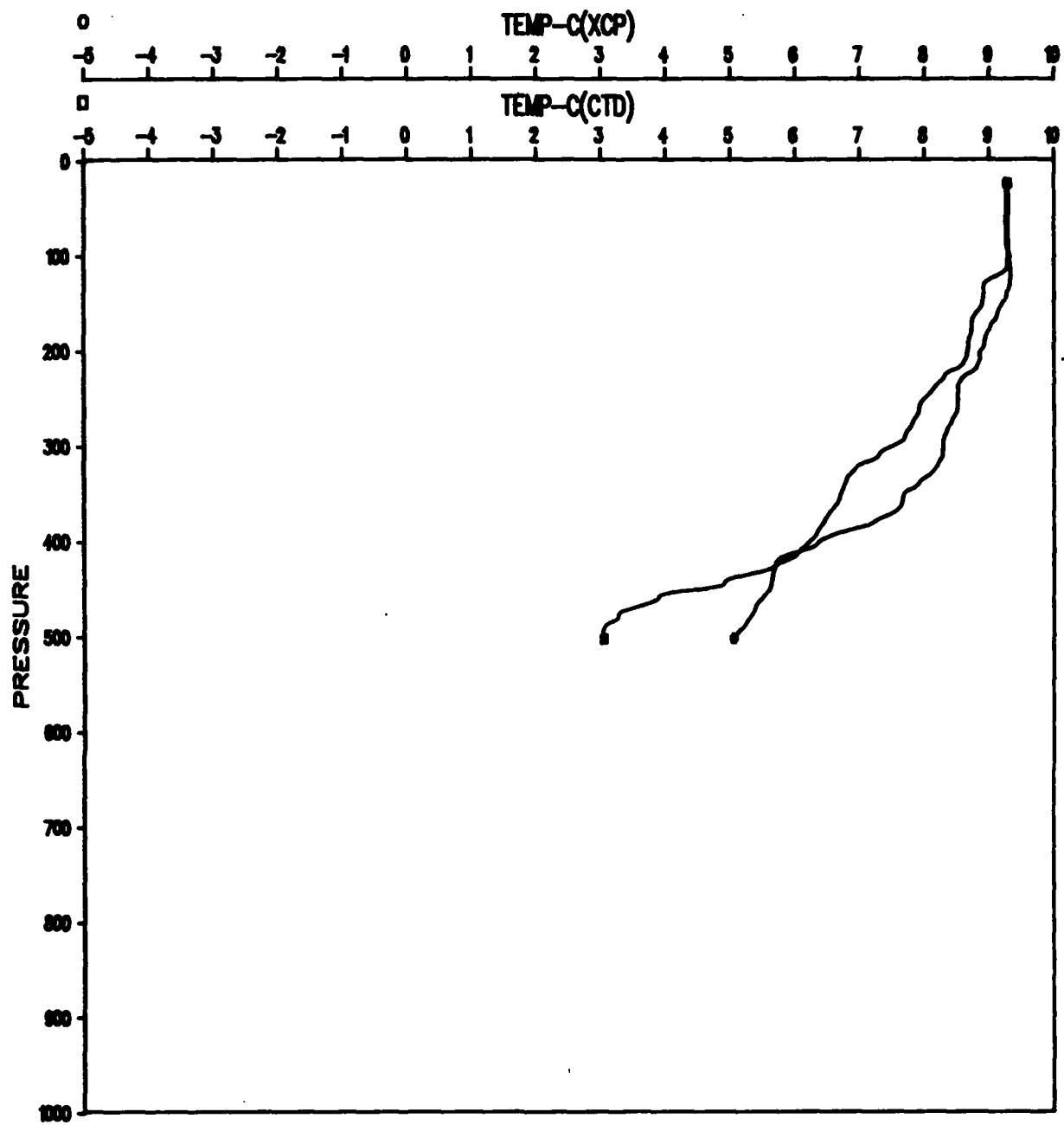


Figure C-1. File: KANE, Segment: C 503

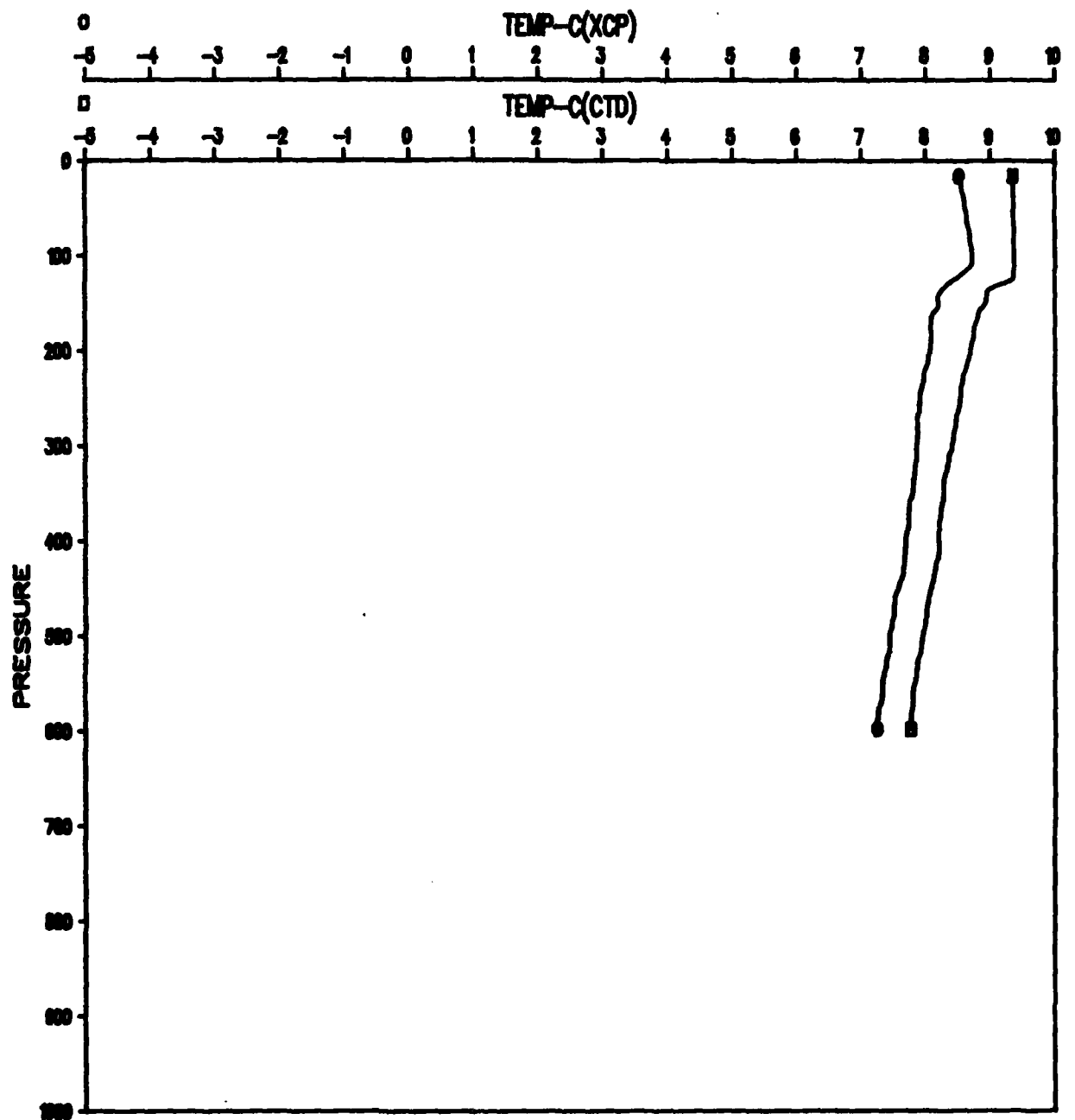


Figure C-2. File: KANE, Segment: C 504

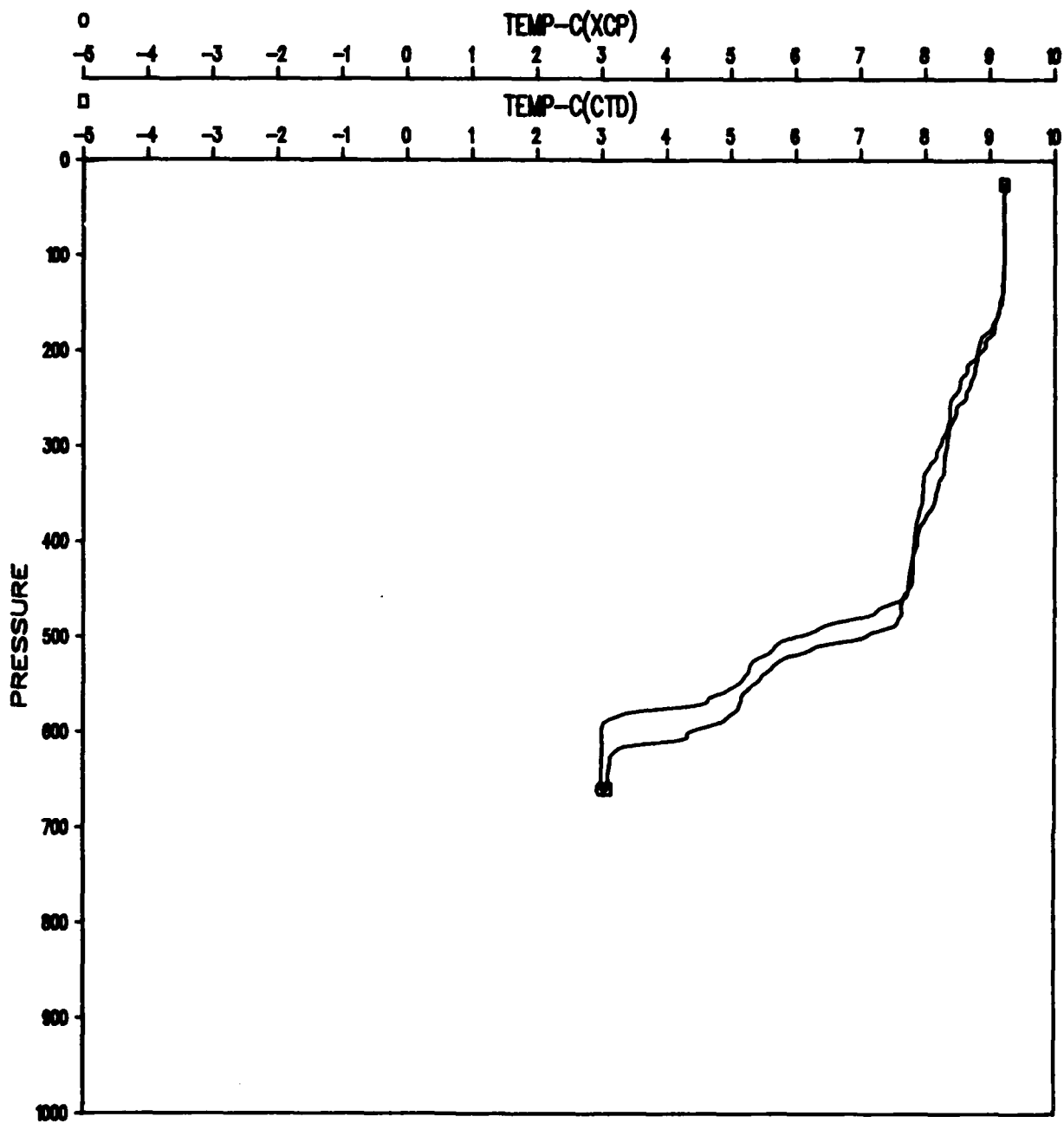


Figure C-3. File: KANE, Segment: C 517

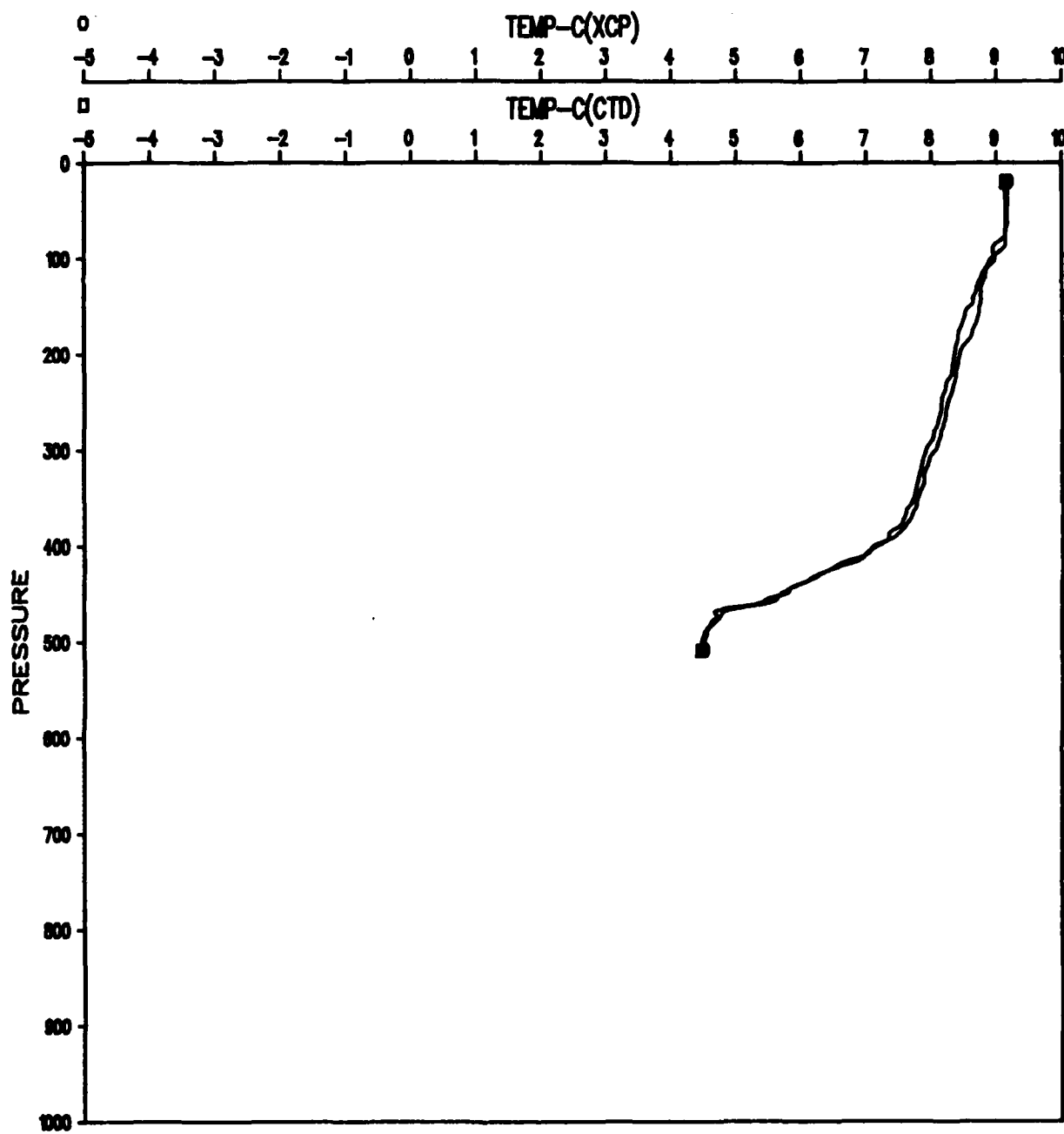


Figure C-4. File: KANE, Segment: C 519

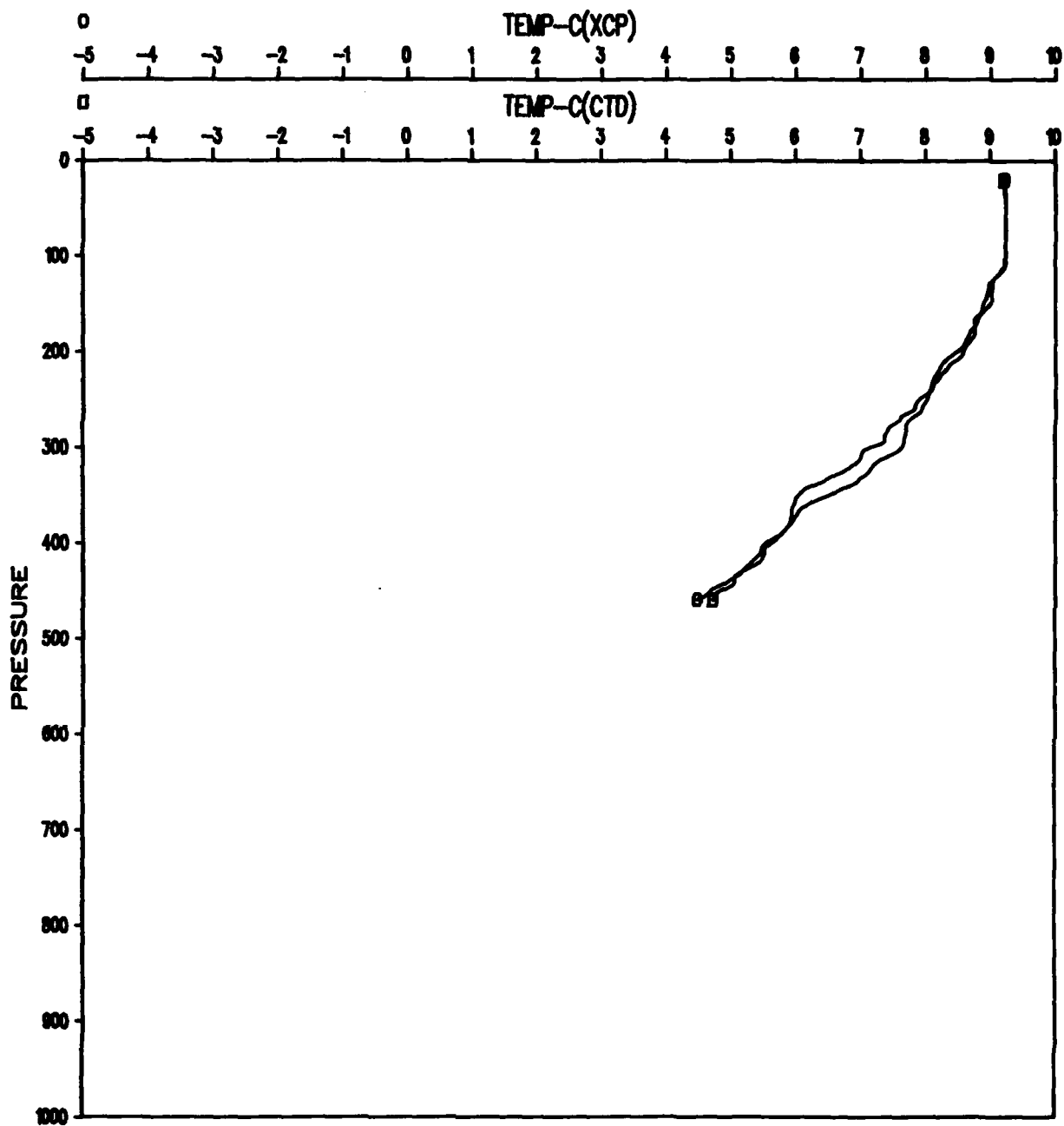


Figure C-5. File: KANE, Segment: C 520

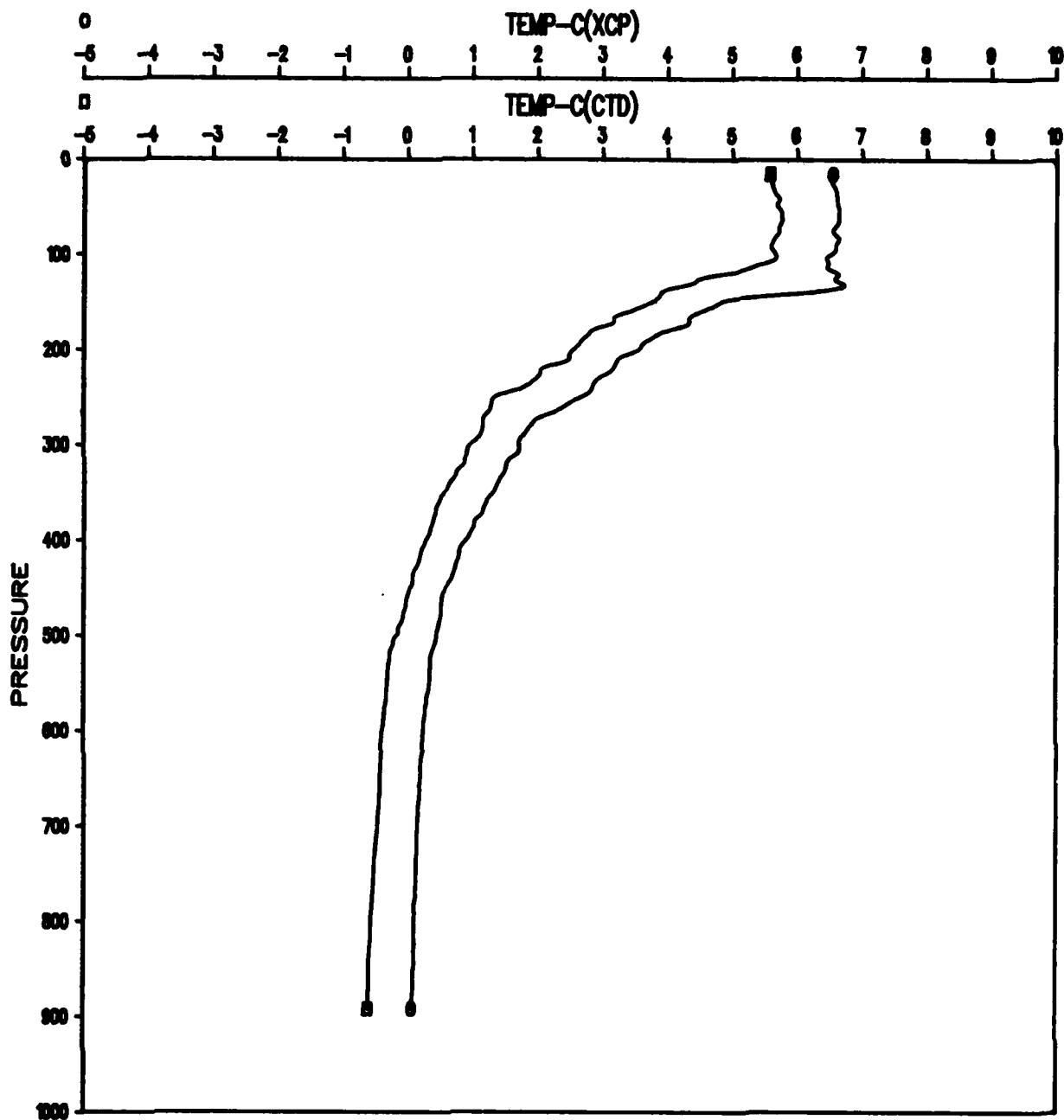


Figure C-6. File: KANE, Segment: C 525

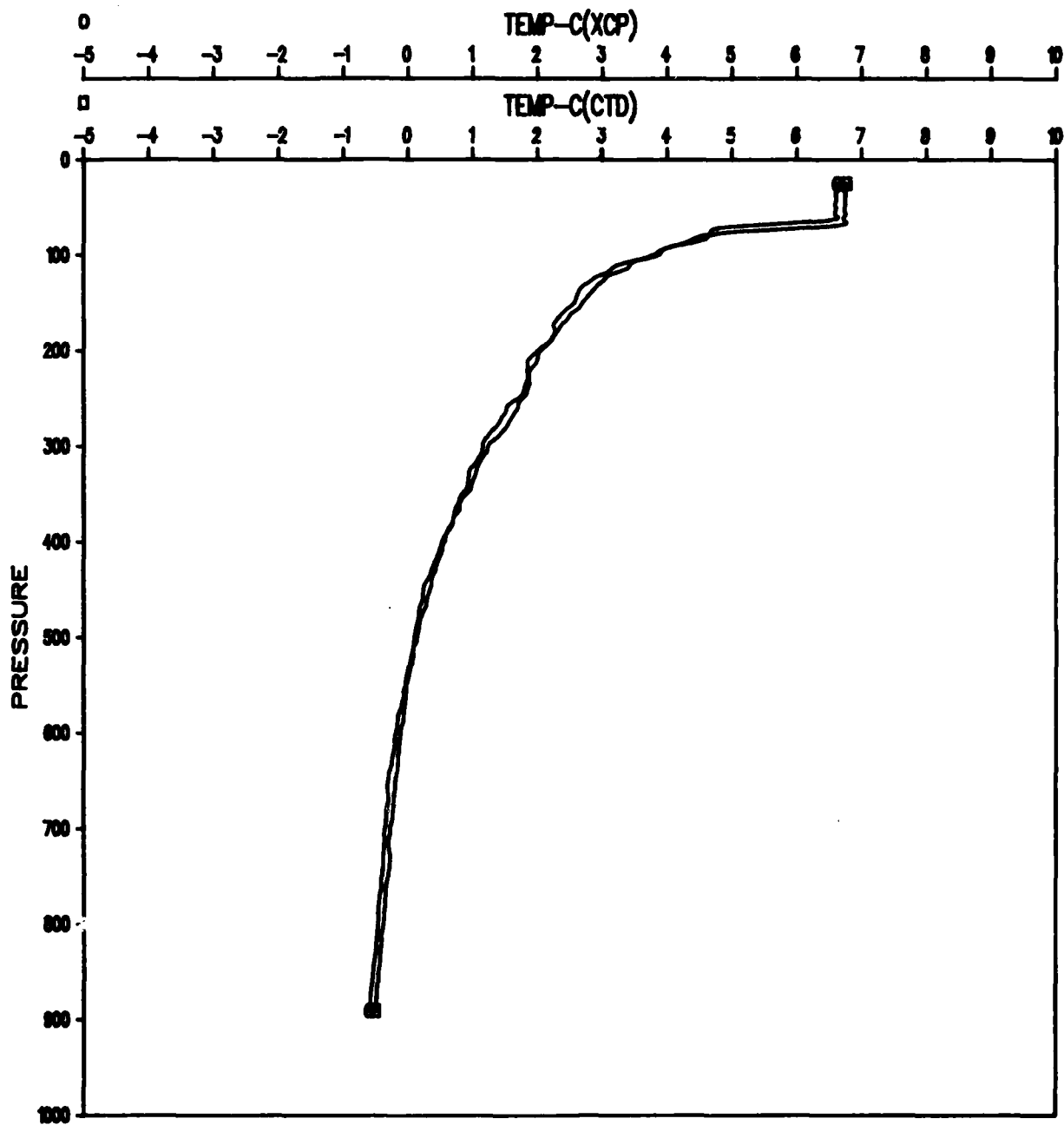


Figure C-7. File: KANE, Segment: C 534

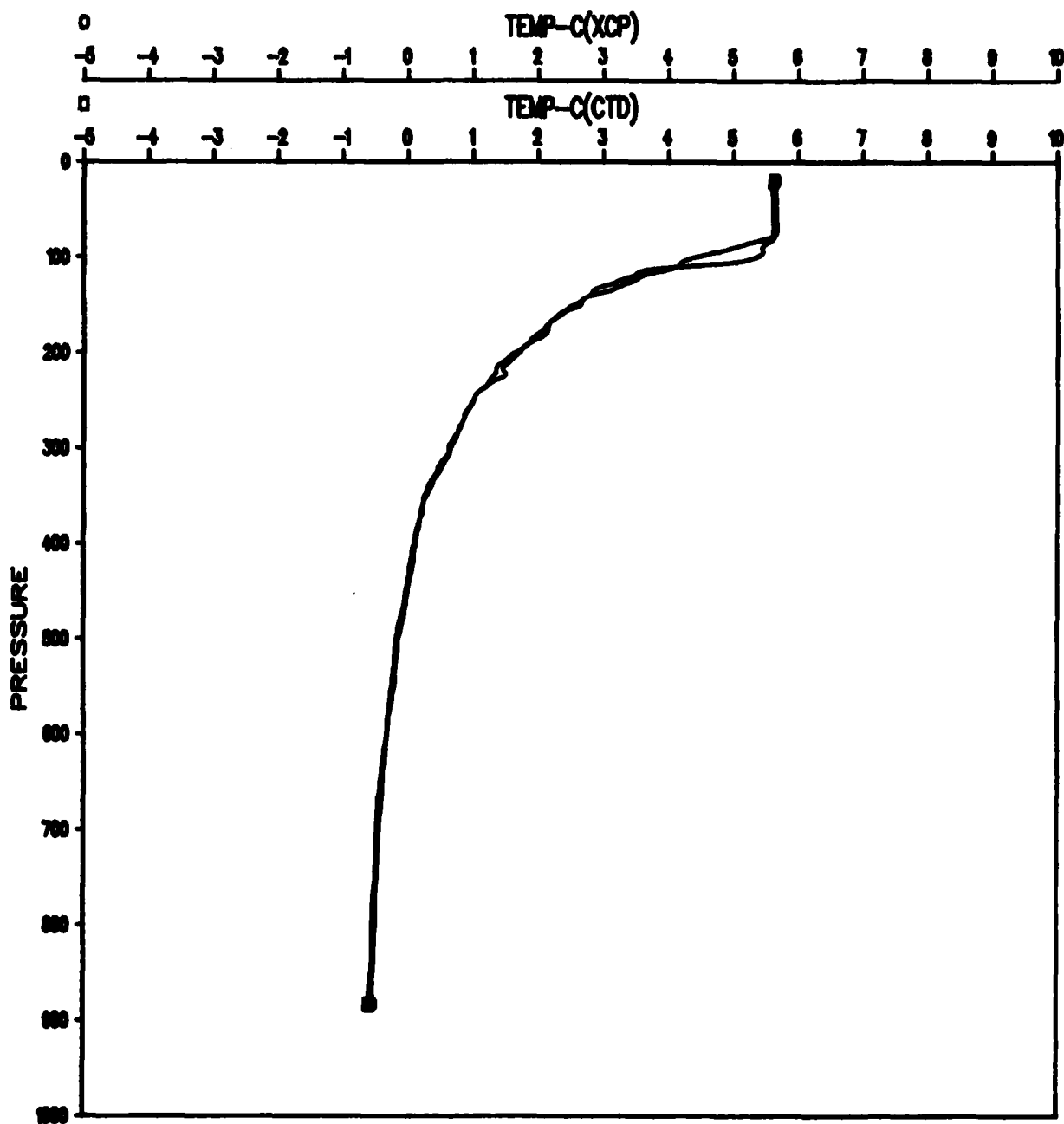


Figure C-8. File: KANE, Segment: C 538

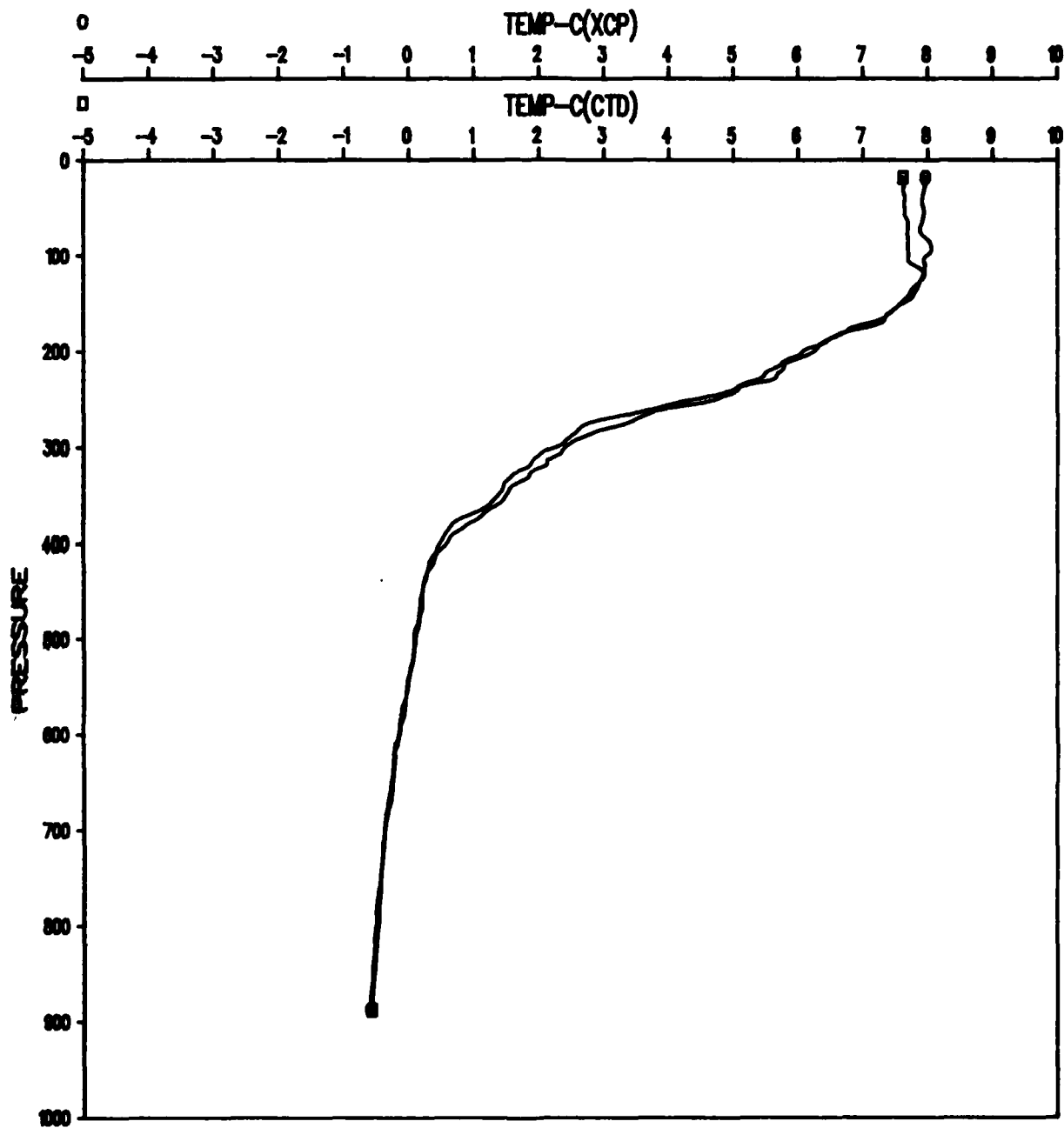


Figure C-9. File: KANE, Segment: C 546

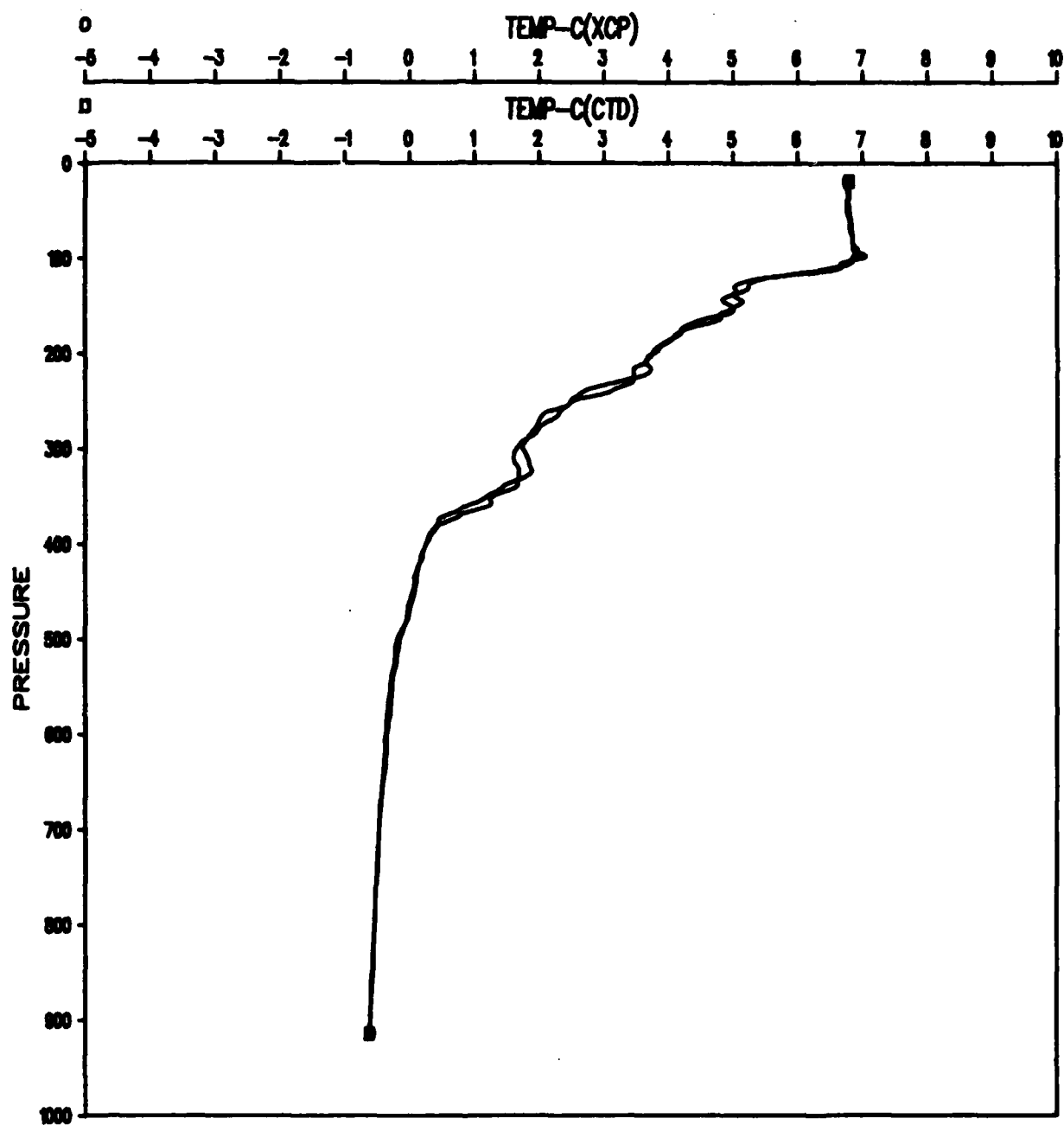


Figure C-10. File: KANE, Segment: C 547

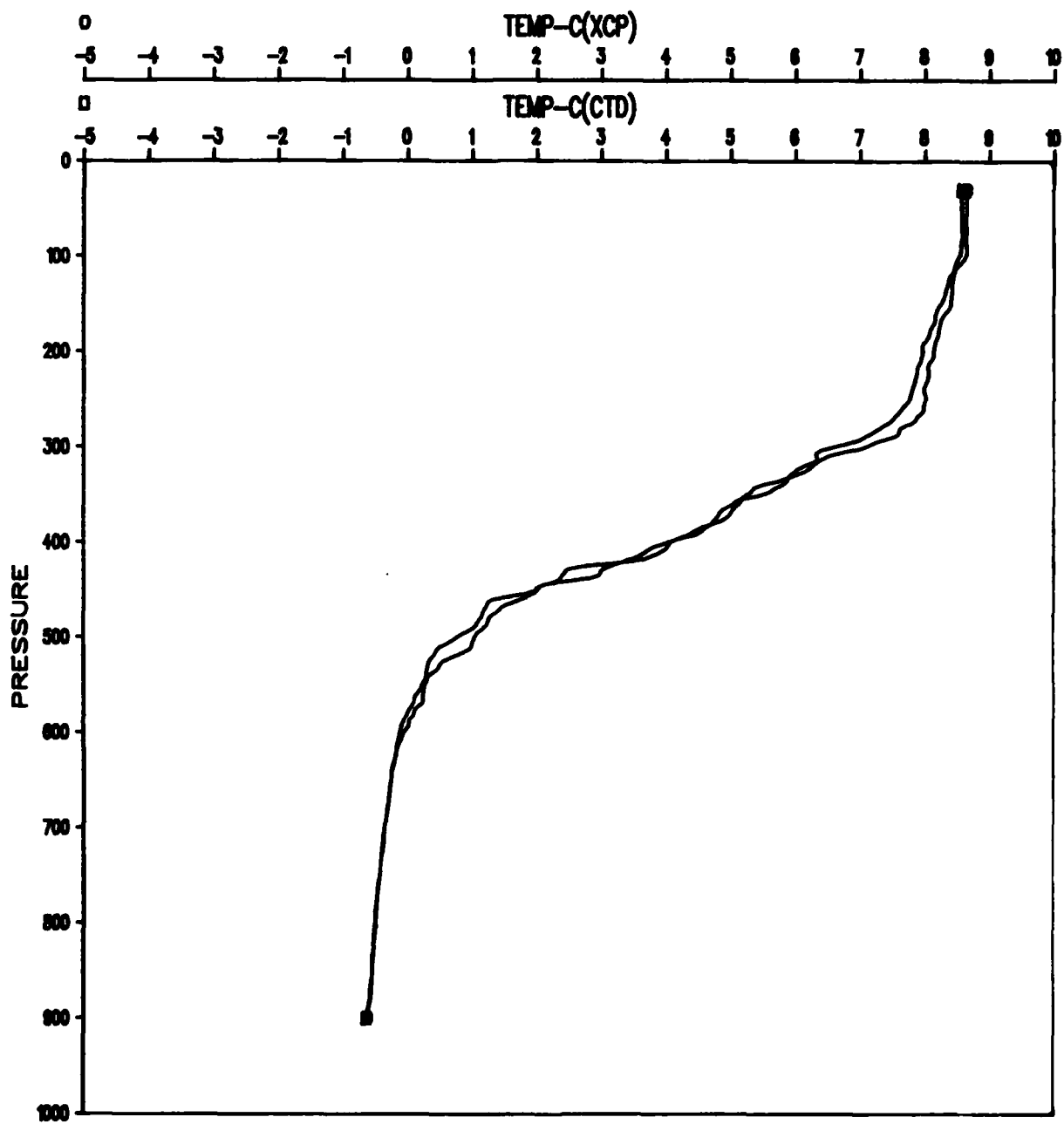


Figure C-11. File: KANE, Segment: C 548

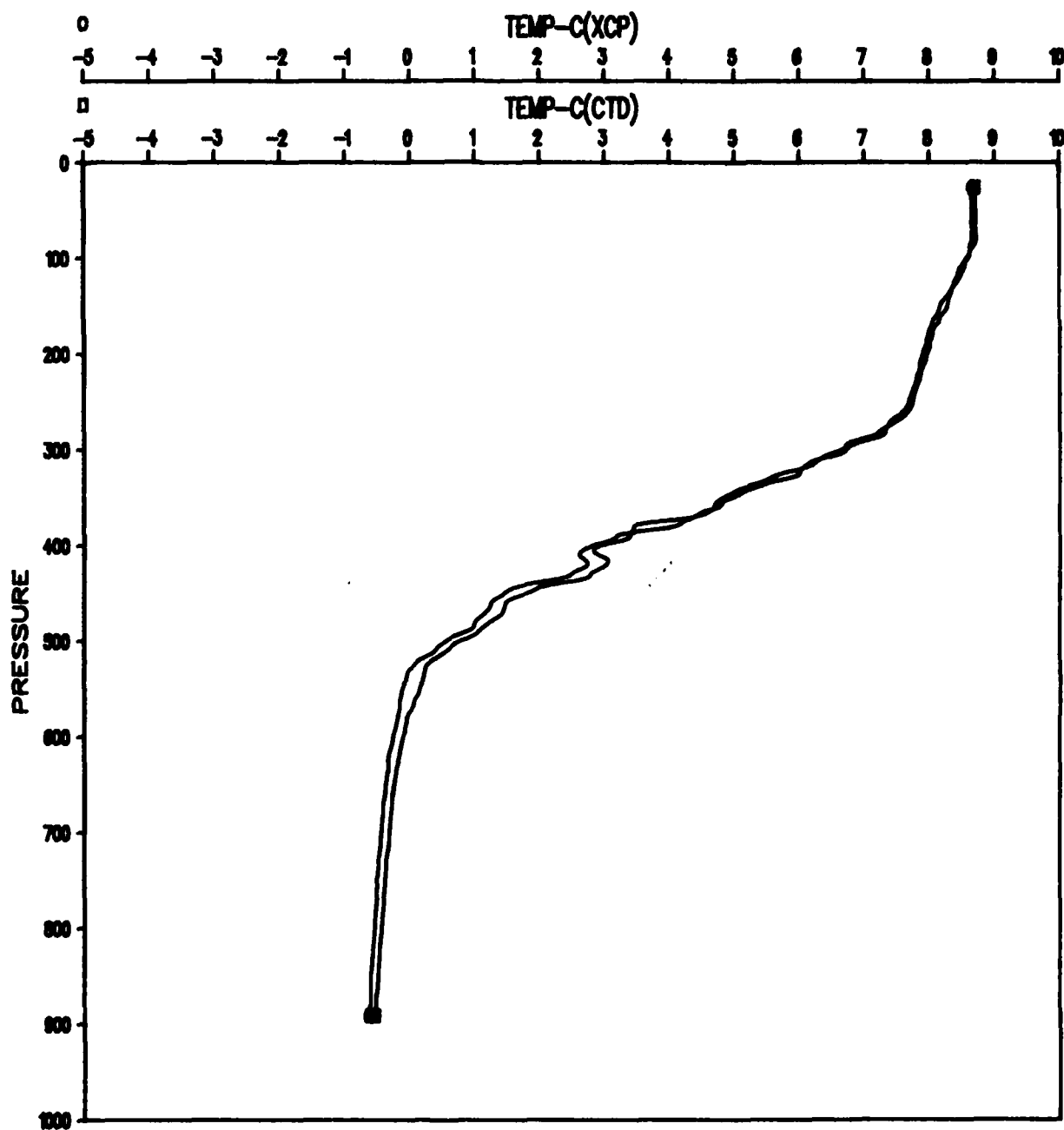


Figure C-12. File: KANE, Segment: C 550

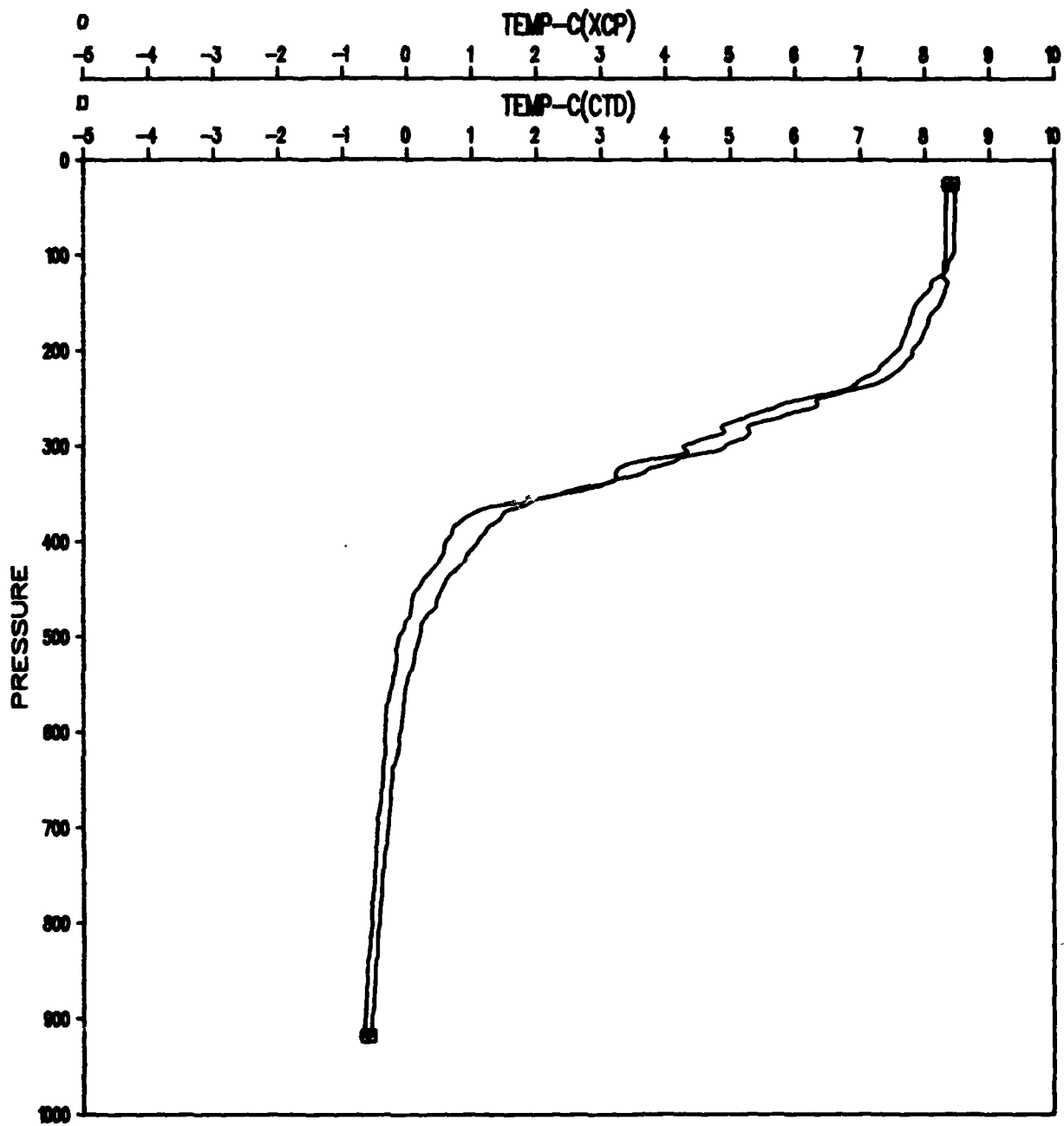


Figure C-13. File: KANE, Segment: C 551

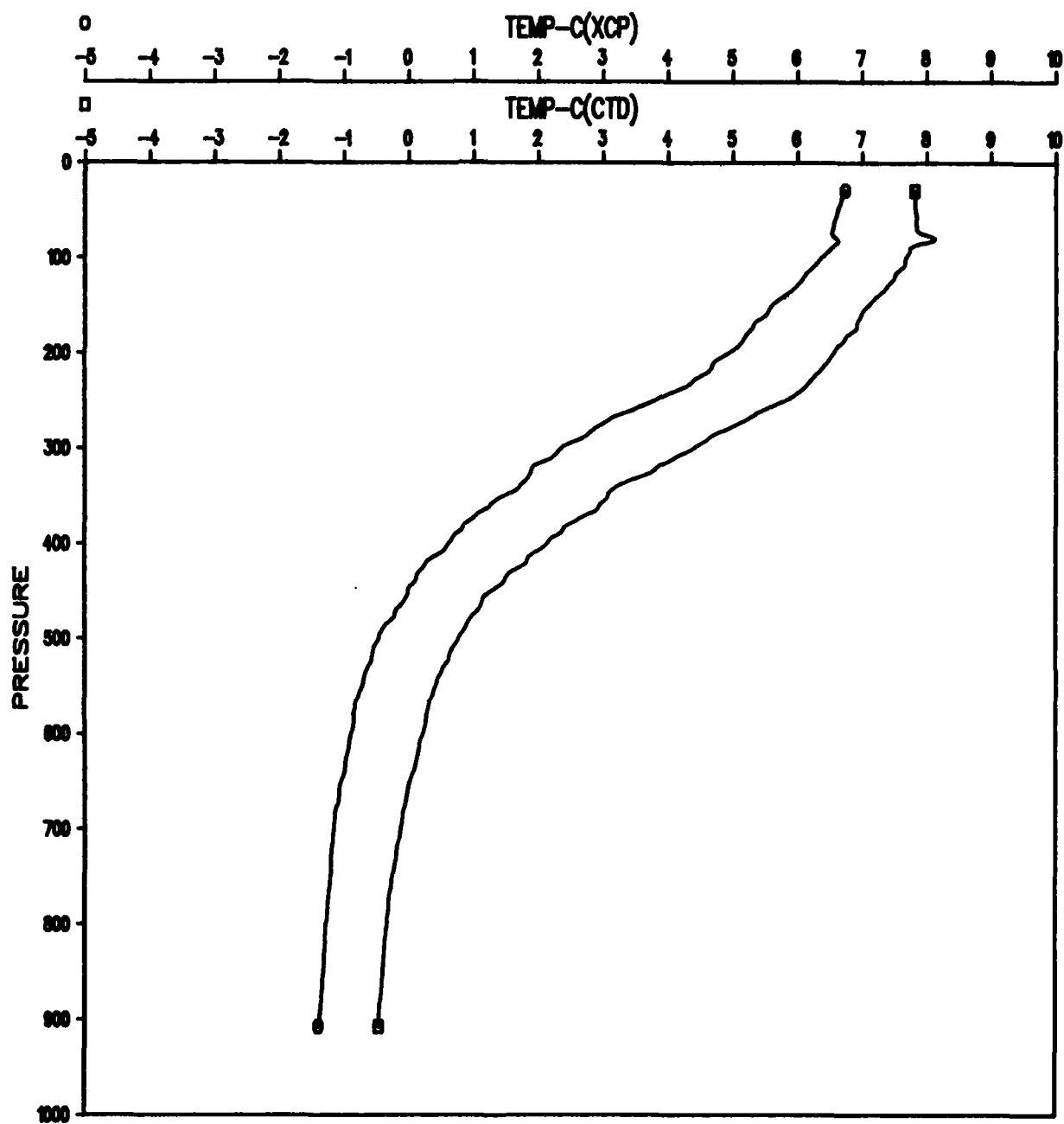


Figure C-14. File: KANE, Segment: C 563

**Appendix D:**

**Selected Vertical Brunt-Väisälä ( $N^2$ ),**

**Shear ( $S^2$ ), and Bulk Richardson**

**Number (RI-NO) Profiles**

**COMMENTS:**

**Low Pass Filtered 10 m Resolution Subsampling Interval 1 m**

**MISSING PAGE BLANK-NOT FILMED**

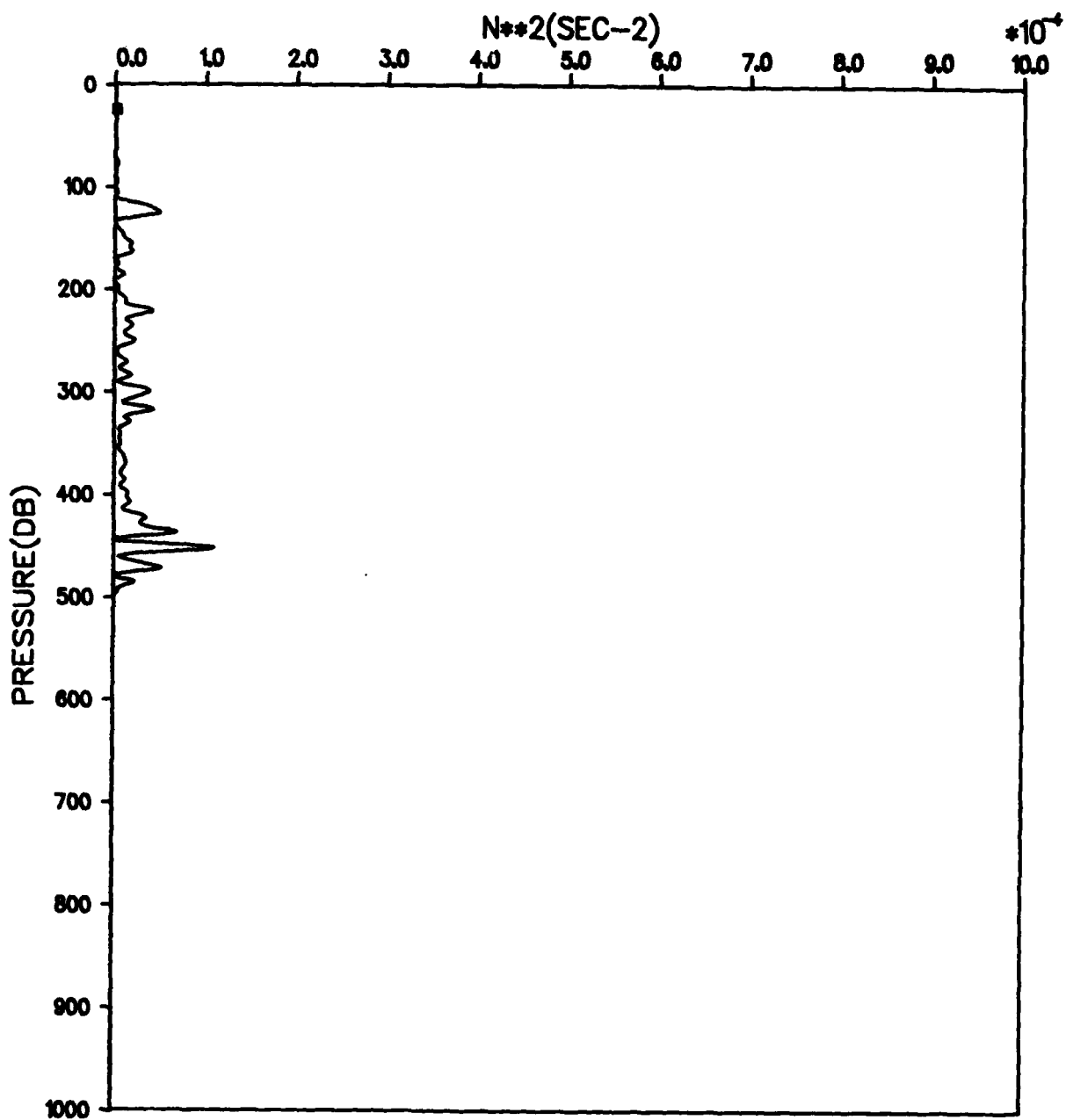


Figure D-1. File: KANE, Segment: C 503

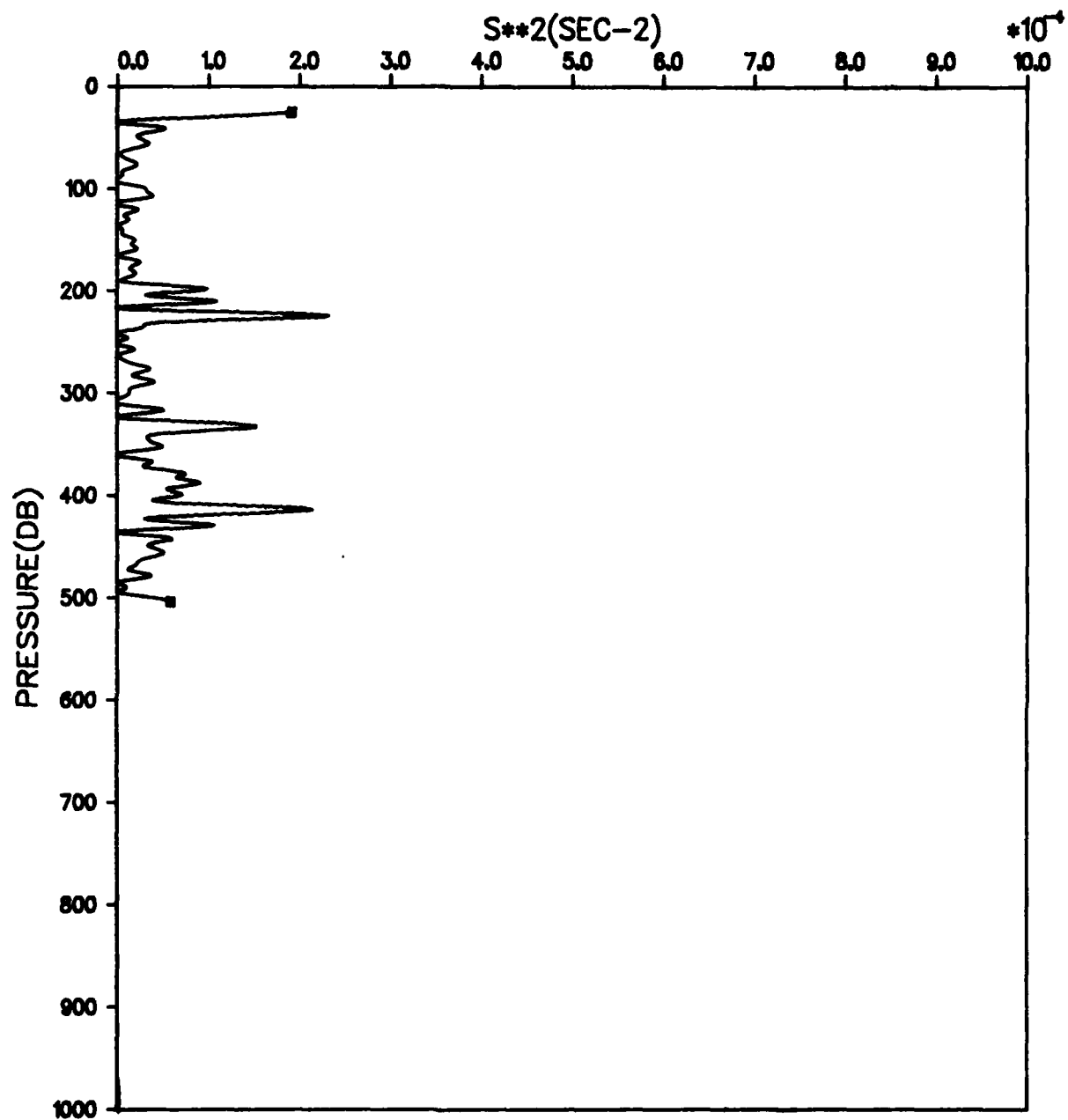


Figure D-2. File: KANE, Segment: C 503

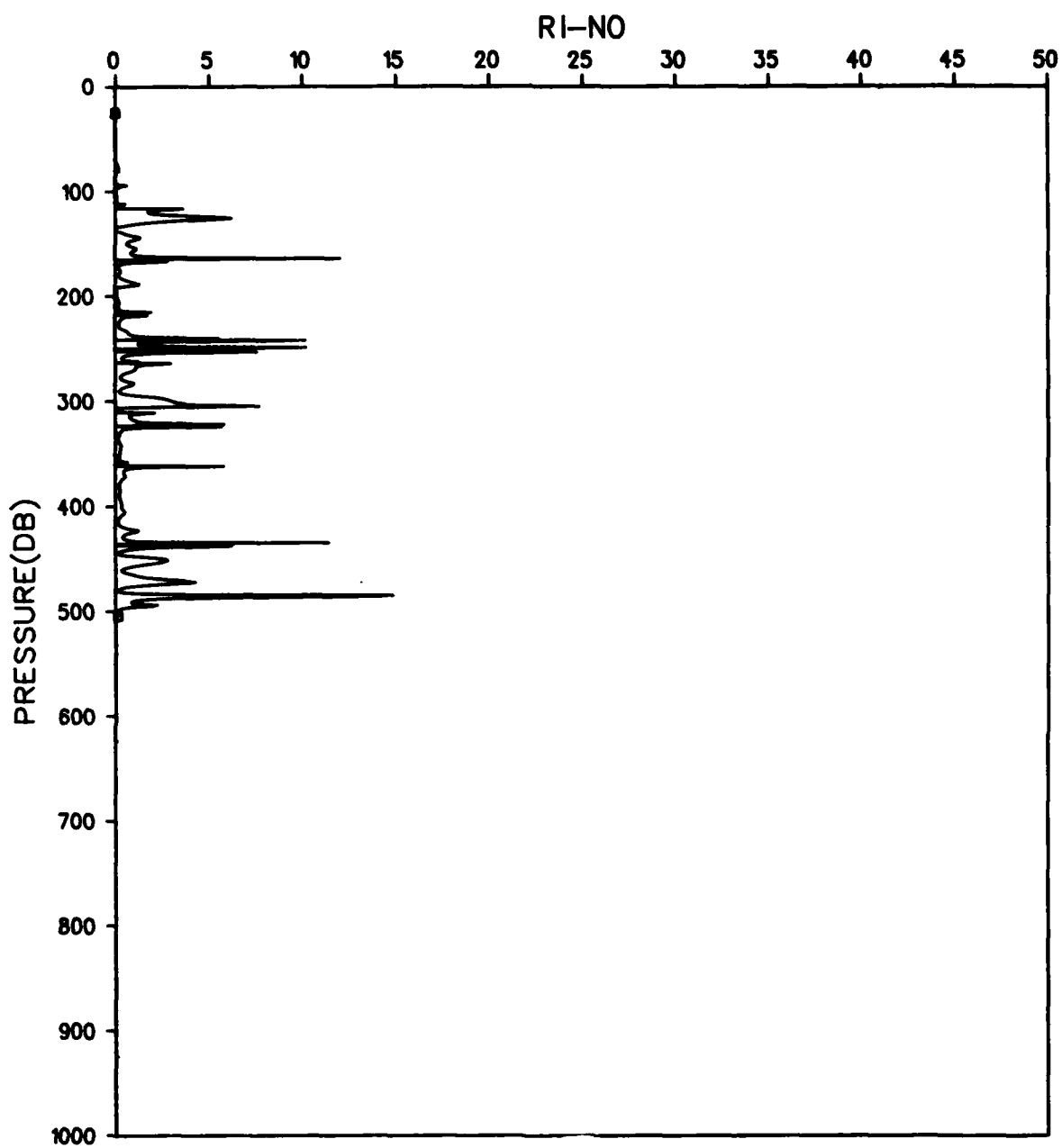


Figure D-3. File: KANE, Segment: C 503

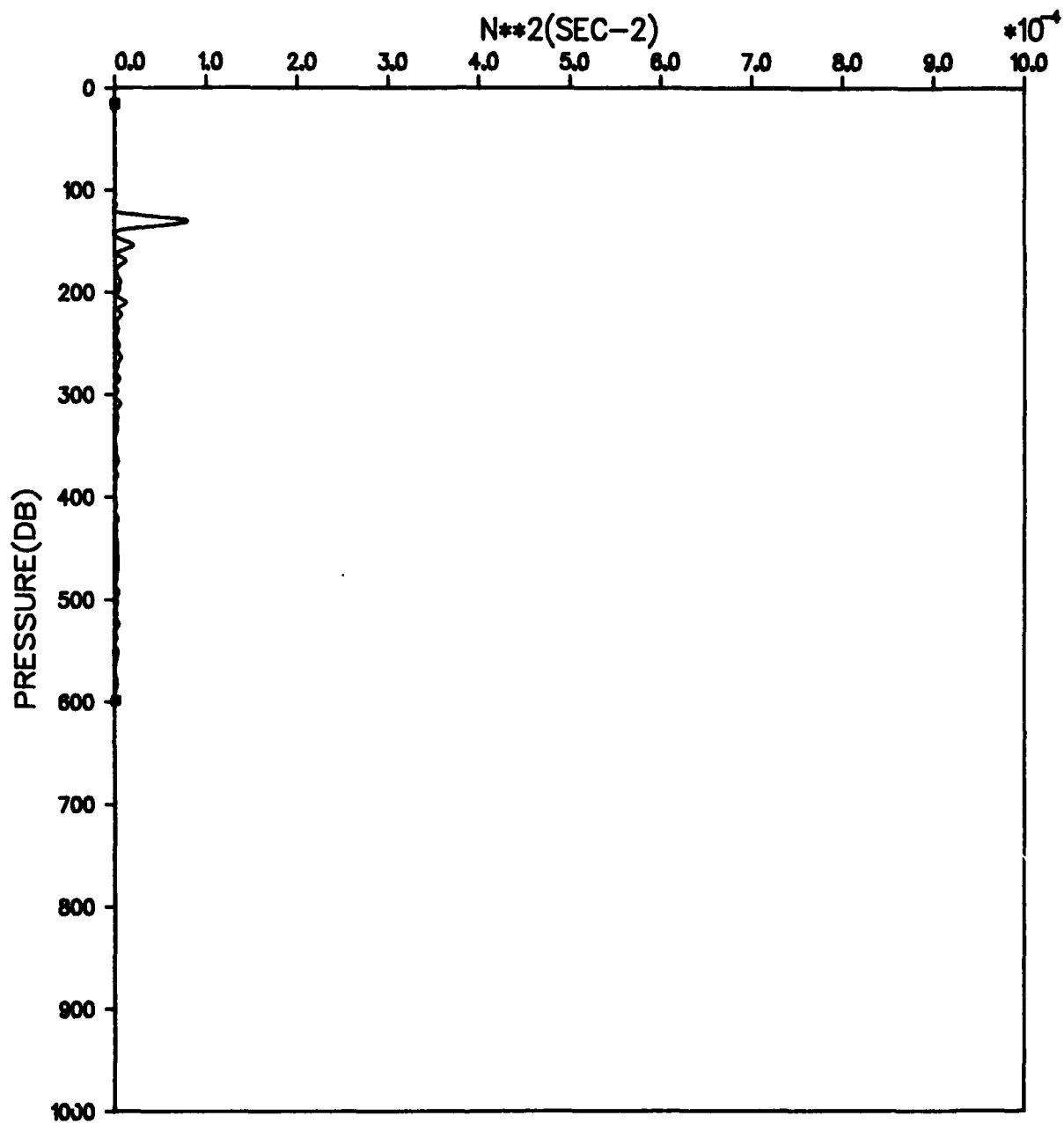


Figure D-4. File: KANE, Segment: C 504

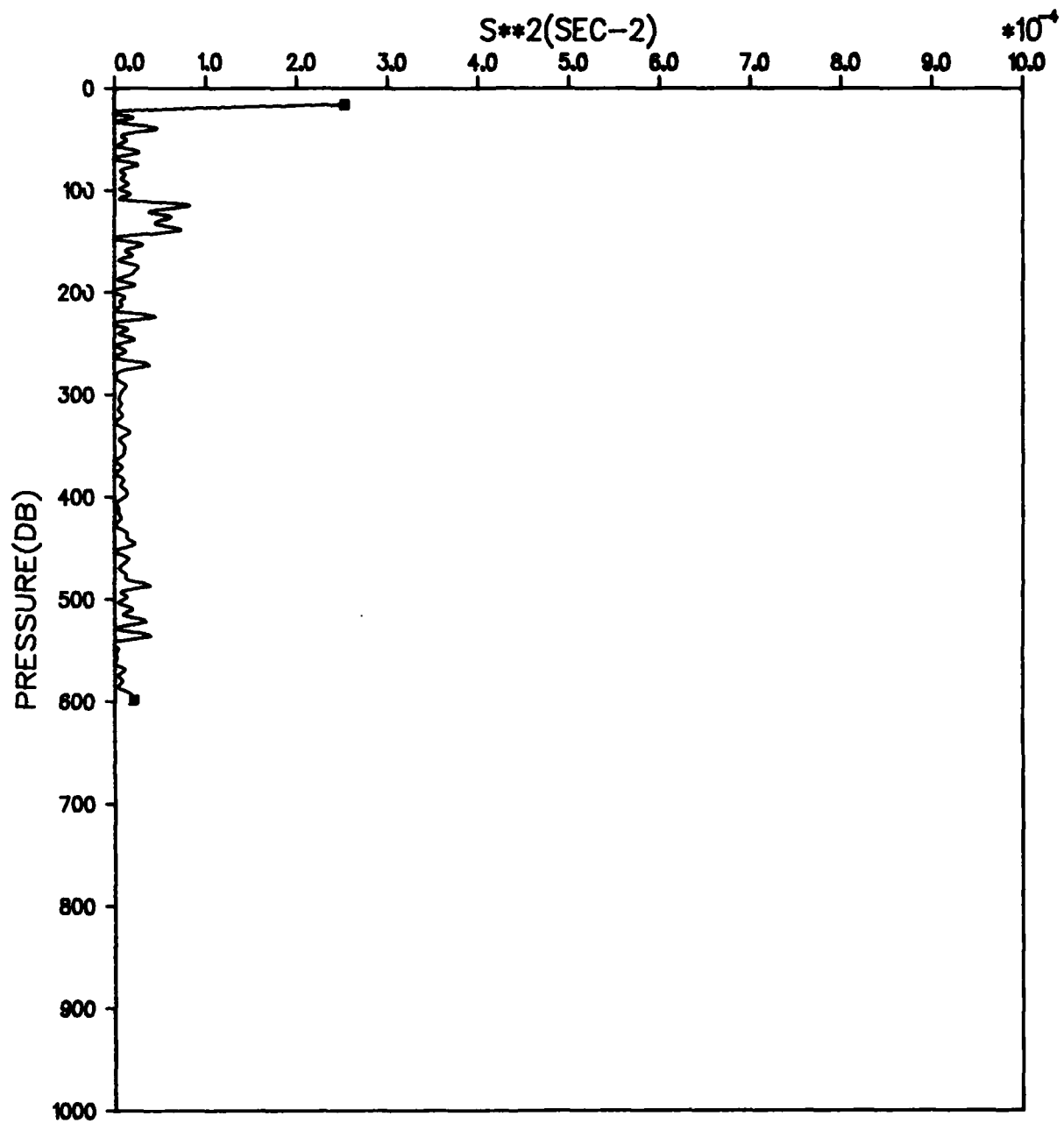


Figure D-5. File: KANE, Segment: C 504

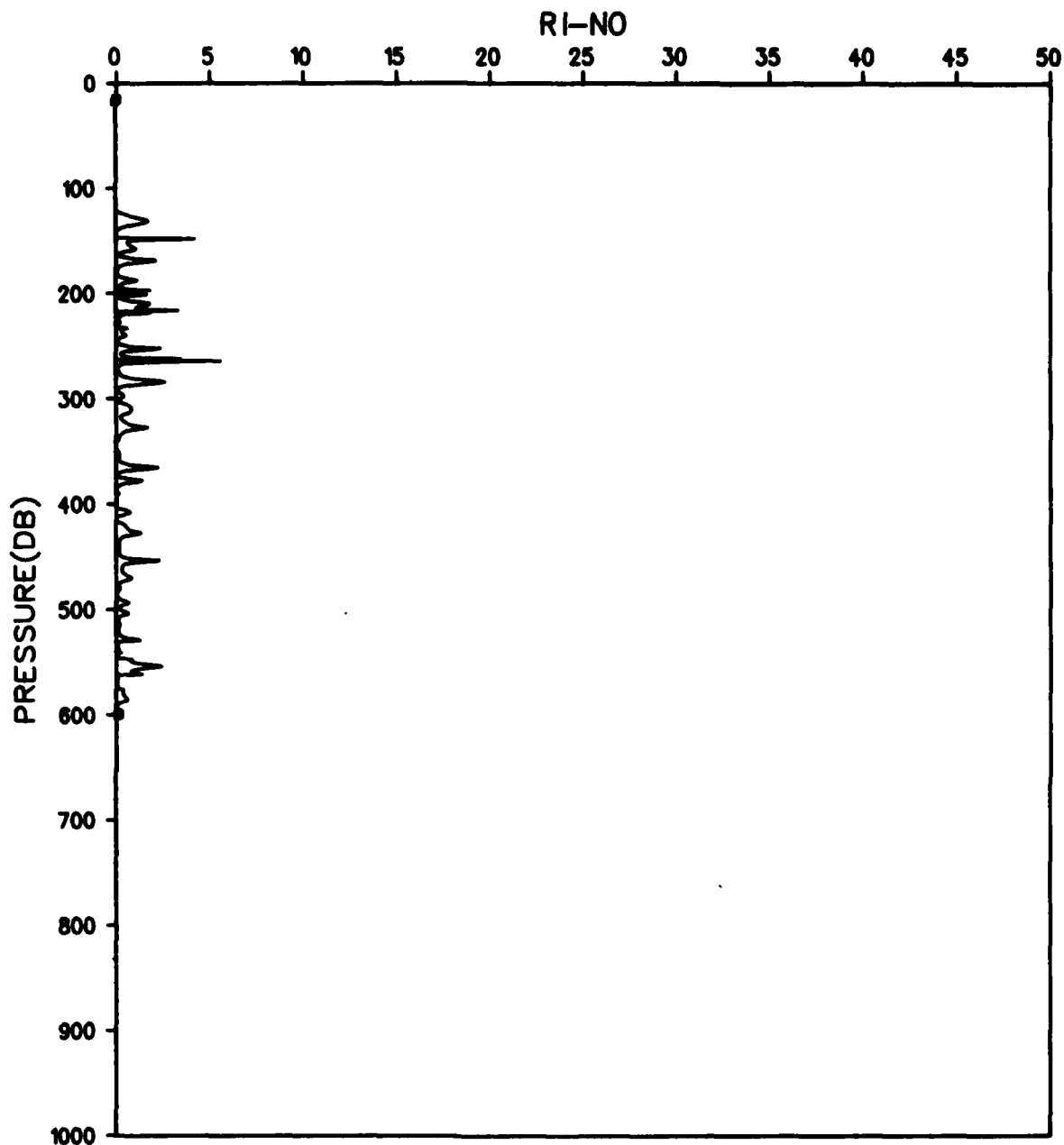


Figure D-6. File: KANE, Segment: C 504

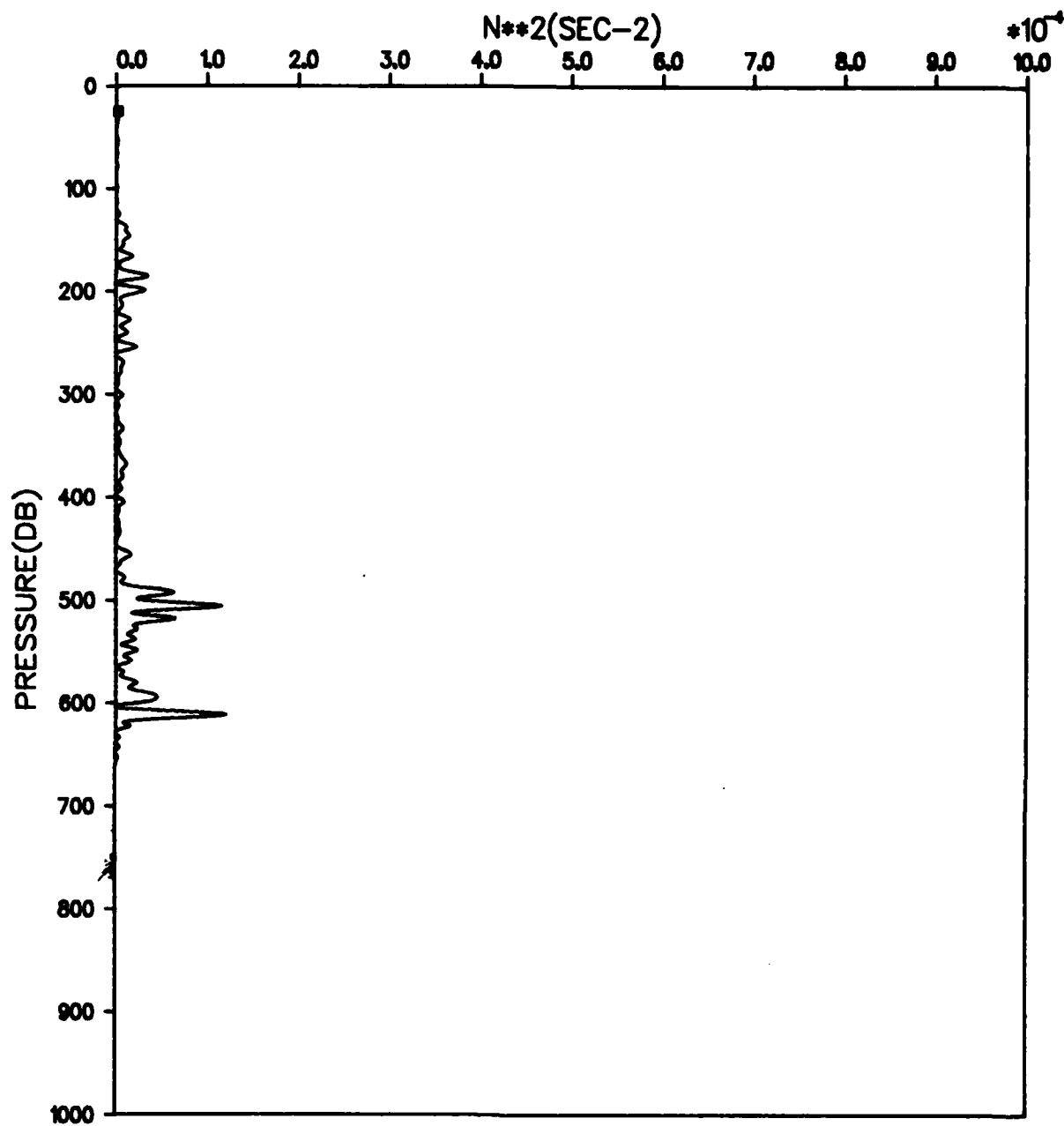


Figure D-7. File: KANE, Segment: C 517

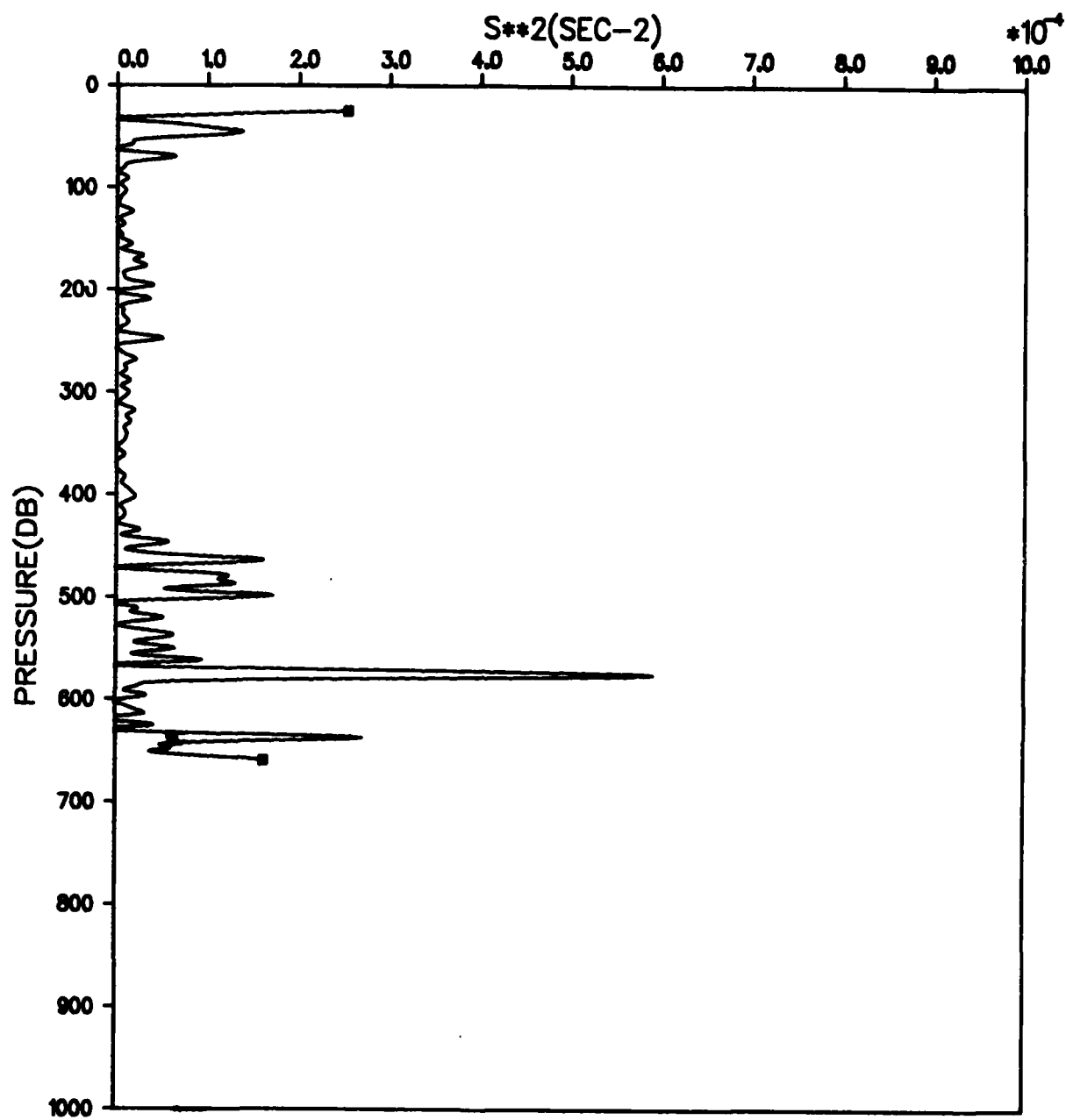


Figure D-8. File: KANE, Segment: C 517

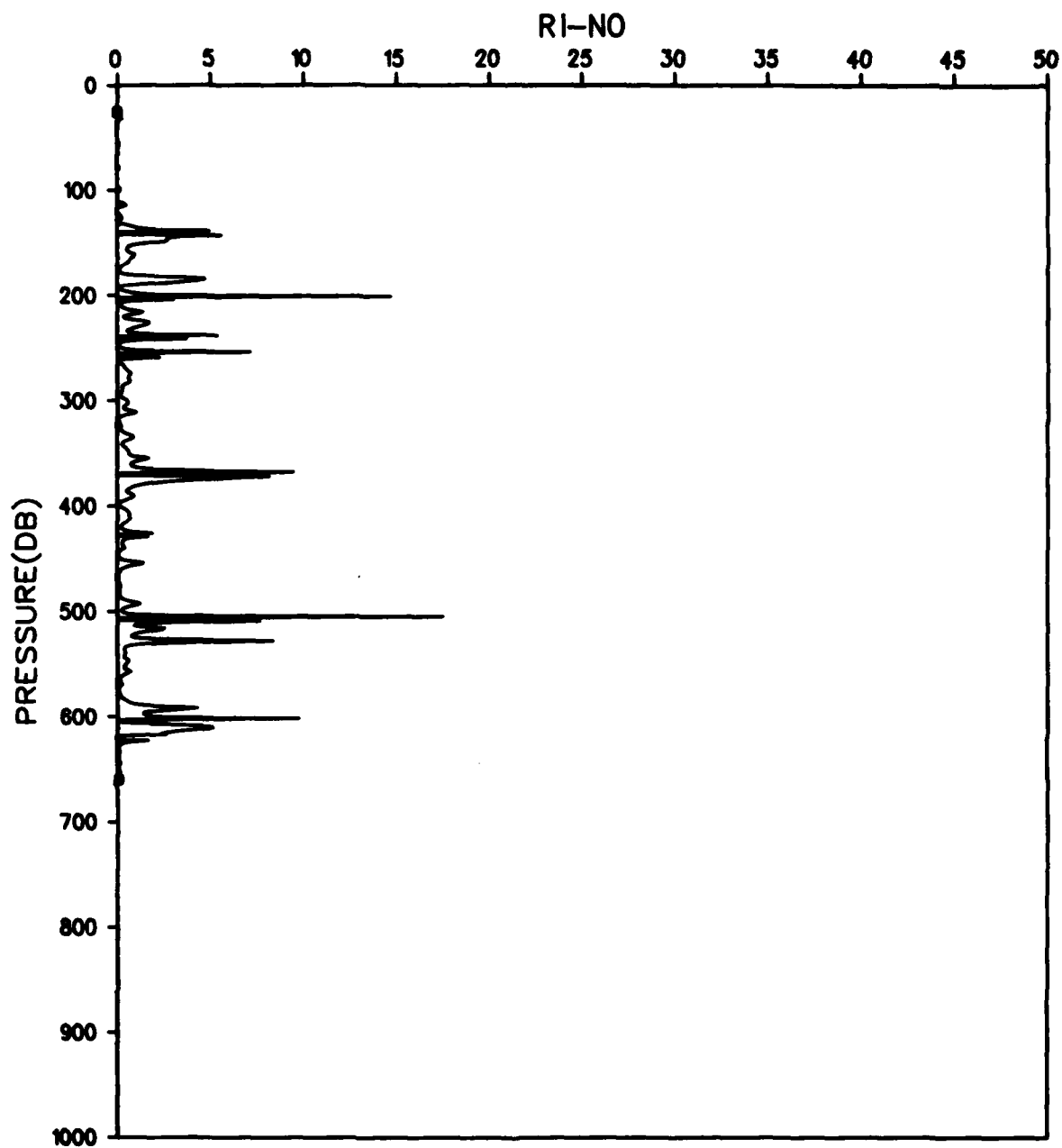


Figure D-9. File: KANE, Segment: C 517

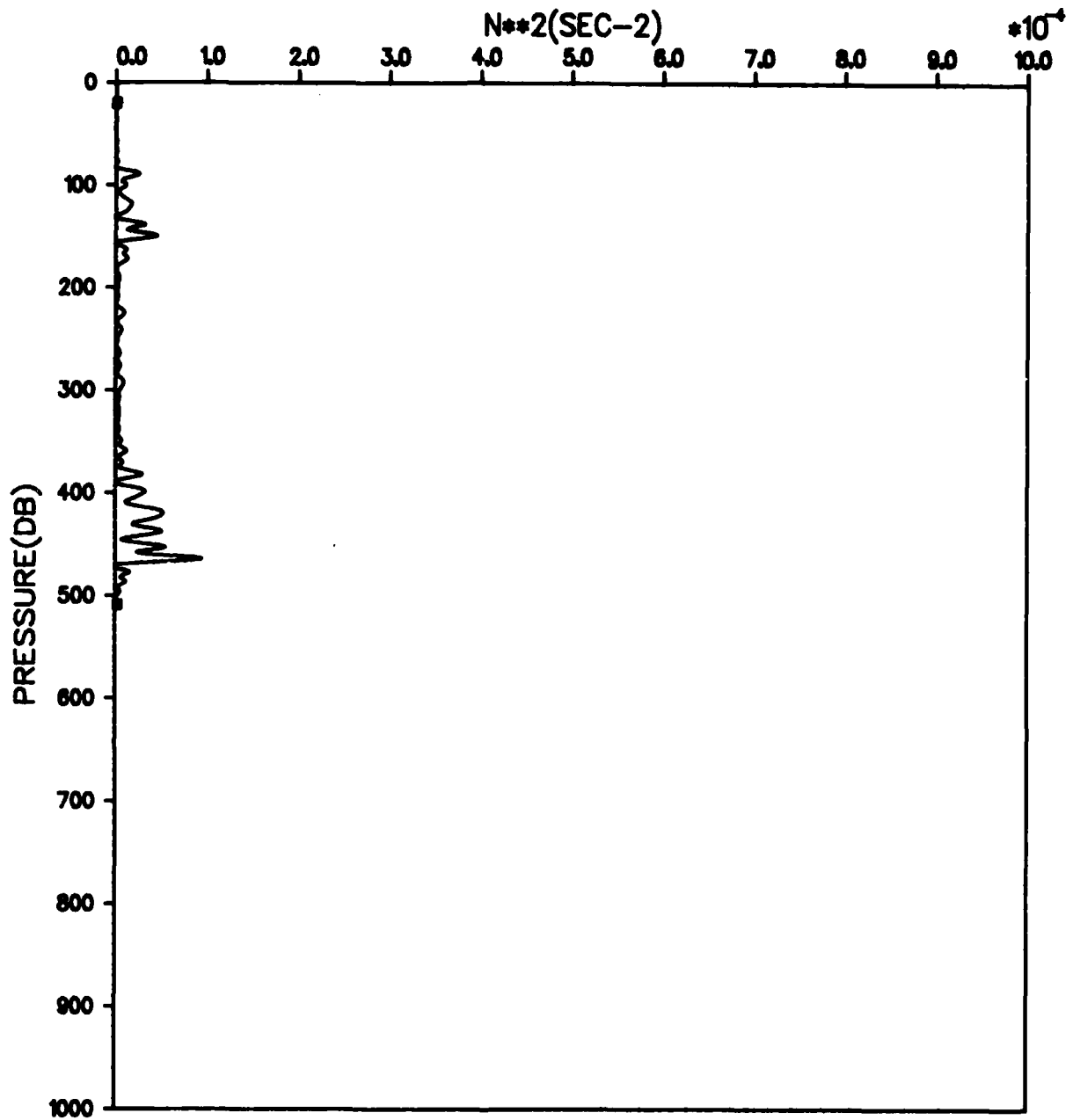


Figure D-10. File: KANE, Segment: C 519

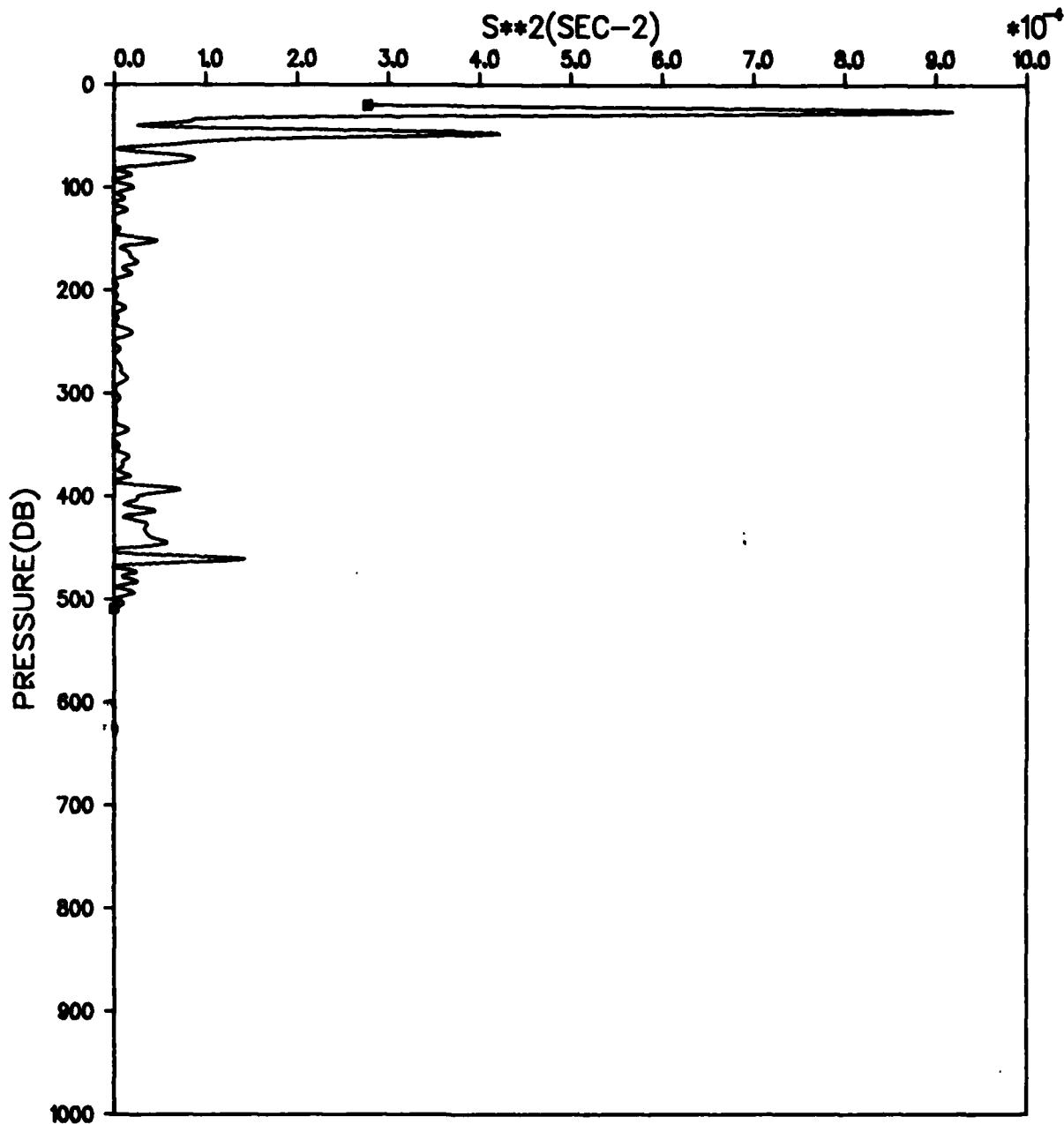


Figure D-11. File: KANE, Segment: C 519

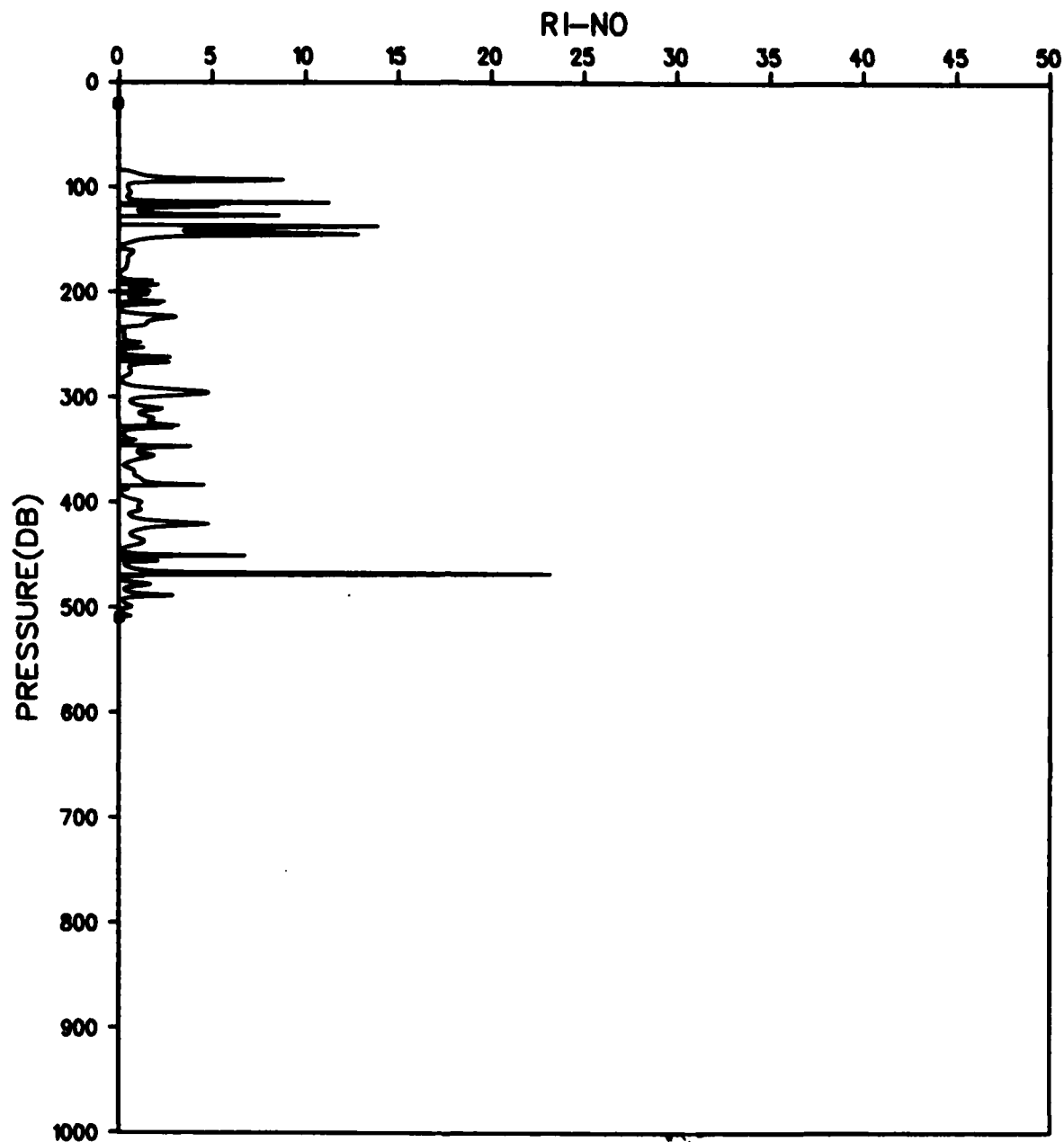


Figure D-12. File: KANE, Segment: C 519

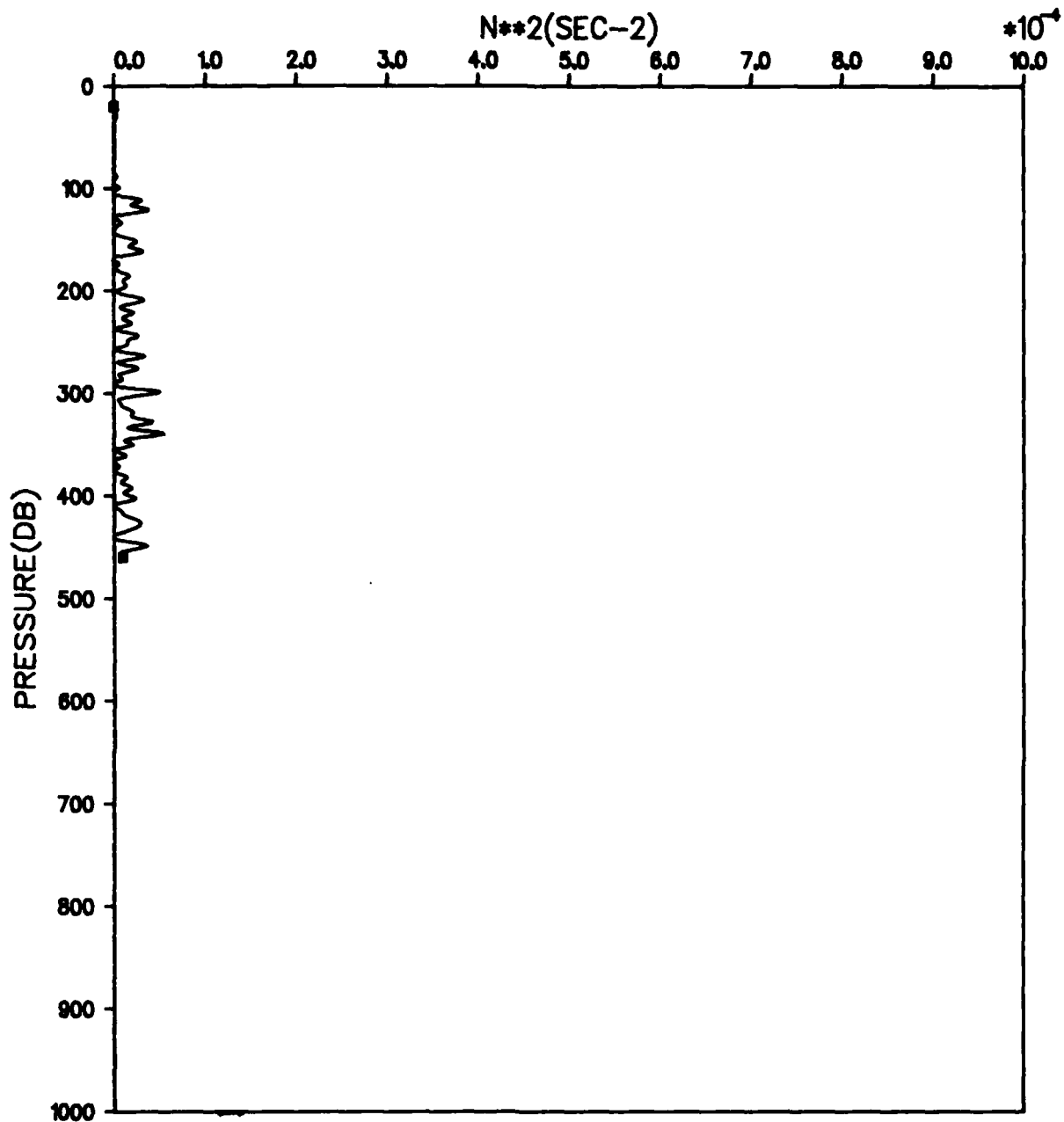


Figure D-13. File: KANE, Segment: C 520

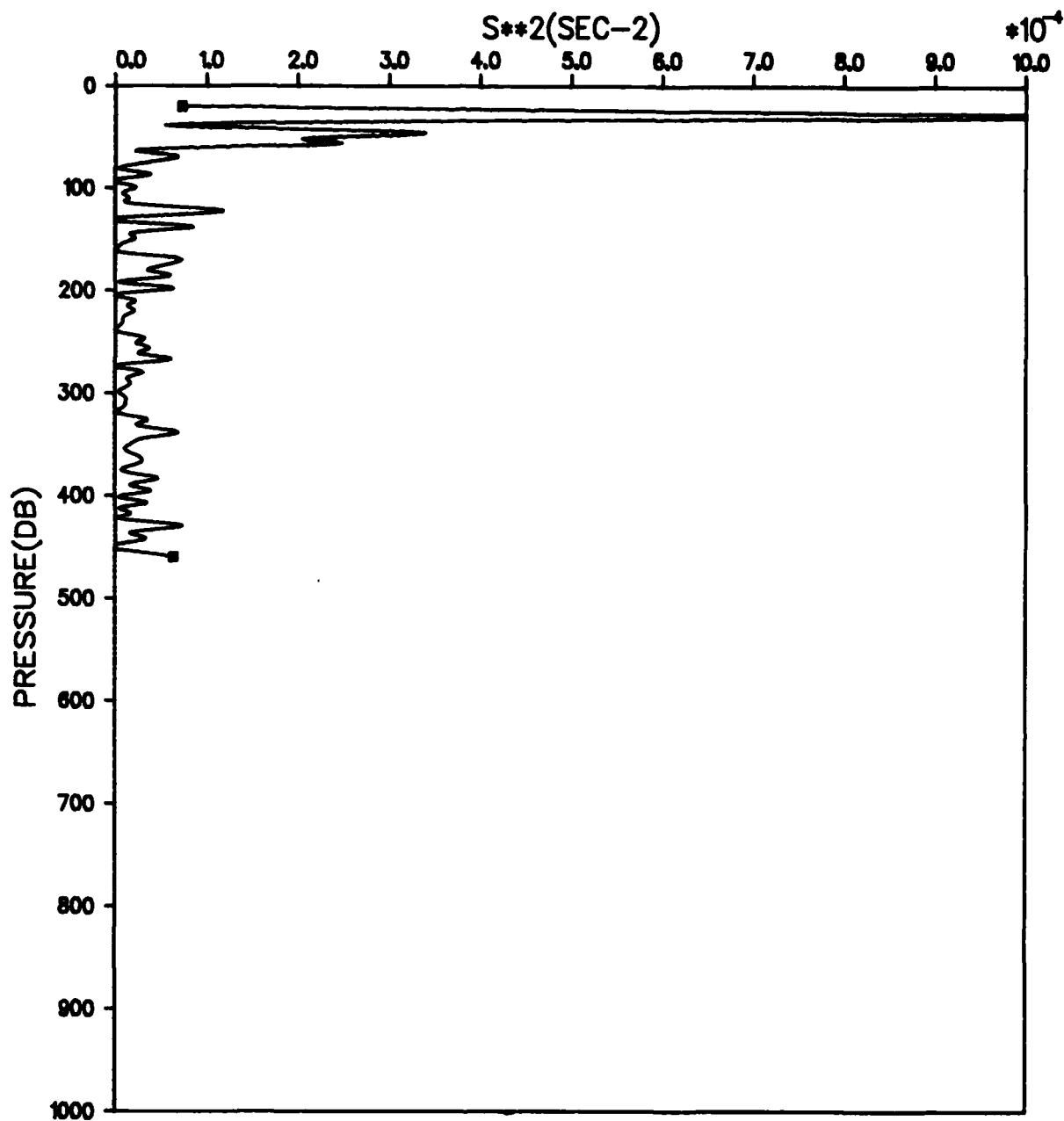


Figure D-14. File: KANE, Segment: C 520

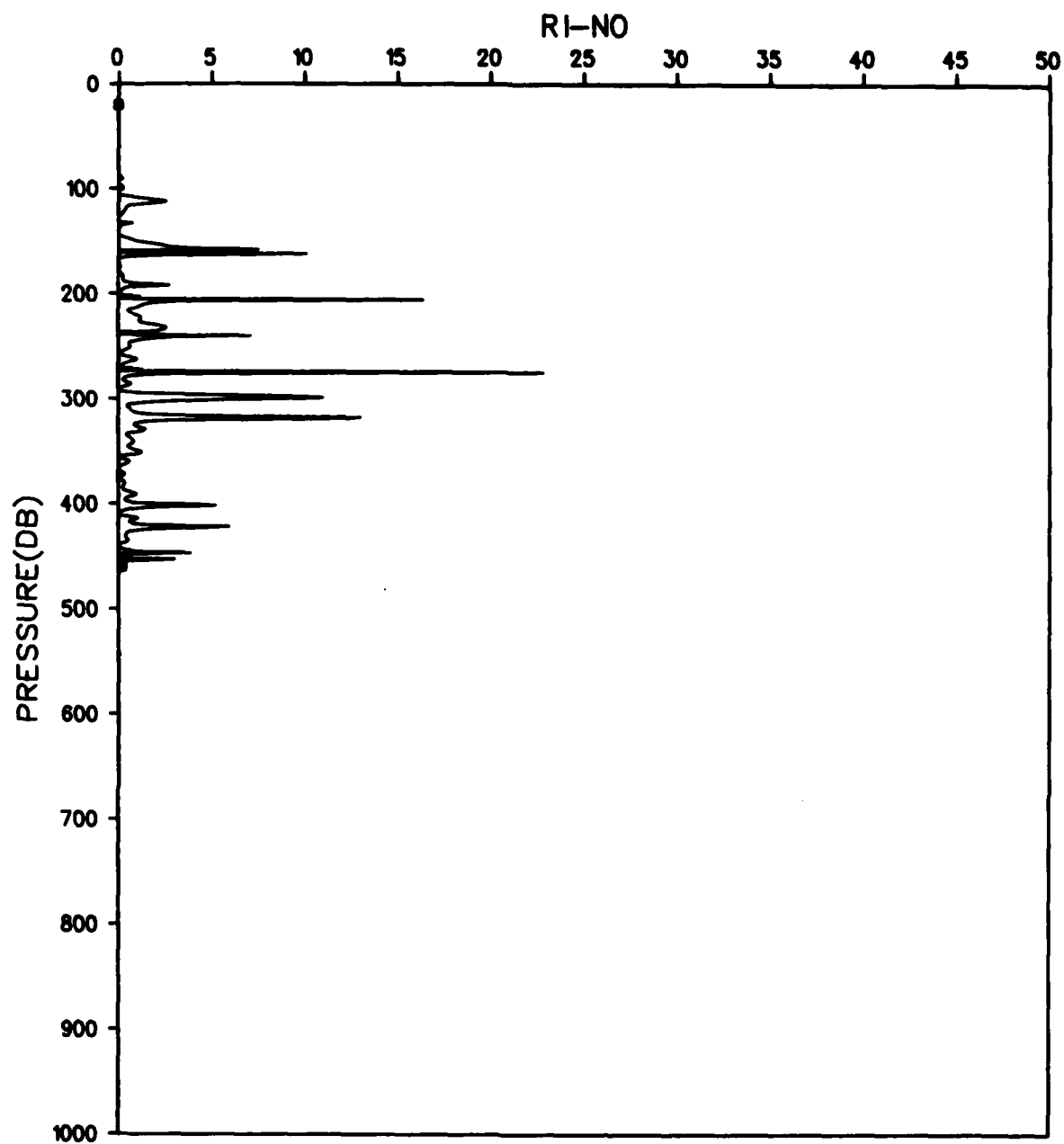


Figure D-15. File: KANE, Segment: C 520

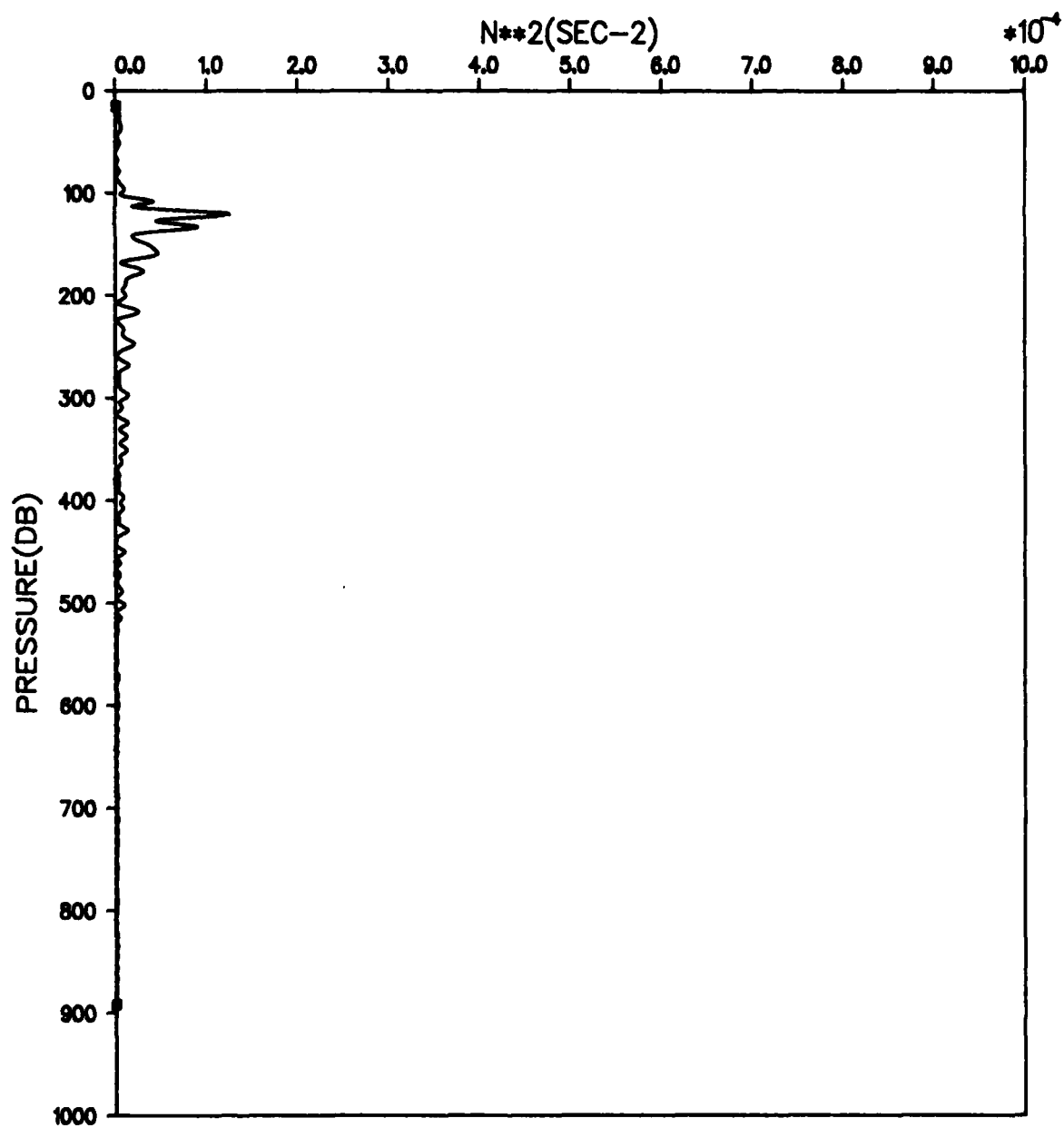


Figure D-16. File: KANE, Segment: C 525

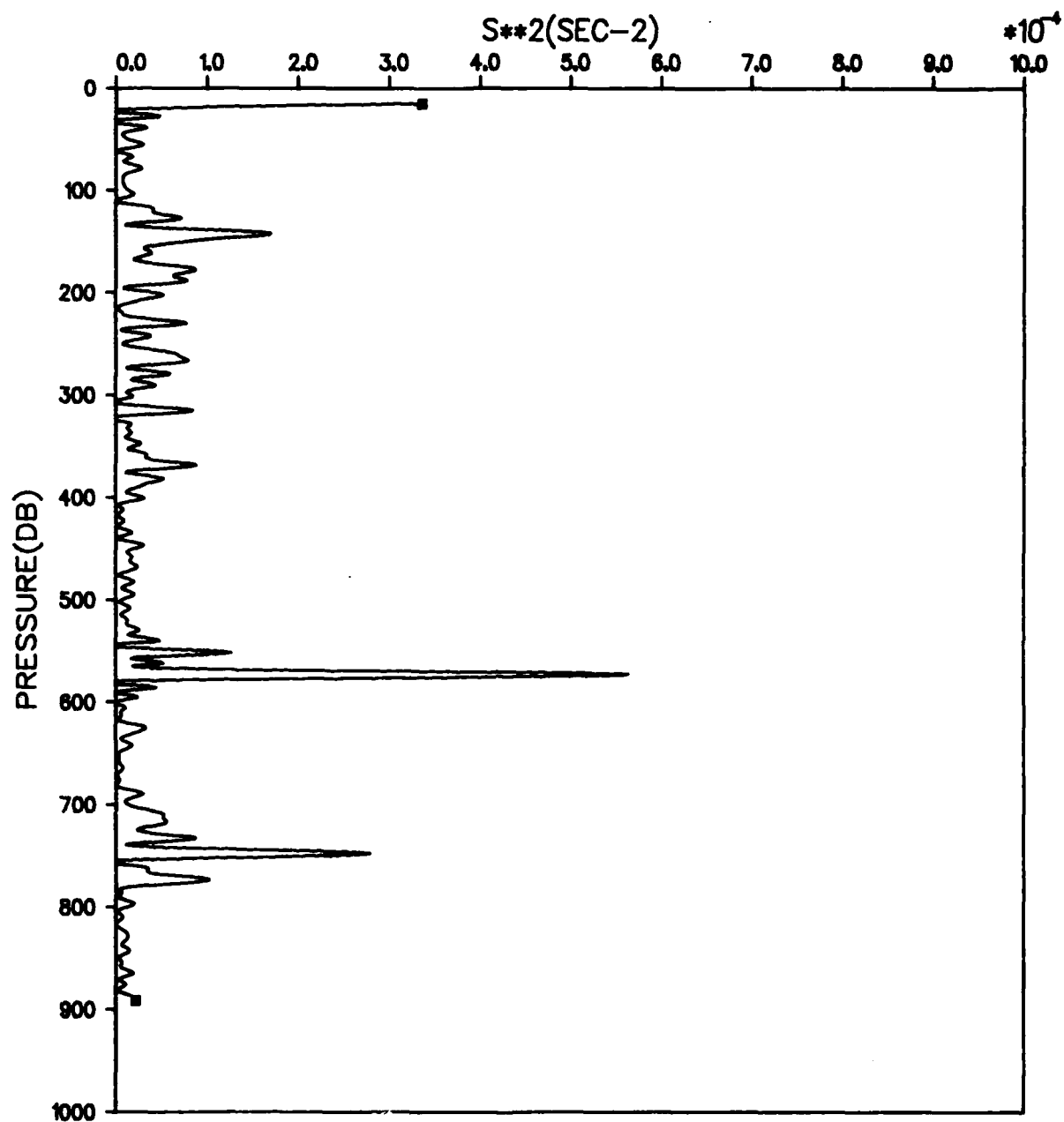


Figure D-17. File: KANE, Segment: C 525

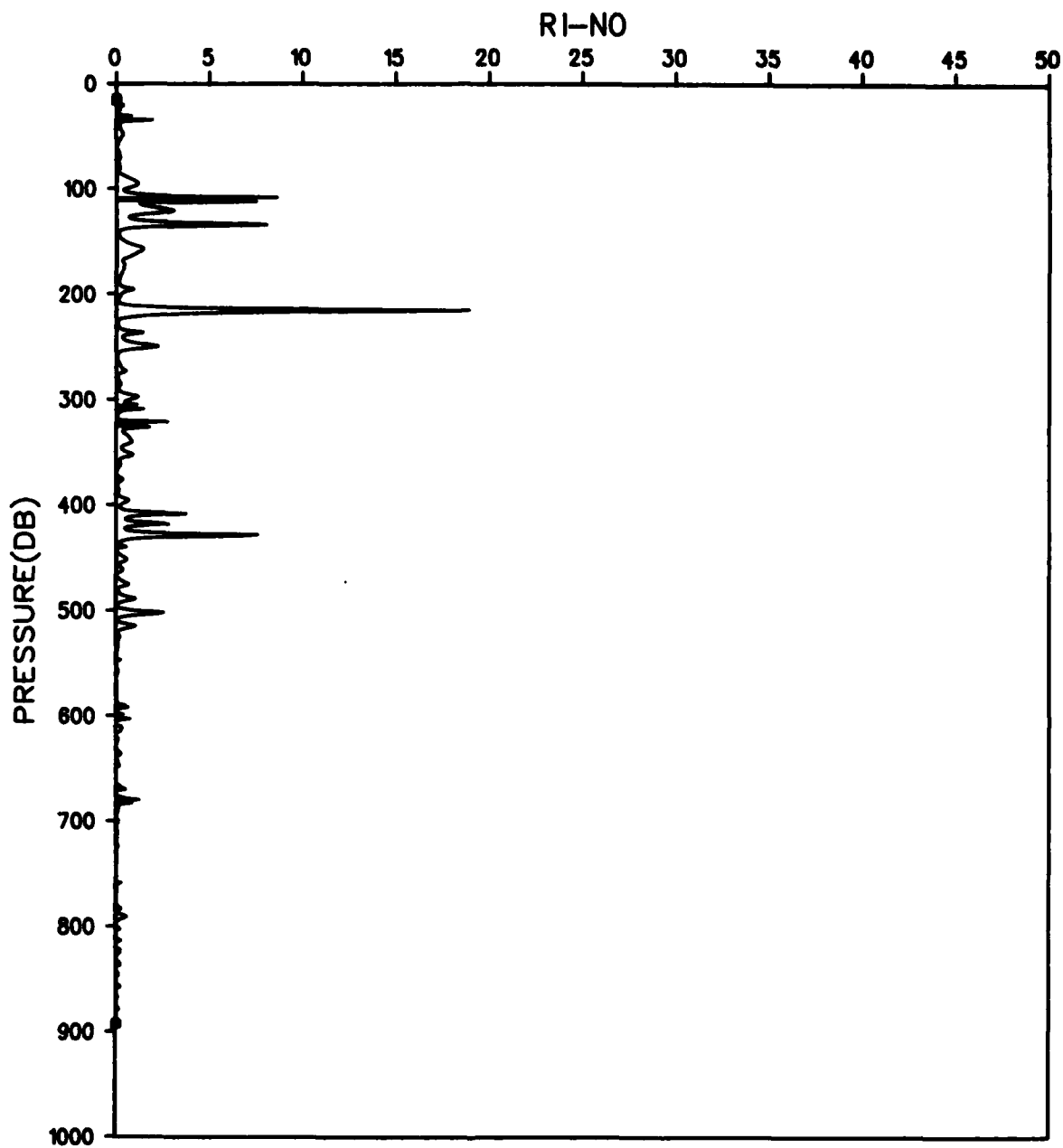


Figure D-18. File: KANE, Segment: C 525

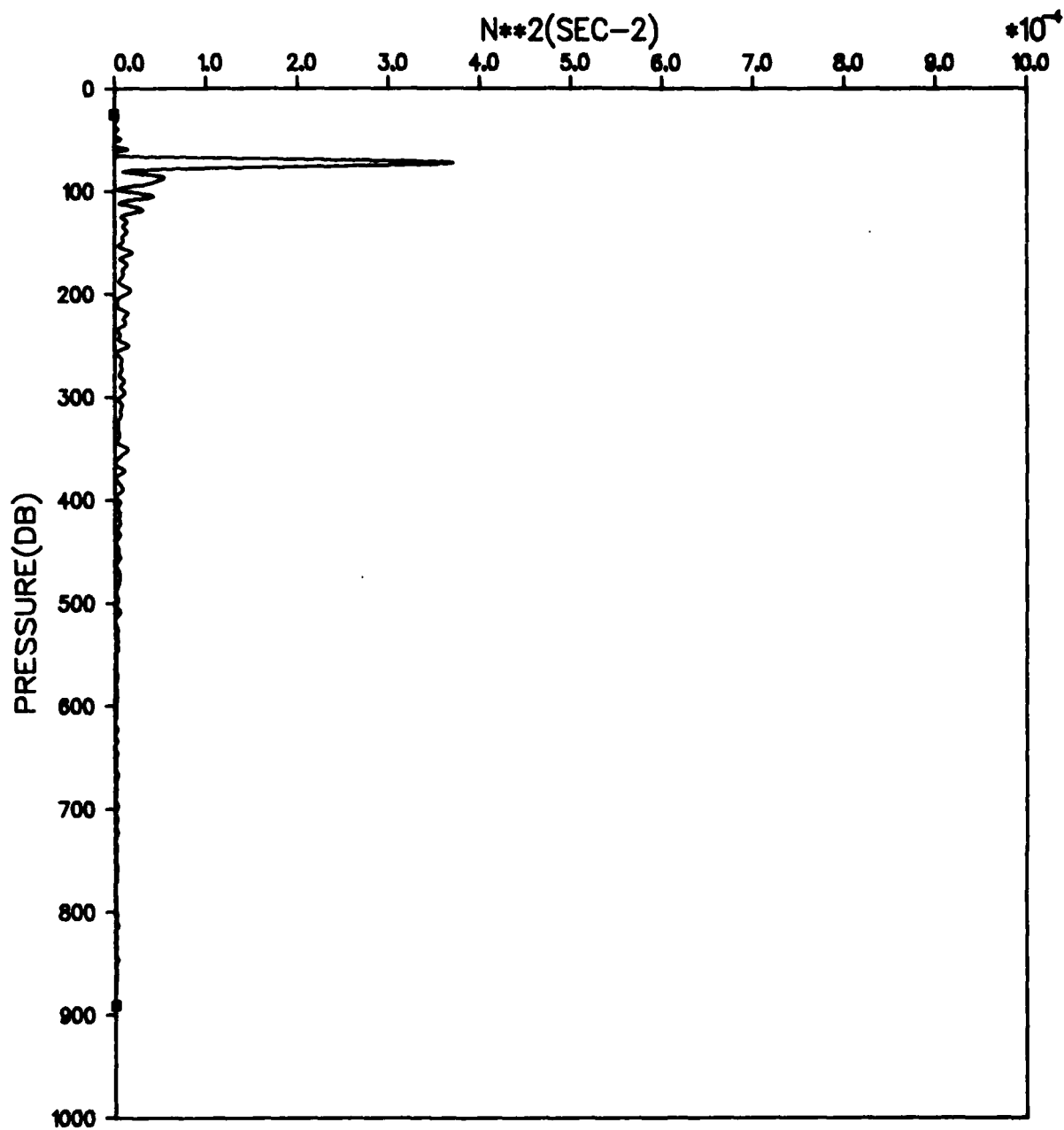


Figure D-19. File: KANE, Segment: C 534

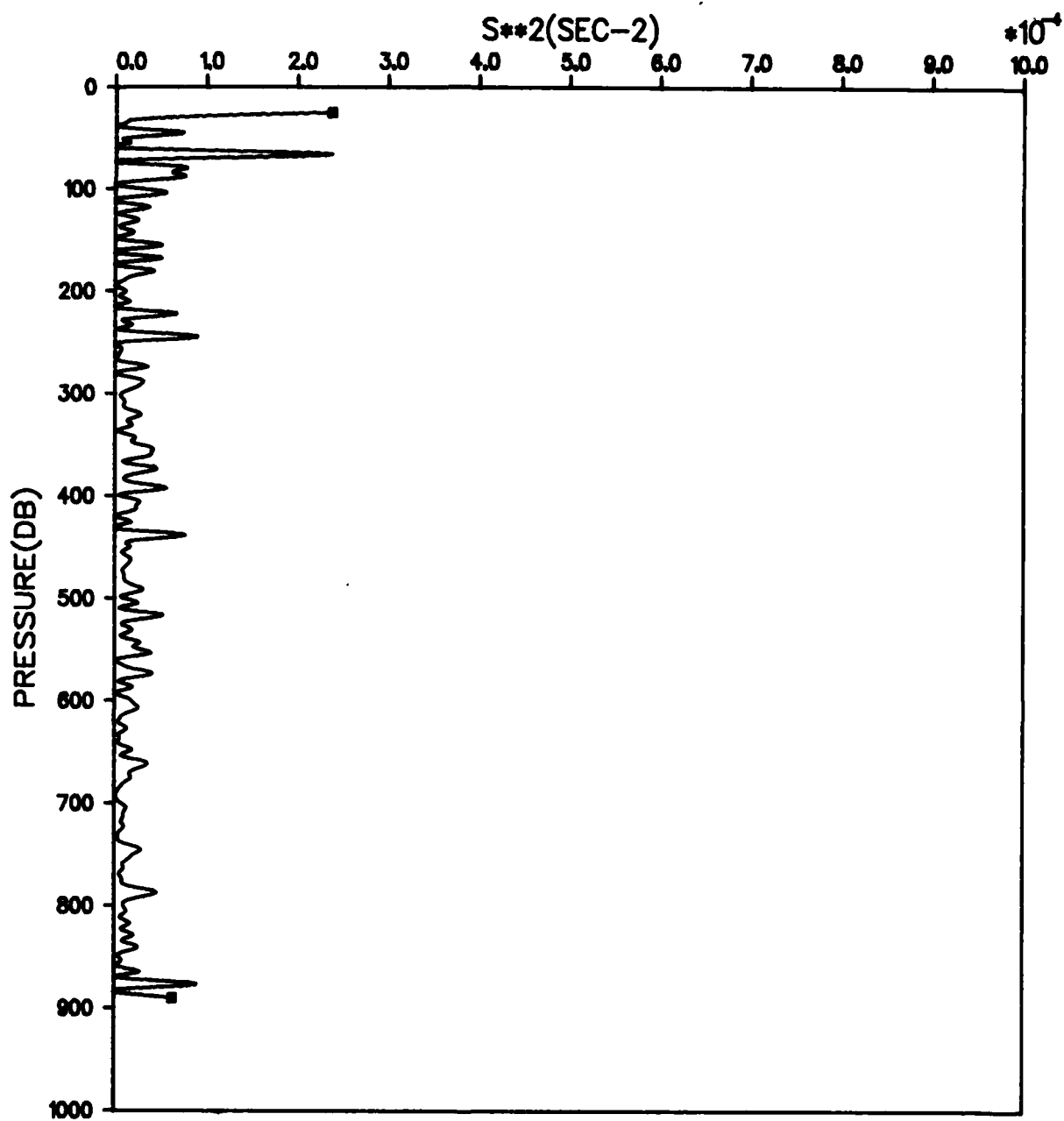


Figure D-20. File: KANE, Segment: C 534

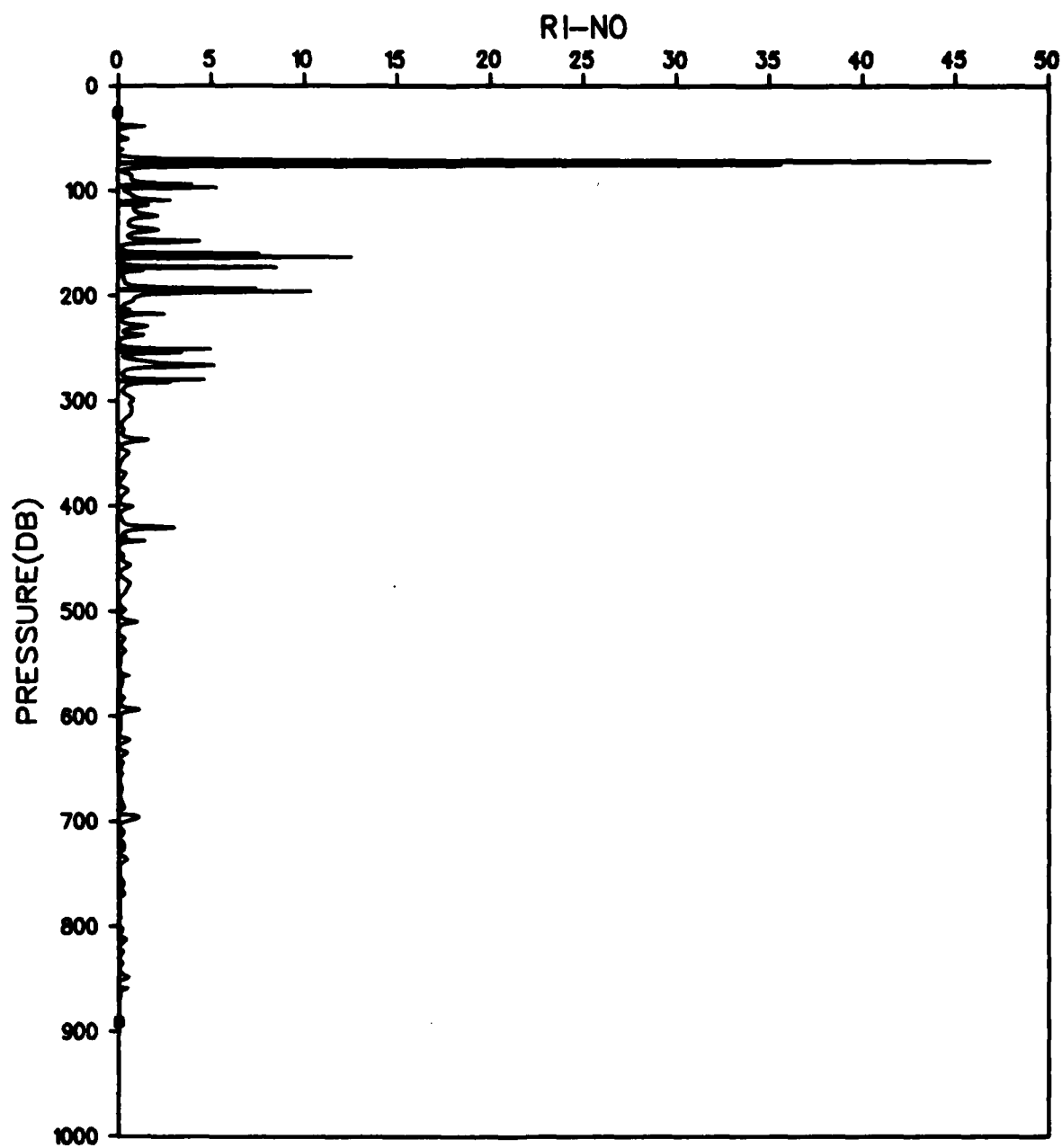


Figure D-21. File: KANE, Segment: C 534

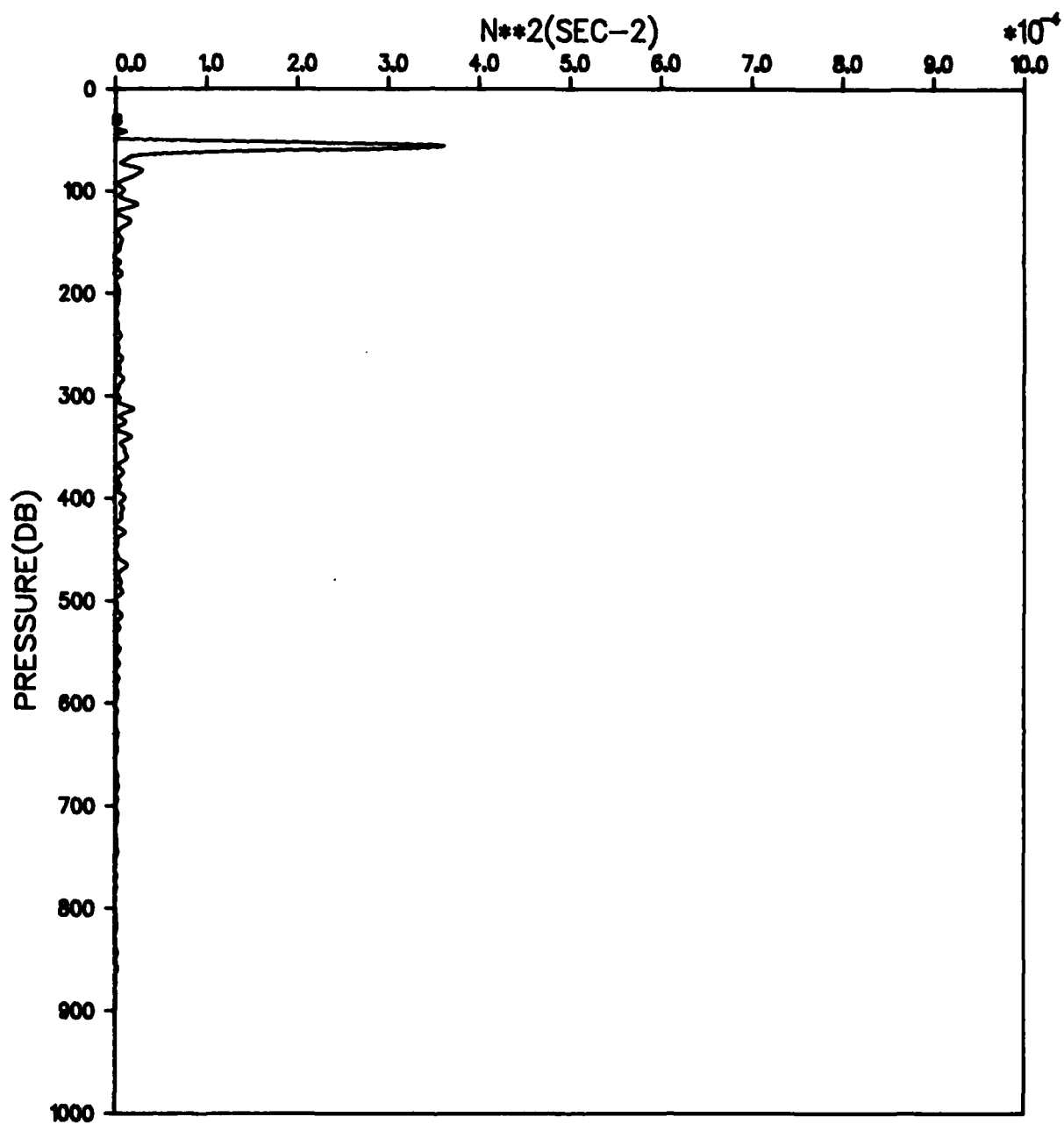


Figure D-22. File: KANE, Segment: C 535

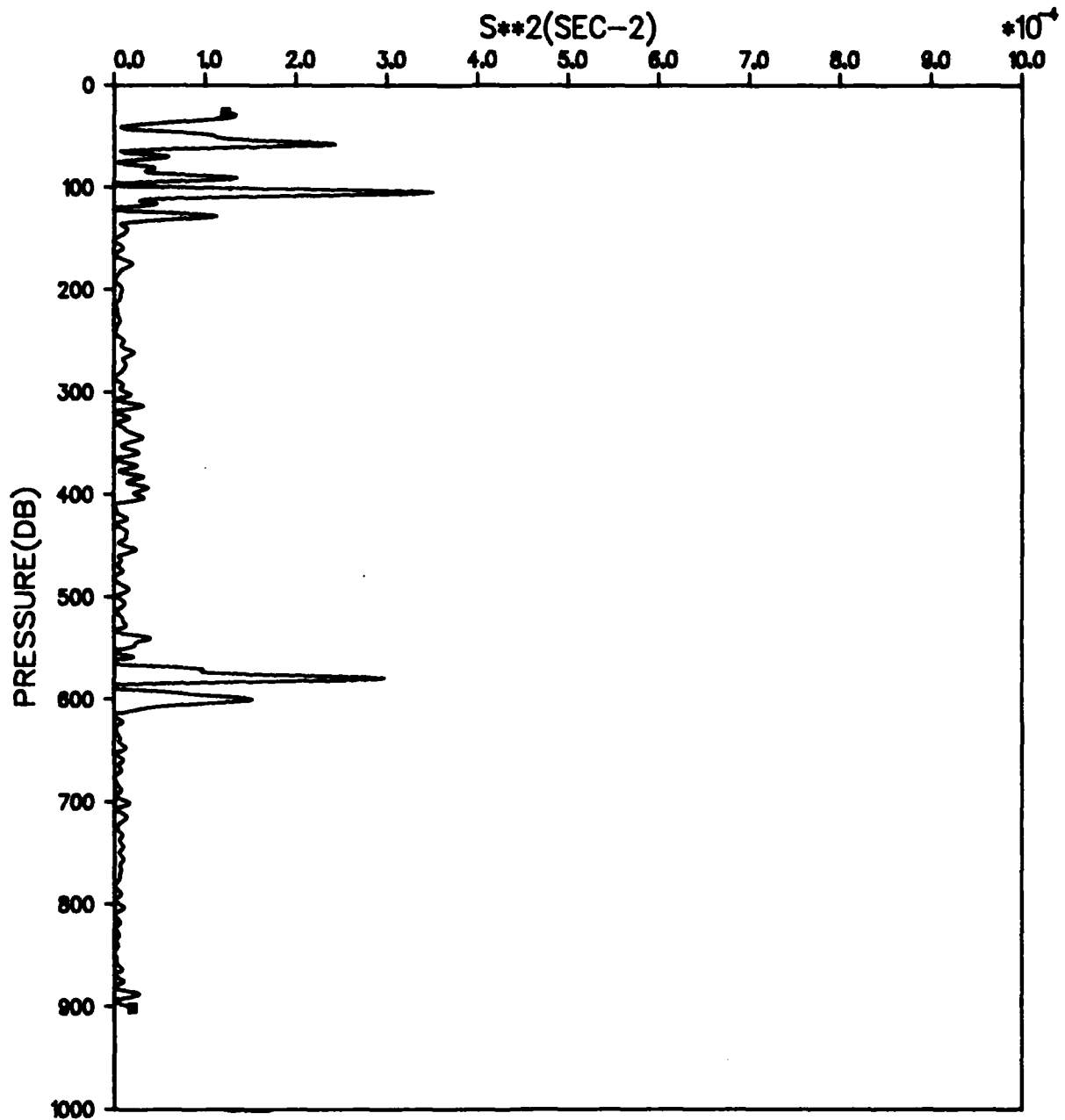


Figure D-23. File: KANE, Segment: C 535

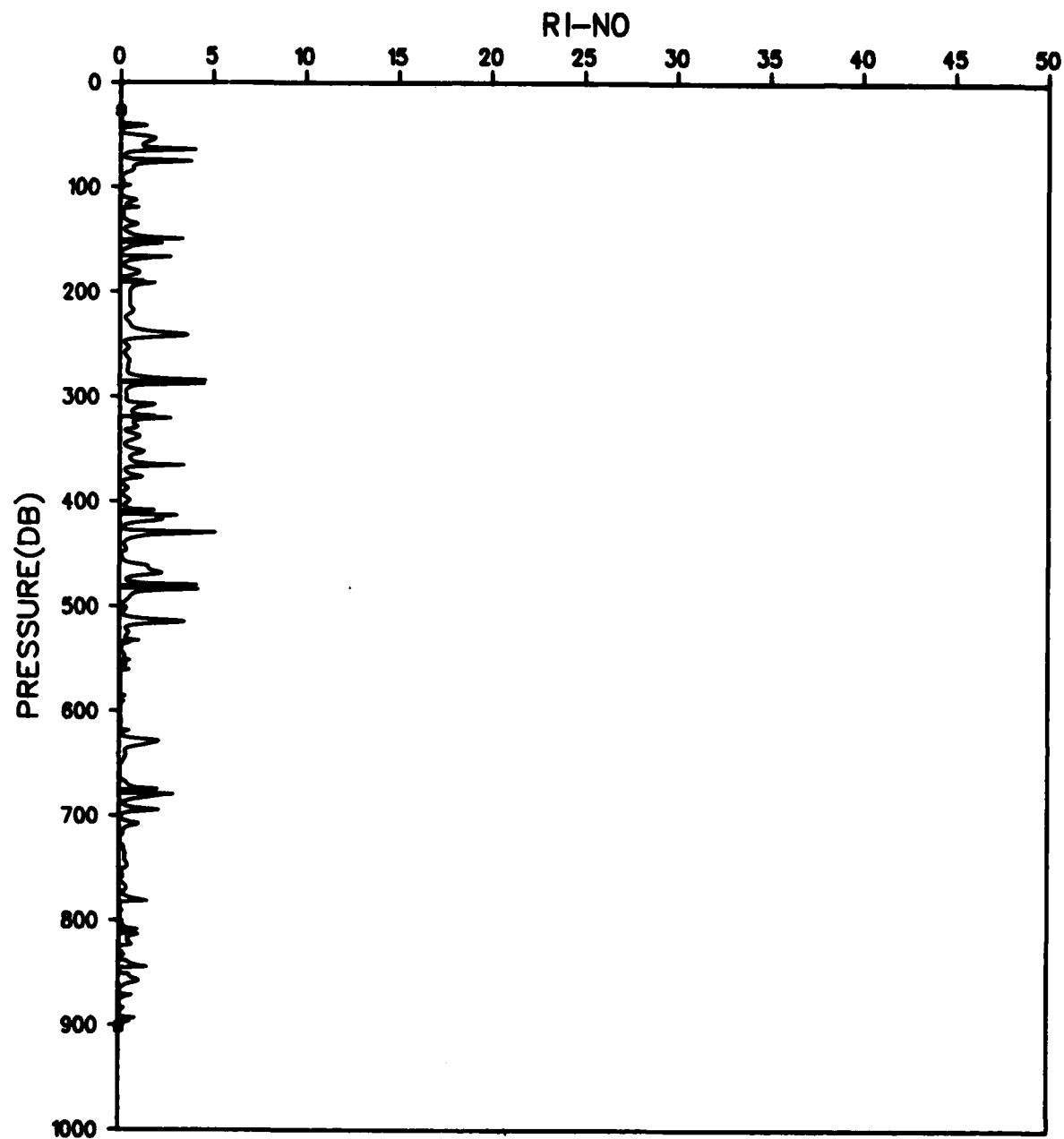


Figure D-24. File: KANE, Segment: C 535

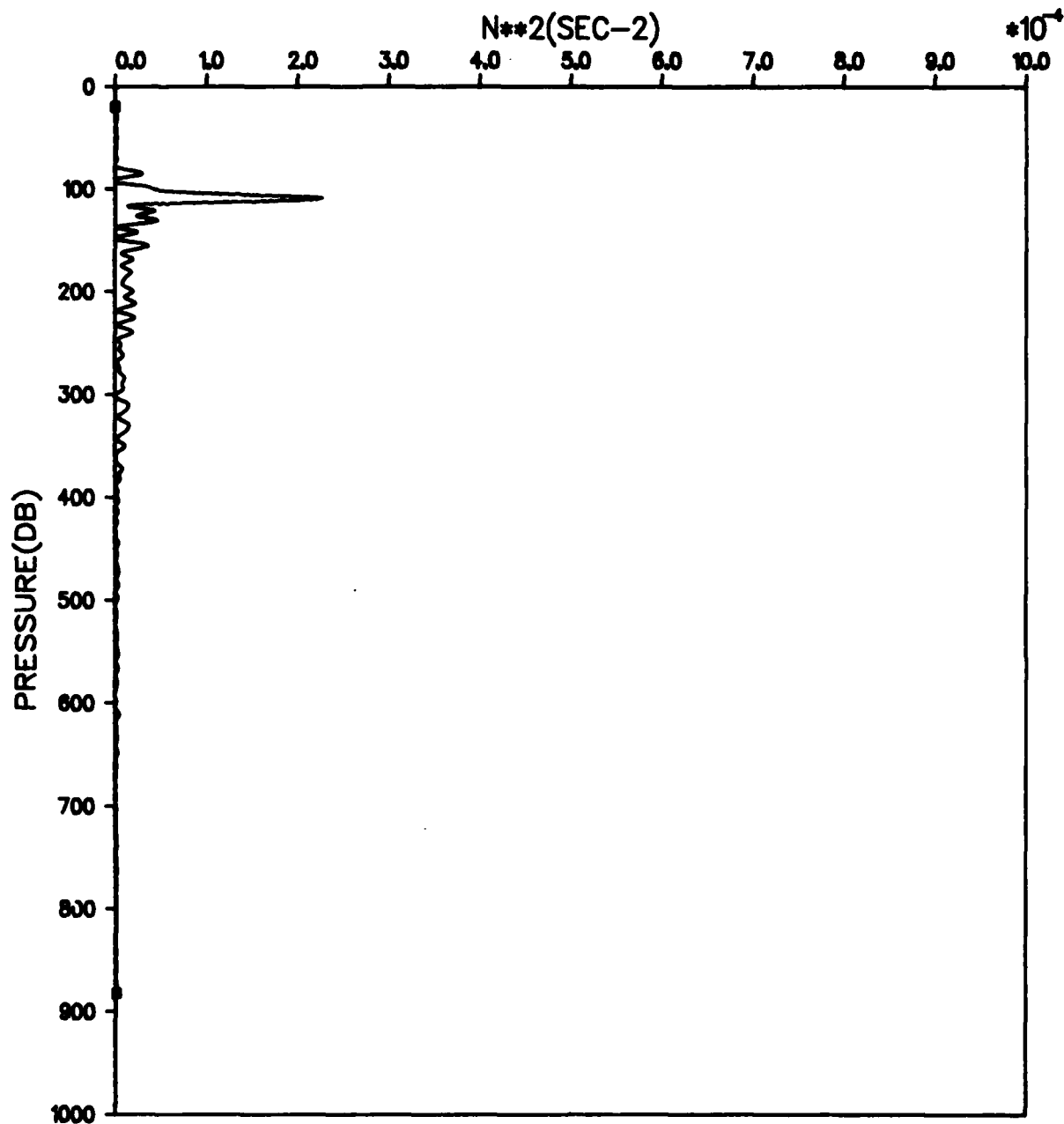


Figure D-25. File: KANE, Segment: C 538

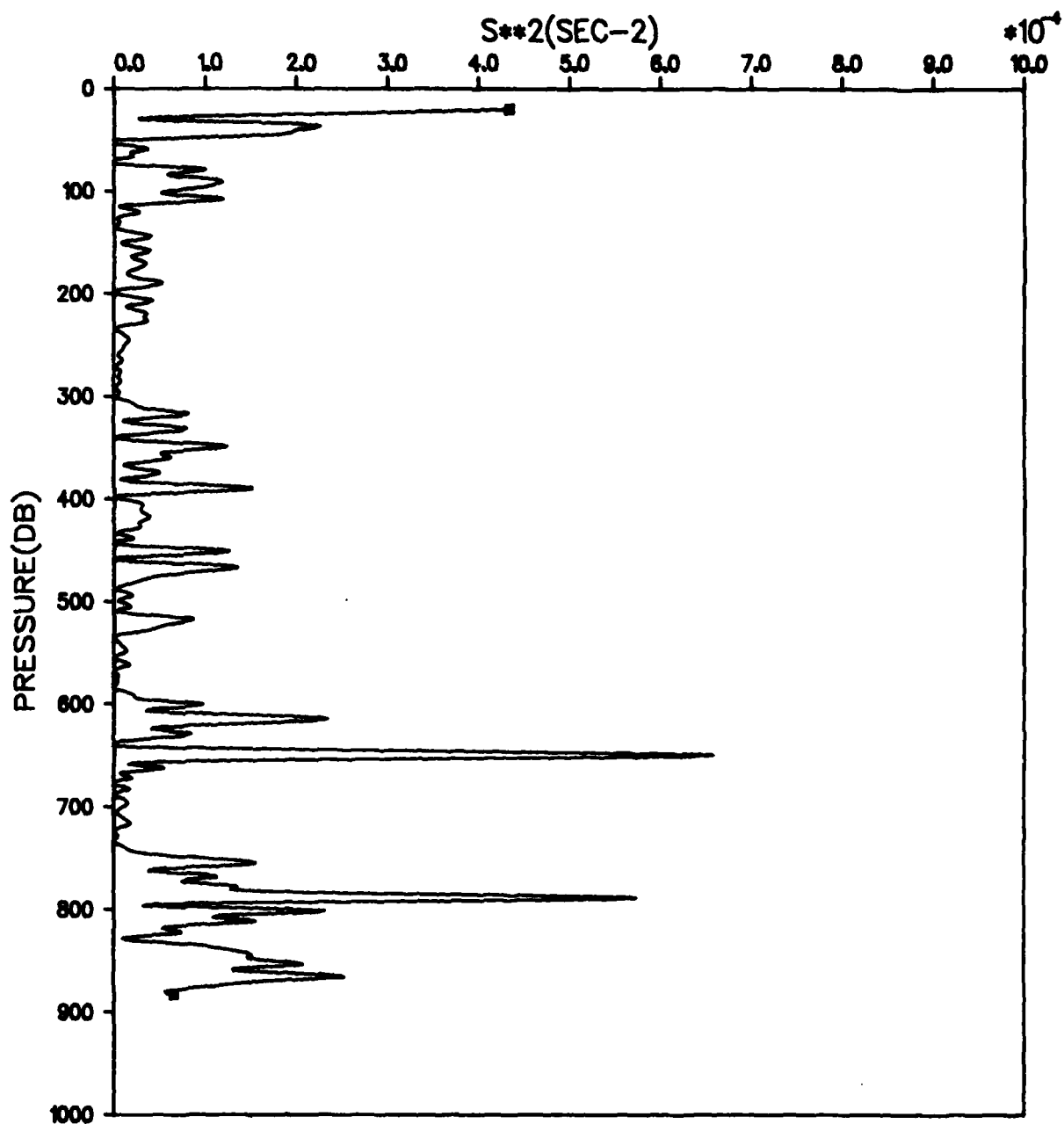


Figure D-26. File: KANE, Segment: C 538

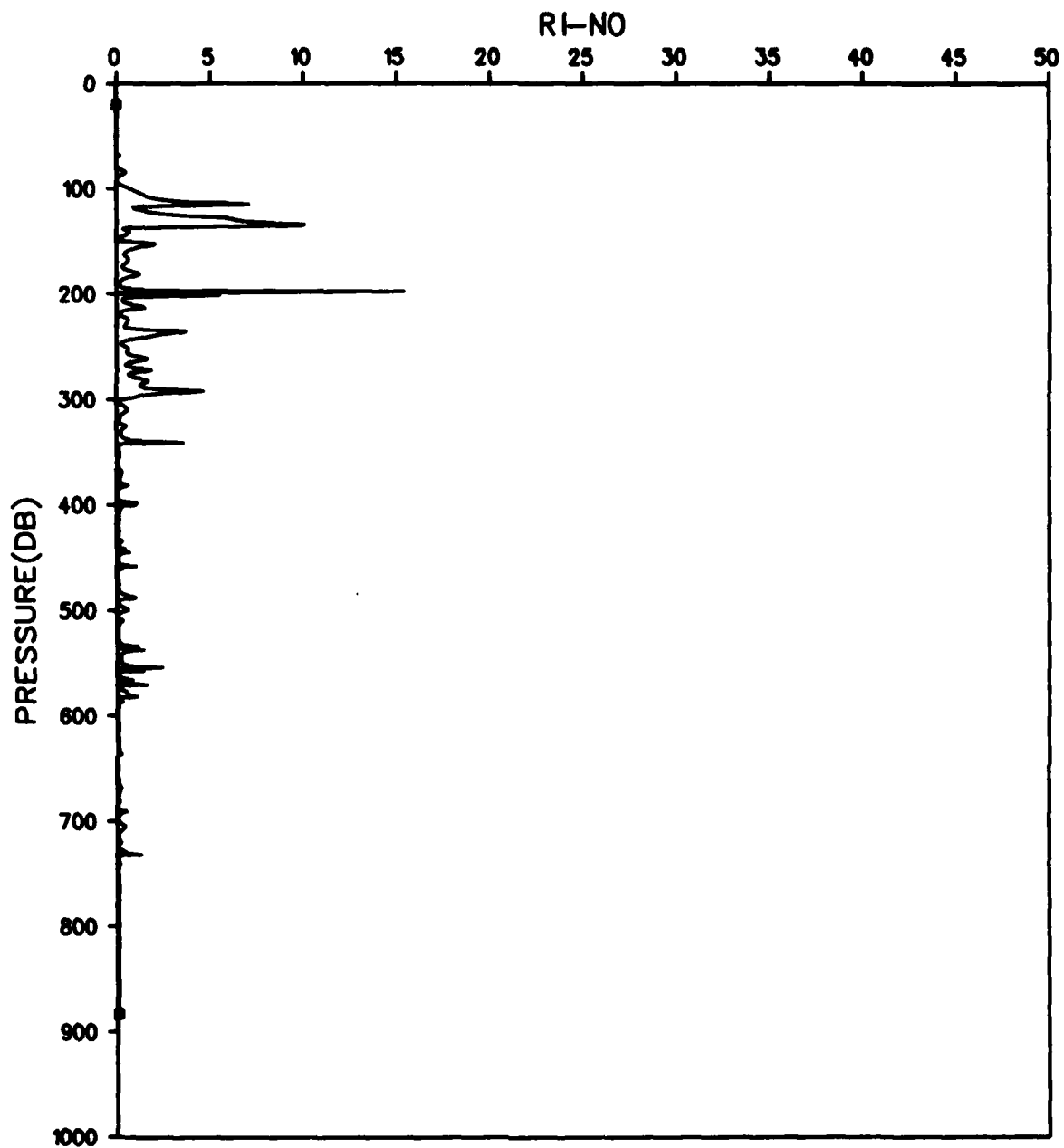


Figure D-27. File: KANE, Segment: C 538

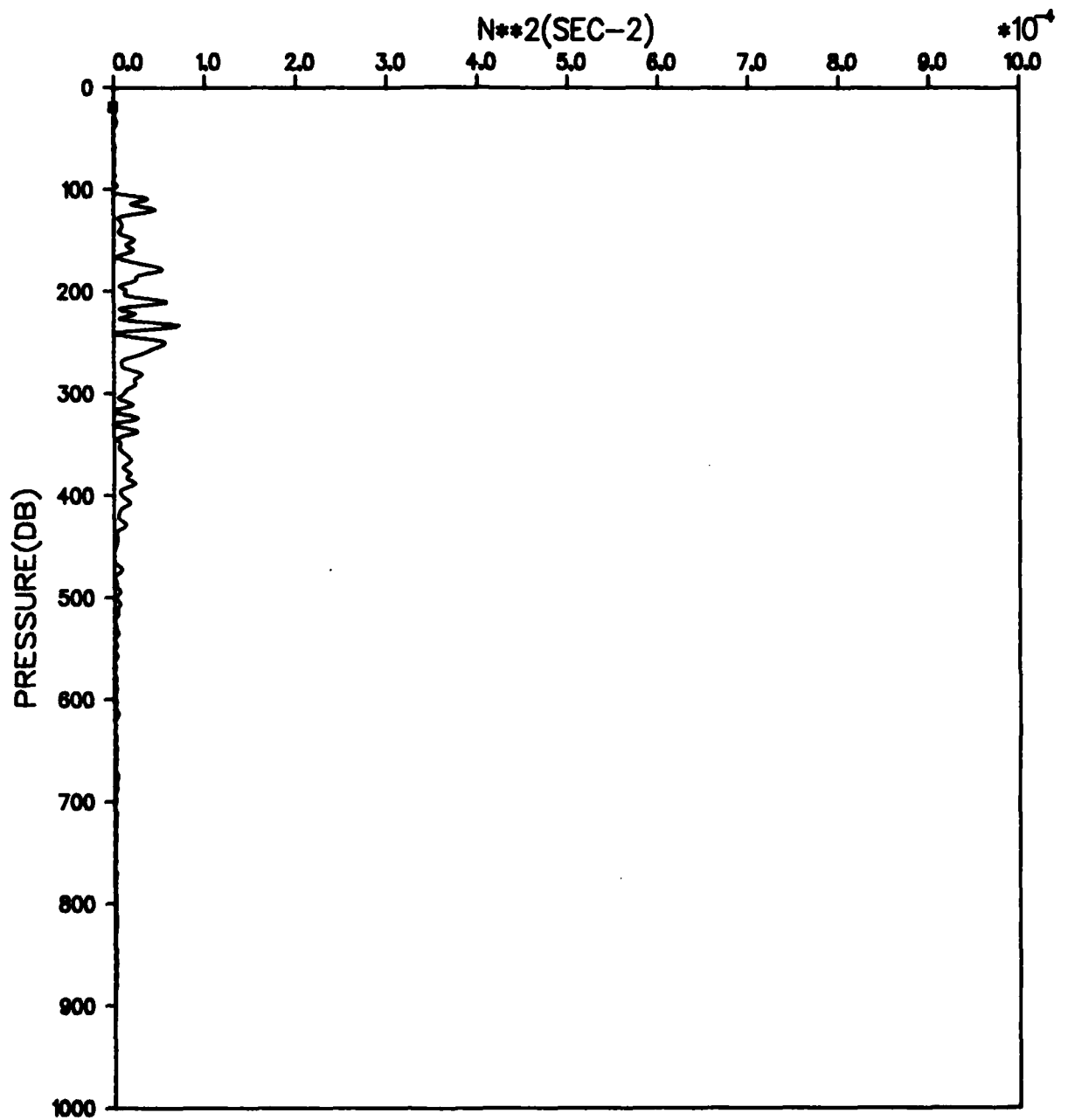


Figure D-28. File: KANE, Segment: C 546

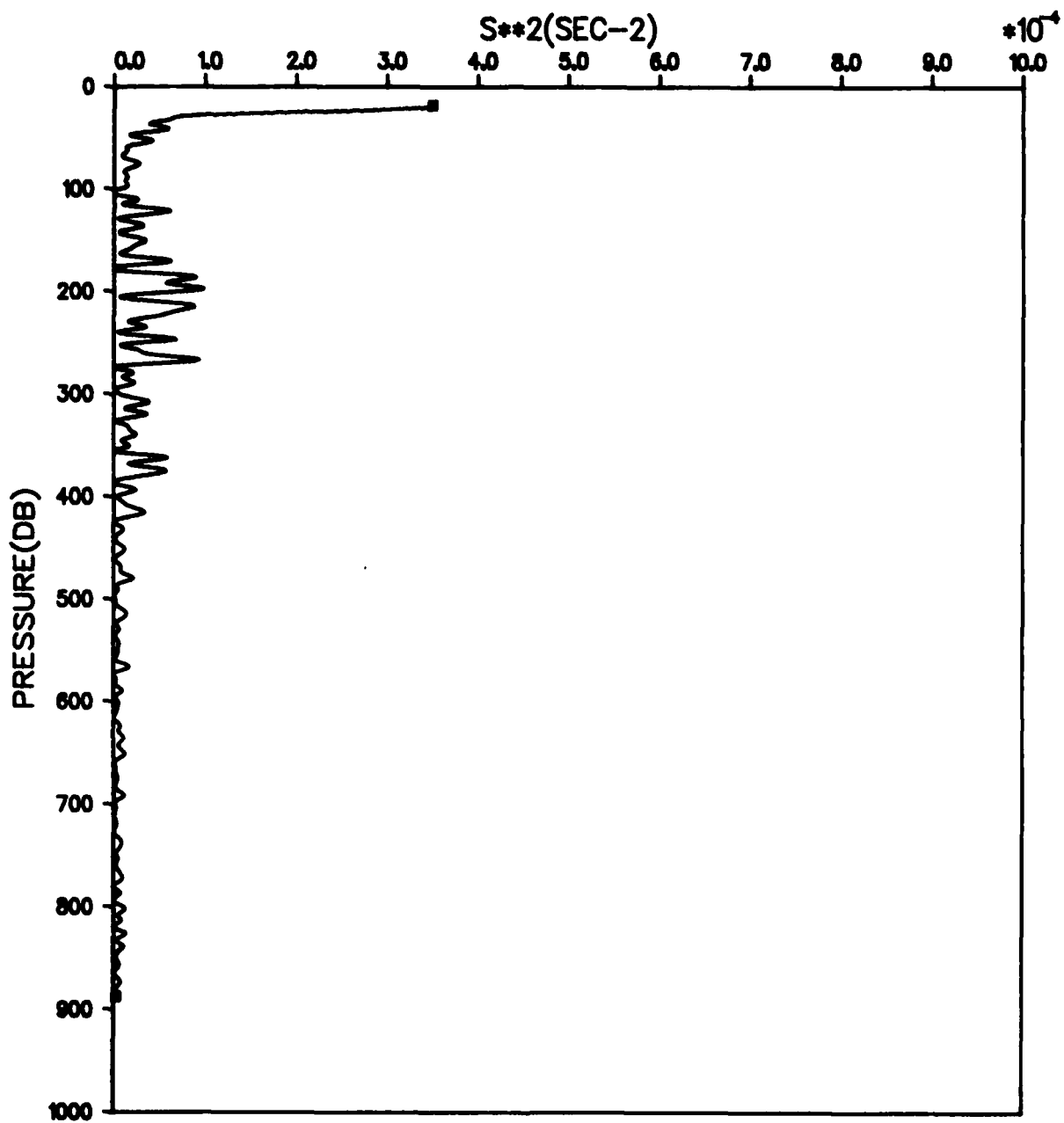


Figure D-29. File: KANE, Segment: C 546

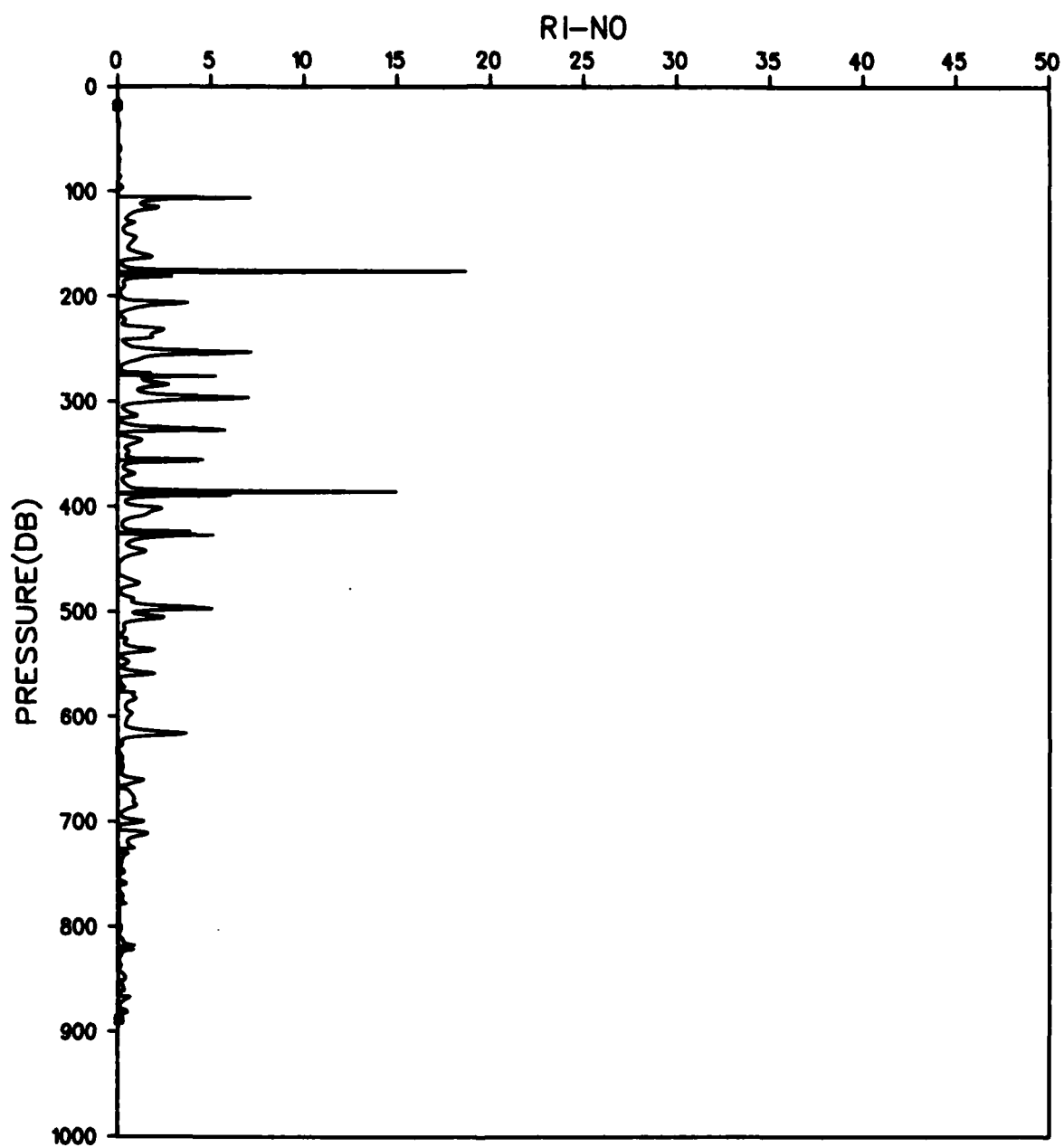


Figure D-30. File: KANE, Segment: C 546

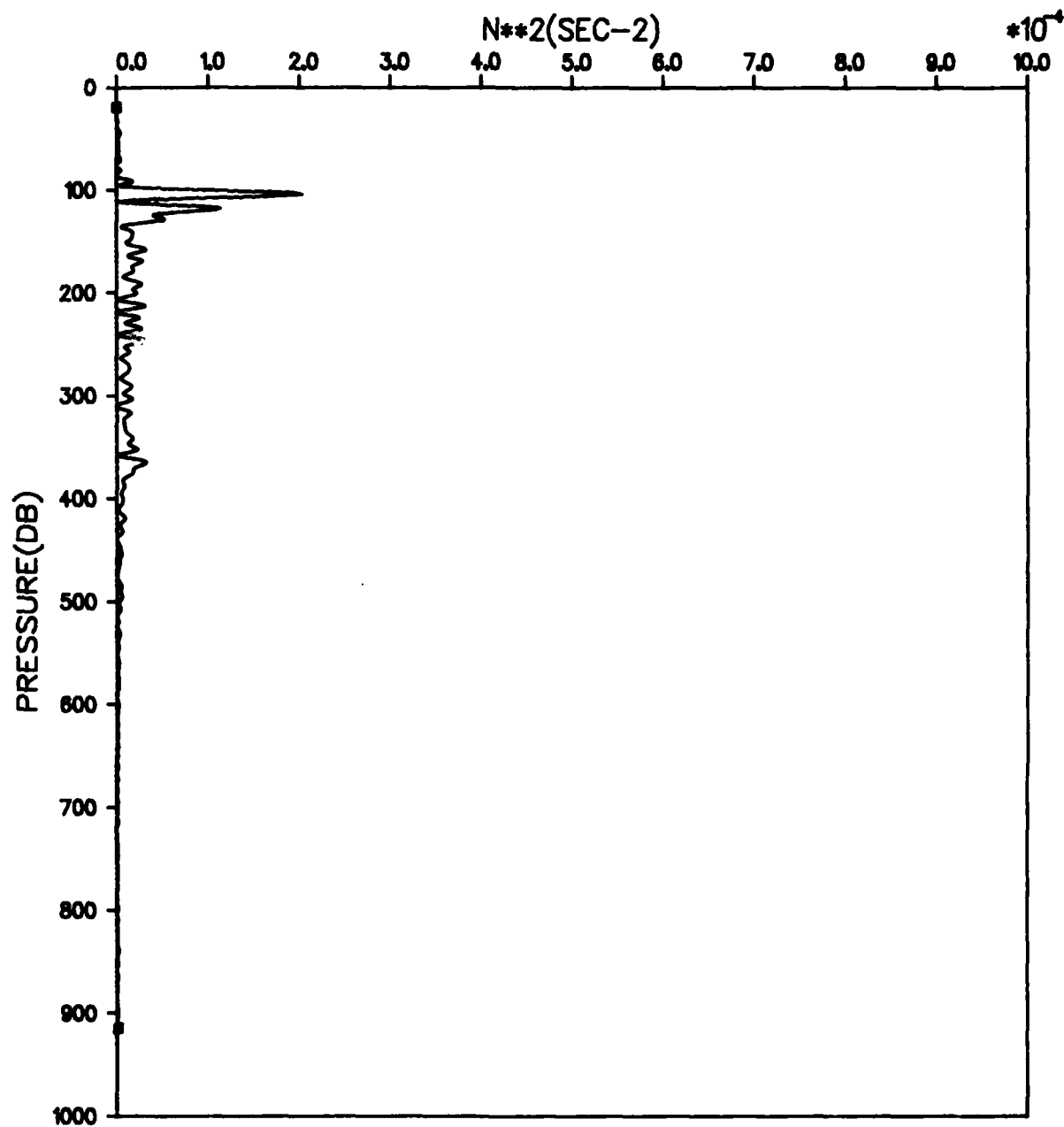


Figure D-31. File: KANE, Segment: C 547

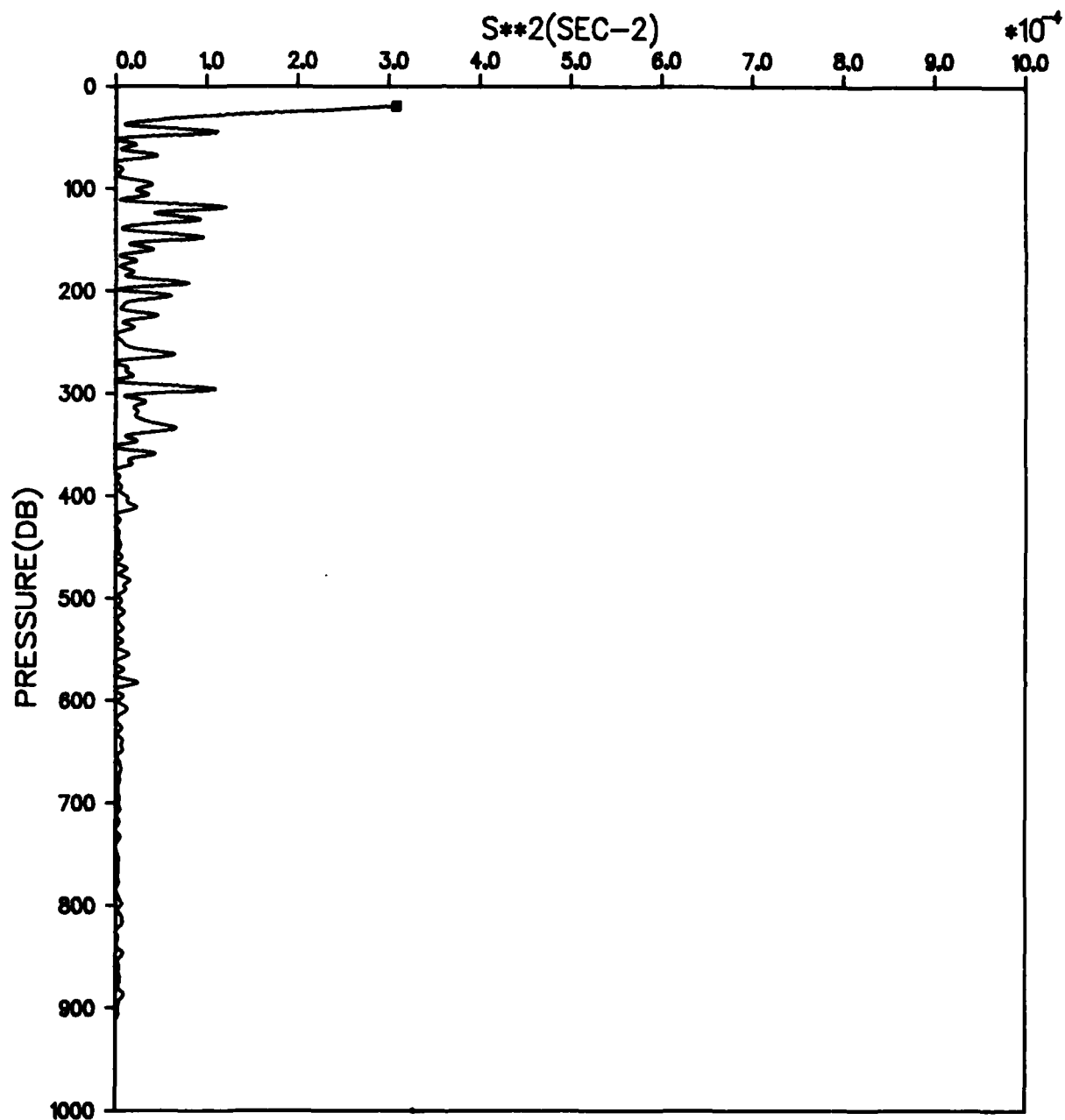


Figure D-32. File: KANE, Segment: C 547

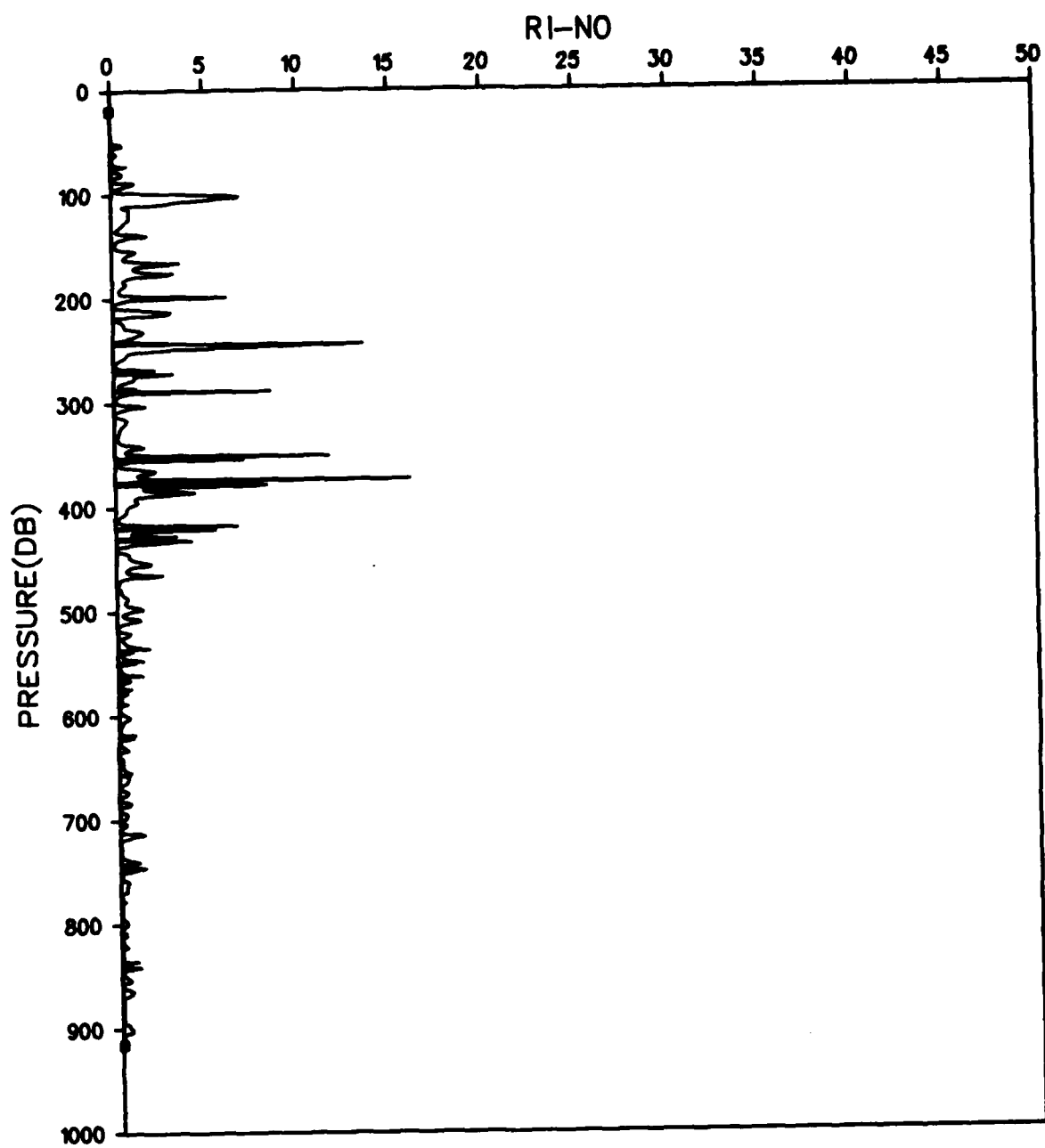


Figure D-33. File: KANE, Segment: C 547

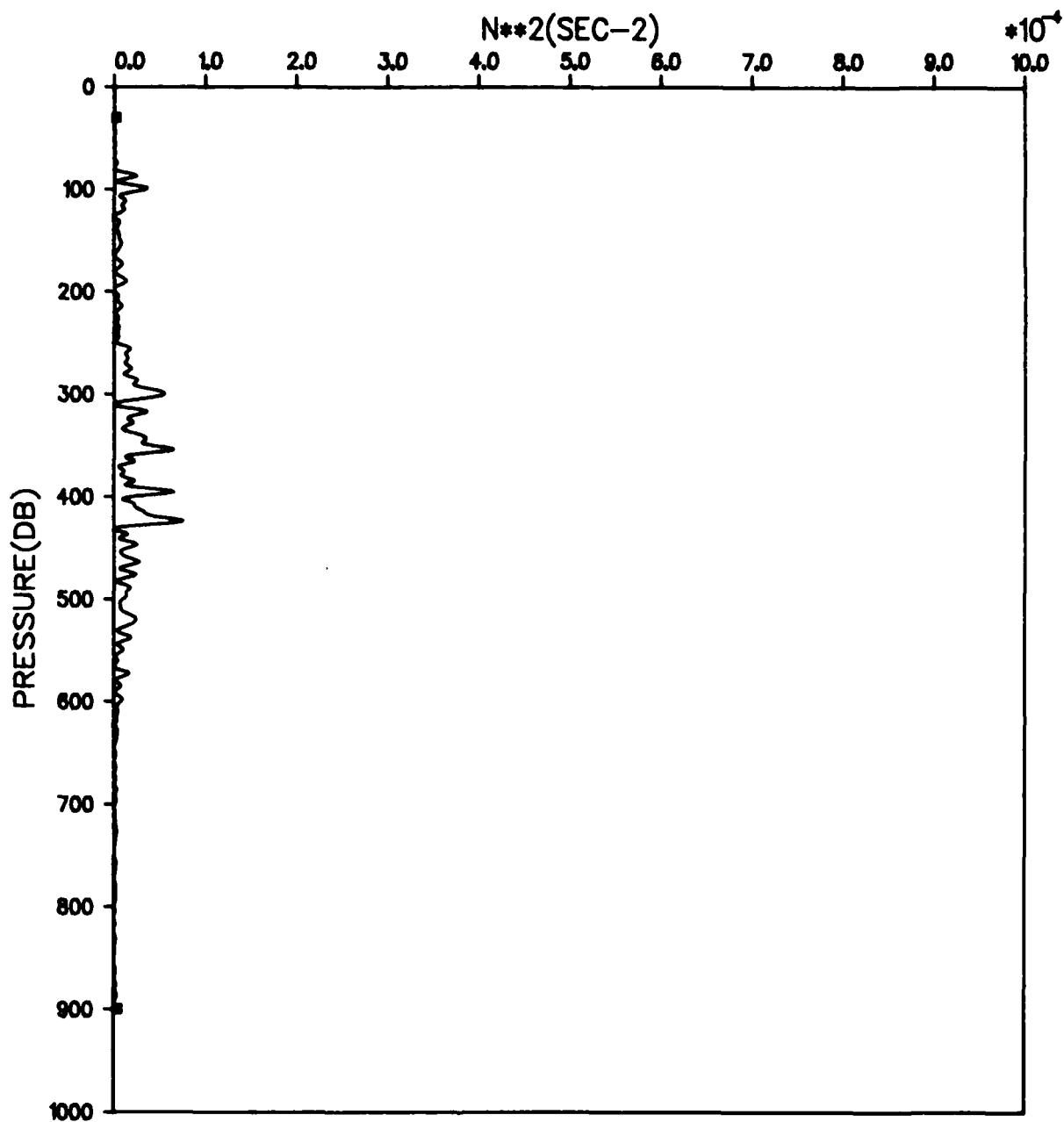


Figure D-34. File: KANE, Segment: C 548

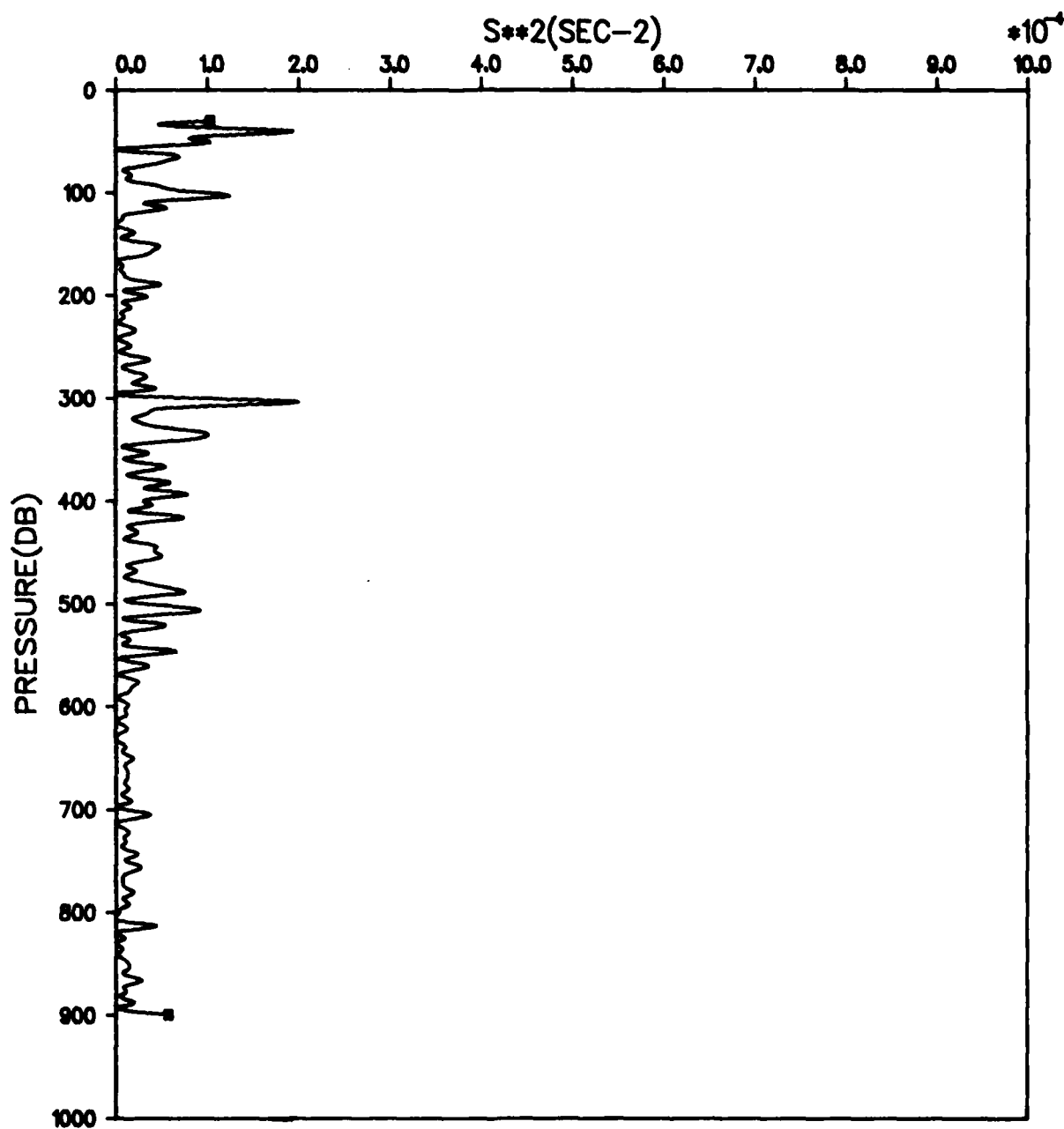


Figure D-35. File: KANE, Segment: C 548

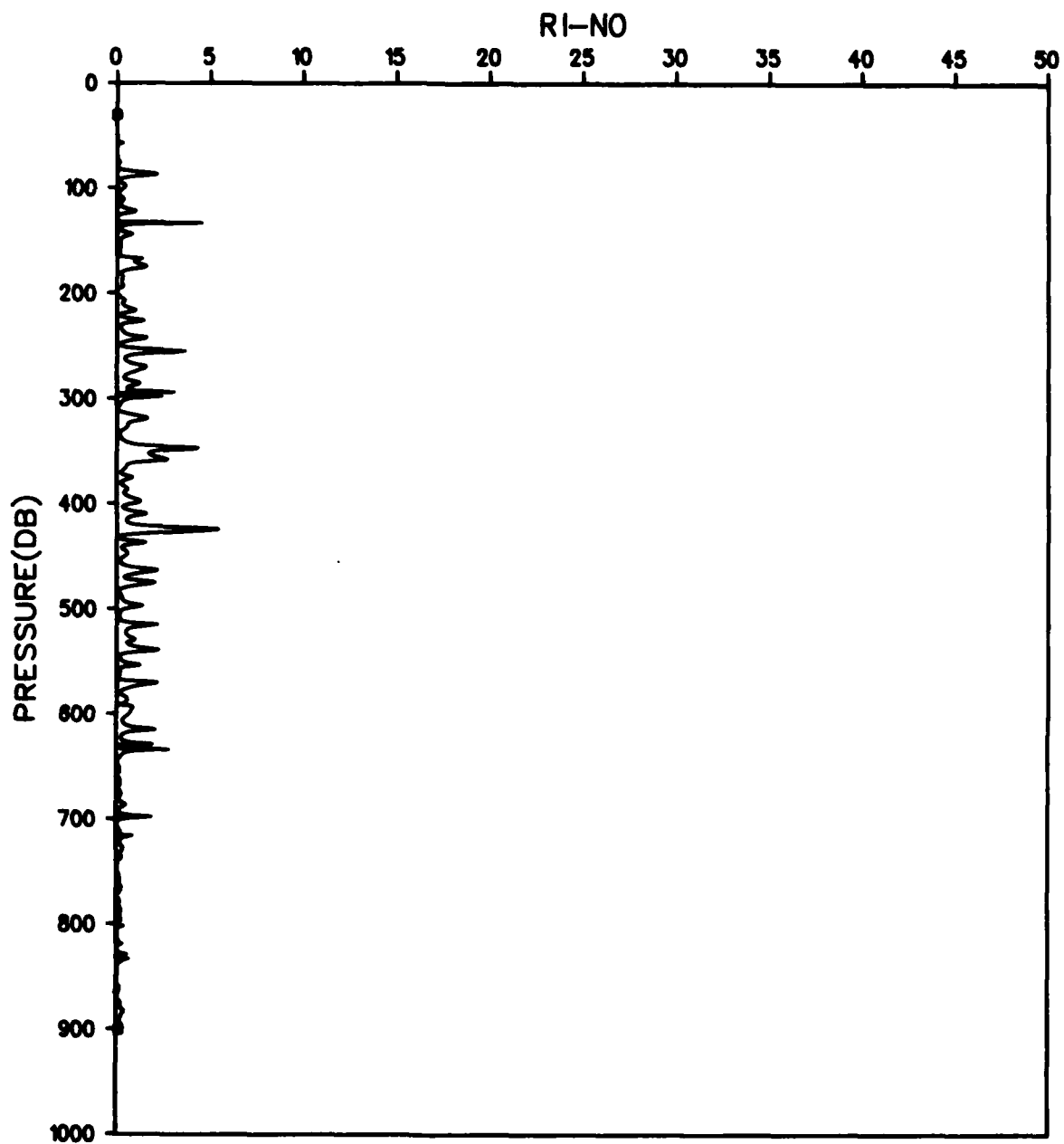


Figure D-36. File: KANE, Segment: C 548

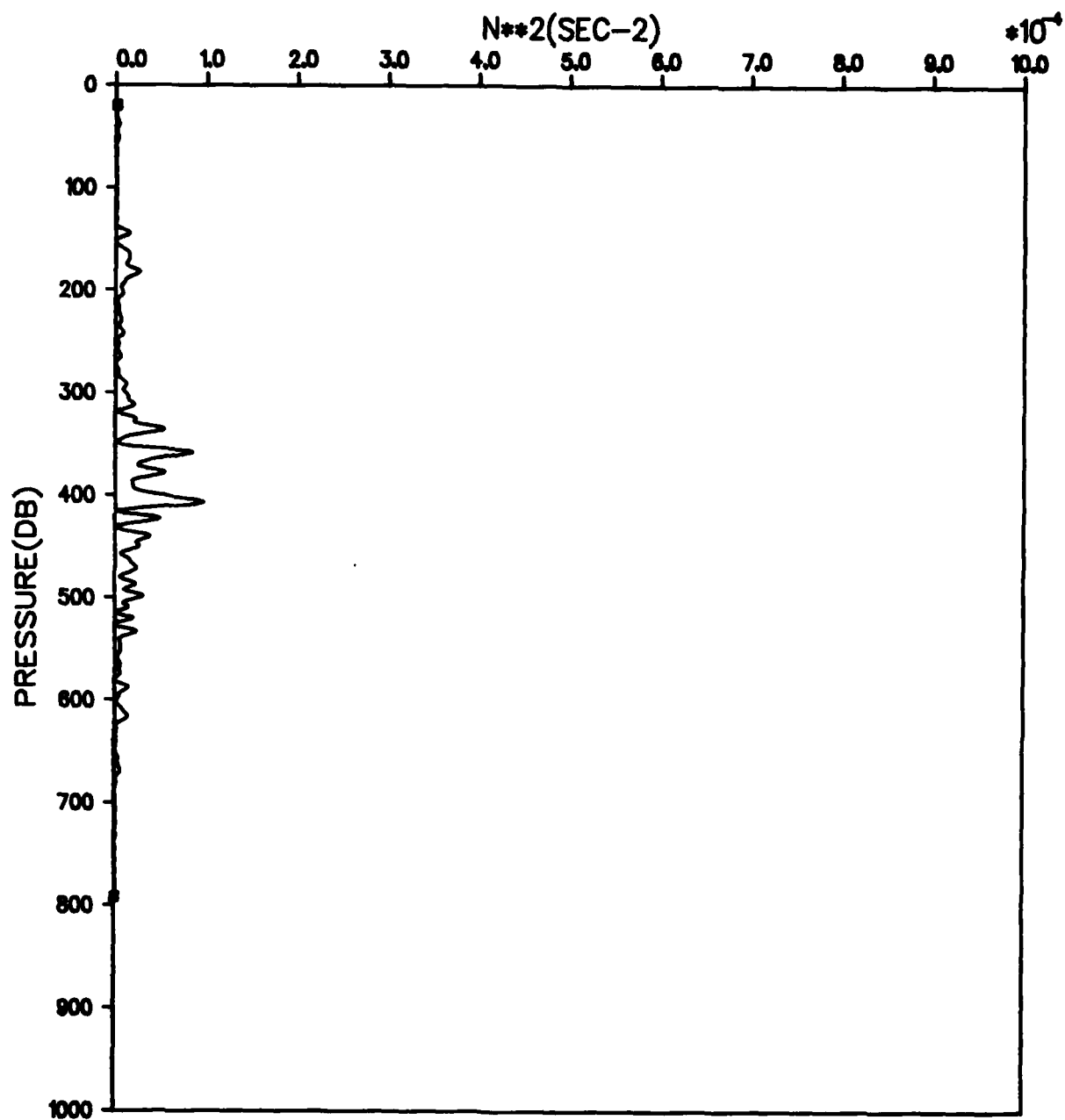


Figure D-37. File: KANE, Segment: C 549

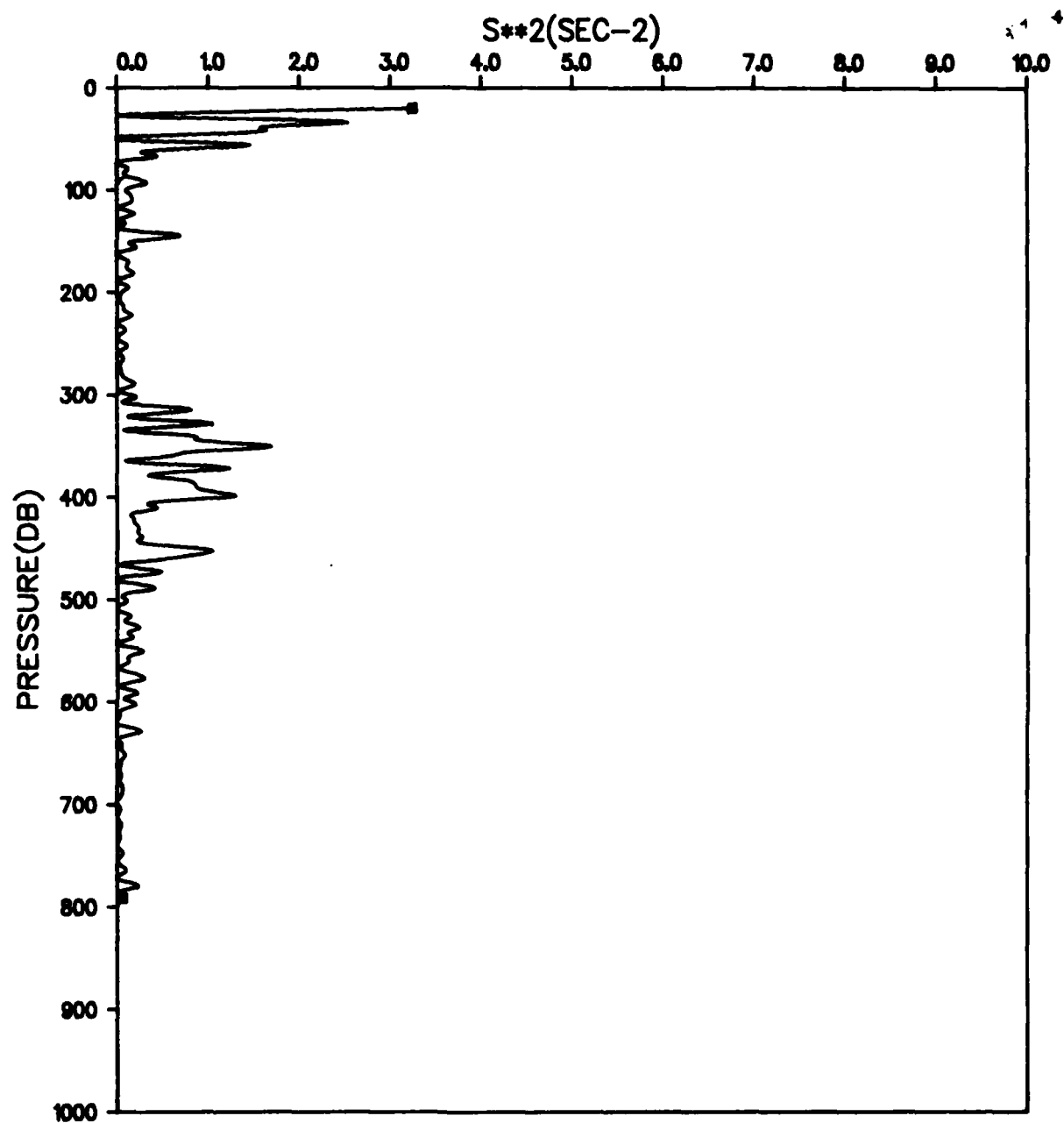


Figure D-38. File: KANE, Segment: C 549

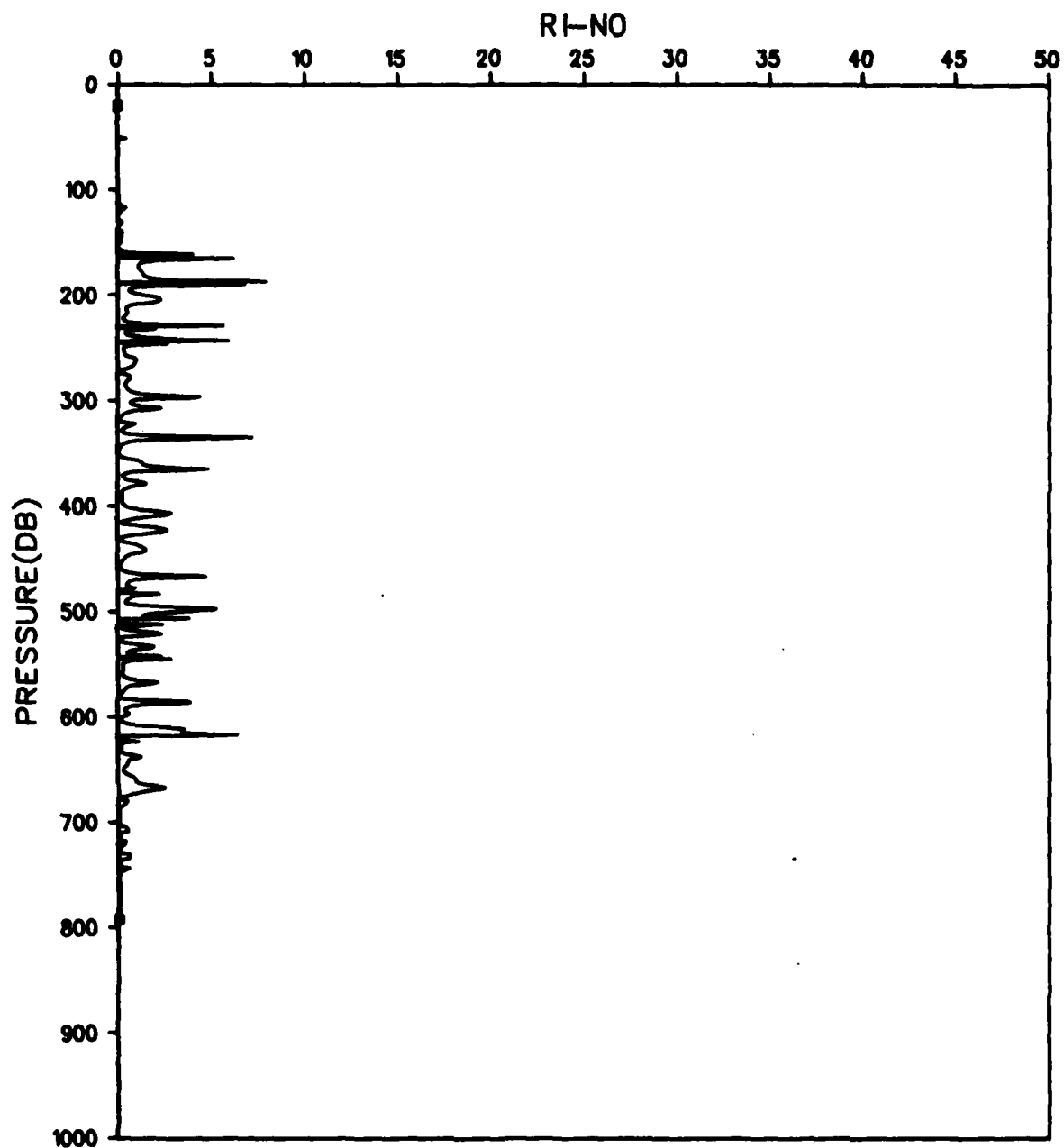


Figure D-39. File: KANE, Segment: C 549

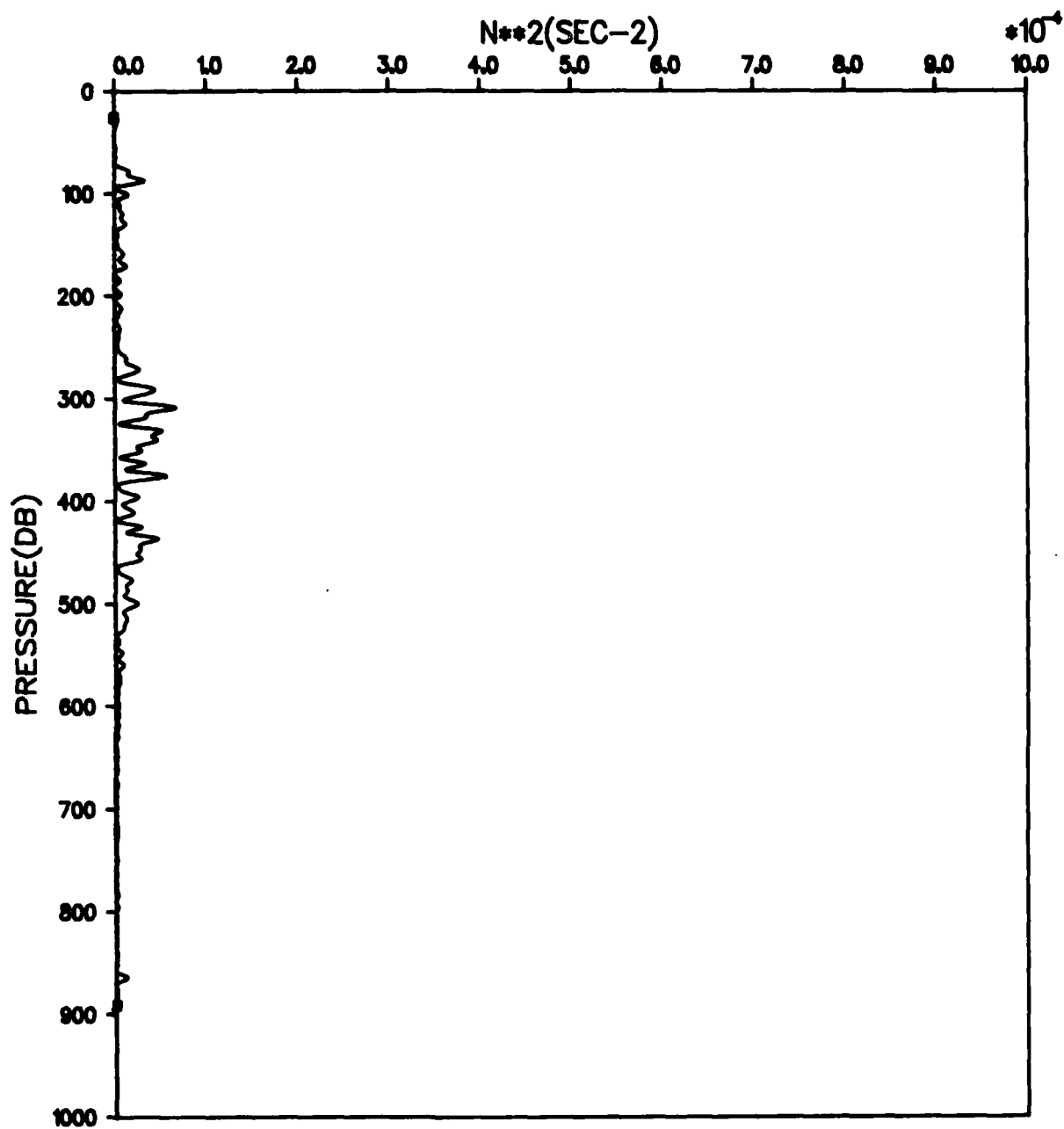


Figure D-40. File: KANE, Segment: C 550

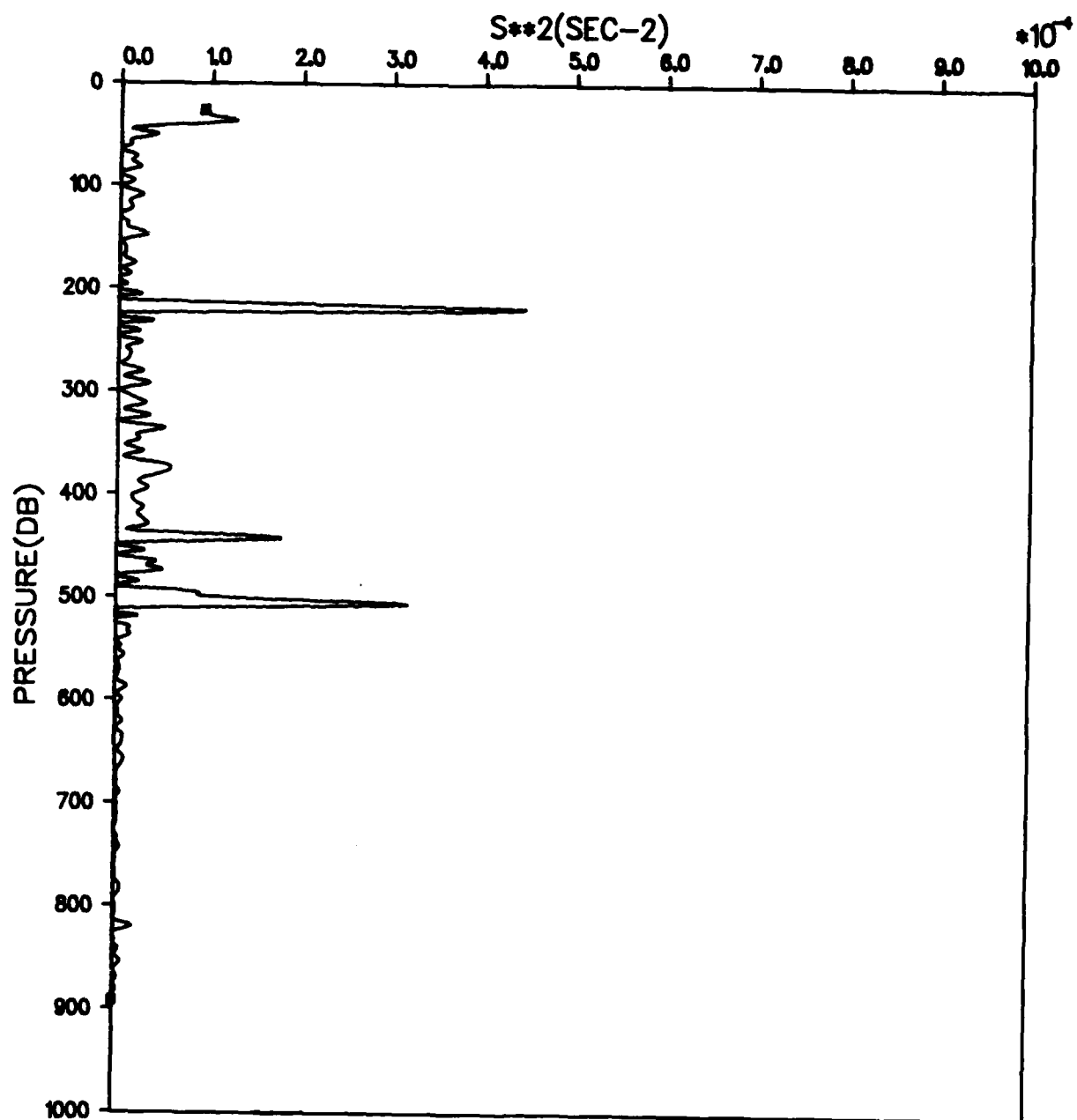


Figure D-41. File: KANE, Segment: C 550

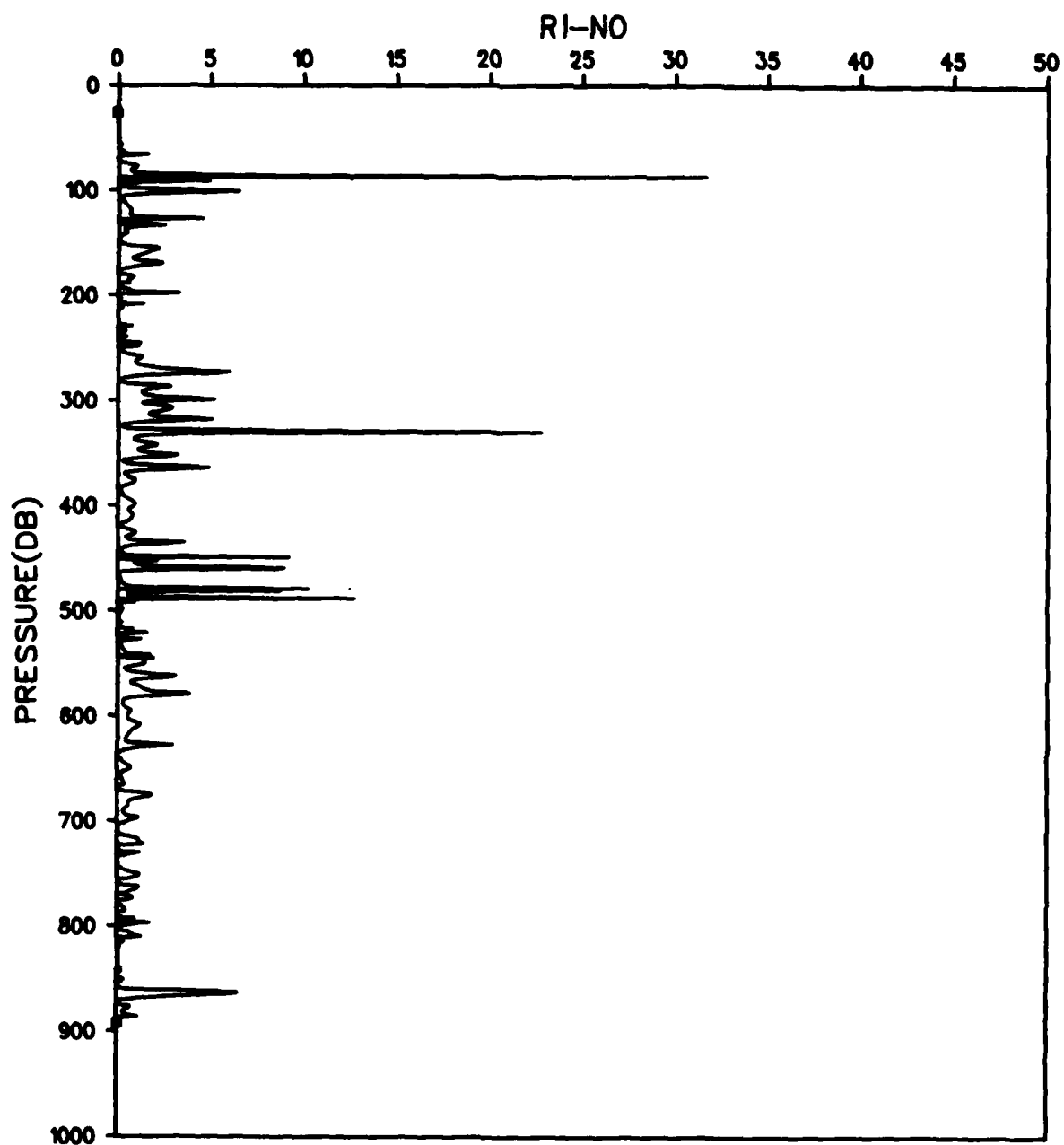


Figure D-42. File: KANE, Segment: C 550

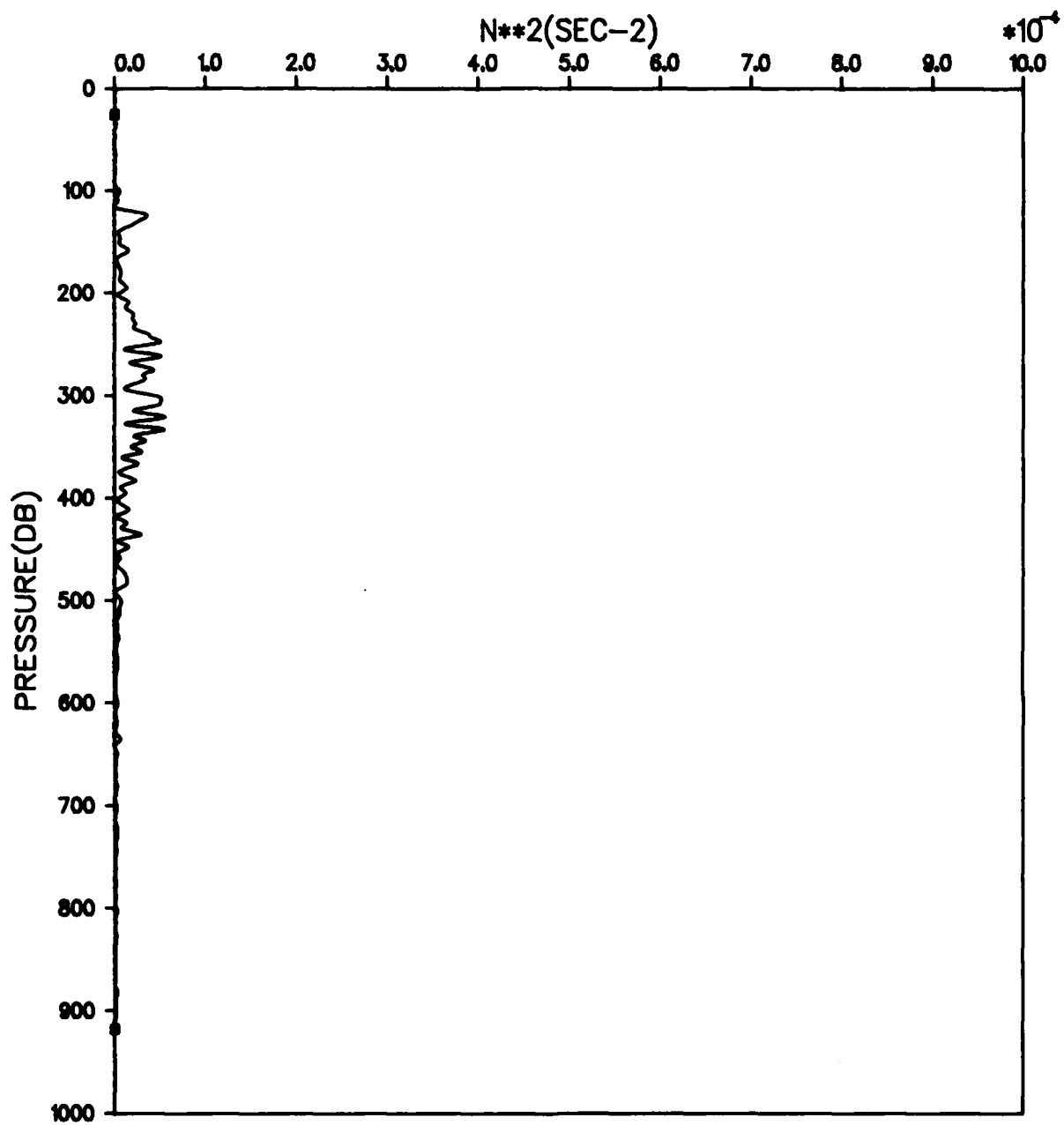


Figure D-43. File: KANE, Segment: C 551

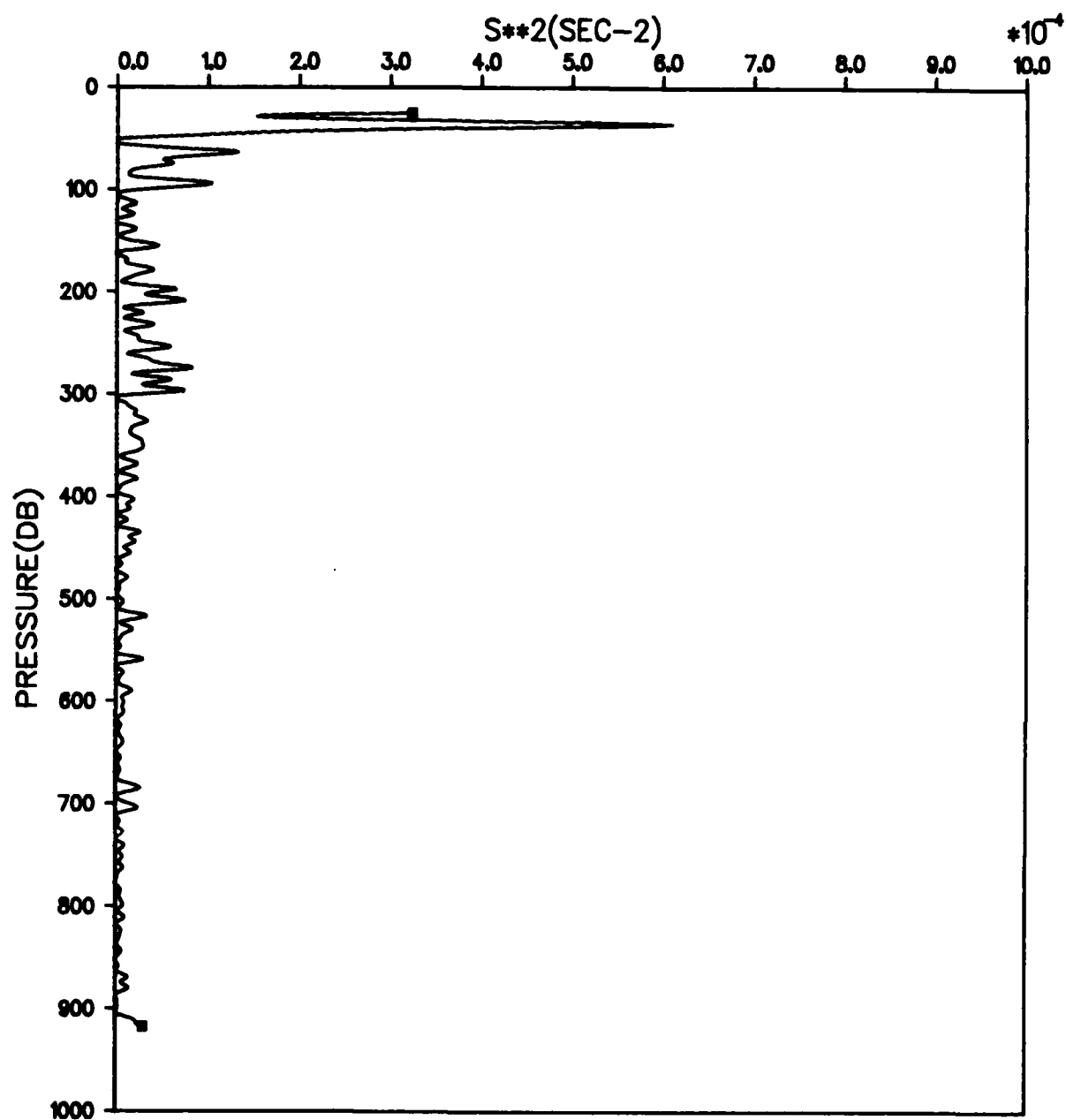


Figure D-44. File: KANE, Segment: C 551

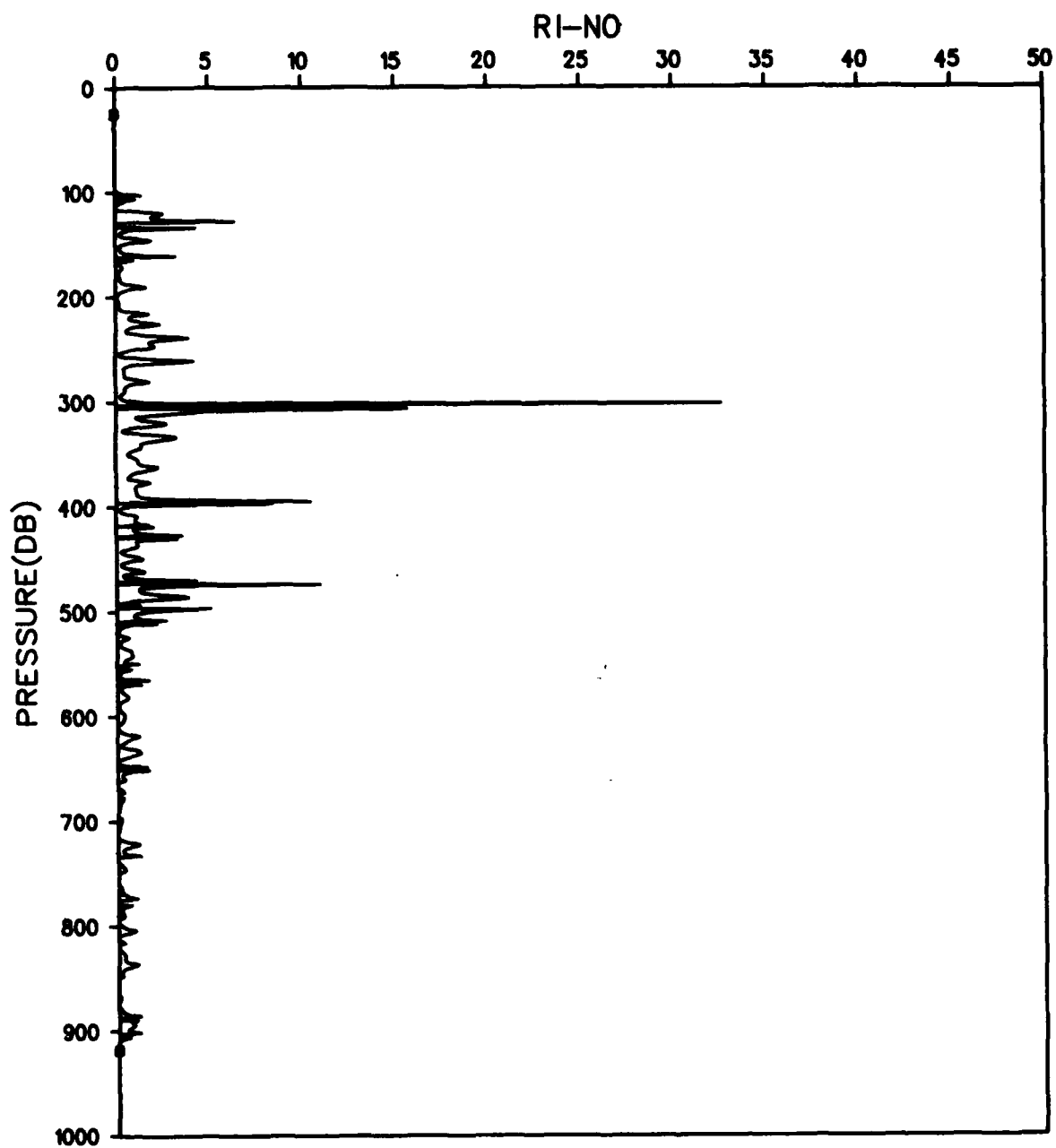


Figure D-45. File: KANE, Segment: C 551

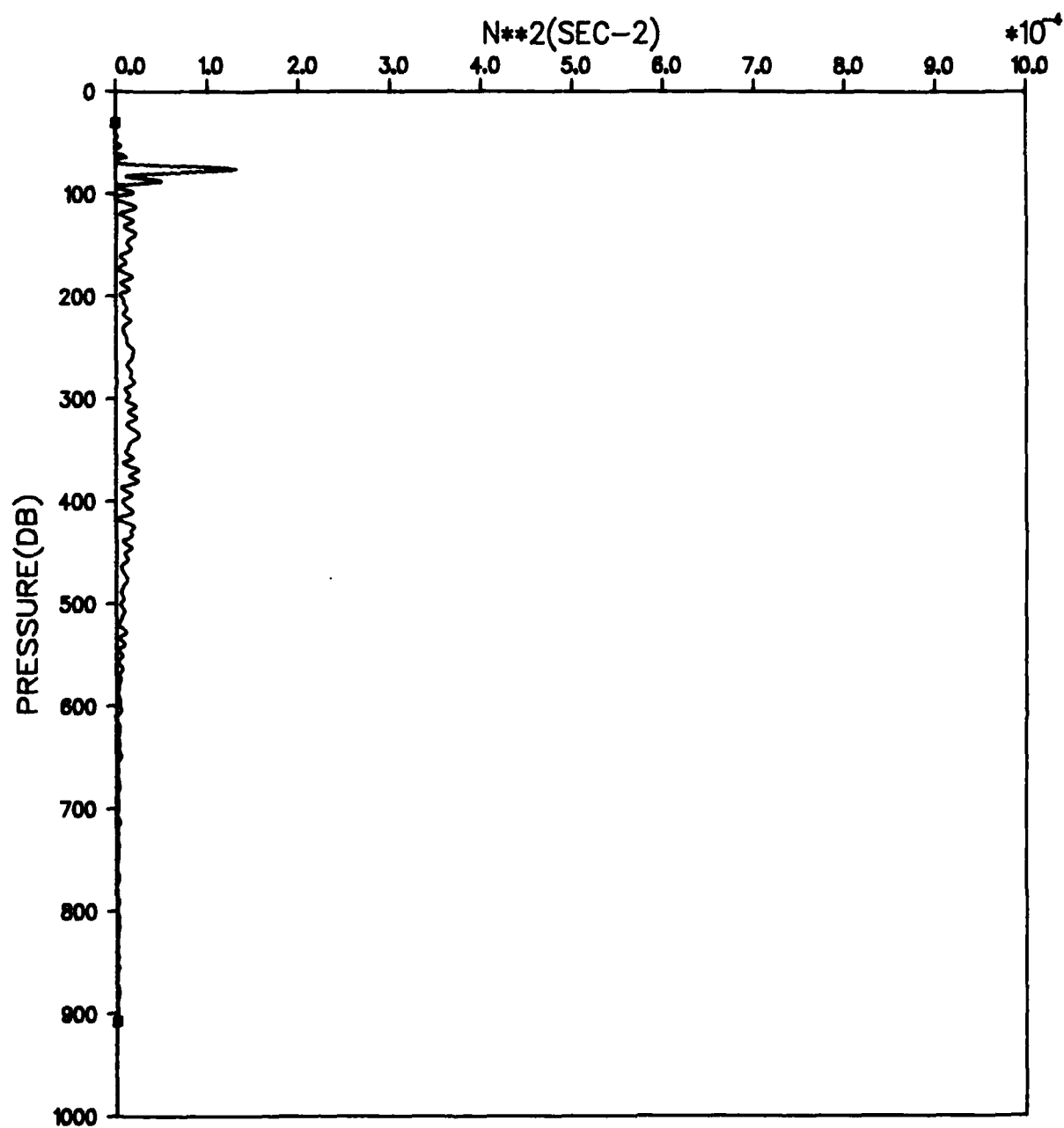


Figure D-46. File: KANE, Segment: C 563

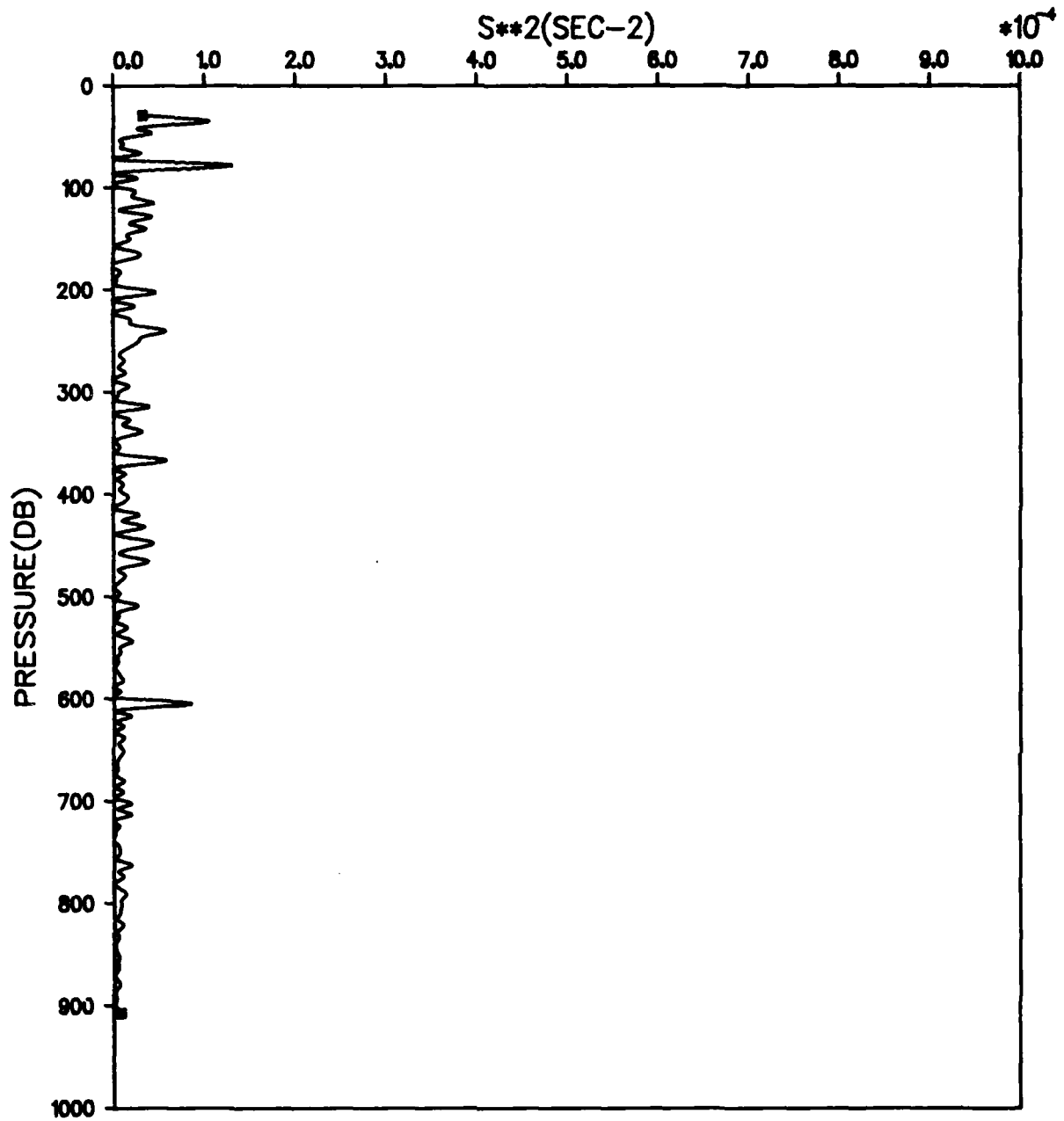


Figure D-47. File: KANE, Segment: C 563

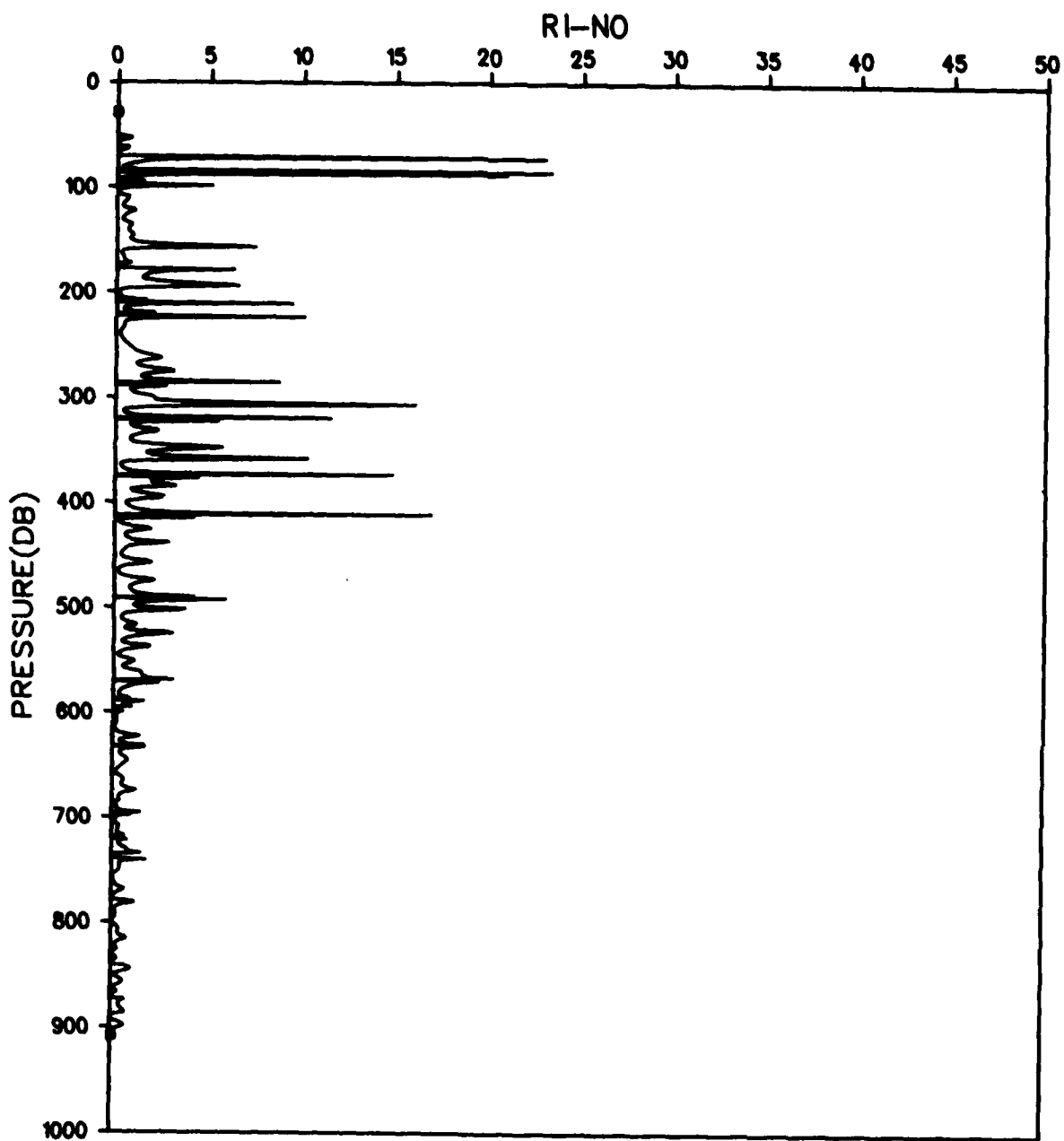


Figure D-48. File: KANE, Segment: C 563

Appendix E:

Log  $S^2$  vs Log  $N^2$

(Bulk Richardson Numbers)

COMMENTS:

Low Pass Filtered 10 m Resolution Subsampling Interval 1 m

PRECEDING PAGE BLANK-NOT FILMED

The vertical (horizontal) line drawn parallel to the  $\log N^2(\log S^2)$  axis represents the value of  $\log S^2(\log N^2)$  for which the estimated signal-to-noise ratio is 1. Points plotted to the left (below) of the vertical (horizontal) line have an estimated signal-to-noise ratio of less than 1. Points in quadrant 1 have a signal-to-noise ratio of at least 1.

Negative values of  $N$  did occur in several of the profiles. These negative values were set to zero and not plotted. All non-zero values of  $S^2$  were plotted.

The slanted lines represent Richardson numbers in the range  $RI=0.0001$  to  $RI=100$ .

The original XCP data sets as received from APL/UAW had a vertical sample interval of about 2 to 3 m. We interpolated these profiles to 1 m intervals and then low passed the data with a half-power wave length of 10 m. Although the cutoff wave-length was set to 10 m, scales down to about 7 m still contributed to the record variance after filtering. Profiles were then subsampled at a vertical interval of 1 m.

Newman (1981) argues that this smoothing technique is statistically equivalent to "boxcar averaging." In the smoothed data, points at 7 m intervals represent an average of 7 samples of 1 m spacing in the unsmoothed profiles. Smoothing over an effective scale of 7 m reduces noise contributions by a factor of  $1/\sqrt{7}$ .

The XCP can resolve changes in velocity (rms) of about 1 cm/sec (Sanford, 1980). Smoothing the data over an effective 7 m scale length reduces this rms error by about  $1/\sqrt{7}$ , or  $\sigma u = 3.780 \times 10^{-1}$  cm sec.

A minimum uncertainty ( $\sigma S^2$ ) based only on velocity resolution (assuming equal error from both  $u$  and  $v$  components) may be estimated as follows (Newman, 1981, personal communication):

$$\sigma S^2 = \frac{4S}{\Delta Z} \cdot \sigma u = (\text{Sec}^{-2})$$

where  $S$  is the vertical shear and  $\Delta Z$  is the effective sample interval.

For a signal to noise ratio of unity  $\sigma S^2 = S^2$  and

$$S^2 = \frac{4S}{\Delta Z} \cdot \sigma u$$

$$S = \frac{4}{\Delta Z} \cdot \sigma u$$

$$\begin{aligned} \Delta Z &= 700 \text{ cm} \\ \sigma u &= 3.78 \times 10^{-1} \text{ cm sec}^{-1} \\ S &= 2.16 \times 10^{-3} \text{ sec}^{-1} \\ S^2 &= 4.6656 \times 10^{-6} \text{ sec}^{-2} \\ \log S^2 &= -5.33 \end{aligned}$$

The Neil Brown CTD sensor can resolve changes in temperature and salinity with a precision (rms) of about  $0.005^\circ\text{C}$  and  $0.005 \text{ ‰}$ .

Using representative values of the coefficients of thermal expansion and haline contraction (Evans et al., 1979; Newman, 1981) an estimate of noise associated with the Brunt-Väisälä frequency (N) may be given approximately by

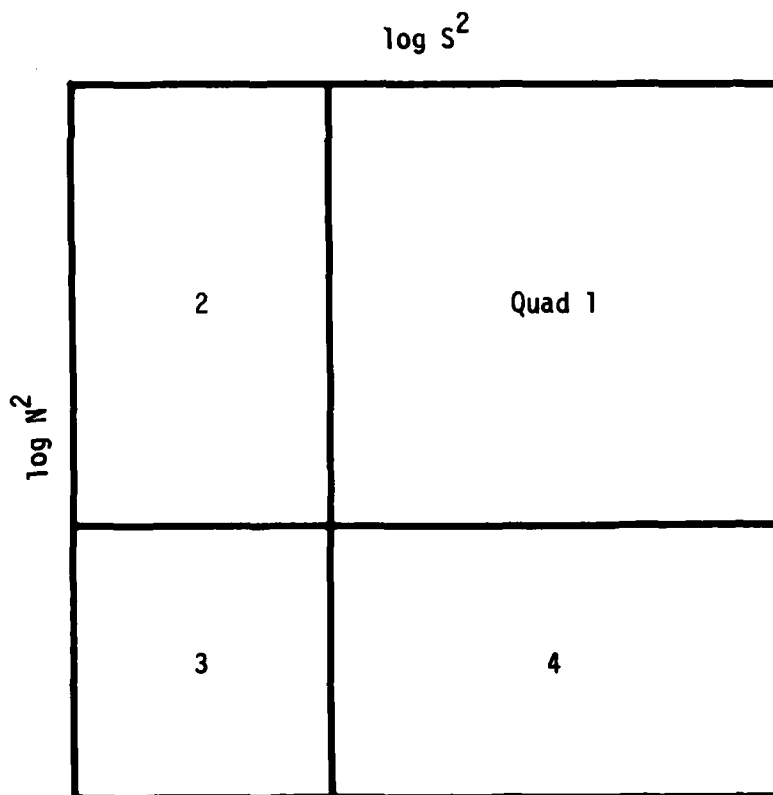
$$\rho_0 \Delta N^2 \approx \frac{g(a\Delta T \pm BS)}{\rho_0 \Delta Z}$$

$$\begin{aligned} g &= 980 \text{ cm sec}^{-2} \\ a &= 3 \times 10^{-4} \text{ g cm}^{-3} (\text{°C})^{-1} \\ B &= 8 \times 10^{-4} \text{ g cm}^{-3} (\text{‰})^{-1} \\ \rho_0 &= 1.0 \text{ g cm}^{-3} \\ \Delta Z &= 700 \text{ cm} \\ \Delta S &= 0.005 \text{ ‰} \sqrt{T} = 1.8898 \times 10^{-3} \text{ ‰} \\ \Delta T &= 0.005 \text{ °C} \sqrt{T} = 1.8898 \times 10^{-3} \text{ °C} \end{aligned}$$

Smoothing of the data reduces the noise level in  $\Delta S$  and  $\Delta T$  by a factor of  $1/\sqrt{T}$ .

$$\begin{aligned} \Delta N^2 &= 2.9103 \times 10^{-6} \text{ (sec}^{-2}\text{)} \\ \log \Delta N^2 &= 5.54 \end{aligned}$$

We selected  $\log N^2 = \log S^2 = -6$  ( $S = N = 1.0 \times 10^{-6} \text{ sec}^{-1}$ ) as being a reasonable cutoff level for a signal-to-noise ratio of 1.



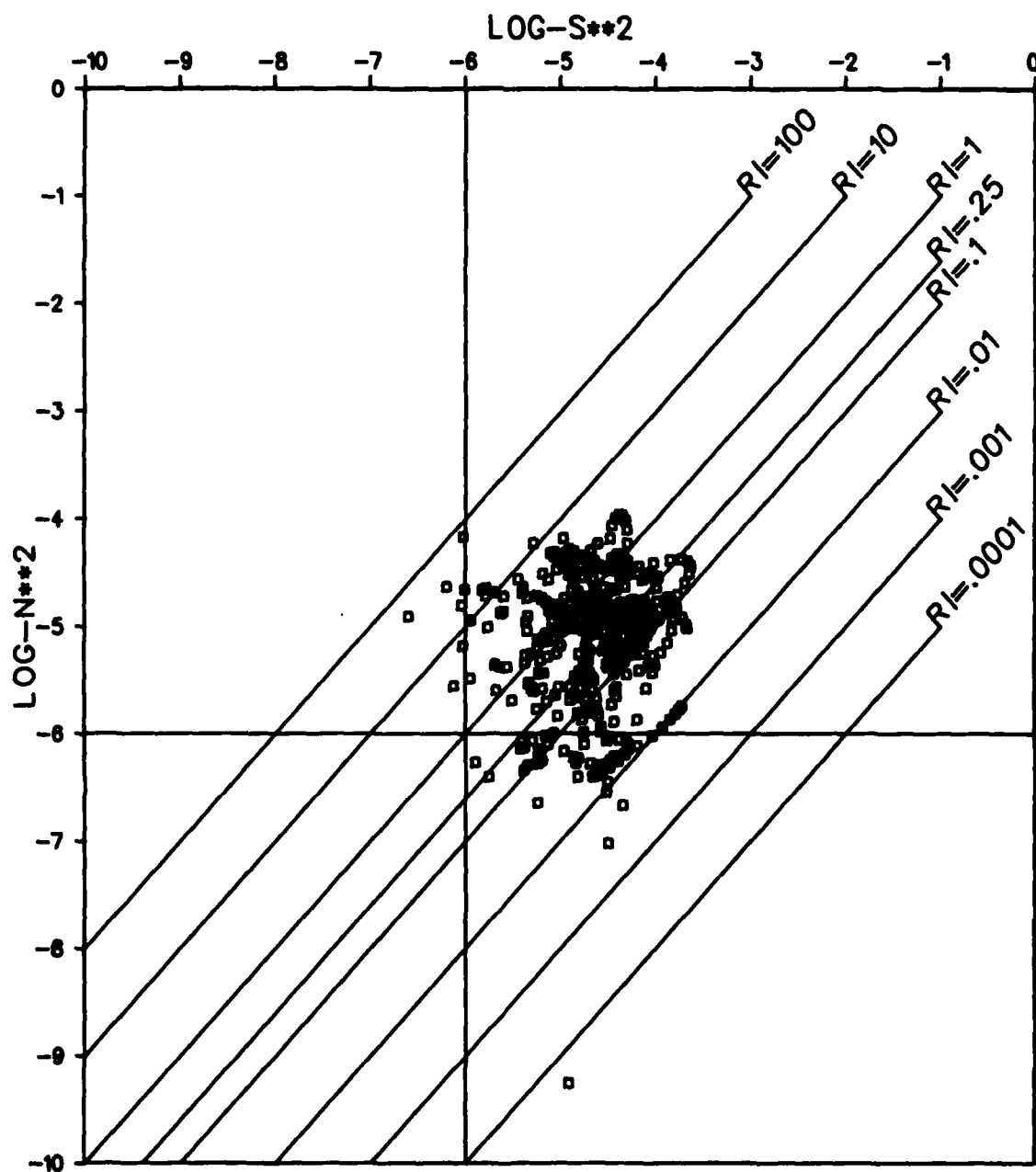


Figure E-1. File: KANE, Segment: C 503

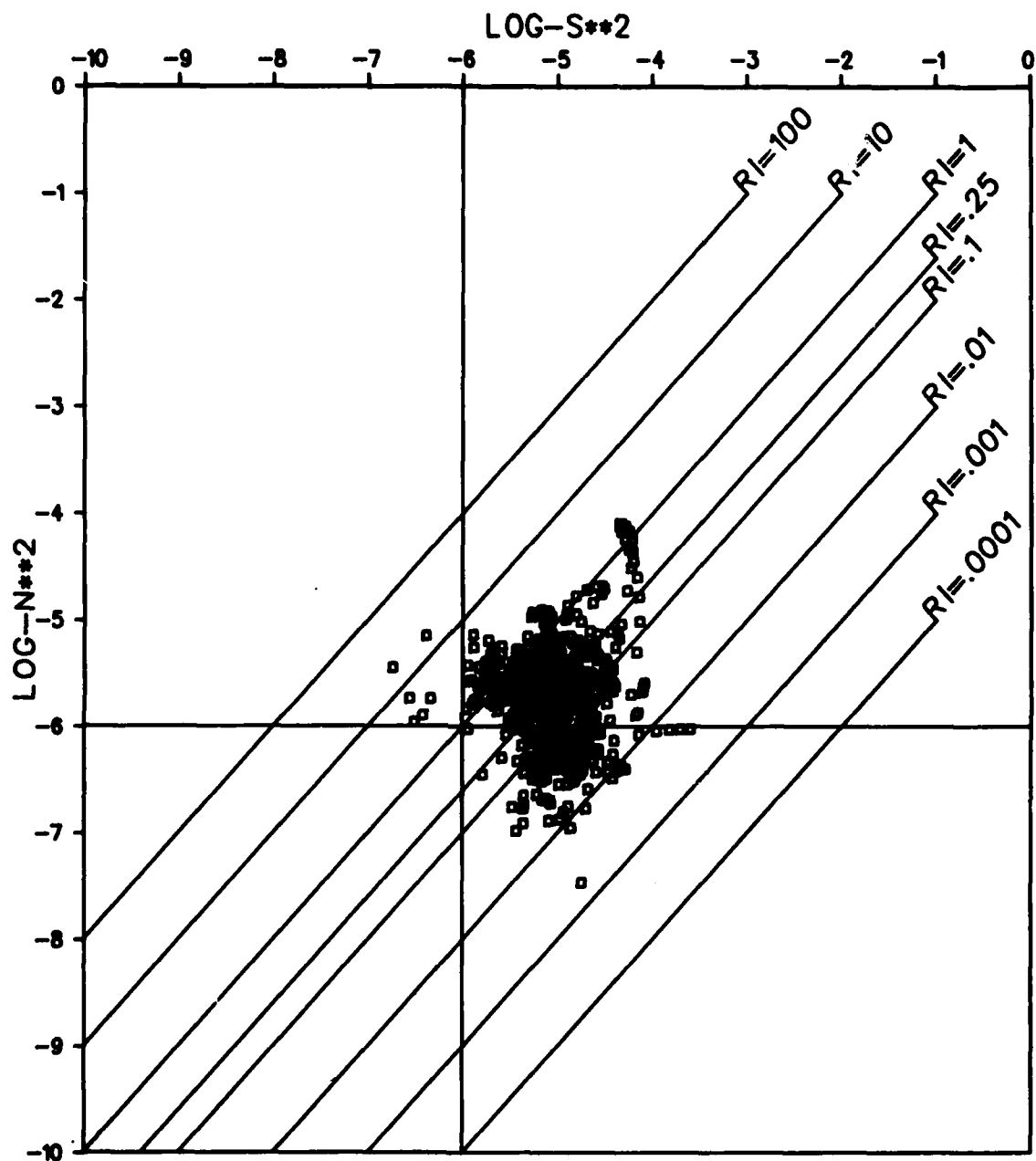


Figure E-2. File: KANE, Segment: C 504

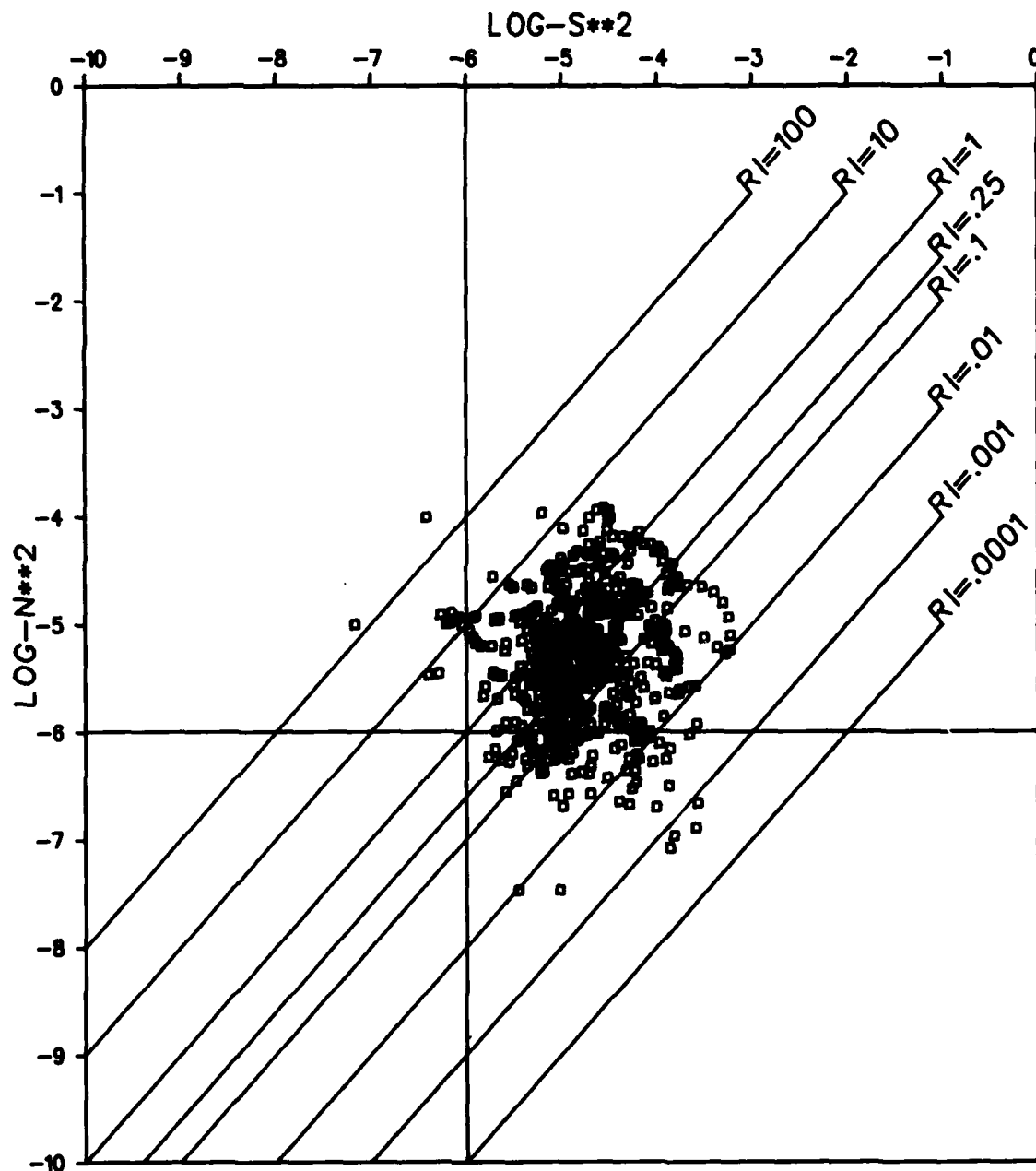


Figure E-3. File: KANE, Segment: C 517

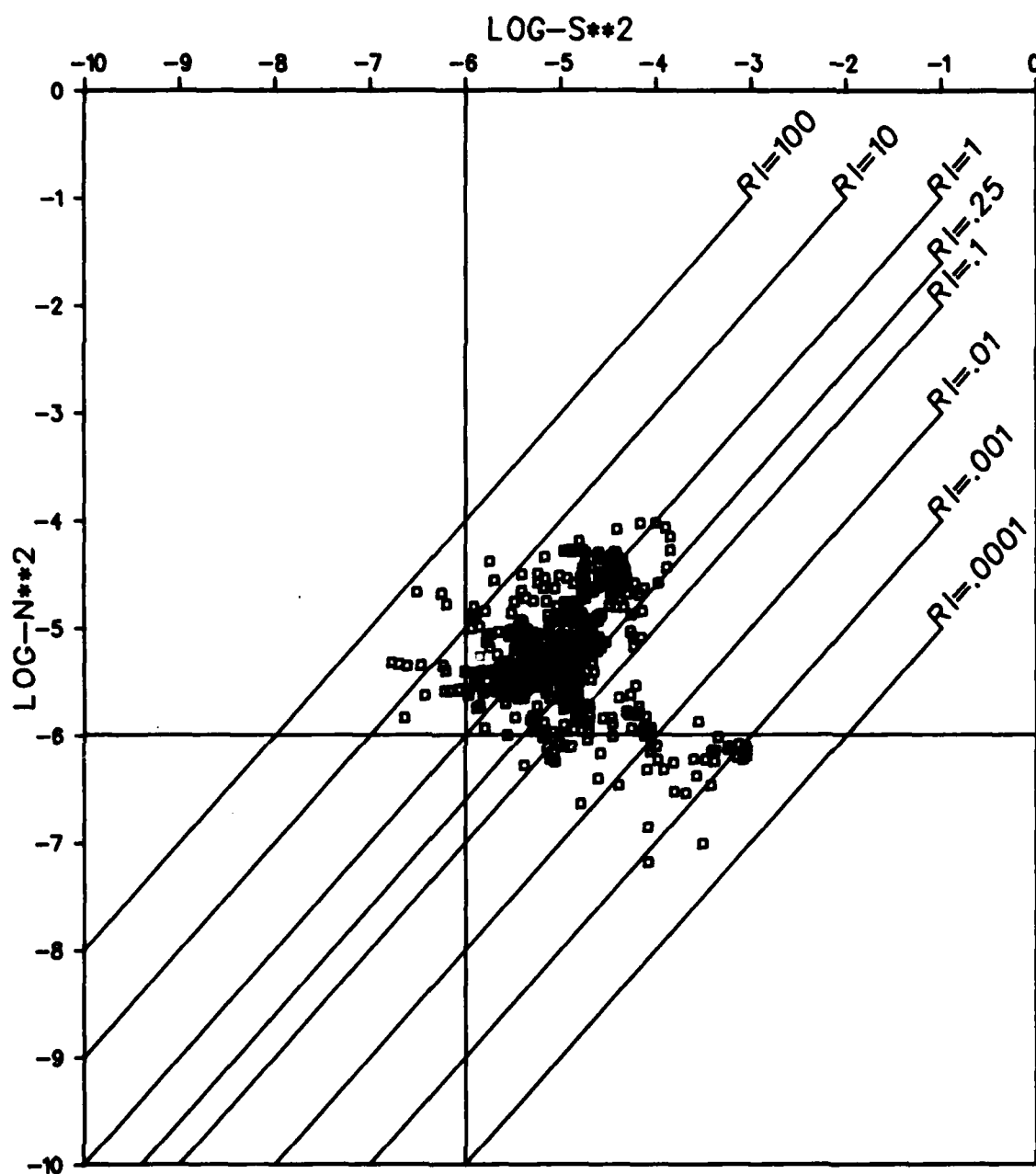


Figure E-4. File: KANE, Segment: C 519

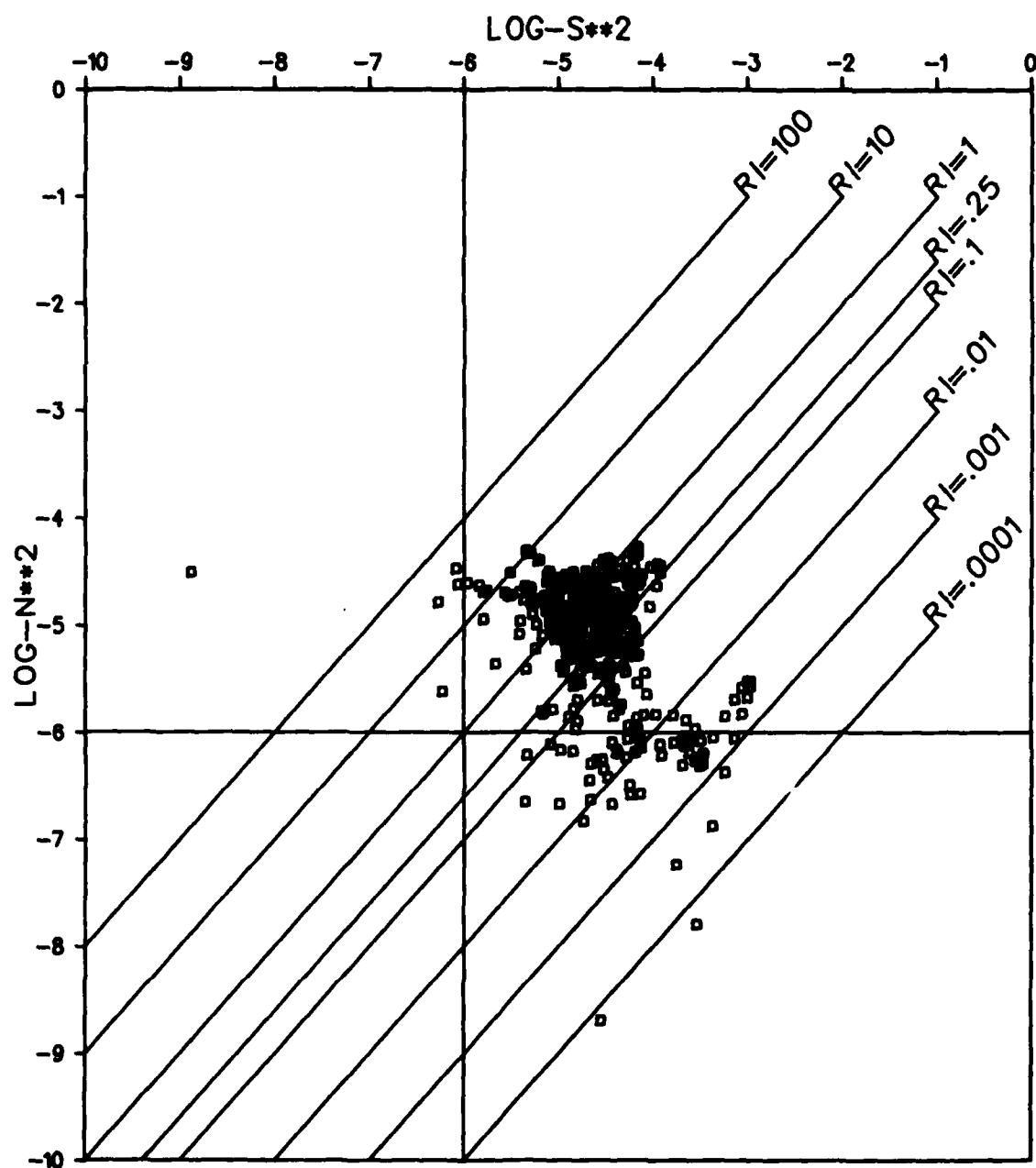


Figure E-5. File: KANE, Segment: C 520

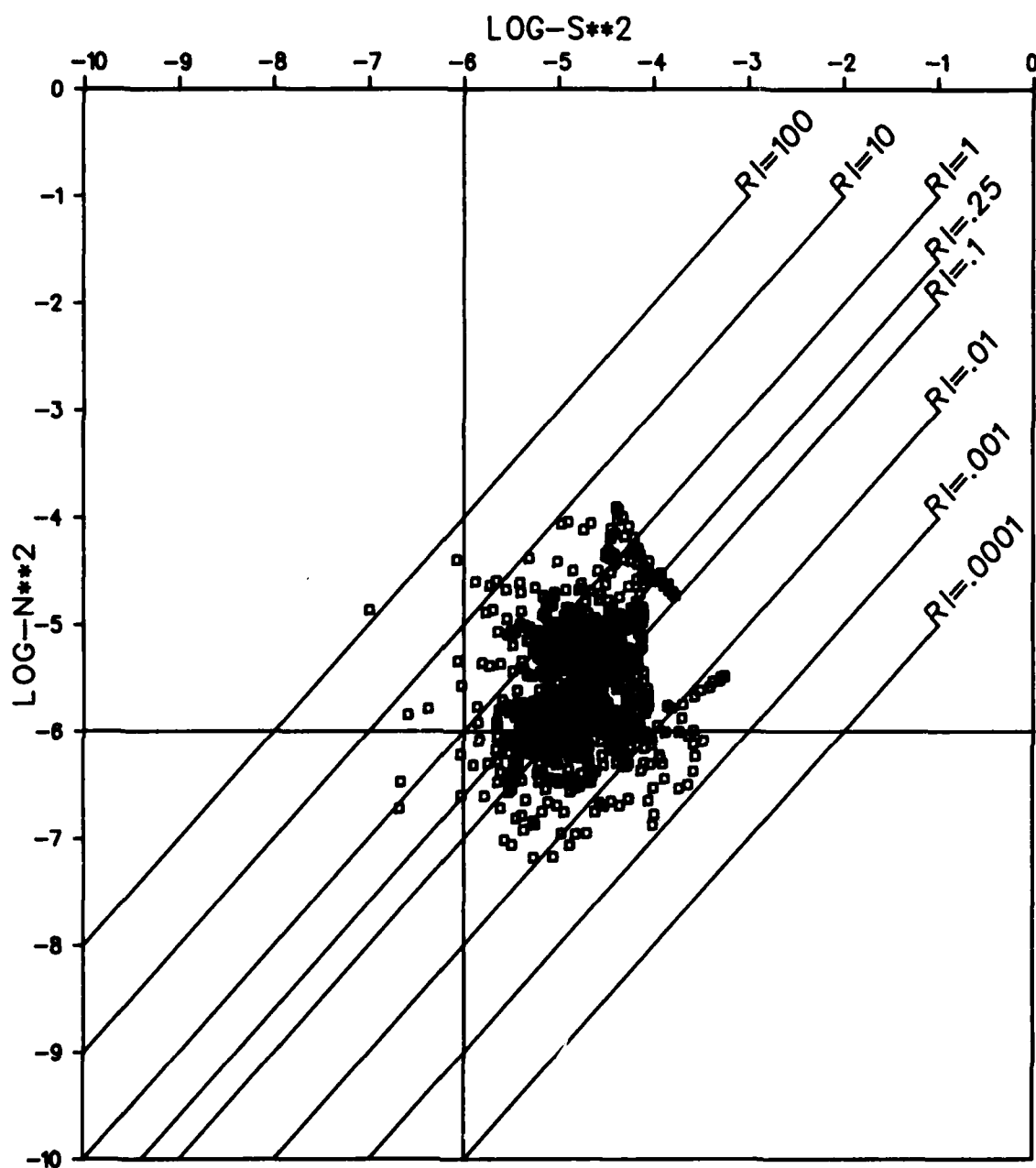


Figure E-6. File: KANE, Segment: C 525

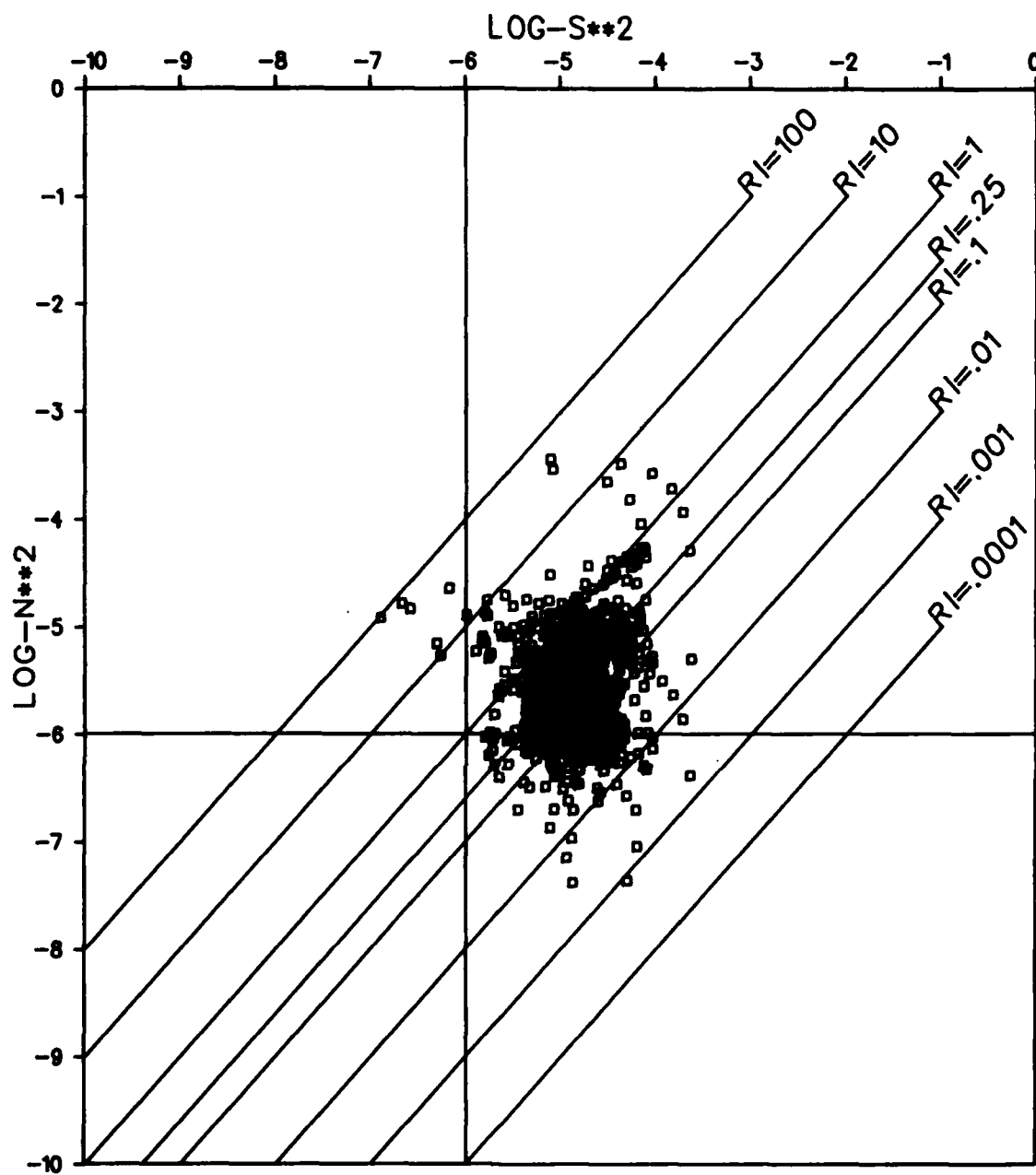


Figure E-7. File: KANE, Segment: C 534

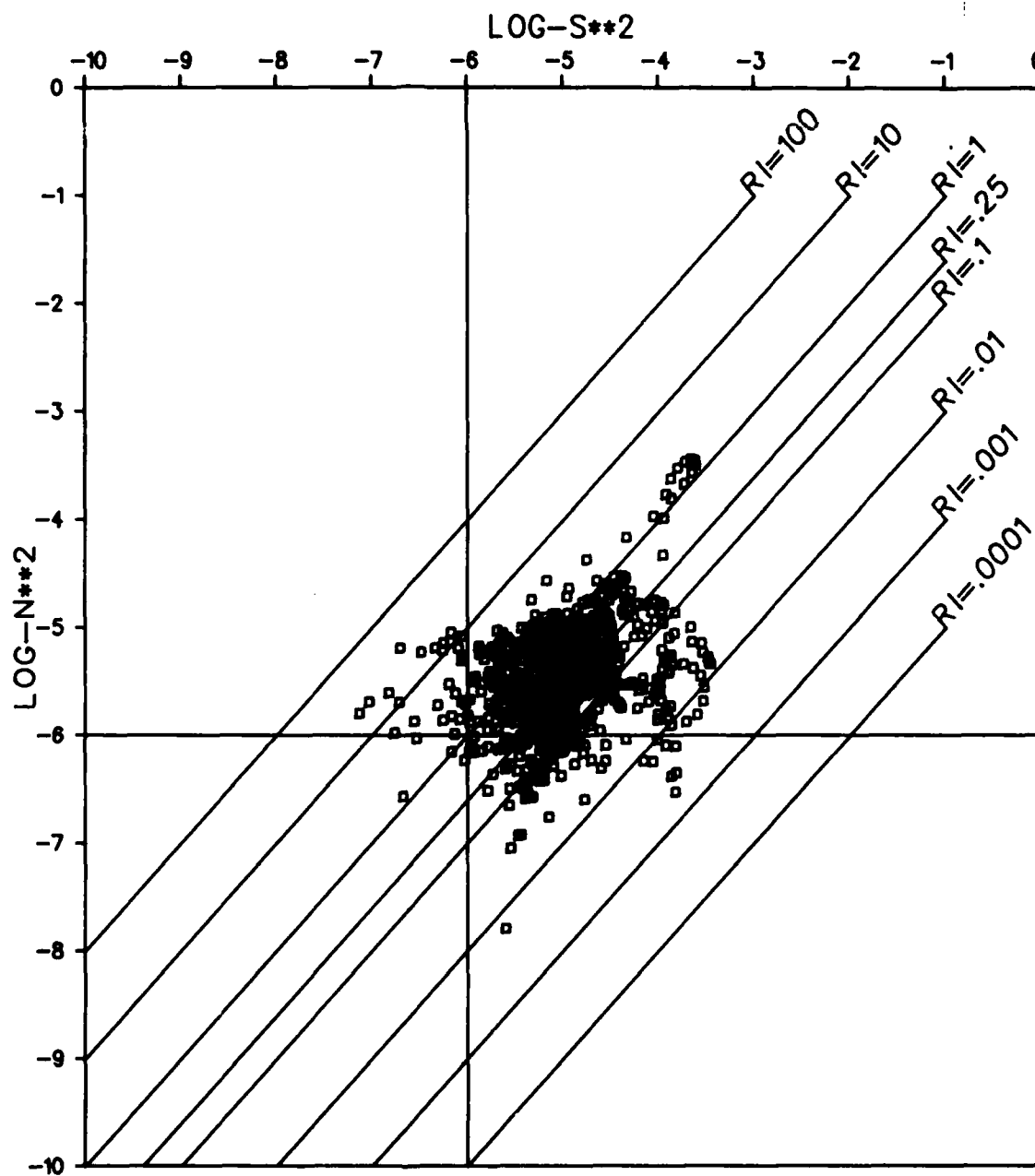


Figure E-8. File: KANE, Segment: C 535

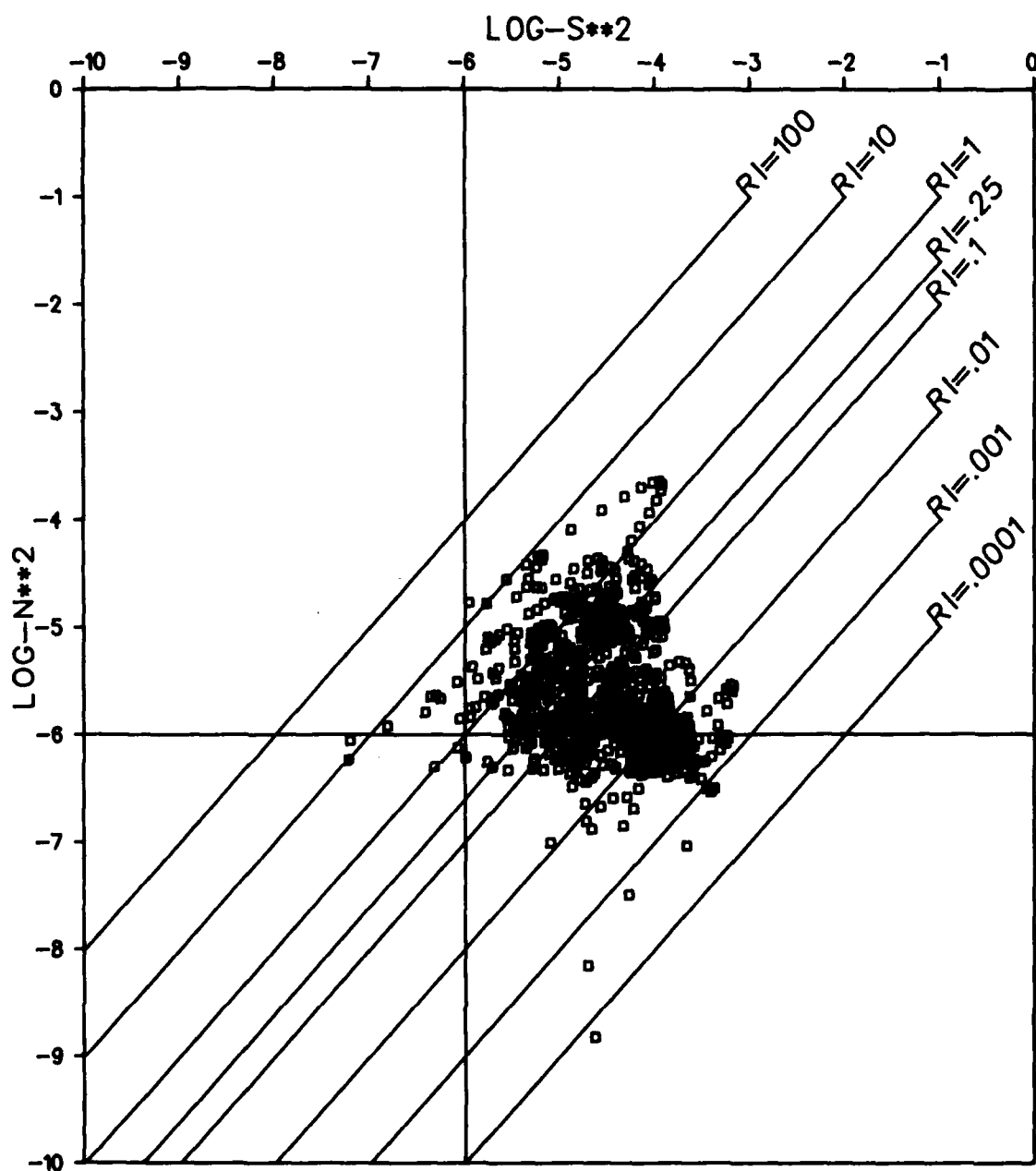


Figure E-9. File: KANE, Segment: C 538

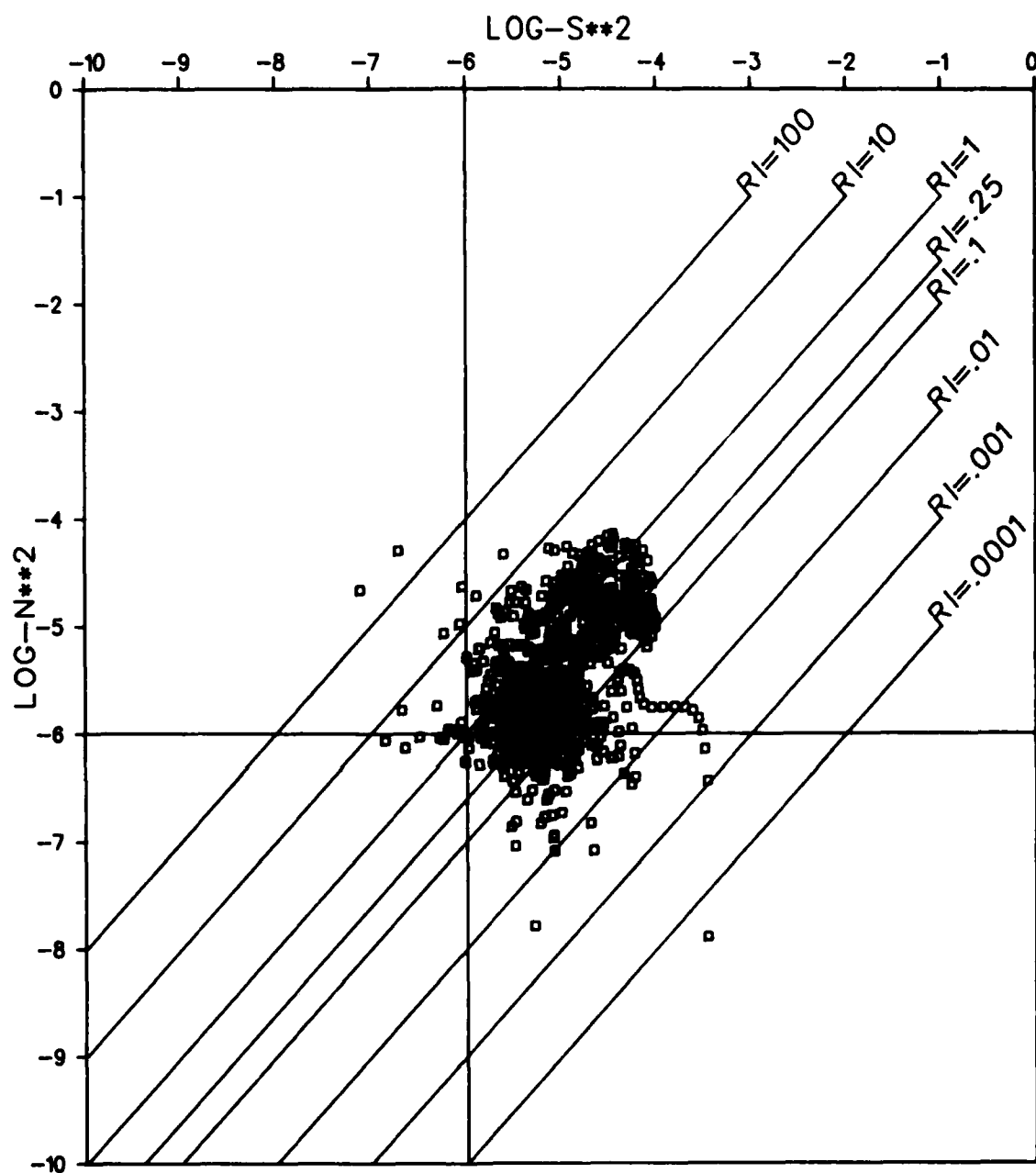


Figure E-10. File: KANE, Segment: C 546

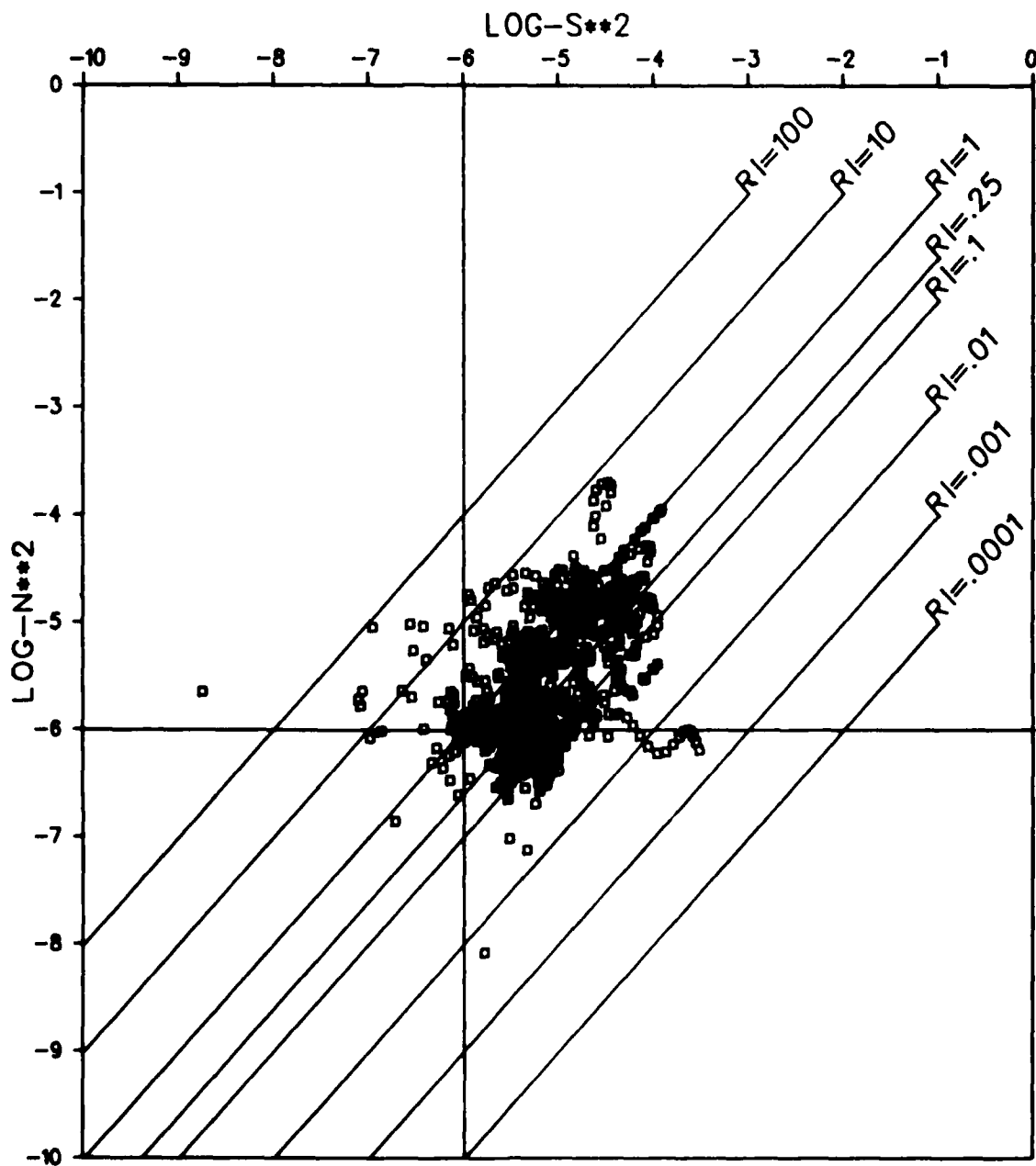


Figure E-11. File: KANE, Segment: C 547

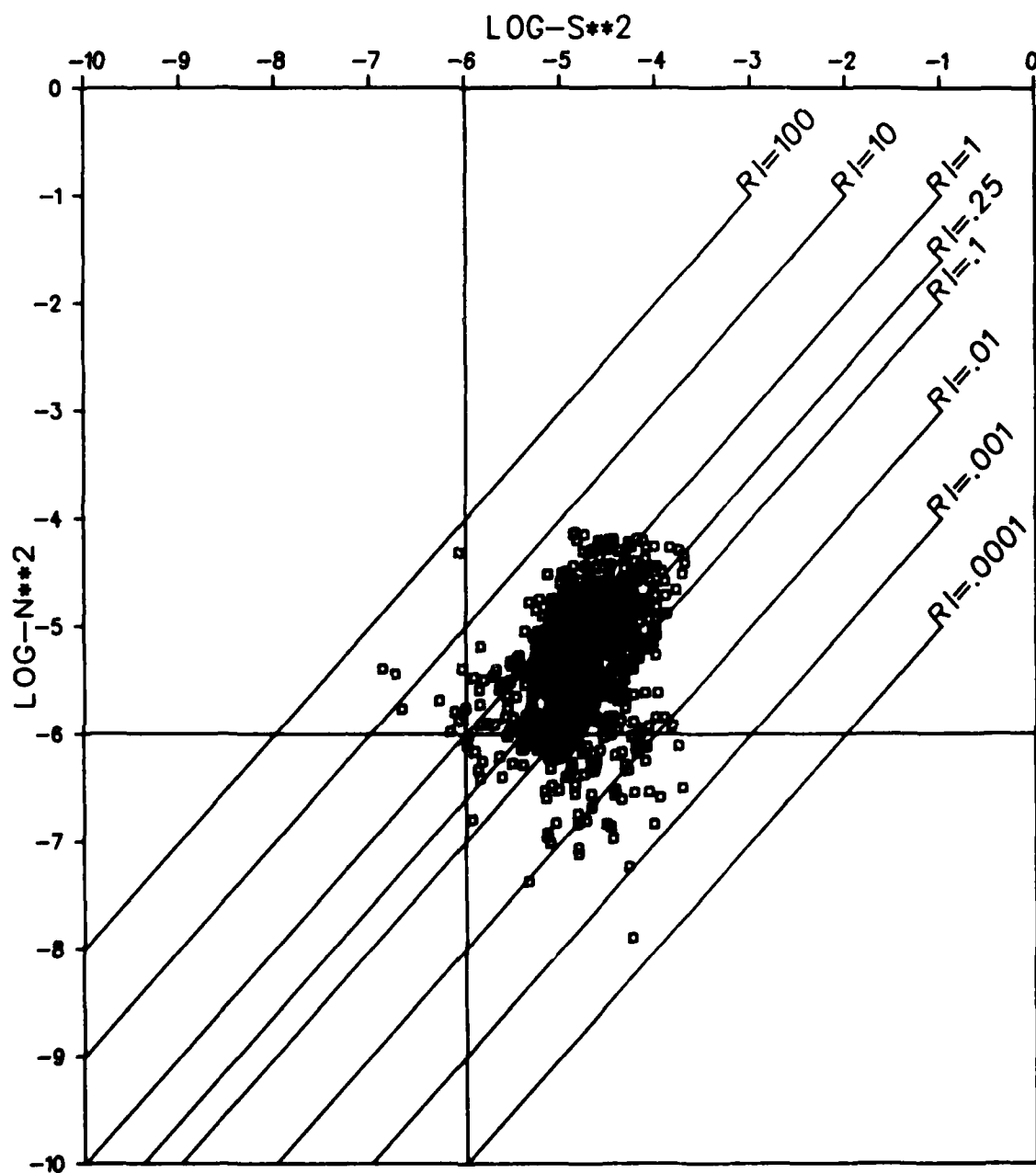


Figure E-12. File: KANE, Segment: C 548

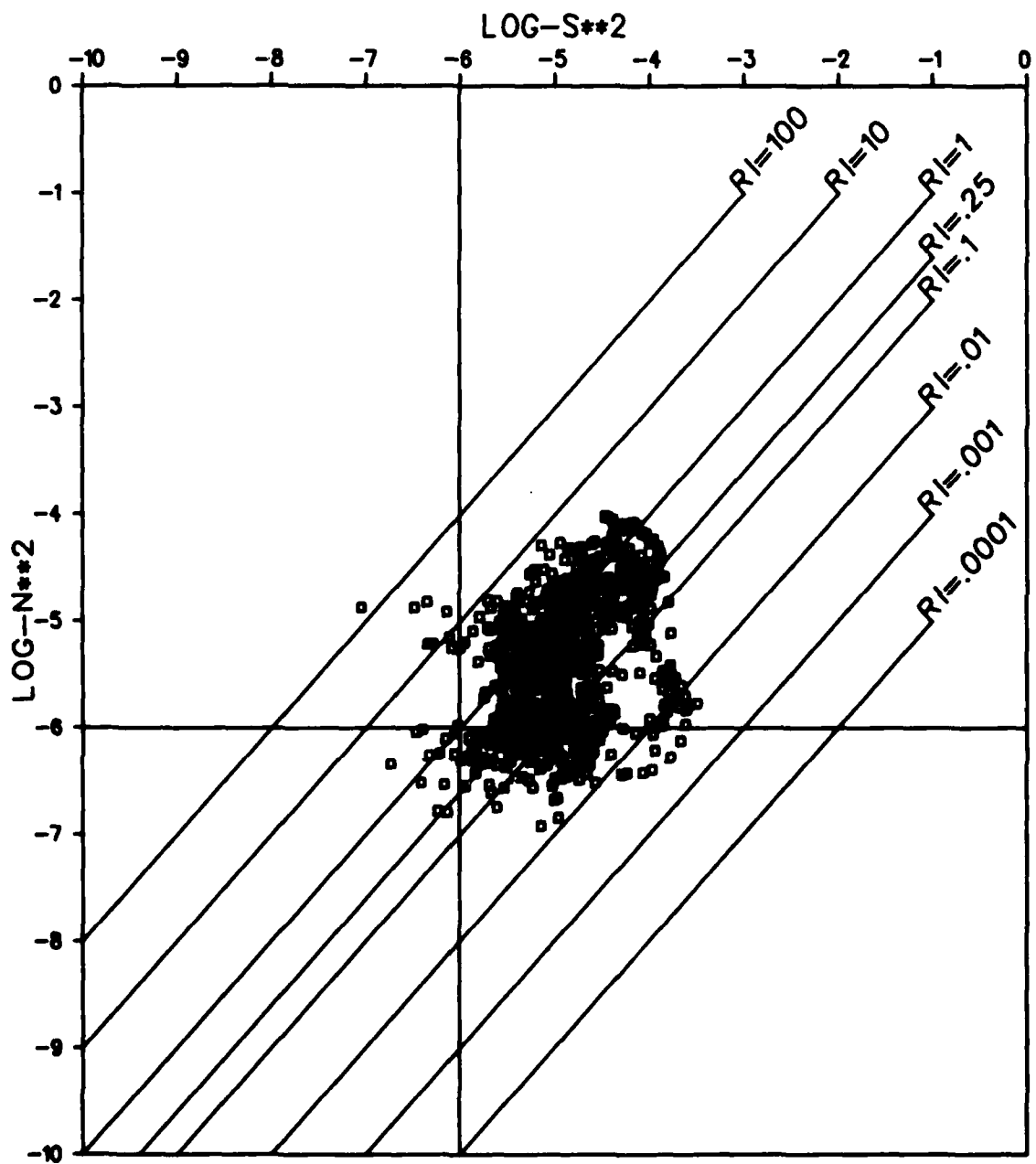


Figure E-13. File: KANE, Segment: C 549

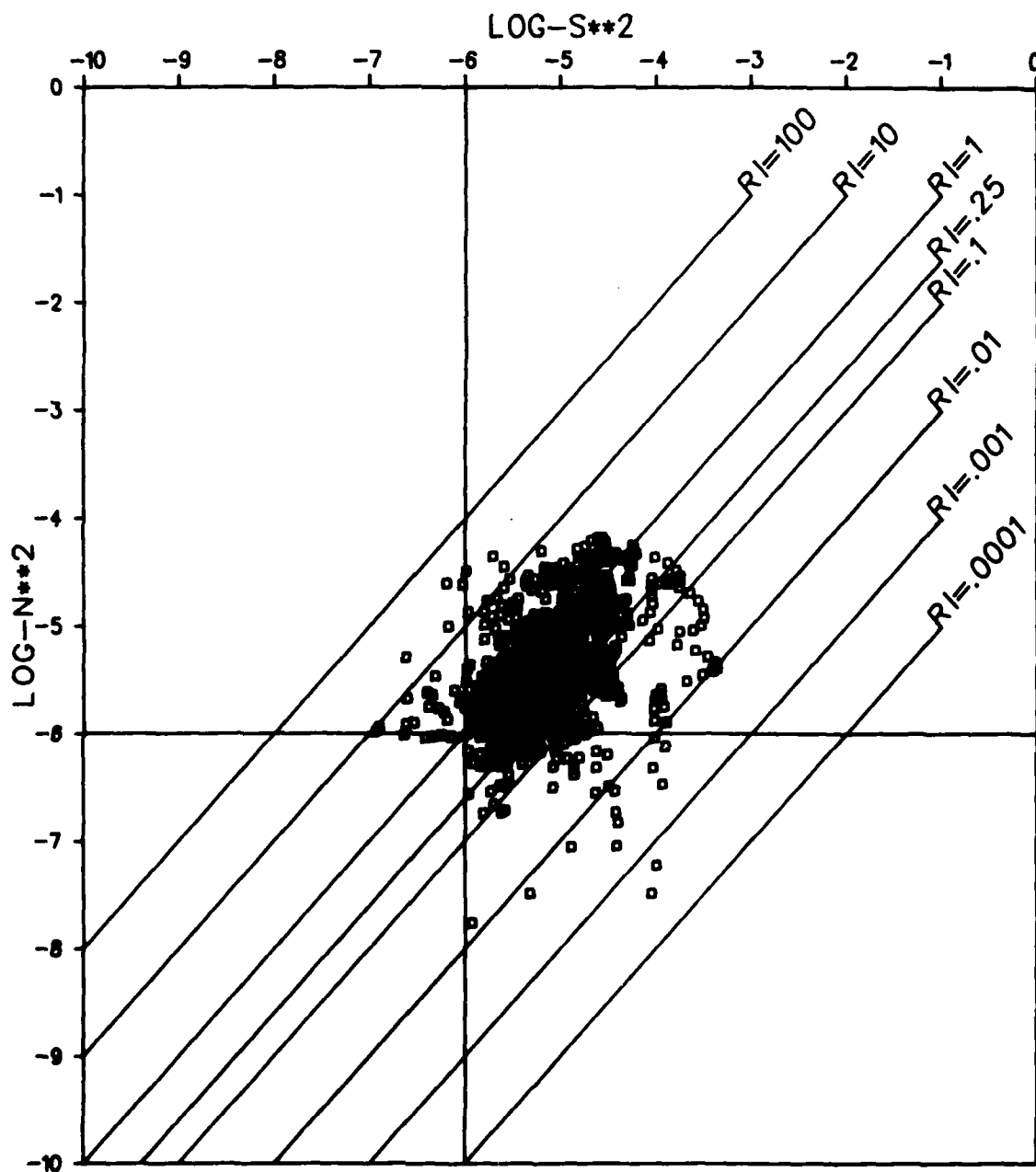


Figure E-14. File: KANE, Segment: C 550

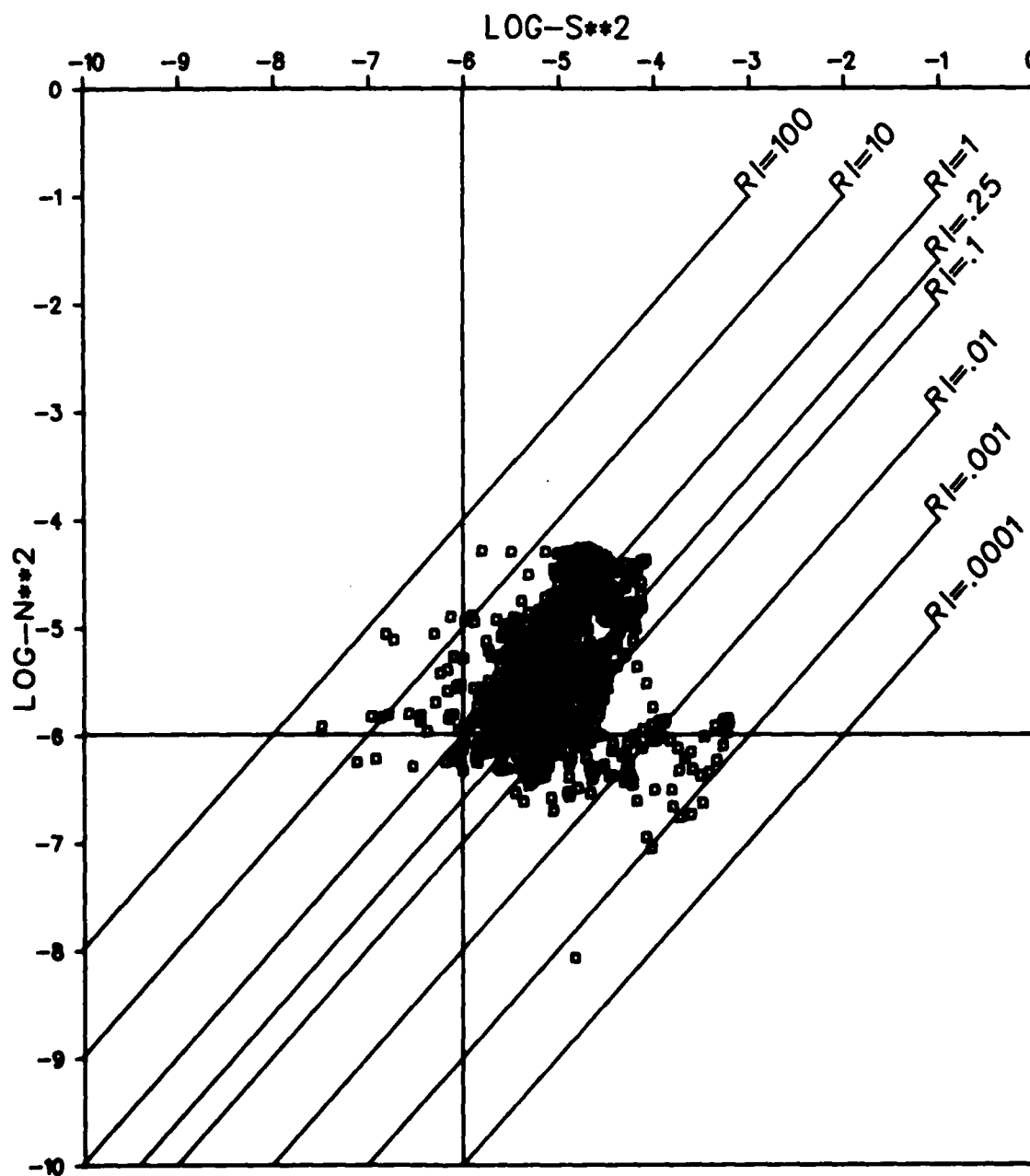


Figure E-15. File: KANE, Segment: C 551

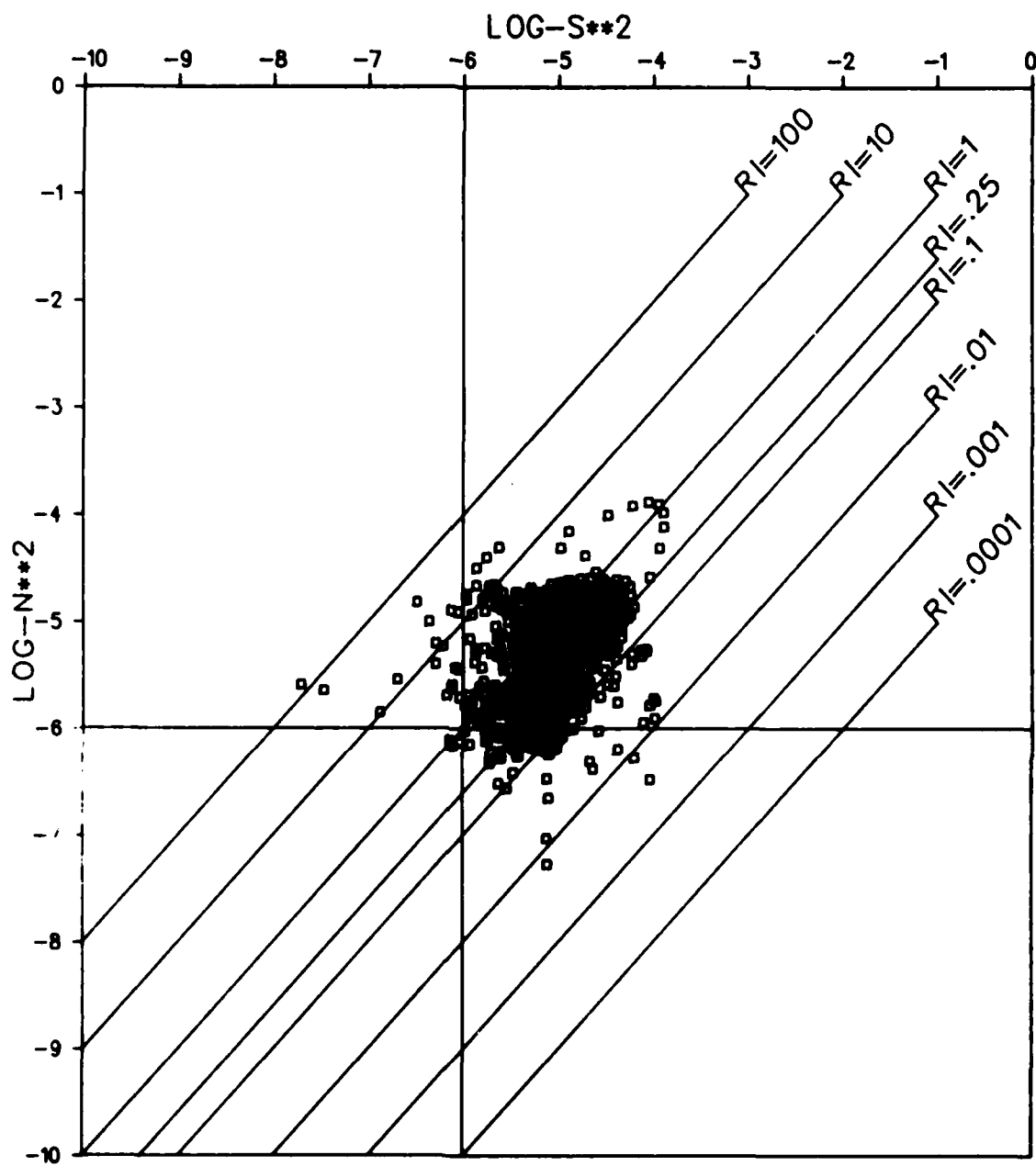


Figure E-16. File: KANE, Segment: C 563

**UNCLASSIFIED**

SECURITY CLASSIFICATION OF THIS PAGE (When Data Entered)

REPORT DOCUMENTATION PAGE		READ INSTRUCTIONS BEFORE COMPLETING FORM
1. REPORT NUMBER <b>NORDA Technical Note 142</b>	2. GOVT ACCESSION NO. <b>42-41528</b>	3. RECIPIENT'S CATALOG NUMBER
4. TITLE (and Subtitle) <b>Data Summary - XCP Profiles in the Vicinity of the Faeroe Islands During October 1980</b>		5. TYPE OF REPORT & PERIOD COVERED
7. AUTHOR(s) <b>D.A. Burns</b>		6. PERFORMING ORG. REPORT NUMBER
9. PERFORMING ORGANIZATION NAME AND ADDRESS <b>Naval Ocean Research and Development Activity NSTL Station, Mississippi 39529</b>		8. CONTRACT OR GRANT NUMBER(s)
11. CONTROLLING OFFICE NAME AND ADDRESS <b>Naval Ocean Research and Development Activity NSTL Station, Mississippi 39529</b>		10. PROGRAM ELEMENT, PROJECT, TASK AREA & WORK UNIT NUMBERS
14. MONITORING AGENCY NAME & ADDRESS (if different from Controlling Office)		12. REPORT DATE <b>April 1982</b>
		13. NUMBER OF PAGES <b>185</b>
		15. SECURITY CLASS. (of this report) <b>UNCLASSIFIED</b>
16. DISTRIBUTION STATEMENT (of this Report) <b>Unlimited</b>		15a. DECLASSIFICATION/DOWNGRADING SCHEDULE
17. DISTRIBUTION STATEMENT (of the abstract entered in Block 20, if different from Report)		
18. SUPPLEMENTARY NOTES		
19. KEY WORDS (Continue on reverse side if necessary and identify by block number) <b>Shear Probe                      Faeroe Islands</b> <b>Subpolar Front                Iceland-Faeroe Ridge</b> <b>Richardson Number           Stratification</b> <b>Brunt-Vaisala Frequency     Hydrography</b> <b>Current Shear                 XCP</b>		
20. ABSTRACT (Continue on reverse side if necessary and identify by block number) <p>In support of the Ocean Measurements Program in the Iceland-Faeroe (Subpolar) oceanic front region, Expendable Current Probes (XCP) were deployed at four time series stations and in four circulation regimes. Forty-six of seventy-three probes deployed transmitted usable data. We discuss data editing and matching of CTD and XCP casts. We present vertical profiles of XCP data and CTD data. We discuss the primary water types present and their relationship to the subpolar front. We discuss the determination and variation of bulk Richardson numbers.</p>		

DD FORM 1 JAN 73 1473

EDITION OF 1 NOV 65 IS OBSOLETE  
S/N 0102-LF-014-6601

**UNCLASSIFIED**

SECURITY CLASSIFICATION OF THIS PAGE (When Data Entered)

DATE  
FILME  
7-8